Vol. 145, January 1, 1983 ISSN 0003-2670
Complete in one issue

INTERNATIONAL CONFERENCE ON FLOW ANALYSIS II, LUND, SWEDEN, JUNE 18–21, 1982

ANALYTICA CHIMICA ACTA

International journal devoted to all branches of analytical chemistry

ELSEVIER SCIENTIFIC PUBLISHING COMPANY

ANALYTICA CHIMICA ACTA

International journal devoted to all branches of analytical chemistry
Revue internationale consacrée à tous les domaines de la chimie analytique
Internationale Zeitschrift für alle Gebiete der analytischen Chemie

PUBLICATION SCHEDULE FOR 1983

	J	F	M	A	M	J	J	A	S	O	N	D
Analytica Chimica Acta	145	146	147	148	149	150/1 150/2	151	152	153/1	153/2	154	155

Scope. *Analytica Chimica Acta* publishes original papers, short communications, and reviews dealing with evei aspect of modern chemical analysis, both fundamental and applied.

Submission of Papers. Manuscripts (three copies) should be submitted as designated below for rapid and efficier handling:

Papers from the Americas to: Professor Harry L. Pardue, Department of Chemistry, Purdue University, West Lafayett IN 47907, U.S.A.

Papers from all other countries to: Dr. A. M. G. Macdonald, Department of Chemistry, The University, P.O. Box 36 Birmingham B15 2TT, England. Papers dealing particularly with computer techniques to: Professor J. T. Cler Universität Bern, Pharmazeutisches Institut, Sahlistrasse 10, CH-3012 Bern, Switzerland.

Submission of an article is understood to imply that the article is original and unpublished and is not being considere for publication elsewhere. Upon acceptance of an article by the journal, authors resident in the U.S.A. will be asked t transfer the copyright of the article to the publisher. This transfer will ensure the widest dissemination of informatio under the U.S. Copyright Law.

Information for Authors. Papers in English, French and German are published. There are no page charge Manuscripts should conform in layout and style to the papers published in this Volume. Authors should consu Vol. 132, p. 239 for detailed information. Reprints of this information are available from the Editors or from: Elsevi Editorial Services Ltd., Mayfield House, 256 Banbury Road, Oxford OX2 7DH (Great Britain).

Reprints. Fifty reprints will be supplied free of charge. Additional reprints (minimum 100) can be ordered. An ord form containing price quotations will be sent to the authors together with the proofs of their article.

Advertisements. Advertisement rates are available from the publisher.

Subscriptions. Subscriptions should be sent to: Elsevier Scientific Publishing Company, P.O. Box 211, 1000 A Amsterdam, The Netherlands.

Publication. *Analytica Chimica Acta* appears in 11 volumes in 1983. The subscription for 1983 (Vols. 145–155) Dfl. 1980.00 plus Dfl. 220.00 (postage) (total approx. U.S. $880.00). Journals are sent automatically by airmail to th U.S.A. and Canada at no extra cost and to Japan, Australia and New Zealand for a small additional postal charge. A earlier volumes (Vols. 1–144) except Vols. 23 and 28 are available at Dfl. 182.00 (U.S. $72.80), plus Dfl. 14.00 (U.S $5.60) postage and handling, per volume.

Claims for issues not received should be made within three months of publication of the issue, otherwise they cann be honoured free of charge.

Customers in the U.S.A. and Canada who wish to obtain additional bibliographic information on this and oth Elsevier journals should contact Elsevier Science Publishing Company Inc., Journal Information Center, 52 Vanderbi Avenue, New York, NY 10017. Tel: (212) 867-9040.

ANALYTICA CHIMICA ACTA
VOL. 145 (1983)

ANALYTICA CHIMICA ACTA

International journal devoted to all branches of analytical chemistry

ELSEVIER SCIENTIFIC PUBLISHING COMPANY

Anal. Chim. Acta, Vol. 145 (1983)

SPECIAL ISSUE

FLOW ANALYSIS II

Proceedings of a Conference held in Lund, Sweden, June 18–21, 1982

Analytica Chimica Acta, 145 (1983) 1—15
Elsevier Scientific Publishing Company, Amsterdam — Printed in The Netherlands

RECENT DEVELOPMENTS IN FLOW INJECTION ANALYSIS: GRADIENT TECHNIQUES AND HYDRODYNAMIC INJECTION

J. RŮŽIČKA and E. H. HANSEN

Chemistry Department A, Building 207, The Technical University of Denmark DK-2800 Lyngby (Denmark)

(Received 23rd April 1982)

SUMMARY

Some of the most exciting recent advances in flow injection analysis (f.i.a.) have involved gradient techniques, which, founded on the key role of dispersion controlled in space and time, are based on the feasibility of identifying and selecting reproducibly suitable sections of the dispersed sample zone and exploiting the specific concentrations at these points for analytical purposes. A comprehensive review of these techniques is given; in addition to the well established f.i.a. titrations and stopped-flow reaction rate procedures, methods have been developed for gradient dilution and calibration, gradient scanning, and selectivity evaluation. Finally, a detailed description of the most recent development within f.i.a., a hydrodynamic injector with no moving parts and zero dead volumes, is presented.

The initial purpose behind the development of flow injection analysis [1] (f.i.a.) was to design a continuous flow method which would be faster and more economical for assays on liquid samples than the well-established method of Skeggs [2], based on air segmentation. The advantages of f.i.a. i.e., the simplicity of the experimental setup, the economy of sample and reagent consumption, and the very rapid availability of the analytical read-out, are winning the method wider acceptance; its versatility, which allows dialysis, gas diffusion and solvent extraction to be done at unprecedented speed [3], is just being recognized. Among the more recent developments, gradient f.i.a. techniques offer new ways of solving analytical problems. In fact, the potential of the gradient approach suggests that f.i.a. techniques are not restricted to providing convenient analytical methods but are becoming generally applicable solution-handling techniques.

The concept of controlled dispersion of the injected sample zone has played the key role in the development of f.i.a., as it has allowed optimization of flow designs and has assisted in the understanding of why and how f.i.a. works. The quantitative description of dispersion simply relates the original concentration of the sample material C^0 to its concentration C in an element of fluid which has undergone dispersion: $D = C^0/C$. For $C = C^{max}$, $D = C^0/C^{max}$, where C^{max} is the concentration at the peak maximum. In this way the dispersion coefficient D describes the dilution ratio of sample

material prior to injection to that measured by the detector. So far the main attention has been focused on peak maximum measurement as the source of the analytical readout, simply because the distance between the summit of the response curve and the baseline is the easiest one to identify and measure. The thus-defined dispersion coefficient D has recently [4] been related to the linear dispersion number δ by

$$D = 2\pi^{3/2} r^2 L^{1/2} F^{1/2} \delta^{1/2} \bar{T}^{1/2} S_v^{-1} \quad (1)$$

where the dispersion number, as given by Levenspiel and Smith [5], is

$$\delta = \frac{1}{8}\left[(8\sigma^2 + 1)^{1/2} - 1\right] \quad (2)$$

for a non-Gaussian curve (as shown in Fig. 1); hence the variance σ is related to the dispersion number δ through Eqn. (2). Thus the tube radius r, the length L, the linear flow velocity F, the mean residence time $\bar{T}$, and the sample volume S_v can be manipulated to achieve the required degree of dispersion.

The interrelated D and σ values describe, of course, the same physical phenomenon, yet they are not equally well suited for description of all continuous flow systems. For chromatography, the use of σ is most appropriate as resolution is the key issue of all separations, and as σ contains "horizontal" information it is superbly suited for descriptions of peak width and overlap. The σ value allows estimation of the maximum sampling frequency S_{max} (in samples/hour) in f.i.a. [3]:

$$S_{max} = 60\,Q/4\,\sigma_v = 3600/4\,\sigma_t$$

where Q is the volumetric pumping rate and σ is the variance in units of time (t) or volume (v). Yet the D value, which contains the "vertical" information, is much more useful in f.i.a., where the analytical readout is based mainly on measurement of peak height.

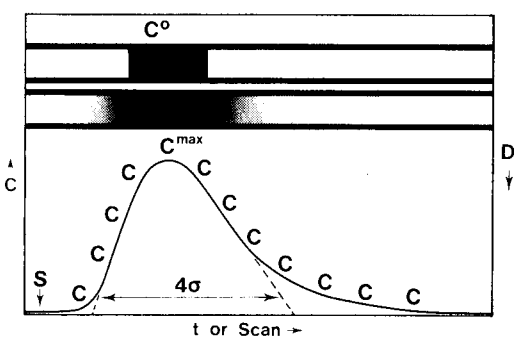

Fig. 1. Dispersed sample zone, of original concentration C^0 injected at position S, and the corresponding recorder output. To each individual concentration C corresponds a specific dispersion value D which is minimum at C^{max} and increases to larger values along the continuous gradient.

The key role of dispersion and its description by the D value should, however, be viewed in a broader context. While the σ value is related to peak width, and describes only the time window of the signal duration, the D value describes the concentration (C, Fig. 1) within any element of fluid constituting the continuous concentration gradient. This straightforward concept thus emphasizes the significance of the analytical information contained within these segments of fluid and has led to designs involving gradient dilution [6], gradient calibration [6], stopped-flow reaction rate measurements [3, 6], gradient scanning methods [3, 7], gradient f.i.a. titrations [3, 4], and selectivity evaluation methods [8].

Along with these recent theoretical advances, technical developments have resulted in improved performance and reliability of various forms of f.i.a. equipment. New means of propelling solutions, connecting and assembling the components, or constructing flow cells have been described but these are outside the scope of this paper. There is, however, one significant exception, a design for a hydrodynamic injector [9] with no moving parts and zero dead volumes. Because of its reliability, this device allows the transfer of f.i.a. technology into the field of automated continuous monitoring. Thus, besides conceptual advances, there is also technological evidence pointing to the future role of f.i.a. as a generalized solution-handling technique.

GRADIENT TECHNIQUES IN FLOW INJECTION ANALYSIS

Gradient dilution

The principle of gradient dilution [6] is simple and it is best understood from Fig. 2 (left), which is self-explanatory: any element of the dispersed sample zone yields as useful information as the element corresponding to the peak maximum. This means that the read-outs, which are usually obtained

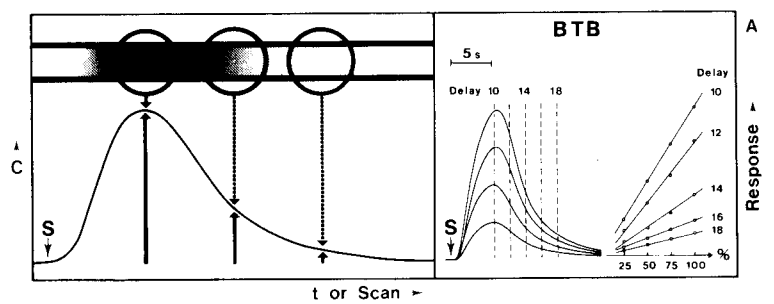

Fig. 2. The principle of the gradient dilution technique. To each delay time, measured from the time of injection, S, corresponds a specific D value of the dispersed sample zone. To the right, is shown the recorder output for a series of injected bromothymol blue (BTB) dye solutions (the most concentrated one being denoted by 100%) and the corresponding calibration curves obtained at different delay times [6].

from peak maxima, may, if desired, be replaced by the read-outs collected at any other section of the peak, provided that they are always taken at exactly the same delay time after the point of injection (Fig. 2, right). The nature of the physical process of dispersion on which f.i.a. is based ensures that the response is linear, and that the calibration curves obtained from data collected at fixed delay times are linear (Fig. 2, far right). Linear relationships will also be found if the physical dispersion is accompanied by a resulting chemical reaction provided that the reaction is also linear in nature, because "if a number of independent linear processes are occurring simultaneously in a system, their over-all effect is also a linear process" [10]. Consequently, the linearity of the calibration graphs, whether obtained from peak maximum measurements, or from peak heights corresponding to successive sections of the dispersed sample zone, will be preserved even if the species to be measured is produced by a chemical reaction during sample zone dispersion, provided that: (a) there is a sufficient excess of all necessary reagents in the element of fluid to be monitored; (b) that there is no inhibition caused by reaction products; and (c) that the detector responds linearly to the generated species. As a matter of fact, these conditions are least likely to be fulfilled at the peak maximum, as with a high sample concentration any of (or even all three) of those unwanted situations may occur. Therefore, the linearity of response will be afflicted first at the peak maximum, while more delayed peak sections will still yield a linear response. Even a trivial error of injecting a too concentrated sample material, which would yield a peak "out of range" of both recorder and detector, can be corrected for by using a delayed read-out. As this is best done electronically, by means of a microcomputer, the gradient dilution technique has also been termed "electronic dilution" [6].

Gradient calibration

This technique is a logical extension of the gradient dilution procedure as it relies on the strict reproducibility of the same phenomena: physical dispersion accompanied by chemical reactions. Its main goal is to avoid the usual repetitive calibration by means of serially diluted solutions, as the information sought is in fact already contained within some of the segments of fluid originating from a sample zone of the most concentrated standard sample material. Thus, by identifying on this curve the time delays associated with those segments of fluid which have concentrations corresponding to the concentrations that would provide the same read-outs if the signals were collected from the peak maxima obtained by separate injections of serial dilutions, one can obtain a multipoint calibration curve from a single injection. In other words, the highest (C^{max}) value can be supplemented by a series of sequential C values empirically spaced along the gradient and identified through increasing delay times. The empirical formula describing $C = f$ (delay time) is obtained from a normal calibration evaluation and stored by a computer [6].

Stopped-flow reaction-rate measurement

This approach is, apart from f.i.a. titrations, the most thoroughly tested gradient technique [3, 6, 11]. It is based on a combination of stopped-flow measurement and of gradient dilution. The most reliable approach to reaction-rate measurement is to hold the reaction mixture within the observation volume of the flow-through detector and to measure the rate of change of the signal with time. This is most readily accomplished by the f.i.a. stopped-flow technique which relies on a combination of a suitable dispersion of the sample material within the reagent stream and on the subsequent reaction-rate measurement, when the carrier solution is held still. The recorded signal has a characteristic shape (Fig. 3, right) which contains a portion of the reaction-rate curve yielding the read-out, and the calibration curve.

An additional feature of the stopped-flow gradient technique is that it allows a fine adjustment of the reagent-to-sample ratio by electronic means, i.e., by choosing an appropriate delay time. It is self-evident that the ratio between the sample material and the reagent varies along the dispersed sample zone, as much as the D value does. (Fig. 3, left). Therefore, close to the peak maximum the sample material is most concentrated and the reagent is in the smallest excess. The opposite is true at the peak tail (or foot), and the intermediate situations offer a wide choice for selection of optimum conditions for reaction-rate measurements. Therefore, closest to the peak maximum (Fig. 3, left) the highest slope of the response curve (but the least linear response) is found, whereas the opposite is true for longer delays. When the optimum reaction-rate curve is to be selected, and the respective delay time for commencing the stop period has been identified, then the reaction-rate measurement can be performed in the usual way [3, 6]. The possibility of combining the present approach and that of gradient calibration naturally occurs at this juncture. This somewhat complicated combination

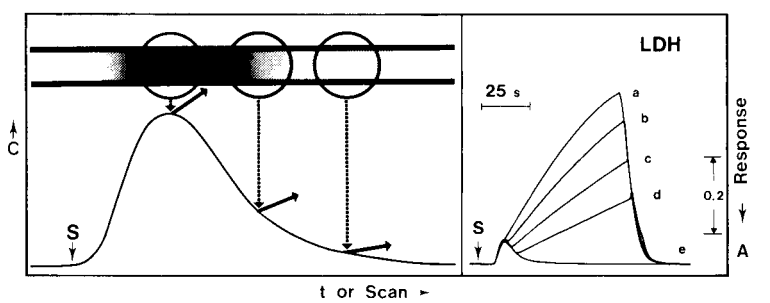

Fig. 3. Dispersed sample zone and corresponding recorder output. The slopes of the individual reaction-rate curves, recorded at stopped-flow conditions at increasing delay times, decrease because of increasing dispersion. To the right is shown a series of stopped-flow recordings of lactate dehydrogenase (LDH) obtained by injecting identical concentrations of LDH but stopping at different delay times (a—d; e, continuous flow) [6].

will have to be resolved by a computer. Even the simple version outlined can, however, be put to good use in clinical applications. Thus it is useful in enzymatic assays (of either substrate content or of enzyme activity) where the ratio of sample and reagent material must be carefully controlled, along with all other reaction conditions, to obtain a meaningful result. Scarcity of sample material and cost of the reagents also call for the economical approach which the f.i.a. gradient technique offers. So far, f.i.a. gradient methods for assay of glucose [11], urea [3], ethanol [12] and of lactate dehydrogenase [6] have been developed.

The gradient scanning method

While the previously described gradient techniques are aimed at various improvements in assays of a diversity of samples, the gradient scanning technique [7] provides a very convenient means of studying the chemical and physical phenomena which take place when solutions are mixed.

The principle of the method is as simple as that of all f.i.a. techniques: a physical parameter is measured continuously within a certain range (e.g., absorbance vs. wavelength or current vs. potential) along the dispersed sample zone (Fig. 4, left). Provided that the rate of the scanning is much faster than the movement of the carrier stream, the dispersed zone may be advanced during the scan and still appear as to be stationary. If this is not the case, or if the chemical reaction occurring is too slow, then selected sections of the zone can be stopped consecutively within the detector. The resulting record will have a multidimensional form, like the three-dimensional voltammogram obtained on a zone containing copper(II) ions dispersed into a solution of complexing agent (NH_3; Fig. 4, right) [7].

The combination of advanced rapidly scanning instruments (both optical and electrochemical) with the f.i.a. gradient approach is natural. The conventional tedious manual solution handling necessary to prepare solutions for

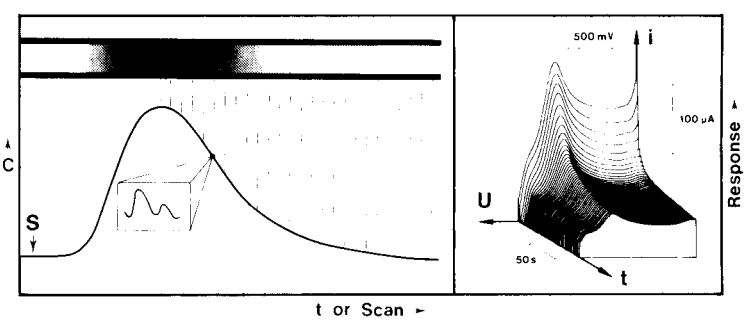

Fig. 4. The principle of the gradient scanning technique, where individual segments of the dispersed sample zone are sequentially monitored. To the right is shown a series of successive voltammetric scans recorded on the descending part of a dispersed zone of Cu(II) in a carrier stream of ammoniacal ammonium nitrate [7].

further measurement in these advanced instruments is simply not sufficiently flexible and does not exploit their full potential. Seen from a purely analytical viewpoint, the advantages of gradient scanning will become even more apparent if a multicomponent analysis is performed on an unknown sample by a spectrometer. Some work has already been done in combining f.i.a. and inductively-coupled plasma emission spectrometry [13]. However, an emission spectrum generated by an inductively-coupled plasma inevitably contains a combination of weak and strong lines, and these could all be accommodated within the optimum detector range if the dispersed sample zone were repeatedly scanned while it gradually passed into the plasma torch. Combination of the gradient scanning technique and electronic calibration would be a logical extension of this approach.

Gradient f.i.a. titrations

The f.i.a. titrations are the oldest gradient technique [3, 14], and the basic principles remain the same although the technical development has already advanced through various stages. If a sample zone of, say, an acid is injected into a carrier stream of a base, then the dispersed zone will become gradually neutralized by the base penetrating through the interfaces with the carrier stream at the leading and trailing sections (Fig. 5, left). Therefore, both at the front and at the tail of the dispersed sample zone an element of fluid exists within which the acid is exactly neutralized by the base. These two equivalence points form a pair, having the same D value, and their physical distance (measured as Δt for a constant flow rate Q) will increase with increasing concentration of the injected acid C_A^0 and decrease with increasing concentration of the base, C_B^0, contained in the carrier stream. The concentration dependence of the time span Δt depends on the concentration profile formed by the dispersion of the zone on the way from the injector to the detector. It has been shown [3, 14] that as long as the concentration profile conforms with the model known as "one mixing stage" [10] then

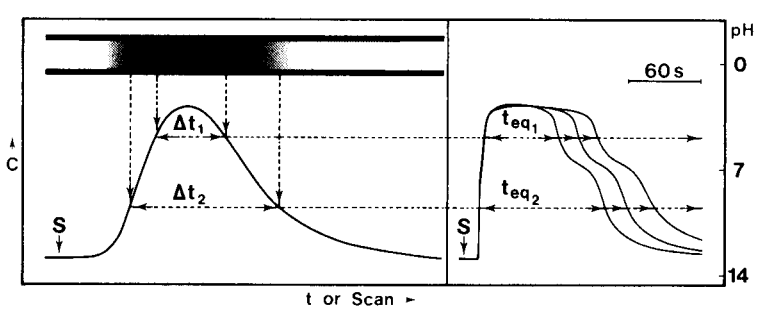

Fig. 5. Gradient f.i.a. titration, based on identifying pair(s) of segments with identical D values in the dispersed sample zone. The time span Δt between these segments is related to the total concentration of analyte. To the right is shown the stepwise potentiometric titration of three different concentrations of phosphoric acid by sodium hydroxide.

$$\Delta t = (V_m/Q) \ln 10 \log (C_A^0/C_B^0\, n) + (V_m/Q) \ln 10 \log (S_v/V_m) \quad (3)$$

where n is the molar ratio of reacting components, S_v is the sample volume and V_m is the volume of the mixing stage. Originally [14] the mixing stage was actually a small mixing chamber (equipped with a magnetic stirrer), the volume of which (ca. 1 ml) dominated the flow design. Further studies have shown, however, that the injection process itself conforms with the "one mixing stage" model and this discovery allowed miniaturization and simplification of the f.i.a. titration system [4].

Such f.i.a. titrations naturally follow all the underlying principles of classical titrimetry. Returning to the example of acid—base titration, it is obvious that an acid, with two protons dissociating at sufficiently different pK values ($pK_2 \geqslant pK_1 + 4$), will be titrated in two steps. Such is the case with phosphoric acid ($pK_1 = 2.15$, $pK_2 = 7.21$, $pK_3 = 12.36$, so that $pH_{eq1} = 4.7$ and $pH_{eq2} = 9.8$); the titration of phosphoric acid by 1×10^{-3} M sodium hydroxide as carrier stream is shown on Fig. 5. (The sample volume was 75 μl; $V_m = 150\ \mu$l; the pH was measured by a microquinhydrone electrode; and the experimental setup was a FIAstar [15]). The concentrations of phosphoric acid in the three injected samples were chosen to be in ratio 1:2:4 (0.05 M, 0.10 M, and 0.20 M H_3PO_4) and the carrier stream was 1×10^{-3} M NaOH containing 1×10^{-2} M quinhydrone) so that according to Eqn. (3) the horizontal distances between the equivalence points of curves 1 and 2, and 2 and 3, respectively, should be equal. As the photographic reproduction of the curves recorded from the same start (S, Fig. 5) shows, this is indeed the case.

The parallel between f.i.a. and batch titrations is so obvious that it may seem unnecessary to emphasize it. However, certain doubts have been expressed [16, 17] that the term "titration" is appropriate for this f.i.a. technique, and have been implied in a recent review [18]. The argument was along the lines that replacement of the carrier stream with water left the exponential concentration profile unaffected, that the sensitivity increased, as Δt will increase as $C_B^0 \rightarrow 0$ (Eqn. 3), and that as neutralization can be replaced by a mere dilution with the carrier stream, the ordinary vertical (lin—C) information is replaced by the horizontal (log—C) information. This suggested that the method is a "dilution" rather than a "titration" technique. Apart from the fact that this argument does not hold for redox, complexometric and precipitation titrations which are possible by the f.i.a. procedure (an aqueous carrier stream alone cannot reduce, oxidize, complex or precipitate the analyte contained in the injected zone), it does not hold for the above-described titration of phosphoric acid. With water alone in the carrier stream, the pH would never rise above 7, and Δt_{eq_2} would not be observed.

Selectivity evaluation

The ability of any assay to provide a result unbiassed by the presence of foreign species is crucial to its practical use. This complex problem cannot be treated in detail here, but it seems appropriate to indicate that the unusual

properties of the f.i.a. gradient method can greatly simplify evaluation of selectivity [8]. Under f.i.a. conditions, all experimental variables are strictly controlled and so readily reproducible that it makes sense to express the selectivity of a method for species A towards an interfering species B by a numerical value. As any interfering species will always appear as the pseudo-A species, it is suggested [8] that the selectivity coefficient for any f.i.a. method can be defined by

$$C'_A = C_A + k_{AB}C_B \tag{4}$$

where C'_A is the apparent concentration of species A and k_{AB} is the selectivity coefficient, and where the concentrations of each species are related to the originally injected concentrations C^0 by the D-value, i.e., $D_A = C^0_A/C_A$ and $D_B = C^0_B/C_B$. If the use of a linearly responding detector is assumed, and the fact that all f.i.a. measurements are made at identical dispersion is exploited, then the value of k_{AB} can be expressed as

$$k_{AB} = (C^0_A/C^0_B)\,[(H_2/H_1) - 1] \tag{5}$$

where H_1 and H_2 are the peak heights recorded by the detector from injections of species A alone and A plus interfering species B, respectively. Thus, the higher the k_{AB} value, the greater will be the interference of the foreign species B in the measurement of the primary species A. The interfering effect may be either positive (more species A found than actually present), or negative (depression of signal generated by A in the presence of B), and therefore this selectivity coefficient may either have a positive or a negative sign.

In f.i.a. two approaches can be used to measure a k_{AB} value: the premixed solution technique, and the individual solution or gradient technique. The first approach requires preparation of a series of mixtures containing always the same level of the primary species A and increasing concentrations of the foreign (secondary) species B. As an example, the interference of silver(I) on the determination of iron(III) by the 1,10-phenanthroline method [19] is shown in Fig. 6. A diluted sulphuric acid solution is used as the carrier stream to which is subsequently added a mixture of 1,10-phenanthroline and hydroxylammonium chloride followed by addition of citrate buffer; the colour of the iron(II)—1,10-phenanthroline complex is monitored at 510 nm. Thus when mixtures of a fixed level of iron(III) (5 ppm) and increasing concentrations of silver(I) (0, 2.5, 5.0, 10, 20, 40, 80, 120, 160, and 200 ppm) are injected, a series of peaks is recorded. The increase of peak height indicates the interference of B on A, and the k_{AB} value can then either be estimated from the position of the break point [P is the maximum permissible level of B in the presence of A, i.e., for no apparent interference; here, 10 ppm silver(I) for 5 ppm iron(III)], or computed from Eqn. (5) which, when extrapolated to that signal level which is twice as high as that of A species alone, yields $k_{AB} = C^0_A/C^0_B$. The $k_{Fe\,Ag}$ value experimentally determined was 2.5×10^{-2}. This experimental approach was first tested on a spectrophotometric method for calcium [15]. It is a useful, but tedious

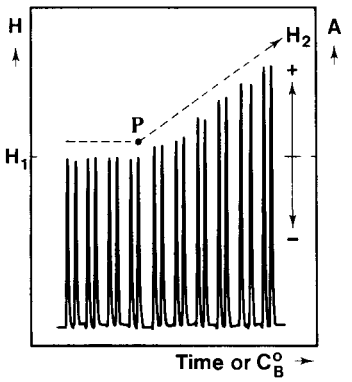

Fig. 6. Selectivity evaluation by the premixed solution technique, where a series of mixtures containing a fixed concentration of the primary species A and increasing concentrations of the secondary (interfering) species B are injected, each set in duplicate. When no interference is observed, the signal response is constant (H_1); interference of B is reflected in increasing (+) — as shown here — or decreasing (—) peak height (H_2). The interference of Ag(I) on the determination of Fe(III) by the 1,10-phenanthroline method is shown.

approach as it requires manual preparation of a number of solutions in which A and B are premixed in well defined ratios.

The gradient approach, however, requires only a few individual solutions to be prepared: essentially only a single solution of A and a single solution of B (for each interfering species). The solutions of A and B are injected separately by means of a double valve, furnished with sample loop A and sample loop B, and allowed to merge asynchronously in the flow channel (Fig. 7, top) on the way towards the detector; advantage is thus taken of the fact that within that region where the two zones overlap there exists a segment of fluid, characterized by a certain delay time M (Fig. 7, left), where the dispersion for both sample zones is equal. This delay time M is readily determined by injecting identical sample concentrations from each loop sequentially. Thus curve A in Fig. 7, left, was recorded by injecting C_A^0 alone by sample loop A, whereas curve B, recorded from the same start (S) as curve A, was obtained by injection of C_A^0 alone by sample loop B. Shown in this figure are also several composite curves A + B, which were obtained by injecting increasing concentrations of B (prepared by sequential dilutions of C_A^0) by loop B while the concentration of species A in loop A was maintained constant at C_A^0. As indicated above, the sum of a set of linear processes will yield a linear response and therefore the peak height of any composite curve A + B at delay time M, where the dispersion for both curves A and B is identical, will be a linear function of the concentration of B injected into loop 2 (see Fig. 7, right). From the previous discussion, it follows that the secondary species B poses as pseudospecies A, the concentration of which is equal to the product $k_{AB} C_B^0$; i.e., if $k_{AB} C_B^0 = 0.01\ C_A^0$,

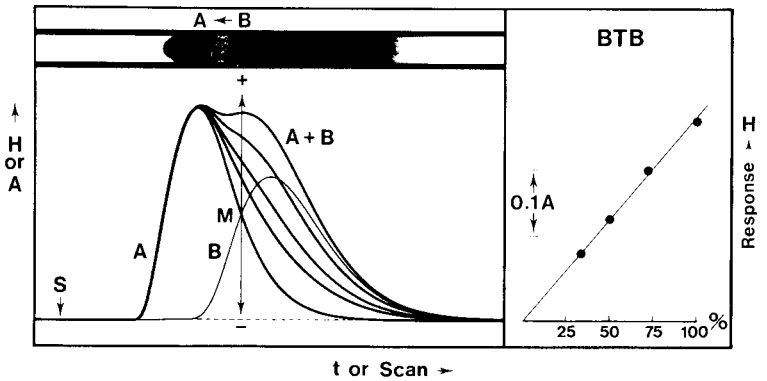

Fig. 7. Selectivity evaluation by the gradient approach where the primary species A and the secondary (interfering) species B are injected simultaneously by a double-valve and allowed to merge asynchronously. Curves A and B are the recorder outputs obtained when the two species are injected separately; A + B indicates the composite curves recorded for simultaneous injections. To the right is shown the calibration graph for the system obtained by injecting a fixed concentration of bromothymol blue (BTB) as A (C_A^0 = 100%) and decreasing concentration of the same dye solution as B. The peak height (H) measured at delay time M is then plotted against the concentration of B (C_B).

there is a 1% interference at point M and if $k_{AB}C_B^0 = C_A^0$ the peak height at delay time M will be doubled. Thus, the selectivity coefficient k_{ABi} for a given interfering species B_i may be obtained by simultaneous injection of A and B_i from loops A and B, respectively, measuring the peak height of the composite curve A + B_i at delay time M and then either computing the value from Eqn. (5) or deriving it from a calibration graph such as that shown in Fig. 7 (right) which was obtained by injecting C_A^0 from loop A and standards of A from loop B. If the distance is greater than between point M and the baseline (Fig. 7), then there is a positive interference (positive k_{AB} value); if it is shorter then the interference is negative (negative k_{AB} value); if the distance is the same, then the foreign species does not interfere (the composite curve A + B will actually be reduced to curve A).

Depending on the actual manifold construction, zones A and B may merge partially, as just described, or can perfectly overlap each other. Both cases yield the same result and the detailed discussion is given in the original paper [8]. The approach suggested above for selectivity studies may be equally useful for the generalized standard addition method [20] as the injected zone A may be merged with zone B containing an exactly known concentration of the standard.

HYDRODYNAMIC INJECTION

It is well recognized that the weakest link in f.i.a. technology is the means for reproducible injection of a well defined sample volume into the carrier

stream. Numerous designs have been tried, often characterized by increasing levels of complexity. The initial approach with a syringe furnished with a hypodermic needle [1] was replaced by a syringe in combination with a flap valve [21]. A valve alternating between high and low pressure lines [22] and a rotary valve serving low pressure lines [3] have been suggested. An ingenious sliding valve commutator has been designed in Brazil [23], while a multiple magnetic valve system controlled by a microprocessor has become the core of the commercial FIAtron SHS-200 system.

All these designs have one common denominator: the solution to be injected into the carrier stream (in the form of a well-defined zone) is, at least for an instant, contained within a hermetically closed container (i.e., in a valve bore or in an external loop of a valve) the purpose of which is to meter an exact volume and transfer it reproducibly into the carrier stream. For this purpose, either a piston has to be compressed, a valve rotated or moved, or conduits constricted and released by magnetic valves. Thus, all these designs comprise finely manufactured moving parts which eventually become worn.

It is, however, possible to meter a column of liquid exactly into a geometrically well defined conduit (of length L and internal radius r, Fig. 8) which is at all times open to other channels, provided that these channels are filled by a liquid held still in place (STOP, Fig. 8, top). These columns of liquid of the carrier stream exert a hydrostatic force which serves as a lock while the sample volume $S_v = \pi r^2 L$ is being filled. Thus by an alternate and

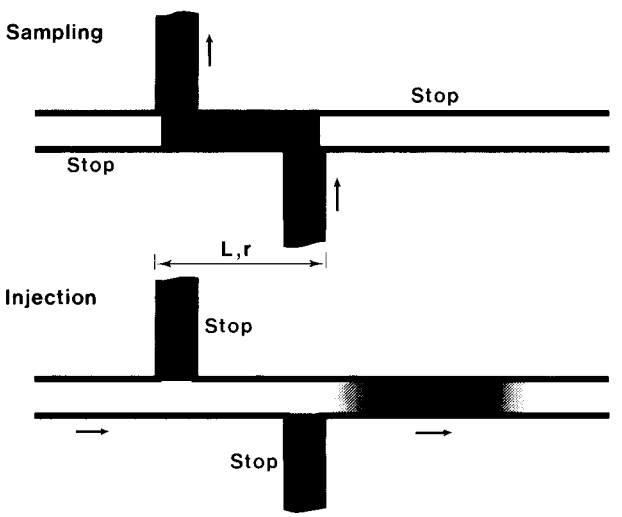

Fig. 8. The principle of hydrodynamic injection. A fixed volume of sample solution is metered into a conduit, of length L and internal radius r (Sampling), and this volume is subsequently propelled downstream by the carrier stream (Injection). During the sampling cycle, the carrier stream circuit is stopped, and vice versa (see also Fig. 9).

intermittent pumping of carrier and sample solutions, a well defined sample zone can be formed and then inserted into the carrier stream (Fig. 8, bottom). The manifold serving for this purpose (Fig. 9) uses two peristaltic pumps to control the movement of sample and carrier solutions. It is obvious that if $x = z$ and if the pumps follow the sequence indicated in Fig. 9, then the sample conduit L will be filled by sample solution from sample reservoir S when pump (1) is in motion, and during the next cycle, when pump 1 is stopped and pump 2 operates, the carrier stream will empty this exactly metered volume of sample solution from conduit L and will carry it further towards the detector (D). Various other schemes employing combinations of hydrostatic and hydrodynamic forms are conceivable [9].

The obvious question is, however, how this hydrodynamic injection compares in terms of reproducibility and of flexibility of adjustment of the sample volume, with the above-described mechanical methods. The well known f.i.a. colorimetric method for chloride was used for testing; a calibration run (with solutions containing 10, 20, 30, 40, and 50 ppm chloride) was run first (Fig. 10 a) followed by a stopped-flow f.i.a. experiment (Fig. 10 b). The relative standard deviation for a series of 10 injections of a chloride standard was better than 0.5%; the value compares well with that obtained by means of a rotary valve (RSD $\leqslant$0.3%). These experiments were all run using the BIFOK-5020 Flow Injection Analyser and a Bausch and Lomb Mini 20 spectrophotometer equipped with a FIAstar tubular flow cell [15]. The FIA-5020 is equally suitable for operation with a rotary valve or in the valveless hydrodynamic injection mode.

Thus, with a slight sacrifice of reproducibility, the f.i.a. system is ready to be transferred from the analytical laboratory, to perform various continuous monitoring tasks. The absence of mechanical valves makes the technique more reliable and will allow simplification of the necessary f.i.a. equipment. Thus a portable f.i.a. monitor is within reach for clinical and industrial applications. Its main advantage would be its reliability: the monitoring would not rely on detector stability (baseline drift) or sensitivity (slope of

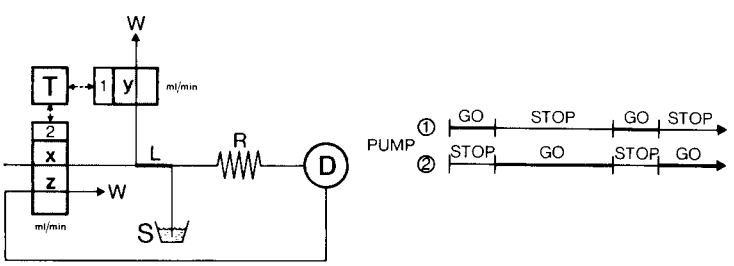

Fig. 9. Manifold for hydrodynamic injection. The sample solution is aspirated by pump 1, operating at a pumping rate of y ml min^{-1}, and a fixed volume of sample from reservoir S passes into conduit L. Subsequently pump 2 is activated, pumping at rates $x = z$ ml min^{-1}, and the sample is flushed through reactor R to the detector D. The operation of the two pumps is controlled by the timer T, the time sequence of events being as depicted.

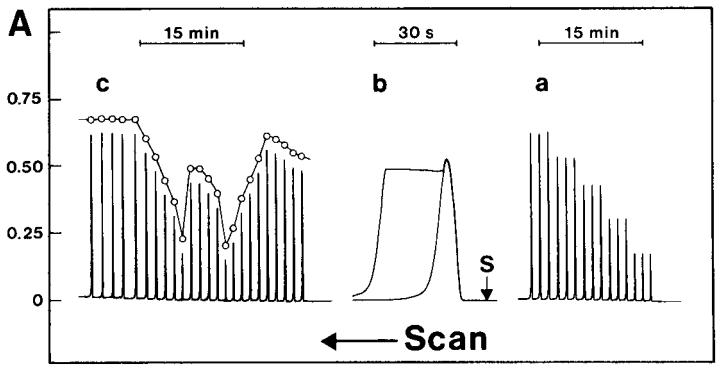

Fig. 10. Determination of chloride by the mercury thiocyanate method with the hydrodynamic injection manifold in Fig. 9, where R was 100 cm long (0.5 mm i.d.) and the volume of the conduit L was 25 μl. The pumping rate $x = z$ was 1.1 ml min^{-1} and the aspiration rate y was 3.0 ml min^{-1}, operated for 12 s. The detector was fixed at 490 nm. (a) Standard calibration run (10, 20, 30, 40 and 50 ppm chloride); (b) stopped-flow experiment with the 40 ppm chloride standard; and (c) monitoring of chloride. The concentration of a pool of sodium chloride was altered at will and monitored by the system. All measurements were conducted with the BIFOK FIA-5020 analyzer programmed for hydrodynamic injection.

calibration response), because regular checks with standard solution(s) can be repeated at any time (cf. Fig. 10 a, c).

DISCUSSION

The very simple design of the hydrodynamic injector offers an opportunity to place the roles of the technical and conceptual developments into proper perspective. The discovery of a new method should not be confused with the tools and means of its experimental realization. Kučera's dropping mercury electrode, Kohlrausch's drum and Weston's standard cell were essential parts of the first polarograph, yet the name and concept of polarography, originated by Heyrovsky, has remained the basis of the method throughout the decades of technological development. Analogously, it is the concept of controlled dispersion which is the thought underlying the theory and development of f.i.a. and not the individual means, such as the method of injection, application of a flow-through detector, or use of an unsegmented stream. These tools have been known for a long time, and used in chromatography, process control equipment or air-segmented systems. It is unfortunate that in recent "historical" reviews [18, 24] the key role of the dispersion concept has not been appreciated.

The key role of dispersion, controlled in space and time, is further advanced by the advent of the gradient techniques, which open a range of new possibilities, not only for conducting serial assays, but also for general studies on the chemistry of solutions. While attention previously has been

focused mainly on the peak maximum as the source of analytical information, the advent of gradient techniques widens the range of f.i.a. applications. It is important to realize that whereas previously the limited, medium and large dispersions were achieved primarily by manipulating the sample volume and the geometry of flow, it is now being recognized that segments of liquid with such properties are found along any dispersed sample zone (Fig. 1). Thus the previously formulated seven rules [3] for optimization of f.i.a. designs can be supplemented by the eighth rule: "as any dispersed sample zone is composed of a continuum of concentrations, a desirable degree of dispersion can most conveniently be chosen by locating the analytical readout within a suitable segment of fluid within this continuum".

The authors express their gratitude to Svend Olsen and Lars Nygaard of this Department and to Jiri Janata of the University of Utah for help, advice and critical comments, and to Inge Marie Johansen for conscientious technical assistance. This work was in part supported by the Danish Council for Scientific and Industrial Research and by the Danish International Development Agency.

REFERENCES

1 J. Růžička and E. H. Hansen, Anal. Chim. Acta, 78 (1975) 145; Dan. Pat. Appl. No. 4846/74, Sept. 1974; subsequent US Pat. No. 4,022,575.
2 L. T. Skeggs, Anal. Chem., 38(6) (1966) 31A.
3 J. Růžička and E. H. Hansen, Flow Injection Analysis, Wiley-Interscience, New York, 1981.
4 A. U. Ramsing, J. Růžička and E. H. Hansen, Anal. Chim. Acta, 129 (1981) 1.
5 O. Levenspiel and W. H. Smith, Chem. Eng. Sci., 6 (1957) 227.
6 S. Olsen, J. Růžička and E. H. Hansen, Anal. Chim. Acta, 136 (1982) 101.
7 J. Janata and J. Růžička, Anal. Chim. Acta, 139 (1982) 105.
8 E. H. Hansen, J. Růžička, F. J. Krug and E. A. G. Zagatto, Anal. Chim. Acta, in press.
9 J. Růžička and E. H. Hansen, Dan. Pat. Appl. No. 81.5148, Nov. 1981, and subsequent U.S. Pat. Appl. No. 385 049.
10 O. Levenspiel, Chemical Reaction Engineering, 2nd. edn., Wiley, New York, 1972.
11 J. Růžička and E. H. Hansen, Anal. Chim. Acta, 106 (1979) 207.
12 P. J. Worsfold, J. Růžička and E. H. Hansen, Analyst, 106 (1981) 1309.
13 S. Greenfield, Ind. Res. Dev., August (1981) 140.
14 J. Růžička, E. H. Hansen and H. Mosbaek, Anal. Chim. Acta, 92 (1977) 235.
15 J. Růžička, E. H. Hansen and A. U. Ramsing, Anal. Chim. Acta, 134 (1982) 55.
16 H. L. Pardue and B. Fields, Anal. Chim. Acta, 124 (1981) 39.
17 H. L. Pardue and B. Fields, Anal. Chim. Acta, 124 (1981) 65.
18 H. A. Mottola, Anal. Chem., 53 (1981) 1312A.
19 Z. Marczenko, Spectrophotometric Determination of Elements, Ellis Horwood, Chichester, 1976.
20 B. E. Saxberg and B. R. Kowalski, Anal. Chem., 51 (1979) 1031.
21 J. W. B. Stewart, J. Růžička, H. Bergamin F° and E. A. Zagatto, Anal. Chim. Acta, 81 (1976) 371.
22 K. K. Stewart, G. R. Beecher and P. E. Hare, Anal. Biochem., 70 (1976) 167.
23 H. Bergamin F°, J. X. Medeiros, B. F. Reis and E. A. G. Zagatto, Anal. Chim. Acta, 101 (1978) 9.
24 K. K. Stewart, Talanta, 28 (1981) 789.

Analytica Chimica Acta, 145 (1983) 17—26
Elsevier Scientific Publishing Company, Amsterdam — Printed in The Netherlands

THE PERFORMANCE OF SOME LIQUID PHASE FLOW-THROUGH DETECTORS

H. POPPE

Laboratory for Analytical Chemistry, University of Amsterdam, Nieuwe Achtergracht 166, 1018 WV Amsterdam (The Netherlands)

(Received 10th May 1982)

SUMMARY

Miniaturization of flow-through analytical systems such as flow injection analysis and liquid chromatography is necessary to achieve higher rates of sample throughput and smaller absolute detection limits. During this miniaturization, however, it is essential to preserve the concentration detection limits of the devices used. Some principles for liquid phase flow-through detection, u.v.-visible absorption photometry, fluorimetry and electrochemical detection, are discussed from this point of view. It appears that, although technical difficulties will be large, there are good prospects of detecting concentrations of about 1 ng ml^{-1}, while keeping the peak broadening down to values of about 1 nl.

Some general principles for the characterization of liquid phase flow-through detectors were discussed in a previous paper [1]. Apart from various aspects, such as selectivity of detection, compatibility with various solvents, ease of operation, linear range, etc., two characteristics of detectors were found to be of prime importance, the concentration detection limit, c_d, and the contribution to peak width, σ_{vd}.

The first is the smallest concentration (change) that can be indicated by the device with a given statistical risk factor. It is intrinsically an approximation, as the application of noise theory to the detection of time-dependent signals shows [2] that the detection limit depends on the duration of the signal in a manner dependent on the power spectrum of the noise. However, in the discussion of cases in which the signal duration does not change over many orders of magnitude, as is the case in flow injection analysis (f.i.a.) this effect can be neglected. The concentration detection limit of the device, c_d, is the starting point for any discussion or prediction of the performance of the complete analytical system in this respect. In normal applications of f.i.a., where the various other parts of the system can only bring about dilution, c_d is the limiting sample concentration detection limit of the complete system, which can be obtained only provided that the dilution in the other parts of the system can be made negligible. The performance of a complete system, however, can be better than that. This is the case in chromatography with on-column concentration procedures [3, 4] in which a

phase transfer leads to a concentration effect, and in correlation chromatography [5, 6] where time (and sample amount) is traded for detectability as it is in other signal-enhancement methods. Nothing seems to inhibit the application of such principles in flow injection systems if concentration detection limits were to be the critical point. The elegant simplicity and low price of the f.i.a. approach would be lost, though.

The second "figure of merit", the contribution to peak width, was defined [1] as the standard deviation in time units, σ_{td}, of the signal response to an injection which is infinitely sharp in time. It is experimentally obtained as such, but it may be converted to a volume standard deviation, σ_{Vd}, by means of

$$\sigma_{Vd} = f_v \, \sigma_{td} \tag{1}$$

in which f_v is the flow rate. This conversion has advantages in discussions of the effects of cell volumes, connecting tubes, etc., on peak broadening. However, it conceals the fact that some peak broadening mechanisms such as slow sensor equilibration, or band-width limitations in amplifiers, may have nothing to do with any volumes in the system. Of course, σ_{td} and σ_{Vd} depend on the operating conditions, and especially on the flow rate f_v.

Although this kind of detector non-ideality was discussed in terms associated with peak-shaped signals, such as are observed in f.i.a. and chromatography, leading naturally to the concept of a standard deviation σ, it was noted that the effect itself is much more general. Thus, it is only the description with σ increments that is specialized towards peak-shaped signals; e.g., in the case of batch-wise measurements or of block-shaped signals, one would probably use terms like time constant, response time, band-width limitation, equilibration time, etc. However, these can in principle be estimated (provided that the systems behave linearly) from the standard deviations and vice versa. Likewise, the rule of the additivity of variances (σ^2) is only a specialized way of expressing the general rule that in a series system the weakest link in the chain determines the time constant, band width, etc.

It was demonstrated theoretically in the previous paper [1] that the value of σ_{td} of a detector system determines the upper limit to the sampling frequency obtainable with a flow injection system. This limit is approached when the other subsystems (injection, reactors, mixers) do not contribute significantly to the final peak width. Appreciable sample dilution is inevitable in that case. The contribution to peak width in volume units (σ_{Vd}) is important for the minimum detectable quantity, $\underline{M}$, which can be obtained with the device. As derived earlier,

$$\underline{M} = k_2 \, \sigma_{Vd} \, c_d$$

in which k_2 is a statistical confidence limit factor. The importance of low values for σ_{Vd} is already apparent from this equation for those cases where the minimum detectable quantity plays a crucial role, as often happens in

clinical analysis, biochemical research and forensic science. However, in the following paragraphs, additional reasons for aiming at very low σ_{Vd} values will be given.

MINIATURIZATION

The systems approach to f.i.a. detection has so far been considered on tacit assumption that the flow rate f_v in the detector is a constant, and given in some way. However, there are many convincing reasons for developing systems with lower flow rates than are usual at present. Two obvious advantages are the lower consumption of solvents and especially reagents, and the smaller sample amounts needed for the smaller systems.

A much more important reason for going towards lower flow rates is given in the paper by Reijn et al. [7] : a careful analysis of the dispersion in various types of reactor reveals that lower flow rates are needed for obtaining higher sample frequencies. For tubular reactors, this approach was indicated by Tijssen two years ago [8]. The two requirements, for low reagent consumption and high sampling rates, point in the same direction, that of miniaturization and low flow rates. The low flow rates, together with the small values of σ_{td} aimed at, set a very low value for the required σ_{Vd}, and in fact in the analysis by Reijn et al. [7] the minimum attainable value for σ_{Vd} is taken as a boundary condition (constraint) in the optimization, in much the same way as was done in the analysis by Knox and Gilbert [9] of the feasibility of open tubular liquid chromatography.

For these reasons, it appears worthwhile to investigate the various detection principles with respect to their ability to perform at low σ_{Vd} values while preserving the lowest concentration detection limit possible.

It is clear that a trade-off exists here. Small σ_{Vd} values can be achieved only when the detection process takes place in a volume of comparable magnitude; and depending on the measurement principle involved, this restriction is more or less likely to affect the detecting power of the method. Apart from the detection volume per se, one has of course to consider the peak-broadening effects arising from the "plumbing" and the time constants. However, as these are usually amenable to adjustment to low flow rates and σ_{td} values, and are not closely related to the measuring process itself, they can be neglected for the moment. With a tighter specification on the contribution to peak broadening, there is simply less volume and consequently less analyte available for detection.

The trade-off becomes immediately manifest if it is realized that the effective σ_{Vd} value of a device can be diminished at the expense of detecting power by simply admixing a solvent in a T-piece immediately in front of the detector (make-up flow). The cell or the detection volume is swept faster and this system behaves with respect to peak broadening as if the cell had a much smaller volume. The solution is of course diluted, so that the detecting power is adversely affected. It is to be noted that, when this is done, the

detection limit in amount, the minimum detectable quantity, M, remains the same.

In order to have some point of reference in the following discussion of various measuring principles, a concentration detection limit $\underline{c}_d$ corresponding to 1 ng ml^{-1} (a reasonable average for u.v.-visible absorption) and a contribution, σ_{Vd}, of 1 nl to the peak width are aimed at. The latter figure may appear extremely low in view of present experimental possibilities, and indeed it is, but was chosen as it follows from the work of Tijssen [8], Knox and Gilbert [9] and Reijn et al. [7] that with this order of magnitude very significant exploitation of the speed advantage of miniaturized systems is possible.

ULTRAVIOLET-VISIBLE ABSORPTION PHOTOMETRY

Ultraviolet-visible absorption photometry is by far the most important detection system in h.p.l.c., and for the rapidly expanding f.i.a. area the same will probably be true in the future, because of the storehouse of selective colour reactions available for all sorts of compounds and elements in the literature.

The detecting power of these devices is conveniently expressed as the smallest absorption coefficient (absorbance per unit length) k in cm^{-1} which can be detected. Current "state of the art" performance for rather expensive devices is of the order of $\underline{k} = 10^{-5}$ cm^{-1}. This is accomplished with cell volumes of the order of 10 μl and observed σ_{Vd} values range around this value, with flow rates around 1 ml min^{-1}. (It should be noted that σ_{Vd} values can only be obtained by experimental determination in the laboratory, because manufacturers generally refuse to give specifications on this point; this is a surprising and unfortunate situation which persists despite the fact that the same manufacturers have papers published on such topics.)

A further decrease of the σ_{Vd} value, and consequently of the cell volume, appears to be possible only at the expense of a drastic increase in the detection limit characterized by $\underline{k}$. This problem was addressed some years ago by Baumann [10] who mainly considered the influence of shot noise. As the stability of source and photo-detection (which Baumann treated as technical imperfections) is often equally important, the present discussion will take this limitation into account as well.

When the source is of sufficiently large dimensions, the amount of light (photons/second, $\dot{n}_{cell}$) which can be passed through the cell is given by

$$\dot{n}_{cell} = b(\lambda)\,\Delta\lambda\,\Omega\,S \qquad (2)$$

where $b(\lambda)$ is the equivalent of the radiance of the source $B(\lambda)$, but expressed as a photon rate; $\Delta\lambda$ is the spectral band width; Ω is the solid angle from within which light can be projected through the cell; and S is the area of the source which can be exploited in this projection.

An analysis of the geometrical optical conditions prevailing in such

systems [10, 11] reveals that the product $S\ \Omega$ has a maximum value which depends on the most critical part of the complete optical system, i.e., that with the smallest optical conductance (area). For microcells, this is the cell itself and the product $S\ \Omega$ is maximal when it is equal to

$$S = S_1\ S_2/b^2 = V_{cell}^2/b^4 \tag{3}$$

where S_1 and S_2 are the areas of the front and rear window of the cell, and b is the cell length (optical path length). In the second part of Eqn. (3), the relation between the areas and the cell volume is substituted, which is useful if a value for the latter is specified.

The number of photons transmitted per second by the (empty) cell is therefore

$$\dot{n}_{cell} = b(\lambda)\ \Delta\lambda\ V_{cell}^2/b^4 \tag{4}$$

The shot noise, i.e., the noise resulting from statistical fluctuations in the stream of independent photons, is conveniently expressed as the relative standard deviation in $\dot{n}_{cell}$. It also depends on the measuring time constant Δt, which can be set about equal to the peak broadening in time σ_{td}. The result is

$$s_{\dot{n}(cell)}/\dot{n}_{cell} = (\dot{n}_{cell}\ \sigma_{td})^{-1/2} = [b(\lambda)\ \Delta\lambda\ V_{cell}^2 b^{-4}\ \sigma_{td}]^{-1/2} \tag{5}$$

This is also equal to the relative standard deviation of the error in the transmission when this is equal to one. The expression has to be corrected for the various processes with less than 100% efficiency, such as the transmission of the optics, background absorption in the solvent and quantum yield of the photodetector. When these effects are summarized in a factor T, the detection limit expressed as $\underline{k}$ can be calculated as

$$\underline{k} = k_2\ [b(\lambda)\ \Delta\lambda\ T]^{-1/2}\ b\ V_{cell}^{-1}\ \sigma_{td}^{-1/2} \tag{6}$$

The surprising result is that, at a specified cell volume, longer cells result in worse detection limits. The larger absorbance values obtained in a long cell for the same concentration are more than counterbalanced by the increased noise level in the measurement of the smaller amount of light which can be transmitted by the narrow cell. However, movement towards smaller b values (wide, short cells) which according to Eqn. (6) would favour detectability, is limited by the instability of the source and the receptor. If a relative standard deviation s_b is assumed to characterize this kind of instability, valid for a time constant σ_{td}, the detection limit in the absorption coefficient is equal to:

$$\underline{k} = k_2\ s_b\ b^{-1} \tag{7}$$

When both effects, shot noise and instability, are significant, the terms described by Eqns. (6) and (7) have to be added quadratically. The result is:

$$\underline{k} = k_2\ \{[b(\lambda)\ \Delta\lambda\ T]^{-1}\ V_{cell}^{-2}\ \sigma_{td}^{-1}\ b^2 + s_b^2\ b^{-2}\}^{1/2} \tag{8}$$

This function has a minimum at that value of b where both contributing terms are equal; i.e., when shot noise and instability yield the same contribution to the uncertainty.

The calculations and data given by Baumann for a number of sources indeed justify the conclusion that, for cell volumes around 10 μl, present low-noise u.v.-visible detectors operate quite near to the optimum. In this context, it is noteworthy that some of the designs issued during the last years employ shorter cell lengths b. This suggests that shot noise becomes predominant when 1-cm cells are used.

The prospects for miniaturized equipment appear to be very bad in view of the above derivation, at least when conventional sources like deuterium and low-pressure mercury lamps are to be used. These feature values of $b(\lambda)$ around 10^{16} photons cm^{-2} sr s and the use of cells smaller than 1 μl is only possible at the expense of detection limit.

An interesting feature of Eqn. (6) is that it predicts for the shot noise-limited case (if V_{cell} can be taken for σ_{Vd}) that the detection limit in amount (minimum detectable quantity) depend on the source exclusively and not on the volume of the cell.

In view of the importance of the intensity of the photon flux it is an obvious approach to look for more intense light sources, such as xenon arcs and lasers. However, the problem with such sources is to keep the magnitude of the second term of Eqn. (8) within reasonable limits, as such sources tend to be much less stable than the sources normally applied.

Nevertheless, there seems to be no doubt that for significant miniaturization of absorption detection systems, the use of lasers is inevitable. Fortunately, the prices of these devices is going down steadily.

Measurement of absorption in the emission mode

The shot-noise limitation and the instability limitation are so important in absorption methods because the absorption is measured via the transmitted light. This is basically equivalent to establishing the absence of a few photons in an overwhelmingly large number of photons. Therefore, it looks attractive to find ways for measuring absorption in a positive mode, via an effect brought about by the absorption of radiant energy. Photoacoustic methods are an example of this. However, no attempts appear to have been made to examine this technique for miniaturized liquid-phase detection.

A related approach has resulted in extremely interesting work by Harris and co-workers [12, 13]. The heat produced by the absorption leads to a change in refractive index of the solution and this can be measured optically. Leach and Harris [12] described the first use of the thermal lens effect, observed when a laser beam passes through an absorbing solution, for liquid-phase detection purposes. Later [13], more sophisticated designs, involving grating-like interference patterns, monitored with a second laser, showed very promising performance, capable of detecting 10^{-5} changes in absorption coefficient in volumes of less than 0.1 μl; the actual measuring volume is even smaller.

Such approaches have the very great advantage that increase of the source intensity improves detection limits, even if the stability of the source is not optimal.

FLUORIMETRY

This same advantage holds for fluorimetry. A drawback of the method is that the effect is displayed by a very limited number of compounds. However, the application of chemical reactions, tailored to this application, can enlarge the scope of the method considerably. In view of the significant advantages of this measuring technique, its selectivity, low detection limit, suitability for miniaturization, and relatively low cost, work in search of selective fluorogenic reagents suitable for inorganic f.i.a. applications, seems to be in order.

Present flow-through fluorimeters are capable of detecting 10^{-10} M quinine in volumes of 10—20 μl. Miniaturization poses similar problems as occur in absorption photometry, with the major difference that source stability is less of a problem. The application of laser excitation is therefore available and in fact, e.g., Hershberger et al. [14] and earlier Diebold and Zare [15] and Folestad et al. [16] have shown that the detection of low concentration levels in very small volumes is possible.

The fundamental approach to this problem has likewise been given by Baumann [10]. The reasoning can be illustrated in an approximate manner by considering that lasers of 1-mW continuous power with a suitable wavelength are becoming available at prices compatible with routine analytical equipment. In a cell of 0.1-mm length, representing a hypothetical cubic cell with a volume of 1 nl, an absorption coefficient of 10^{-5} cm^{-1} will lead to the absorption of a fraction equal to 10^{-7} of this power. This represents roughly 3×10^{8} photons/second. Even with moderate quantum efficiencies for the fluorescence process, the light collection in the emission path and the photoelectric detection, the signal can be expected to be measurable against the background.

It should be noted that, although the feasibility of detection in submicroliter volumes can be safely assumed, much work is also necessary on the hydrodynamic design. Classical approaches, in which a cell is connected with the reactor or column by means of tubes and fittings, probably will not be compatible with the requirement of extremely low volume broadening. Designs with "in-reactor" or "in-column" measurement, or such elegant approaches as that given by Hershberger et al. [14] presumably will play an important role. In the latter design, a sheathing flow, surrounding the exit flow of the reactor or column, is used to maintain the integrity of the latter. This avoids the problems of dispersion in wide connecting tubes or clogging of narrow ones and has the additional advantage that scattering on the cell walls, which is likely when existing systems are simply scaled down, does not occur.

ELECTROCHEMICAL DETECTION

The very nature of the electrochemical processes, which occur at a surface rather than in a volume, makes these attractive for miniaturized detection. This holds for all kinds of methods relying on electrochemical reactions at an electrode, such as potentiometry (redox, pH, selective electrodes), voltammetry or amperometry, whereas conductometry, being essentially a volume effect, may form an exception. The following discussion will be focused, rather arbitrarily, on the controlled voltage techniques, while referring for other modes to the excellent review by Pungor et al. [17].

With respect to the popularity, field of application and performance of amperometric detectors, it is necessary to distinguish between designs involving solid electrodes and dropping mercury electrodes (DME). The DME has the important advantage of a constantly renewed electrode surface, which guarantees a stable sensitivity and base-line level. In addition, the mercury electrodes have a uniquely large negative potential range. However, these advantages are largely offset by the drawbacks of their practical awkwardness in flow systems and the less favourable detection limits obtainable.

The latter feature is the negative aspect of the renewal of the surface: the surface has to be charged to the prevailing potential at every renewal. The resulting current can, of course, be offset in the amplifiers; this is also valid for the current arising from the reduction of dissolved oxygen, which is difficult to remove completely. However, such offset does not remove the fluctuations in these currents caused by variations in drop time or drop size, and the resulting base-line noise limits the detectability in the range 10^{-7}—10^{-8} M.

After pioneering work in the fifties by Kemula [18], and adaptation to the requirements of h.p.l.c. by Koen et al. [19] in 1970 (σ_{Vd} 10—20 μl), Hanekamp et al. [20] made a thorough study of the improvement of measuring conditions for flow-through employment of the DME. High drop rates, horizontal capillaries and alternating current methods improved the detection capabilities. A pressure-resistant electrochemical scrubber allowed the quantitative removal of oxygen from flowing liquids. It is difficult to speculate about the feasibility of miniaturized detection with the DME, in view of the complicated hydrodynamic conditions.

The other main branch of electrochemical detection is that involving solid electrodes like carbon paste, glassy carbon and the like [21, 22]. The hydrodynamic conditions are usually those of a thin (10—100 μm) film of liquid flowing along a flat electrode, which can be circular or rectangular in shape. This method features very low detection limits (down to 10^{-10} M) and is mainly limited to anodic reactions, but is plagued by problems of electrode ageing (changing sensitivity factors and base-line levels). Contribution to peak width σ_{Vd} can easily be kept below 10 μl with present designs.

The field of application of these devices encompasses the determination at very low concentrations of physiologically active compounds like neuro-

transmitters and their precursors and metabolites. This important application has given a strong impetus to scientific and commercial activities in this area. Numerous new proposals for cell designs have been made in the literature. However, in the opinion of the author, the geometric design of the cell does not have much influence on the most relevant performance parameters, the detection limit and the electrode stability. More relevant in these respects are the studies in which new electrode materials [23—26] or modifications of these are studied. Indeed, it has been shown by van Rooijen [27] that the noise level is governed by the electrical capacity of the electrode surface, and also the chemical nature of the electrode surface is of decisive importance for the ageing problem. Such studies on new materials are therefore extremely useful. Unfortunately, progress in this field is hampered by the general lack of insight into surface phenomena.

A position half way between the two extremes described above is taken by the static mercury drop electrode (E. G. and G. Princeton Applied Research) and the use of mercury layers on solid electrodes (gold, etc.), which brings cathodic reactions within reach of thin-layer cells [28]. It is not yet clear whether these techniques will find general acceptance.

The miniaturization of thin-film designs appears to be a very promising field. The results given by van Rooijen [27] show that the noise level is proportional to electrode surface area. As the signal under most conditions is less than proportional to this area, the miniaturization of the cell (surface area) does not present noise problems until the point where the currents become so small that there the measurement would become difficult from the electronic point of view. This does not seem likely, at least during the first steps in the miniaturization process.

Real progress in this direction can also be expected in view of the success of ultramicro in vivo sensing devices for neurotransmitters used in brain research [29, 30].

Conclusions

Miniaturization of liquid phase flow-through detectors is needed for increase in the sample frequency in both liquid chromatography and flow injection analysis. It is reasonable to speculate about the feasibility of detection in volumes of about 1 nl, with a detection limit of about 1 ng ml^{-1}, because the first figure would allow for the exploitation of significant speed advantages, while the latter figure represents most present requirements with respect to concentration detection limits.

This combination is tantamount to the detection of 10^{-15} g of analyte or about 10^5 molecules. Although only a few methods are discussed above from this point of view, it appears that such detection performance is by no means impossible in principle. Techniques not taken into consideration, such as mass spectrometry (m.s.) with direct liquid inlet and atomic spectrometry may also be considered. In this area a laser-m.s. microanalysis combination capable of detecting 10^{-20} g of material may be cited [31].

The analytical advantages of miniaturized systems with respect to absolute detection limits and speed of analysis are of such great importance and general significance that further extensive work in this direction appears to be indicated.

REFERENCES

1 H. Poppe, Anal. Chim. Acta, 114 (1980) 59.
2 H. C. Smit and H. L. Walg, Chromatographia, 8 (1975) 311.
3 J. Lankelma and H. Poppe, J. Chromatogr., 149 (1978) 587.
4 C. E. Werkhoven-Goewie, U. A. Th. Brinkman and R. W. Frei, Anal. Chem., 53 (1981) 2072.
5 Tj. Th. Lub, H. C. Smit and H. Poppe, J. Chromatogr., 149 (1978) 721.
6 H. C. Smit, T. T. Lub and W. J. Vloon, Anal. Chim. Acta, 122 (1980) 267.
7 J. M. Reijn, H. Poppe and W. E. van der Linden, Anal. Chim. Acta, 145 (1983) ■■■.
8 R. Tijssen, Anal. Chim. Acta, 114 (1980) 71.
9 J. H. Knox and M. T. Gilbert, J. Chromatogr., 186 (1979) 405.
10 W. Baumann, Fresenius Z. Anal. Chem., 284 (1977) 31.
11 G. Hansen and E. Mohr, Spectrochim. Acta (Berlin), 3 (1949) 584.
12 R. A. Leach and J. M. Harris, J. Chromatogr., 218 (1981) 15.
13 M. J. Pelletier, H. Thorsheim and J. M. Harris, Anal. Chem., 54 (1982) 239.
14 L. W. Hershberger, J. B. Callis and G. D. Christian, Anal. Chem., 51 (1980) 1444.
15 G. J. Diebold and R. N. Zare, Science, 196 (1977) 1439.
16 S. Folestad, L. Johnson, B. Josefsson and B. Galle, Anal. Chem., 54 (1982) 925.
17 E. Pungor, Z. Féher and M. Varadi, CRC Crit. Rev. Anal. Chem., 9 (1980) 97.
18 W. Kemula, Rocz. Chem., 26 (1952) 281.
19 J. G. Koen, J. F. K. Huber, H. Poppe and G. den Boef, J. Chromatogr. Sci., 8 (1970) 192.
20 H. B. Hanekamp, Doctoral Thesis, Free University, Amsterdam, 1981; H. B. Hanekamp, W. H. Voogt and P. Bos, Anal. Chim. Acta, 118 (1980) 73.
21 P. T. Kissinger, C. Refshauge, R. Dreiling and R. N. Adams, Anal. Lett., 6 (1973) 465.
22 J. Lankelma and H. Poppe, J. Chromatogr., 125 (1976) 375.
23 F. G. Gonnor, C. M. Fombarlet, M. J. Buda and J. F. Pujol, Anal. Chem., 53 (1981) 1386.
24 D. E. Weisshaar, D. E. Tallman and J. L. Anderson, Anal. Chem., 53 (1981) 1809.
25 R. M. Wightman, E. C. Polk, S. Borman and M. A. Dayton, Anal. Chem., 50 (1978) 1411.
26 D. N. Armentrout, J. D. McLean and M. W. Long, Anal. Chem., 50 (1978) 1411.
27 H. W. van Rooijen, Doctoral Thesis, University of Amsterdam, Amsterdam, 1982.
28 W. A. McCrehan and R. A. Durst, Anal. Chem., 50 (1978) 2108.
29 R. F. Lane, A. T. Hubbard and C. D. Blaha, J. Electroanal. Chem., 95 (1979) 117.
30 J. C. Conti, E. Strope, R. N. Adams and C. A. Marsden, Life Sci., 23 (1978) 2705.
31 E. Denoyer, R. van Grieken, F. Adams and D. F. S. Natusch, Anal. Chem., 54 (1982) 26A.

Analytica Chimica Acta, 145 (1983) 27—39
Elsevier Scientific Publishing Company, Amsterdam — Printed in The Netherlands

ENZYMATIC PREPARATIONS IN ANALYTICAL CONTINUOUS-FLOW SYSTEMS

HORACIO A. MOTTOLA

Department of Chemistry, Oklahoma State University, Stillwater, Oklahoma 74078 (U.S.A.)

(Received 20th April 1982)

SUMMARY

Research on different enzyme preparations in unsegmented continuous-flow systems is discussed. The relative merits of using closed-loop systems, packed reactors with immobilized enzyme, open-tube wall reactors, and single-bead-string reactors are considered for expensive enzymes unstable in solution and for inexpensive stable enzymes. For immobilization, covalent bonding to the surface of a glass matrix is recommended.

Historically, continuous-flow sample processing systems have entered the analytical laboratory as a result of the ever-increasing load experienced in clinical chemistry since the early 1950's [1, 2]. Implementation with air segmentation preceded the more recent developments in unsegmented-flow procedures which had to wait until the mid-1970's to make inroads in analytical methodology [3]. Undoubtedly, segmented continuous-flow systems influenced the birth as well as the development of the unsegmented version. It is gratifying to detect today the influence of unsegmented methodology in some recent developments in segmented systems which address the challenge of simplicity (low cost) [4] and higher sampling rates [5].

Because of the natural adaptation of continuous-flow sample processing to clinical analyses, enzymatic methods have been widely applied in continuous-flow situations. Determinations involving alkaline phosphatase [6, 7] and glucose oxidase [8—10] appear as the earliest applications of enzymatic analyses in segmented systems. Glucose determination based on immobilized glucose oxidase, however, was implemented during what could be termed the prehistory of unsegmented continuous-flow procedures [11]. The use of enzymes as analytical reagents in general and in clinical chemistry in particular has increased greatly in recent years. As biological catalysts which work in complex living systems, enzymes offer two characteristics of paramount importance in analytical chemistry: generally high selectivity (occasional specificity), and capacity of self-regeneration via the catalytic cycle. The second of these two characteristics is particularly relevant to the use of enzymes in continuous-flow systems because it permits the use of enzymes as

main reagents to be recirculated in the implementation of such procedures. It is not surprising then that one of the earliest applications of enzymatic methods in continuous-flow systems coincides with the first report of a closed-loop configuration [11]. Both soluble enzyme preparations and immobilized preparations (packed column-type reactors and open-tube wall reactors) have been used. A general view of these applications and recent developments from our research group, with emphasis on unsegmented systems, is given here with the hope of providing a perspective of the use of enzymes in continuous-flow systems.

EXPERIMENTAL

Experimental details of the work described here have been discussed in several previous reports: closed-loop with amperometric detection [12, 13]; packed-column enzyme reactors [14]; enzymes immobilized on walls of glass tubes (open tube, wall reactors) [15]; and potentiometric proton monitoring [16].

SYSTEMS BASED ON SOLUBLE OR IMMOBILIZED ENZYMES

Early in the development of unsegmented continuous-flow systems, the question of using soluble or immobilized enzyme preparations was discussed. Although no direct documentation appears in the literature, the practitioners' camp was divided. Some believed that immobilized enzymes were the only answer to method development while others expressed strong pessimism about the prospects of success in using such enzymes. As seems to be always the case, a view between the extremes turned out to be more realistic. The extreme views, however, prompted an investigation of their relative validity, with the realization that any findings would fall in generalized categories and that some cases would have to be considered as special, individual ones.

For these studies, a family of enzymes was selected that would catalyze the same overall chemical scheme:

$$S + H_2O + O_2 \overset{E}{\rightleftharpoons} P + H_2O_2 \qquad (1)$$

where S is the substrate, E an appropriate oxidase, and P the product(s). Glucose, uric acid, galactose, and amino acids are examples of suitable substrates determined by methods based on this type of reaction. The progress of this reaction can be conveniently followed electrochemically by measuring either the consumption of oxygen [11—13] or the release of hydrogen peroxide [17]. For direct electrochemical monitoring, the measurement of oxygen consumption seemed more attractive because, although hydrogen peroxide is electroactive, its oxidation and reduction are essentially irreversible. The hydrogen peroxide released in reaction (1) can be expected to interfere with determination of oxygen depending on the level of substrate

being determined and the length of time allowed for reaction. To be on the safe side, glucose oxidase impurified with catalase was chosen; this is inexpensive and insures instantaneous destruction, for all practical purposes, of hydrogen peroxide:

$$H_2O_2 \xrightarrow{\text{catalase}} H_2O + 1/2\ O_2 \qquad (2)$$

The overall reaction of concern in the detection is then

$$\beta\text{-D-glucose} + 1/2\ O_2 \longrightarrow \text{D-gluconic acid} \qquad (3)$$

After the overall type of catalyzed reactions and the monitoring principle had been selected, it was necessary to develop a fast sensor for the dissolved oxygen level; this led to the design of a three-electrode amperometric system with a bare platinum wire working electrode [12]. This sensor offered faster response than the traditionally used Clark-type electrode in which diffusion through a membrane imposes kinetic limitations. It was shown later that materials present in blood serum do not necessarily interfere under flow conditions; over 15 000 samples (10 μl in volume) were processed without serious problems [13]. Periodic washing of the electrodes in warm, aqueous (1 + 4) nitric acid and thorough rinsing with distilled water is recommended for good continuous performance.

On the basis that stability and cost of the enzyme were important factors in deciding between use in solution or in immobilized form, glucose oxidase and uricase were selected as typical examples of extreme situations. Glucose oxidase is relatively stable in solution as well as inexpensive compared to other enzymes commonly used in clinical chemistry. In contrast, uricase is relatively expensive and unstable in solution. A normalized comparison of the stability of these two enzymes is shown in Fig. 1. A survey of prices from two European and two American suppliers of enzymes showed uricase costing about 700 times more than glucose oxidase in preparations typically

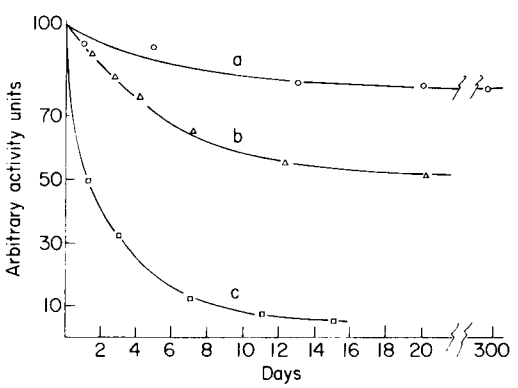

Fig. 1. Long-term operational stability of: (a) uricase immobilized on controlled-pore glass by the glutaraldehyde method; (b) glucose oxidase in solution; (c) uricase in solution. All curves normalized to 100% activity at the time of preparation.

used in analytical work. Studies with these two enzymes and the general scheme of sample processing and detection described earlier [13] led to the conclusion that if an enzyme is relatively inexpensive and relatively stable (so that it retains its activity toward the substrate of interest at reasonably constant level at room temperature with time), it can be used directly in solution for repetitive determinations in closed-flow systems. The closed loop affords enzyme recycling and re-use. Table 1 compares the performance of a soluble enzyme system [13] and a packed-column type reactor [11]. The sampling rate is considerably higher in the open-tube reactor using soluble enzyme and other performance aspects are comparable. The immobilized-enzyme system uses a lesser total amount of enzyme but this argument is weakened by the low cost of glucose oxidase. The reproducibility seems better for immobilized enzyme but this is not related to the form in which the enzyme is used; it seems to depend mainly on the number of replications and the injection system used. In open systems (solutions sent to waste after detection), miniaturization and implementation of the merging zone principle [18] is recommended. The use of soluble enzyme preparation in open tube systems allows more convenient flow characteristics than the forced-flow operation required with packed-type reactors [14]. Actually, the unobstructed nature of the system permits use of gravitational flow [15], which is practically impossible with packed columns.

Some important clinical determinations make use of enzymes that are not sufficiently stable and/or inexpensive to be used in solution for relatively long periods of time and at the high activity levels required for success in closed-loop systems. In order to develop determinations competitive in cost and number of determinations per hour, enzymes such as uricase must be stabilized and need to be present in high local concentrations. This leads to

TABLE 1

Comparison of unsegmented-flow reactors based on soluble and immobilized glucose oxidase for the determination of β-D-glucose in serum samples[a]

	Soluble system [13]	Immobilized system [11][b]
No. of determinations/hour	~800[c]	60
No. of determinations/ reservoir (column)	>15 000 (10-μl sample)	~10 000
Units of enzyme used	50 U ml^{-1} (200-ml reservoir)	50 U
Relative standard deviation (%)	1.7[d]	0.6[e]

[a]Both systems used closed-loop configurations and monitoring of dissolved oxygen levels. [b]Polyacrylamide gel-type immobilization. Relatively coarse-grained carrier packed in column configuration. Geometric dimensions of the column not reported. [c]By exploiting the delay time between the moment of injection and the beginning of the transient signal, the injection rate can be extended to 1700 injections per hour. [d]Based on 40 injections (without rejecting any value). [e]Number of replicates not reported.

the conclusion that for enzymes that are expensive and/or unstable in solution, immobilization offers the only reasonable possibility for use in continuous-flow systems.

Table 2 summarizes the most important avenues for immobilization of enzymes and their relative applicability in continuous-flow reactors. Those interested in a good review on the use of immobilized enzymes in analytical chemistry are referred to a recent monograph by Carr and Bowers [17]. As indicated in Table 2, covalent bonding on the surface of an inert matrix offers the best immobilization approach for preparations to be used in continuous-flow reactors. Covalent attachment of enzymes to an inert matrix takes advantage of exposed reactive groups on the enzyme surface. The most commonly used such groups are those involving primary amino groups and the phenol ring of tyrosine. The choice of method depends on the stability of the enzyme at the pH at which coupling is performed, the stability of the linkage at the pH at which the enzyme preparation will be used, and also the carrier. Background on the different reactions involved can be found in the monograph of Means and Feeney [20]. One of the most widely used methods involves alkylamino glass and glutaraldehyde. Although the detailed chemistry

TABLE 2

Techniques used in enzyme immobilization

Technique	General comments	Suitability for continuous flow
Adsorption	Oldest of the immobilization approaches. Typical case: immobilization by phenoxyacetylcellulose via hydrophobic—hydrophobic interaction [19].	Produces poor preparations with enzyme easily washed out by flow.
Cross-linking	Formation of intermolecular covalent linkages between enzyme molecules and bifunctional species (e.g., aldehydes, alkylating agents, diisothiocyanates).	Immobilized enzyme units buried inside the cross-linked material are not readily accessible for reaction. This imposes kinetic limitations.
Entrapment	Polymeric gel-type materials providing pores small enough to retain the enzyme molecules and allow free movement of smaller molecules such as substrates and products.	Kinetic limitations since the process is controlled by diffusion in and out of gel pores. Relatively poor mechanical stability under flow conditions.
Microencapsulation	Enzymes enclosed by membranes of a variety of polymers in capsule form 5—300 μm diameter)	Kinetic limitations as in entrapment.
Semipermeable membranes	Operation depends on the ability to retain enzymes and allow free movement of products and substrates.	Kinetic limitations as above.
Covalent attachment	Perhaps the most commonly used technique. Terminal, non-essential amino acid residues of the enzyme attached to chemically activated supports such as cellulose, synthetic polymers, glass.	The most adequate immobilization technique for preparations to be used in continuous-flow analyses

of this reaction is not well understood, the individual steps include the reaction of the silica framework with an aminosilane, modification of the product of this reaction with glutaraldehyde, and finally immobilization of the enzyme. These steps can be symbolized as follows:

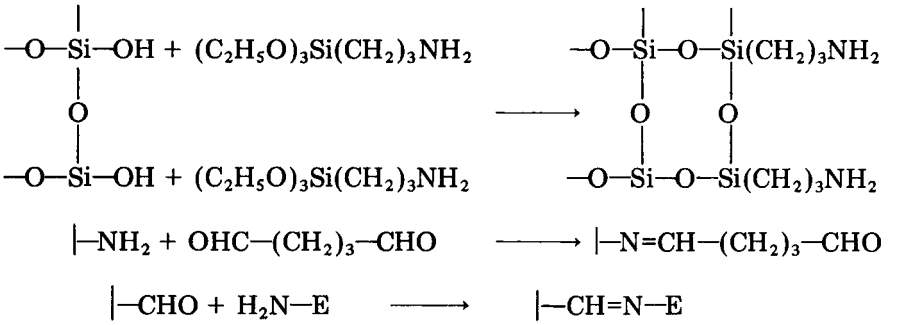

IMMOBILIZED ENZYME REACTOR CONFIGURATION

Packed columns

Immobilization via glutaraldehyde attachment seemed attractive for the following reasons: (1) its simplicity and mild operating conditions [21], (2) the success with quite a variety of enzymes, and (3) the good mechanical properties to flow offered by glass as an inert matrix. Immobilization of uricase on controlled-pore glass proved to be successful. The controlled-pore glass consists of rigid glass chips honeycombed with a very large number of size-controlled pores; Fig. 2 illustrates the topography of these particles , which are described in a commercial handbook (Pierce 1981—82 Catalog, Pierce Chemical Company, Rockford IL). This preparation yielded a material

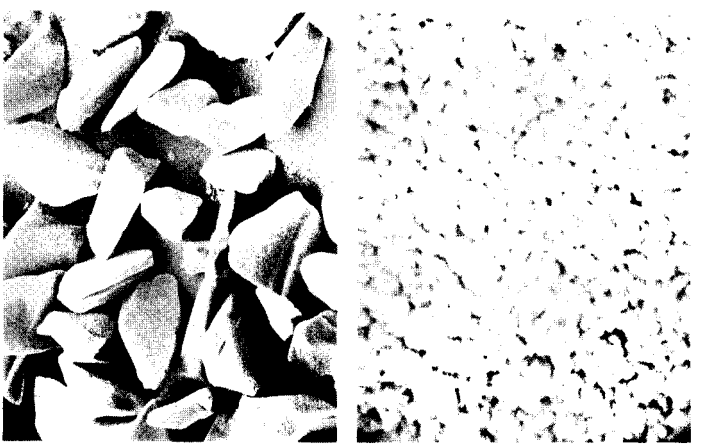

Fig. 2. Scanning electron micrographs for controlled-pore glass: nominal particle diameter of 125—177 μm and nominal pore size of 544 Å. Magnification: right = 15 000× ; left = 50×.

suitable for packed reactors for use in the unsegmented closed-loop determination of uric acid in biological fluids [14]. Uricase immobilized in this manner has shown (Fig. 1) a remarkable retention of activity with time. Worth mentioning here is the comparison illustrated in Fig. 3, which shows signals obtained with packed columns containing the same weight of controlled-pore glass in a packed coil and a straight chamber. Even though the activity of the immobilized enzyme in the packed coil is only one-half to one-third that in the straight chamber, the secondary flow occurring in the coil reactor results in larger peaks (more reaction) and the smaller diameter of the delay-mixing coil adds the extra feature of smaller dispersion. The attractive alternative of immobilization in the form of wall reactors becomes obvious.

Open-tube wall reactors

The use of open tubes with an enzyme immobilized at the inner wall seems to have originated in the work of Hornby and co-workers [22, 23] with polystyrene and nylon tubes. The tubes prepared by Hornby and co-workers contained a monomolecular enzyme layer covalently bound to the etched inner wall of the tubes. This layer had rather low activity requiring a long tube to provide sufficient reaction for detection. Horvath and co-workers [24, 25] developed an alternative providing a thick porous enzymatic annulus

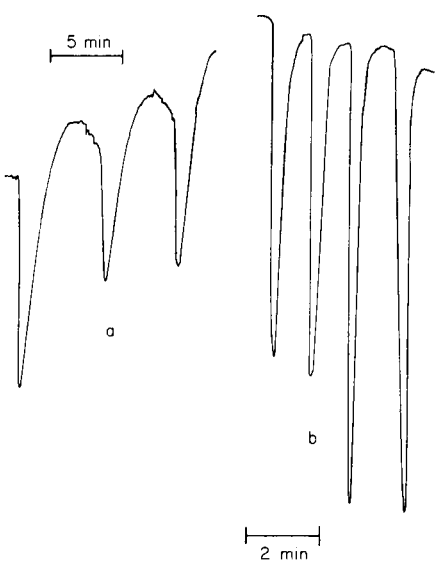

Fig. 3. Typical signal profiles: (a) straight-chamber reactor (60 mm long, 1.7 mm i.d.) packed with controlled-pore glass-3000 (0.75 U of uricase immobilized); (b) delay-mixing coil (75 mm long, 1 mm i.d.) packed with controlled-pore glass-3000 (0.3 U of uricase immobilized). Both cases represent injection of 88 mg of uric acid in 100 ml of sample (shorter peaks correspond to 20-μl samples and larger peaks to 30-μl samples). The uric acid solution was in borate buffer pH 9.4 containing 0.04% lithium carbonate.

in a tubular envelope, the enzyme(s) being bound to a polycarboxylic gel layer attached to the inner wall of small-bore nylon tubes. Horvath and Pedersen [26] have reviewed the fundamental aspects of the use of enzyme tubes in analytical chemistry and have presented a mathematical model describing coil performance in segmented-flow sample processing. The most recent contribution from Horvath and co-workers [27] is the use of a bound-uricase coil made by coating polyamide tubing with uricase, following earlier directions [24], for the determination of uric acid by segmented-continuous-flow sample processing. In this application they used the released hydrogen peroxide to oxidize an organic species which gave a colored product that was detected spectrophotometrically.

Because of oxygen diffusion in and out of plastic materials, glass is the indicated material to provide for transporting tubing and delay-mixing coil, when dissolved oxygen levels are monitored. Effective immobilization of uricase on walls of glass tubes for use as reactors in continuous-flow analyses was reported recently [15]. This contribution resulted from a combination of techniques independently developed in the areas of chromatography and enzyme engineering. The glass wall is modified by growing "whiskers" (silicate filaments) on the inert surface of glass tubing of small diameter; then the silicate surface of the inner wall of the coil is modified with amino-alkylsilyl groups and the steps illustrated earlier for glutaraldehyde and on controlled-pore glass are carried out to immobilize uricase. Gaseous hydrogen fluoride is the most commonly used reagent for roughening glass surfaces; it can be conveniently generated from ammonium hydrogenfluoride at high temperatures [28]. The technique results in filament protrusions (whiskers) of nearly perfect structural form providing a large increase in available surface area (Fig. 4).

These reactors being open tubes offer better flow characteristics than the packed coils and permit faster sampling (typically doubled rates, e.g., about

Fig. 4. Scanning electron micrographs of whiskers grown on the wall of a 2-mm i.d. Pyrex glass tube. Magnification: 2500×.

100 samples per hour with packed coils and 200 samples per hour with open tube wall reactors). Typical signals are shown in Fig. 5.

More recently, it has proved possible to immobilize the enzyme penicillinase (E.C. 3.5.2.6, penicillinase* A; Riker Labs., Northridge, CA) on capillary tubes drawn by a capillary drawing maching (Hewlett-Packard, Model 1045A). The coils have lengths of about 5 m (26 turns, 6 cm diameter) and 0.7 mm i.d. Although complete data on the characteristics of these coils are not yet available, early preparations have shown a retention of activity for about 3 months. These coils are being used in the development of a flow injection procedure for determination of penicillins in biological fluids, pharmaceutical preparations, and cow milk [29]. Penicillinase catalyzes the hydrolysis of penicillins according to

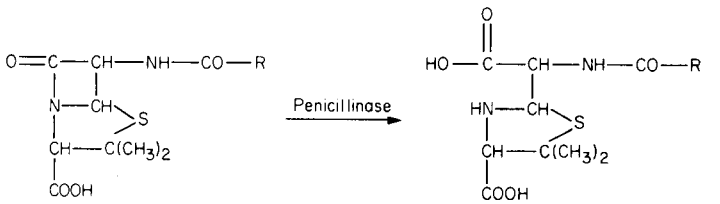

The pH change is monitored with an experimental set-up similar to the one described earlier [16] except that a FIAtron SHS-200 sample handling system (FIAtron Systems, Milwaukee, WI) is used for carrier and sample introduction. As carrier stream a 0.00050 M dipotassium hydrogenphosphate solution with the pH adjusted to 7.00 with hydrochloric acid is used. A pH of 7.00 was adopted on the assumption that this is equal or very close to the optimum pH for enzyme operation [30]. Characterization of the enzyme

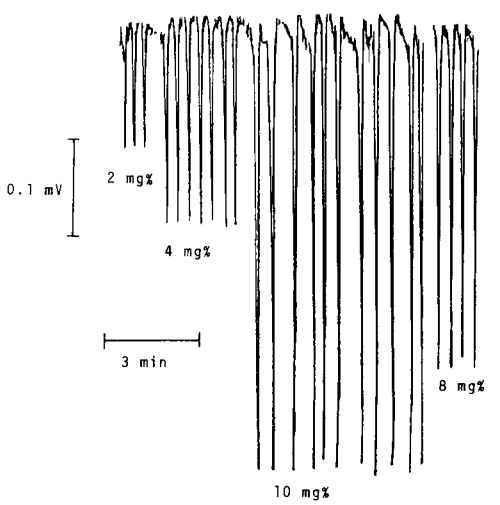

Fig. 5. Typical peak profiles for samples of uric acid determined by use of an open-tube wall reactor containing immobilized uricase [15].

preparation as well as optimization of the procedure and its application are under development.

Single-bead-string reactor

Of interest is the implementation of the concept of preparing a single-bead-string reactor with the enzyme immobilized not only on the walls of the tubing but also on the beads themselves. The single-bead-string reactor introduced by Reijn et al. [31] constitutes a very useful device for enhancing the performance of unsegmented continuous flow. It produces an increase in residence time but a substantial decrease in dispersion in comparison with open tube systems of the same length [32]. Penicillinase was immobilized on the glass beads after hydrogen fluoride treatment of the beads. Figure 6 shows that the surface modification achieved on the glass beads is better described as "volcanic crater erosion" than whisker growth. The increase in surface area is dramatic and provides an adequate surface for enzyme (penicillinase) immobilization as indicated in Table 3 and Fig. 7. It is interesting to note the rather flat surface of the untreated sphere (A, Fig. 6) compared with the surface resulting from treatment (C, Fig. 6).

Table 3 summarizes a comparison of performance of an open-tube reactor and a reactor with a string of single beads with immobilized enzyme on their surfaces. The expected improvement using the single-bead-string reactor is obvious in the data of Table 3. Although the area under the peak for the

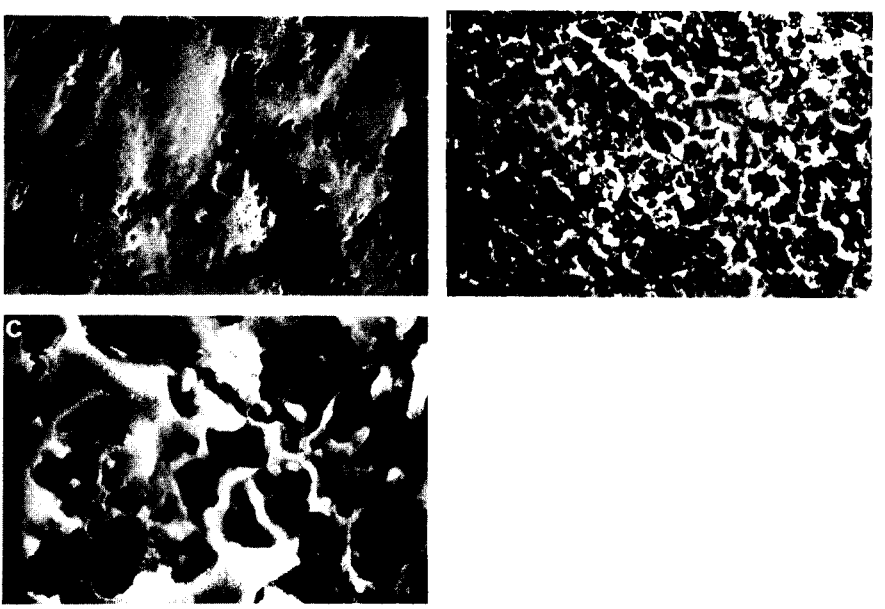

Fig. 6. Scanning electron micrographs for glass beads. A, 5000 magnification of the untreated surface of a 1 mm nominal diameter bead; B, 1000 magnification of the surface of a similar bead after the fluoride treatment intended for silicate filaments (whiskers) growth; C, the same surface as in B but at a 5000 magnification.

TABLE 3

Comparison of signal characteristics obtained with an open tube wall reactor and a single-bead-string reactor with penicillinase A immobilized on the wall of the tube and on the beads.[a] [Penicillin determined: Penicillin V (phenoxymethylpenicillinic acid, potassium salt from Sigma Chemical Company). Carrier stream: 5.0×10^{-4} M phosphate, pH 7.04. Sample size injected: 1.00 ml of 8.0×10^{-4} M penicillin. Flow rate: 1 ml min^{-1}.]

	Open tube reactor	Single-bead-string reactor
Peak height, mV	17.6	44.0
Width at half peak height, arbitrary units[b]	9	6
Area under the peak, arbitrary units[c]	330	585

[a]Coils were both seven 6-cm diameter turns of 1.3 mm i.d. capillary. Glass beads were 1 mm nominal diameter from Propper Mfg. Co., Long Island City, NY. [b]Although the amount of penicillinoic acid released in the single-bead-string reactor is about twice that released in the open tube reactor, the control of dispersion provided by the beads obviates a decrease of sampling rate which, even though not optimized, is about 50 h^{-1} in this case. [c]Graphical integration with an Ott planimeter (A. Ott, Kempton, Federal Republic of Germany).

single-bead reactor is only 1.8 times that of the open tube, the peak is 2.5 times higher. Although more quantitative information and optimization of the system is needed, the three traces compared in Fig. 7 permit one to conclude that packing of a coiled, open-tube, reactor with a single string of beads with immobilized enzyme, significantly enhances the reactor performance. Immobilization on both the walls of the coil and the beads offers very attractive characteristics for application in enzymatic analyses in unsegmented (or even segmented) continuous-flow processing. The large eddy-diffusion effect of the relatively large particles used in this packing and the small pressure drop created are attractive characteristics in an immobilized enzyme reactor. One may speculate that an open-tube wall reactor (enzyme immobilized on the wall of the tube only) of the same volume but with a significantly smaller coil diameter should at least improve the axial and radial dispersion characteristics [33]. The expected benefits of miniaturization, however, find some practical limitations when the growth of whiskers is considered. The smaller the diameter of the glass tubing the less effective is the increase in surface area by whisker growth. The same is true with surface modification of the glass beads. It is worthwhile to point out the implication of curve C in Fig. 7. This curve shows that the glass beads reduce the effective use of enzyme immobilized on the walls of the tube and implies that simple utilization of the enzyme immobilized on the beads alone may be satisfactory in many cases.

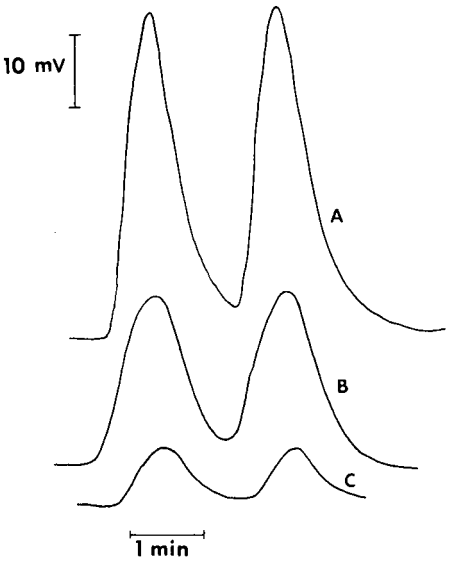

Fig. 7. Signals obtained to compare reactor performance. A, Single-bead-string reactor with enzyme immobilized on both the walls and the beads; B, same reactor as in A but with the beads removed; C, same reactor as in B but packed with untreated glass beads. For the three curves, the carrier (0.00050 M phosphate buffer, pH 7.00 and 0.10 M KCl) and the injected sample (1 ml, 0.8 mM phenoxymethylpenicillinic acid in carrier as in solution background) were the same.

CONCLUSIONS

The results presented here, an accumulation from research work using different enzyme preparations in unsegmented continuous-flow sample processing systems, allow a few general conclusions, some of which have been outlined above.

Inexpensive and relatively stable enzymes can be used conveniently in closed-loop systems and directly in solution. Alternatively, in open systems, miniaturization and the use of merging zones are recommended.

Relatively expensive enzymes of rather unstable nature (with respect to activity retention) are better utilized in immobilized form; covalent bonding to the surface of a glass matrix (or similarly uncompressed surfaces) is the recommended method of immobilization to be used for flow situations.

Open-tube wall reactors offer advantageous characteristics over packed columns. In turn, coiled reactors are to be preferred to straight reactors. Immobilization of the enzyme on the walls of the coiled reactor and on beads so as to form a single-bead-string reactor constitutes an excellent configuration for using immobilized enzyme systems. Use of the enzyme immobilized on the single beads alone may be satisfactory in some cases.

The Analytical Research Services Divisions of CONOCO Inc. (Ponca City, OK) and DOWEL (Tulsa, OK) are thanked for their cooperation in providing scanning electron micrographs. Thanks are extended to FIAtron Systems (Milwaukee, WI) for the loan of the SHS-200 sample handling system. The work reported here was supported by the National Science Foundation (Grant CHE-7923956).

REFERENCES

1 L. T. Skeggs Jr., Am. J. Clin. Pathol., 28 (1957) 311.
2 L. T. Skeggs Jr., Abstracts of Papers, 1982 Pittsburgh Conference and Exposition on Analytical Chemistry and Applied Spectroscopy, Atlantic City, NJ, 1982; Abstr. 006, The Pittsburgh Conf. Inc., Pittsburgh, PA, 1982.
3 H. A. Mottola, Anal. Chem., 53 (1981) 1312A.
4 C. J. Patton and S. R. Crouch, Abstracts of Papers, 1982 Pittsburgh Conference and Exposition on Analytical Chemistry and Applied Spectroscopy, Atlantic City, NJ., 1982; Abstr. 004, The Pittsburgh Conf. Inc., Pittsburgh, PA, 1982.
5 P. W. Alexander and H. Marpaung, Talanta, 29 (1982) 213.
6 W. H. Marsh, B. Fingerhut and E. Kirsch, Clin. Chem., 5 (1959) 119.
7 M. K. Schwartz, G. Kessler and O. Bodansky, Clin. Chem., 5 (1959) 368.
8 M. Tkachuk, Can. J. Med. Technol., 22 (1960) 71.
9 J. B. Hill and G. Kessler, J. Lab. Clin. Med., 57 (1961) 970.
10 C. Wincey and V. Marks, J. Clin. Pathol., 14 (1961) 558.
11 H. U. Bergmeyer and A. Hagan, Fresenius' Z. Anal. Chem., 261 (1972) 333.
12 Ch-M. Wolff and H. A. Mottola, Anal. Chem., 49 (1977) 2118.
13 Ch-M. Wolff and H. A. Mottola, Anal. Chem., 50 (1978) 94.
14 A. Iob and H. A. Mottola, Anal. Chem., 52 (1980) 2332.
15 A. Iob and H. A. Mottola, Clin. Chem., 27 (1981) 195.
16 J. Růžička, E. H. Hansen, A. K. Ghose and H. A. Mottola, Anal. Chem., 51 (1979) 199.
17 P. W. Carr and L. D. Bowers, Immobilized Enzymes in Analytical and Clinical Chemistry, Wiley, New York, 1980; Chapter 3, pp. 131—136.
18 J. Růžička and E. H. Hansen, Flow Injection Analysis; Wiley, New York, 1981, pp. 73—76.
19 L. G. Butler, Arch. Biochem. Biophys., 171 (1975) 645.
20 G. E. Means and R. E. Feeney, Chemical Modification of Proteins, Holden-Day, San Francisco, 1971.
21 P. J. Robinson, P. Dunnill and M. D. Lilly, Biochem. Biophys. Acta, 242 (1971) 659.
22 W. E. Hornby, D. J. Inman and A. McDonald, FEBS Lett., 9 (1970) 8.
23 D. J. Inman and W. E. Hornby, Biochem. J., 129 (1972) 225.
24 C. Horvath and B. A. Solomon, Biotechnol. Bioeng., 14 (1972) 885.
25 C. Horvath, A. Sardi and J. S. Woods, J. Appl. Physiol., 34 (1973) 181.
26 C. Horvath and H. Pedersen, in Advances in Automated Analysis, 7th Technicon International Congress, December, 1976, New York City; Technicon Instrument Corporation, Tarrytown, NY, 1977.
27 L. P. Leon, J. B. Smith, A. Yeung, C. K. Yeh and C. Horvath, J. Autom. Chem., 4 (1982) 11.
28 F. I. Onuska, M. E. Comba, T. Bistricki and J. Wilkinson, J. Chromatogr., 142 (1977) 117.
29 R. Gnanasekaran, Oklahoma State University, unpublished results, 1982.
30 J. F. Rusling, G. H. Luttrell, L. F. Cullen and G. J. Papariello, Anal. Chem., 48 (1976) 1211.
31 J. M. Reijn, W. E. van der Linden and E. Poppe, Anal. Chim. Acta, 123 (1981) 229.
32 S. M. Ramasamy and H. A. Mottola, Anal. Chem., 54 (1982) 283.
33 R. Tijssen, Axial and Radial Dispersion Phenomena in Flow Analysis and Related Techniques, paper read at Flow Analysis II, June, 1982, Lund, Sweden.

Analytica Chimica Acta, 145 (1983) 41—50
Elsevier Scientific Publishing Company, Amsterdam — Printed in The Netherlands

A POLAROGRAPHIC AND SPECTROPHOTOMETRIC ROUTINE ANALYZER FOR ASSAYING CONTENT UNIFORMITY IN PHARMACEUTICAL QUALITY CONTROL

ZSÓFIA FEHÉR, GYÖRGY HORVAI, GÉZA NAGY, ZSUZSANNA NIEGREISZ, KLÁRA TÓTH and ERNÖ PUNGOR*

Institute for General and Analytical Chemistry, Technical University of Budapest, Gellért-tér 4, H-1111 Budapest (Hungary)

(Received 18th June 1982)

SUMMARY

A serial analyzer with polarographic and spectrophotometric detection has been designed to speed up content uniformity tests in pharmaceutical quality control laboratories. The advantages of flow and discrete analysis are combined to provide the required speed and precision. Pharmaceutical preparations of diazepam, nitrazepam, spironolactone and pyridinolcarbamate have been tested satisfactorily. The system is easily constructed from commercially available hardware and a few home-made units. The problem of sample deaeration before polarographic measurements in flow systems is solved succesfully in a very simple way.

An important part of quality control in pharmaceutical factories is the assay of the active ingredient in each batch of tablets, capsules, etc. This is usually done by taking a representative sample of, e.g., ten tablets, homogenization and subsequent chemical analysis. In recent years, there has been a trend towards not only determining the average amount of active ingredient in each batch but also checking the uniformity of the distribution of the active ingredient within the batch. In several cases, tests for content uniformity are required by national Pharmacopoeias [1, 2]. For such tests, at least ten individual dosage units (tablets, capsules, etc.) must be analyzed individually, usually by the same method as is used for the assay of the batch average. This, however, is not always possible because of the much smaller amount of sample (one tablet instead of ten); in some cases, a more sensitive method has to be used, e.g., differential pulse polarography instead of d.c. polarography [3]. Moreover, the introduction of content uniformity tests increases the workload of the quality control laboratory at least ten-fold. This is one reason why automation of assays for content uniformity is very desirable. The situation is actually very suitable for automation, because the samples are not only numerous but also very similar in composition.

Spectrophotometry and polarography are perhaps the most widely used instrumental analytical methods in pharmaceutical quality control, and automation of these two methods for content uniformity tests is therefore

most desirable. There have been many individual efforts to automate these separate techniques, but there appears to be no report on equipment based on the same building blocks, apart from the detector cells themselves, to solve both problems. This would, however, be very useful in laboratories which use both techniques routinely.

Automated spectrophotometric analysis can be completely based on commercially available units [4]. This approach is not necessarily the best or cheapest, if the methodology is very simple (e.g., absorbance measurement at a fixed wavelength in the u.v. region without preceding chemical reaction is possible) or if automation with computers is required in combination with another detection system such as polarography. With spectrophotometric detection, special problems arise if the analytical method requires a partially or completely organic medium; air bubbles may appear and accumulate in the light path causing spurious signals. Attempts have been made to avoid such problems by specially designed flow-through cuvettes [5].

Automation of polarography has been described widely in the literature but no commercial or other system appears to have gained wide acceptance. A commercial batch analyzer (ANSWER, Princeton Applied Research) was on the market for only a short time. Others have used the flow-through principle, which has, however, inherent problems that are not easily overcome. When the dropping mercury electrode is used as the detector in streaming solutions, the polarographic cell must be carefully designed so that the hydrodynamic conditions remain well defined and the long-term stability is adequate. A further crucial problem is how to deoxygenate the streaming solution. Cinci and Silvestri [6] added the oxygen-containing samples to an excess of deoxygenated streaming background solution. Lento [7] and Cullen et al. [8] used nitrogen to segment the solution flowing through a delay coil. Lund and Opheim [9] found earlier deaeration methods unsatisfactory and replaced them by a more efficient but also more complicated technique: nitrogen was bubbled through the samples loaded on a sample tray, but the pump transporting the samples to the detector cell had to be stopped during sample changes to avoid introduction of air bubbles into the sample line. Trojanek and Holub [10] deoxygenated solutions by pumping them through a gas-permeable silicone rubber tube surrounded by a second tube flushed with nitrogen. Polarographic cell designs for use in flowing solutions have been described by many authors (see, e.g., [11—13]). Both fixed potential and potential scanning measurements have been applied.

The aim of the work described here was to build an automatic analyzer for content uniformity tests in which either spectrophotometric or polarographic detection could be used but which would otherwise be built from the same, easily available units. At the present stage, suitable units for dissolved, filtered and occasionally diluted samples have been developed. Computer control of the equipment and on-line data handling are being finalized and will be reported at a later date. Consideration of the problems encountered and practical experience with the difficulties in batch and flow

analysis led to the adoption of a new concept: batch and flow operations are combined so that both retain their advantages while overcoming their separate drawbacks. The system has been tested on four pharmaceutical preparations from the Gedeon Richter Works (Budapest, Hungary): Prodectin, Eunoctin, Seduxen and Verospiron tablets, which have the active ingredients pyridinolcarbamate, nitrazepam, diazepam and spironolactone, respectively.

NITRAZEPAM

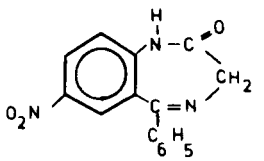

DIAZEPAM

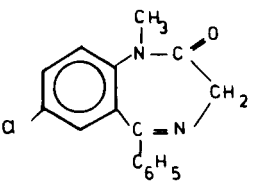

PYRIDINOLCARBAMATE

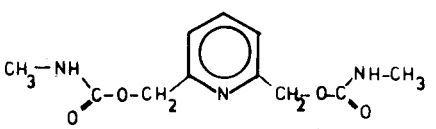

SPIRONOLACTONE

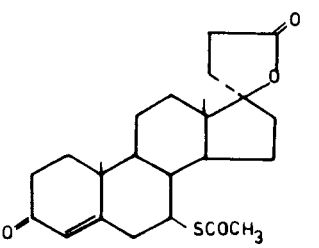

All four active ingredients have analytically useful u.v. absorption bands, and with the exception of spironolactone are also polarographically active at the dropping mercury electrode.

POLAROGRAPHIC SYSTEM

In the course of a detailed study of the problems of automatic deaeration of samples, it became clear that none of the continuous techniques published so far is universally applicable. Other possibilities, such as sine-wave a.c. polarography as well as chemical reduction of oxygen, were tried but it was concluded that the combination of batch and flow analysis principles offered the best and most general solution for the problem. This is also true for the design of the polarographic cell.

Accordingly, in the system developed, the polarographic analysis of the sample solutions is done in static solution, whereas the samples are transported in the analyzer system with the help of a peristaltic pump. A schematic diagram of the polarographic unit is shown in Fig. 1.

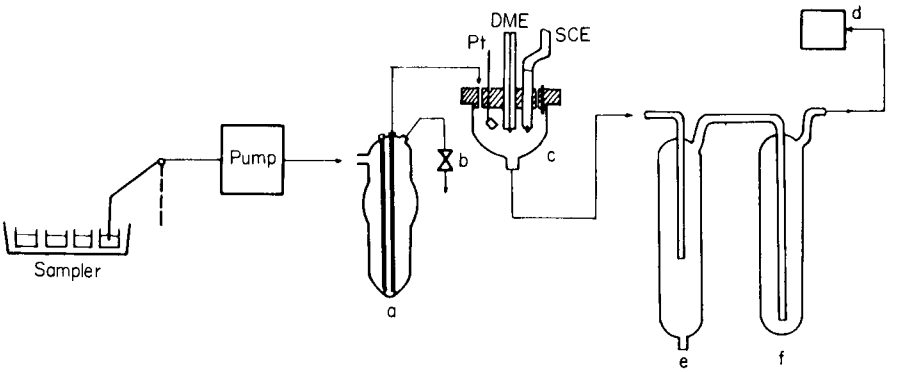

Fig. 1. Polarographic set-up for content uniformity test (for details, see text).

Procedure

About 2.5 ml of the sample solution is pumped into the deaeration cell (a) by means of a peristaltic pump (Type OL-602, Labor MIM, Hungary) from the sampler unit (Type OL-603, Labor MIM, Hungary). After a fixed time interval, sufficient for elimination of the dissolved oxygen by bubbling nitrogen (see below), valve b is closed, an over-pressure of nitrogen develops in the deaeration vessel, and the sample solution is transferred into the polarographic cell (c). The polarographic cell contains the dropping mercury electrode (drop time about 1 s), a saturated calomel reference electrode and a platinum auxiliary electrode. Then either the current–potential curve is recorded for the sample solution or the current is measured at a fixed potential. After this, the sample solution is sucked from the polarographic cell with the help of a very simple membrane pump (d) through the buffer vessels (e, f) to waste.

Between two sample portions, the peristaltic pump is not stopped but transports air. This small amount of air which is led into the deaeration chamber above the liquid level is completely swept out by the nitrogen stream. To avoid any problems caused by oxygen, a nitrogen blanket is ensured in the polarographic cell, by passing nitrogen over the sample solution surface. In this measuring system, the consecutive steps of the procedure occur in parallel for different samples, i.e., during the polarographic measurement of one sample, nitrogen is bubbled through the next sample solution, and so on.

Suitable calibration graphs are used to calculate the concentrations of the sample solutions. The timing of the procedural steps is shown in Fig. 2. The timed operation of the various units in the system is controlled by a home-built electronic unit. Although any commercial polarograph could be used in this system, a home-made polarographic unit will be used in the final system to make computer control and connection with the spectrophotometric unit easier and more economic.

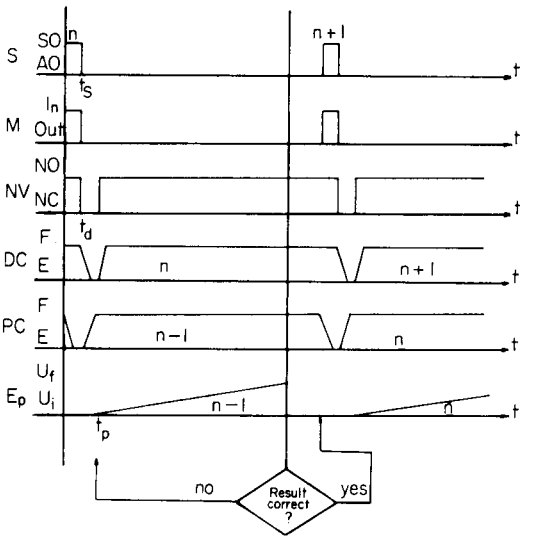

Fig. 2. Timing diagram for the polarographic set-up. S, sampler with sample suction (SO) and air suction (AO); M, membrane pump; NV, nitrogen valve, open (NO) and closed (NC); DC, deaeration cell, filled with sample (F) and empty (E); PC, polarographic cell, filled with sample (F) and empty (E); EP, electrode-potential program with U_i as the initial potential and U_f as the final potential. t_s shows the end of sampling, t_d the end of deaeration, and t_p the start of the potential scan. n is the sample number.

Results and discussion

Appropriate conditions for the polarographic measurements, selected on the basis of data found in the literature and on confirmatory experiments, are summarized in Table 1.

TABLE 1

Conditions for polarographic measurements

Drug (active ingredient)	Supporting electrolyte	Potential scan[b] (V)	Sample concn.[a] ($\times 10^{-4}$ M)	R.s.d.[c] (%)	Linear range ($\times 10^{-4}$)
Prodectin (Pyridinolcarbamate)	Buffer pH 6.6[d]	−1.2 to −1.7	3.95	1.0	0.3–50
Eunoctin (Nitrazepam)	Buffer pH 3.5[d]	0.0 to −0.5	3.39	1.1	0.3–50
Seduxen (Diazepam)	0.1 M H_2SO_4	−0.4 to −0.9	3.51	0.7	0.3–50

[a] Sample concentration corresponding to 0.1 g l^{-1} if the tablet contains the nominal content of active ingredient.
[b] The polarization rate was 5 mV s^{-1}.
[c] For the pure active ingredient; $n = 15$.
[d] Britton–Robinson buffer solutions.

The stability of the sample solutions was studied from the point of view of automated polarography. It was found that the solutions, in the concentration range to be measured, are stable for at least 6 h.

The reproducibility of the polarographic results was investigated first by using standard solutions prepared from the active ingredients; 15 samples of the same concentration were analyzed by recording complete polarograms. The standard deviations are included in Table 1. The relationship between the analytical signal (current) and the concentration of the analyte was found to be linear in the concentration ranges given in Table 1.

Studies of the time necessary for deaeration (nitrogen bubbling) showed that 100 s was sufficient in each case studied.

Carry-over effects were examined as follows: solutions of the lowest (80% of the declared drug content) and highest (120% of the declared drug content) concentrations were processed, first in separate groups and then alternately. The results, summarized in Table 2, indicate that the changes in the measured concentrations when solutions of widely differing concentrations are processed one after another are not significantly different from the statistical error of the concentration determination.

An important step in working out an assay for drug content is an examination of the effects of constituents present in the pharmaceutical preparations in addition to the active ingredient. Experiments showed that none of the components present in the tablets which were analyzed were electroactive, and that they did not cause any change in the shape or height of the polarographic wave of the active ingredient. Thus, polarography is possible after simple pulverization of the tablet and dissolution of the active ingredient in an appropriate medium.

The reproducibility of the drug content determination in tablets was also studied; five portions, each corresponding to one tablet, of a homogenized powder made from a large number of tablets were pumped into the system. The results are compared with those obtained spectrophotometrically for the same homogenized powder in Table 3. The sample through-put in all polarographic measurements was 30 samples per hour.

TABLE 2

Results of carry-over studies on the polarographic measurement of pyridinolcarbamate as model compound[a]

n	Average[b]	R.s.d. (%)	*n*	Average[b]	R.s.d. (%)
5	80.00	1.20	15	79.66	1.35
5	120.00	1.08	15	120.9	1.13

[a]Columns 1—3 refer to separate groups of the same concentration. Columns 4—6 refer to alternating measurements of low and high concentrations.
[b]Percent referred to nominal value.

TABLE 3

Comparison of polarographic and spectrophotometric performance with tablets

Tablet	Polarography		Spectrophotometry	
	Drug content[a] (%)	R.s.d. (%)	Drug content[a] (%)	R.s.d. (%)
Prodectin	103.6	0.6	101.7	0.4
Eunoctin	98.4	0.8	99.2	0.4
Seduxen	98.0	1.3	99.0	0.8

[a]Percent referred to standard solutions of nominal concentrations.

SPECTROPHOTOMETRIC SYSTEM

The automatic sampler and the pump were the same as those used for the polarographic mode. Absorbance was measured by a u.v. spectrophotometer (Type OL-308, Labor MIM, Hungary) and recorded by an OmniScribe recorder (Houston Instruments). The sampler had a capacity for 200 samples. The detector was mounted between the sampler and the pump. Thus the suction line became relatively long and bubble formation before or during detection was more of a problem. However, the adsorption phenomena eventually observed with the pump tubing (both Tygon and silicone rubber) made this sequence of units desirable. The tablets could have been dissolved in acidic solution to decrease the adsorption but under such conditions, spectrophotometric stability was found to be less satisfactory. The problems connected with air bubble formation had then to be avoided by suitable design of the sampling process, sample line and flow-through cuvette. Both the spurious formation of small bubbles and sample carry-over can be diminished by air segmentation at sampling. Segmentation within one sample was found to be unnecessary with the sample line (ca. 40 cm long, 1.2 mm i.d. polyethylene) used to connect the sampler head with the cuvette. Segmentation between consecutive samples was solved simply by keeping the sampler head in air for some time before moving it into the next sample.

Various designs of the flow-through cuvette were tested. Two Z-shaped cells, one with and one without a built-in debubbler, were found to operate less reliably than the cell shown in Fig. 3B. This cell is made from plexiglas with quartz windows glued to each side. It has one inlet and two outlet tubes; the outlets are placed under suction from two separate channels of the peristaltic pump (Fig. 3A) and the flow rates in the two channels are typically about equal. The optical pathlength is 10 mm and the active cell volume is about 500 μl. Samples and air are alternately sucked into the cell by suitable movement of the sampler head; the air suction period is slightly longer than the sampling period. This operation results in alternate filling and emptying of the optical cell, and as the cell is machined from plexiglas, practically no liquid adheres to the walls on emptying. With this arrangement, a sample

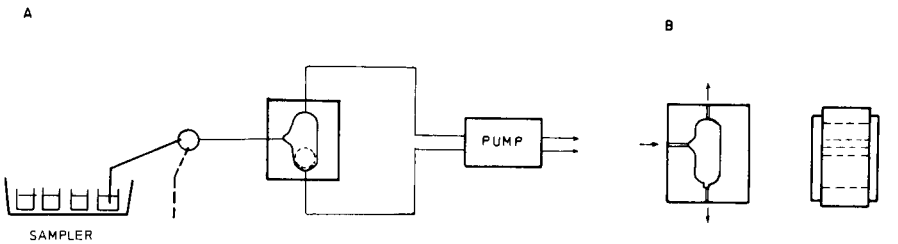

Fig. 3. A, Spectrophotometric set-up for content uniformity tests. B, Cuvette. (For details, see text.)

throughput of 120 samples per hour was easily achieved at a total flow rate of 4.4 ml min^{-1} even though the absorption was always measured at steady state. By the use of scale expansion (i.e., measuring absorbances near 0.5 on the 0.1 or 0.05 scale and using electronic compensation), high sensitivity was achieved (Fig. 4). It is worth noting that with the Z-type flow cell without a debubbler, a sample throughput of more than 500 samples per hour was attainable with alternating suction of samples and air. In this case, however, the flow pattern showed occasional irregularities which caused erroneous readings.

Results and discussion

The working conditions which were found suitable for the four drugs tested are given in Table 4. The sample solutions used were stable for at

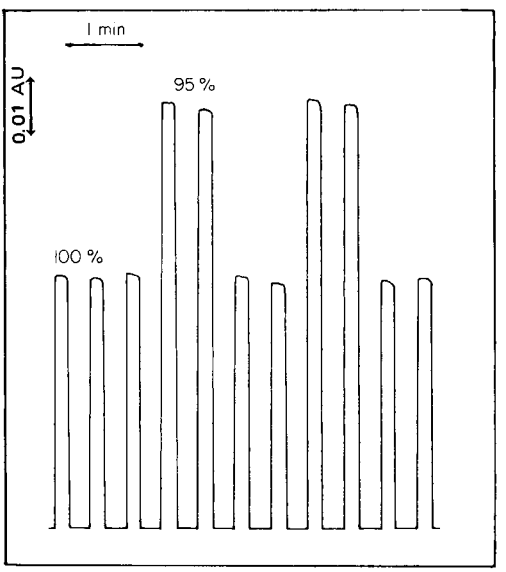

Fig. 4. Typical output from the spectrophotometric system. Replicate analyses of pyridinolcarbamate at two different concentration levels. For the working conditions see Table 4. The nominal concentration is 100%.

TABLE 4

Working conditions for the spectrophotometric system

Drug[a]	Sample concn.[b] (mg l^{-1})	Wavelength (nm)	R.s.d.[c] (%)
Prodectin	0.25	263	0.28
Eunoctin	0.10	259	0.18
Seduxen	0.05	230	0.40
Verospiron	0.10	242	0.18

[a]All samples were dissolved in aqueous 10% ethanol. The active ingredient in Verospiron is spironolactone.
[b]Sample concentration if the nominal content of active ingredient.
[c]For the pure active ingredient; n = 10.

least 3 h. The reproducibility of the absorbance measurements with standard solutions was good (Table 4). Absorbance was found to depend linearly on concentration in the studied range (nominal value ±20%). A study of sample carry-over, similar to the polarographic one, gave the results shown in Table 5. Only minor matrix effects were found with the tablets. The results of reproducibility tests with tablets, for comparison with the polarographic method, are shown in Table 3.

CONCLUSIONS

The polarographic and spectrophotometric set-ups described above are of considerable help in pharmaceutical quality control even in their present form. The throughput of the polarographic unit could be increased by slight modifications. At these high sample throughputs, sample pretreatment and data processing become the rate-limiting factors in the laboratory; their automation is under development.

Although the main intention was to solve a problem arising in pharmaceutical quality control, the measuring systems described would be equally useful in many other routine laboratories dealing with the polarographic

TABLE 5

Carry-over study for the spectrophotometric measurement of pyridinolcarbamate

n	Average[a]	R.s.d. (%)	n	Average[a]	R.s.d. (%)
5	80.0	0	10	79.97	0.14
5	100.0	0.14	10	99.87	0.14

[a]Percent referred to nominal value.

and spectrophotometric analysis of large numbers of samples. The polarographic system is advantageous in this respect, because it can be adapted to most modern polarographic techniques, simply by changing the electronic circuitry. In addition, other working electrodes (e.g., stationary mercury electrode) can easily be incorporated into the polarographic cell. The polarographic unit also offers the possibility of simultaneous selective determinations of components in a mixture, because a complete polarogram is usually taken for each sample. Sample deaeration, which has been a crucial problem in using the dropping mercury electrode in automated analysis, has been solved very simply. As the polarographic and spectrophotometric systems are built from the same units apart from the detectors it is easy to change from polarographic to spectrophotometric operation and vice versa.

The authors express their thanks to the Gedeon Richter Company for the financial support of this work.

REFERENCES

1 The United States Pharmacopeia XX, 1980.
2 British Pharmacopeia, 1980.
3 M. A. Brooks and J. A. F. de Silva, Talanta, 22 (1975) 849.
4 The United States Pharmacopeia XX, 1980, p. 956.
5 See, e.g., H. Gausmann and W. Geis, Ger. Offen. 2,904,909, 1980.
6 A. Cinci and S. Silvestri, Farmaco Ed. Prat., 27 (1972) 28.
7 H. G. Lento, Automation in Analytical Chemistry, Technicon Symposium, 1966, Mediad, White Plains, New York 1967, Vol. I, p. 598.
8 L. F. Cullen, M. P. Brindle and G. I. Papariello, J. Pharm. Sci., 62 (1973) 1708.
9 W. Lund and L. Opheim, Anal. Chim. Acta, 79 (1975) 35; 82 (1976) 245.
10 A. Trojanek and K. Holub, Anal. Chim. Acta, 121 (1980) 23.
11 W. J. Blaedel and J. H. Strohl, Anal. Chem., 36 (1964) 445.
12 E. Scarano, M. G. Bonicelli and M. Forina, Anal. Chem., 42 (1970) 1470.
13 Zs. Fehér and E. Pungor, Anal. Chim. Acta, 71 (1974) 425.

Analytica Chimica Acta, 145 (1983) 51—58
Elsevier Scientific Publishing Company, Amsterdam — Printed in The Netherlands

OPTIMAL SPEED AS A FUNCTION OF SYSTEM PERFORMANCE FOR CONTINUOUS FLOW ANALYZERS

SVETLA ANGELOVA

International Institute of Cellular and Molecular Pathology, Unit of Experimental Medicine, Avenue Hippocrate 75, 1200 Brussels (Belgium)

H. W. HOLY*

Technicon International Division S.A., Case Postale 64, 1211 Geneva 17 (Switzerland)

(Received 21st June 1982)

SUMMARY

The limitation to high rates of sample throughput with continuous flow automated analyzers is unacceptably high sample-to-sample carry-over. Previous programs for carry-over correction have involved relatively large computer capacities. Here, the simple expression derived for carry-over can be easily programmed in BASIC for a Commodore PET operating in real time. The program includes peak picking and calculation of the calibration graph and sample concentrations. At 240 samples per hour, the results obtained for total protein (linear calibration graph) and haptoglobin (non-linear calibration plot) showed acceptable precision and recovery and correlated well with the same determination conducted at normal operating speeds. Standard AutoAnalyzer equipment was used throughout. A parameter which monitors the instrument function is also calculated; this replaces the conventional visual examination of the curve for function monitoring. At high sample rates with degraded curves, visual curve examination is not effective.

Continuous flow with air segmentation has long played an important role in analytical methods partly because of its inherent reliability derived from the shape of the analogue curve. A deformed curve was a doubtful result. However, sample throughputs of 60 h^{-1} have seemed unnecessarily slow for an automated system. Various techniques have been described to increase speed such as flow injection analysis [1, 2], miniaturization [3] and curve regeneration [4, 5]. With curve regeneration, the authors have gone to considerable length to monitor the curve shape as an indicator of system performance, the secret of air-segmented continuous flow success.

Explicitly or implicitly each method is concerned with sample interaction or carry-over as a speed-limiting factor. Yet, only Thiers et al. [6] seem to have analyzed the problem of curve interaction in depth and as early as 1970 described a program written in assembly language for a large computer (LINC 8) to correct for sample interaction; this allowed standard AutoAnalyzer systems to operate at 180 samples per hour even when the calibration graphs were non-linear. In spite of the complexity of the program, curve

monitoring was not included as a check on instrument performance. In this paper, a simpler method than that used by Thiers is described for the correction of carry-over, thus making it possible to program a simple desk computer such as the Commodore PET in BASIC to make the necessary calculations for carry-over as part of a total program of peak picking, calculating the calibration curve, linear or non-linear, and printing out the corrected assay values, all in real time at assay rates of up to 240 h^{-1} At the same time it is possible to calculate the constant B identified by Walker et al. [4] and exploited by de Jong and Weyden [5] as a powerful monitor of system performance, which is an obvious advantage with high assay rates when the curve shape has lost visual significance. In view of the many thousands of continuous flow analyzers currently being used, such a program could significantly increase the efficiency of this equipment at a very moderate cost.

THEORY

In any automated analytical technique, the equipment is calibrated by running a series of standards and assuming that samples to be assayed will produce the same response as the standards of the same concentration. The error introduced by this assumption depends on the carry-over from sample to sample. The simplest method to correct for this carry-over is to reduce each assay for sample or standard to the value it would have had if no sample or standard had preceded it. Carry-over has been defined as the concentration difference between the first sample measured and the value given by that sample after several repetitions [7]. For clarity, carry-over is defined here as the quantity to be subtracted from each measured concentration as a contribution from the preceding peak.

Thiers et al. [8] spent considerable time showing experimentally that, to a sufficient order of precision, the influence on peak 2 is dependent only on the height of the preceding peak 1. Yet this concept is readily derived mathematically if it is assumed that any continuous flow system is only usable if the peak height y_s can be fully described by a generalized equation $y_s = f(B, t_s, t_w, Y_{max})$ where f is any function, t_s is the sampling time, t_w is the wash time, Y_{max} is the peak height if t_s is infinite, and B is a constant incorporating all parameters which may affect peak height such as sample viscosity, dialysis rates, manifold construction, temperature, etc. Because $t_s + t_w = t_c$ (cycle time) is constant for any automated analytical system, the above expression reduces to

$$y_s = f(B, t_c, Y_{max}) \tag{1}$$

Because the above parameters are the only ones which determine the peak height and shape and because sample carry-over in its most general terms must depend on the preceding peak in some way (height, breadth, shape, etc.), the amount of carry-over can be described formally by the function $C_0 = q(B, t_s, t_w, y_i)$, thus

$$C_0 = q(k_c, y_i) \quad (2)$$

where $y_i = f(Y_{max})$. In the linear case (i.e., a function in which Y_{max} remains to the power 1, and which must not be confused with the linear calibration graphs where a straight line relationship exists between instrument response and sample concentration), Eqn. (1) becomes $y_s = k\ Y_{max}$, and Eqn. (2) becomes $C_0 = k_c y_s$. This simply demonstrates mathematically that in a usable continuous flow system, the sample interaction can depend only on the preceding peak height. That the system must be expressable mathematically as a linear function, is not a restriction, as all continuous flow systems can be so expressed.

For example, given the normally accepted model of a continuous flow peak [4] (Fig. 1) to be $y_s = [1 - \exp(-t/B)]\ Y_{max}$ for $0 \leqslant t \leqslant t_s$, the amount of sample carry-over can be expressed by

$$y_w = \exp(-t/B) y_s = C_0 \quad (3)$$

where $t_s \leqslant t \leqslant t_s + t_w$. Then for $t = t_s$,

$$y_s = [1 - \exp(-t_s/B)]\ Y_{max} = k_c Y_{max} \quad (4)$$

because t_s and B are constants. Further, for $t = t_s + t_w$,

$$C_0 = y_w = y_s \exp[-(t_s + t_w)/B] = k_c y_s \quad (5)$$

as t_s, t_w and B are all constants. This expression is consistent with the observation that in the case of equilibrium where $t_s \to \infty$ and $(t_s + t_w) \to \infty$, the amount of carry-over is $C_0 \to 0$ and that it is the cycle time (i.e., the sum of t_s and t_w) which determines the carry-over and not the individual quantities.

From the equation, the following points become obvious. First, the sample carry-over increases as t_c becomes smaller, i.e., as the sampling rate increases, which is in keeping with experience. Secondly, the sample carry-

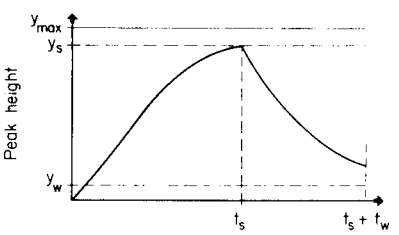

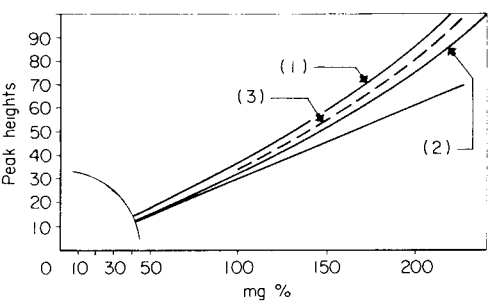

Fig. 1. Typical continuous flow response curve; y_w is the carry-over contribution to the peak formed at $t = t_s + t_w$.

Fig. 2. AIP calibration curves at 240 assays/h for haptoglobin, showing the effect of the order in which standards are run. Curves: (1) curve plotted from standards run in descending concentrations; (2) curve plotted from standards run in ascending order; (3) accepted curve.

over increases as B increases, i.e., as the system performance deteriorates, emphasizing the importance of this factor as a system function monitor. Thirdly, the method of correction for carry-over fails when variations in t_c or B are significantly large relative to t_c/B. Such variations will then increase the imprecision of the peaks themselves, as defined by Eqn. (4), to unacceptable levels quite independently of any sample carry-over correction. There is therefore a limit to the maximum speed achievable, defined by the constancy of the above parameters.

For linear calibration graphs, the k_c value is used very simply to correct each peak height y_i' based on the preceding peak height y_{i-1}', to give the corrected peak height

$$y_i = y_i' - k_c y_{i-1}' \tag{6}$$

For systems based on non-linear calibration graphs, an accurate correction for sample carry-over is possible but extremely complex. If, however, the non-linearity is not excessive, a linear-type correction can be applied effectively. In non-linear systems, the sample carry-over depresses the peaks if standards are used in ascending concentration and vice versa. A close approximation of the true calibration curve is the curve plotted on the mean values between the rising and falling calibration curve (Fig. 2).

For the sample carry-over constant k_c, it is also possible to accept a compromise by assuming that the middle range value is essentially constant. If the middle range peak height is y_M, the low y_L and the high y_H, the interaction constant can be calculated simply as $y_M = y_M' - k_c y_L'$ for the ascending curve and $y_M = y_M'' - k_c y_H''$ for the descending curve, where y_M is the corrected peak height. Therefore $y_M' - k_c y_L' = y_M'' - k_c y_H''$, and

$$k_c = (y_M'' - y_M')/(y_H'' - y_L'') \tag{7}$$

The same formula as is used for the linear case may then be applied to all peak heights with the assumption that the y_M sample is correct and thus

$$y_i = y_1' - k_c (y_{(i-1)} - y_m) \tag{8}$$

The interaction correction is therefore subtracted for values below y_M and added for values above y_M.

EXPERIMENTAL

To check the above theory for a linear system, a Technicon AutoAnalyzer (AAII) was used as described in their method sheet No. N-14b I/II (1969) for total protein. All reagents were obtained from Technicon. Standards were prepared from bovine serum albumin (BSA) as described.

As an example of a non-linear system, a Technicon AIP (automated immuno precipitin) system (method sheet No. 12, Preliminary, 1972) was used for the determination of haptoglobin in serum. Technicon standard serum was used suitably diluted in saline BSA to establish the calibration

curve. Samples were sera from the Clinique St. Luc, Brussels, sent to the laboratory of the Unit of Experimental Medicine for routine assays for 12 immunoproteins including haptoglobin. These samples were run on the day that they were received after routine determination at 120 samples/h on the same apparatus.

In both cases, recorders were connected with a Technicon interface to a Commodore PET computer and the standard program as written for the Technicon Multilyzer for peak picking and calculation of the calibration graphs and results was used.

RESULTS AND DISCUSSION

Determination of k_c

The great advantage of the carry-over constant k_c is that it can be determined very simply by using one standard processed twice at the given rate of sample throughput. Then $k_c = (y_2 - y_1)/(y_1 - N)$ where y_1 and y_2 are the same standard, twice assayed, and N is the baseline value. The advantage of using the present definition of carry-over is therefore obvious. Two calibrating standards are now required in place of the normal six standards (3 high, 3 low) [7] used to determine carry-over in its earlier definition. The earlier concept, furthermore, does not lend itself readily to calculation of the function monitoring parameter B.

To check the hypothesis that the carry-over constant k_c for a linear system was indeed independent of peak height, eight equally spaced standards of bovine albumin (BSA) were prepared between 1 and 8 g dl^{-1}, labelled y_{1-8}, respectively. The samples were then divided into 3 series:

(1) series y_L in which y_1 was followed by y_1, y_1 by y_2, y_1 by y_3, y_1 by y_4 .... y_1 by y_8;

(2) series y_M was similarly arranged, with y_4 used in place of y_1;

(3) series y_H, with y_8 in place of y_1.

The samples were then run at 180 samples/h (Fig. 3), the peak heights being expressed in arbitrary units (Table 1). From the table it is clear that sample y_8 contributes the same amount to peak y_1 as it does to peak y_8, i.e. 40 units, confirming the premise that the carry-over is a constant. In this case, k_c = 40/452 = 0.088. Given $t_s = t_w$ = 10 s, t_c = 20 s (180 samples/h), and from

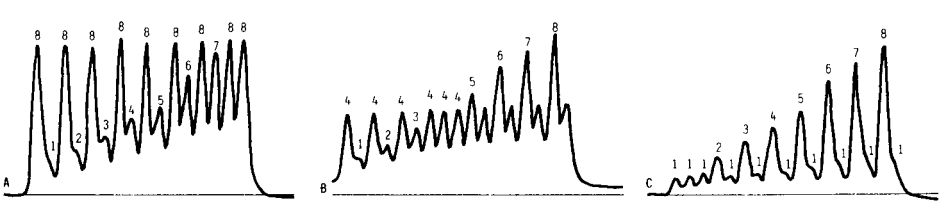

Fig. 3. Eight BSA standards run in sequence at 180 samples/h but each standard preceded by a high standard (A), medium standard (B) and low standard (C) to estimate the effect of peak height on the amount of sample carry-over.

TABLE 1

Change in peak height of standards repeated eight times when preceded by samples of increasing concentration[a]

Conc. of BSA in mg% of preceding sample	Peak heights (arbitrary units)							
	1	2	3	4	5	6	7	8
y_L	50	56	60	65	69	76	89	90
y_M	182	185	195	197	205	108	218	222
y_H	412	425	421	425	434	436	444	452

[a] y_L = 1 mg%, y_M = 4 mg%, y_H = 8 mg%.

$k_c = \exp(-t_c/B)$, B = 8.7 s.

The same total protein method was used with the system running at 240 samples/h for five BSA standards between 1 and 8 g dl^{-1} (Fig. 4). After the carry-over correction had been applied to each peak (*i.e.*, $y_i = y_i' - k_c y_{i-1}'$), the recovery on 40 samples at each level was 101.4% with a coefficient of variation of 2.7%. Obviously the peaks have been so degraded by sample carry-over that any meaningful manual or visual interpretation would be impossible.

In order to test the theory extended to non-linear systems, haptoglobin assays were done at 240 samples/h with 8 s of sample and 7 s of wash (Fig. 5). As expected, the ascending and descending calibration curves were significantly different (Fig. 2). The more accurate calibration curve is therefore the mean between the two. From Eqn. (7), $k_c = (y''_{100} - y'_{100})/(y''_{150} - y'_{50}) = 10/100 = 0.1$, where 100 mg% represents the middle standard y_M. Each peak is then corrected according to Eqn. (8).

In ten series of assays with between 20 and 40 samples in each series, the assay was first run at the normal speed of 120 samples/h and the concentrations were calculated manually from the peak heights. The assays were then immediately repeated on the same system at 240 samples/h but with the new program and interface. The regression equation between the two sets of results could be expressed as

$$y_{240} = 1.7\ (\pm 1.2) + (0.96 \pm 0.06) y_{120}$$

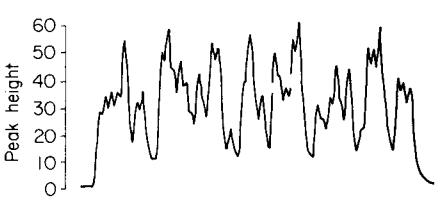

Fig. 4. Chart recording of total protein estimation at 240 samples/h using 5 standards in random order.

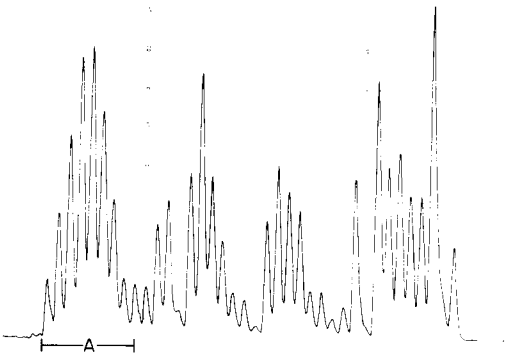

Fig. 5. Haptoglobin standards and samples at 240 assays/h. Curves over A are 4 standards at 50, 100, 150, 200 mg% in ascending/descending order. Subsequent curves are for samples.

Samples ranged from 20 to 280 mg% haptoglobin. Twenty runs of serum standards at 50, 100, 150 and 200 mg% randomly distributed showed a coefficient of variation of 2.3% at 240 samples/h compared to 1.6% at 120 samples/h. While more refined methods of calculating and correcting for sample carry-over would probably have reduced the imprecision, further improvements would not be clinically significant. The advantage of this simple technique is that the program can still be used by the Commodore PET in real time. Furthermore, the monitoring constant B is retained in the calculation for the carry-over constant as a continuous indicator for the operator as to system functioning. Experience with the automated immunoprecipitin system over 6 months has shown the B value to be stable. It retained its value to within ±1.5 s over the several weeks between routine maintenance.

Conclusion

Application of the simplified correction for sample carry-over in a continuous flow system makes it possible to achieve speeds of 240 assays per hour on standard AutoAnalyzers. The simplicity of the approach also makes possible the use of a cheap computer to calculate the corrected results in real time and to monitor system performance by calculating the B constant. Thus, improved automation has been achieved for standard systems with increased speed, with no significant loss of precision and with a continuous check on method reliability. It remains for the operator to decide on the allowable imprecision, to check the optimal performance through the B values and then increase the speed using the carry-over correction described until the imprecision becomes unacceptable.

We thank Dr. Michel Lievens and his staff at the International Institute of Cellular and Molecular Pathology, Unit of Experimental Medicine, Brussels, Belgium for their patient assistance in running the many assays necessary to validate the above technique.

REFERENCES

1 E. H. Hansen and J. Růžička, Anal. Chim. Acta, 87 (1976) 353.
2 J. Růžička and E. H. Hansen, Anal. Chim. Acta, 99 (1978) 37.
3 W. E. Neeley, S. Wardlaw and M. E. T. Swinnen, Clin. Chem., 20 (1974) 78.
4 W. H. C. Walker, J. Townsend and P. M. Keane, Clin. Chim. Acta, 36 (1972) 119.
5 E. B. M. de Jong and A. H. Weyden, Anal. Chim. Acta, 114 (1980) 311.
6 R. E. Thiers, J. Meyn and R. F. Wildermann, Clin. Chem., 16 (10) (1970) 832.
7 P. M. G. Broughton, M. A. Buttolph, A. H. Gowenlock, D. W. Niell and R. G. Skentleberry, J. Clin. Pathol., 22 (1969) 278.
8 R. E. Thiers, R. R. Cole and W. J. Kirsch, Clin. Chem., 13 (6) (1967) 451.

Analytica Chimica Acta, 145 (1983) 59—70
Elsevier Scientific Publishing Company, Amsterdam — Printed in The Netherlands

A POSSIBLE APPROACH TO THE OPTIMIZATION OF FLOW INJECTION ANALYSIS

J. M. REIJN[a] and H. POPPE*

Laboratory for Analytical Chemistry, University of Amsterdam, Nieuwe Achtergracht 166, 1018 WV Amsterdam (The Netherlands)

W. E. VAN DER LINDEN

Laboratory for Chemical Analysis, Twente University of Technology, P.O. Box 217, 7500 AE Enschede (The Netherlands)

(Received 21st April 1982)

SUMMARY

The theory of sample zone dispersion is well known for most cases of practical interest in flow injection analysis. This paper offers a theoretical analysis which allows for the optimal design of single-line flow systems. For various reactor types, a detailed analysis is provided in terms of physical constants, design parameters and constraints.

It is shown that, within practical constraints and using a pressure drop of less than 1 bar, it is possible to operate flow systems at 100 samples per hour, with a residence time of 100 s and a reagent consumption of 8 μl for each determination. Further miniaturization of flow systems must rely on smaller detector volumes than those currently available, a situation not unlike that in liquid chromatography.

This paper is concerned with the performance of systems for flow injection analysis (f.i.a.). Three types of parameters of the flow system can be distinguished: physical constants which are characteristic of dilute aqueous solutions, like the molecular diffusion coefficient D_m and the viscosity; design parameters like the helix diameter in a coiled reactor or the bed diameter in a packed-bed reactor; and performance-limiting parameters (constraints) such as the maximum pressure drop over the reactor, the smallest acceptable tube diameter or the smallest detector volume that is allowed for. Equations for the optimal design of flow injection systems are presented, which show clearly when a constraint parameter actually limits the performance. The values of the constraint parameters are obtained from f.i.a. practice.

Although Růžička and Hansen [1] have pointed out correctly the differences between f.i.a. and high-performance liquid chromatography (h.p.l.c.), the present treatment is based on optimization studies in h.p.l.c. by Knox et al. [2, 3] and Guiochon [4]. Throughout this work, it is assumed that the elution (response) curve of the flow reactor (column) is Gaussian. It

[a]Present address: Department of Bioengineering, University of Utah, Salt Lake City, UT 84112, U.S.A.

was shown earlier [5] that the flow conditions must be chosen in such a way that the number of tanks to which the reactor is equivalent is greater than 50 ($Pe_L > 100$) in order to satisfy this condition.

The following chromatographic definitions are used. The plate height H is defined as:

$$H = L\ (\sigma_t/m_t)^2 \tag{1}$$

In this definition L is the length of the reactor, and m_t is the mean and σ_t^2 the variance of the response curve. For small sample volumes, the mean virtually equals the residence time t_v. The plate number N (which in f.i.a. is known as the number of tanks) is given by

$$N = L/H = (m_t/\sigma_t)^2 \tag{2}$$

In chromatography the plate number is related to the chromatographic resolution, whereas in f.i.a. the number of tanks is related to the maximum sampling frequency:

$$f_{max} = k_1/\sigma_t \text{ or } N = (f_{max}\, t_v/k_1)^2 \tag{3}$$

(For convenience, all symbols are defined in Table 1.) When f_{max} is expressed in $(h)^{-1}$ and a pessimistic value for the base-width of the peak of 6 σ_t is taken, the numerical value of k_1 is 600. Most authors [1] take k_1 equal to 900 corresponding to a base-width of 4 σ_t. For a given reactor, the plate number is determined by the dispersion, when the injection volume is sufficiently small. The relevant equations for the flow conditions and the dispersion are summarized in Table 2. When a characteristic length d is introduced, these equations are generally valid for any reactor type. In open tubes, this length is equal to the tube diameter d_t; in packed reactors it is equal to the particle diameter d_p.

TABLE 1

List of symbols

A	Free cross-sectional area of packed reactor	N	Plate number
A_c	Constant in plate height equation of coiled tube	ΔP	Pressure drop over the reactor
C	Constant in plate height equation of straight tube	Pe_L	Péclet number
d	Characteristic length	Re	Reynolds number
d_h	Helix diameter (coiled tube)	Sc	Schmidt number
d_p	Particle diameter	$\langle v \rangle$	Linear velocity of fluid
d_t	Tube diameter	v	Reduced velocity
D_m	Molecular diffusion coefficient	α	Ratio of sample volume and reactor volume
Dn	Dean number	ϵ	Void fraction of packed reactor
f_{max}	Maximal sampling frequency	η	Dynamic viscosity
f_v	Volumetric flow rate	κ	Peak width reduction coefficient
h	Reduced plate height	λ	Aspect ratio of coiled tube (d_h/d_t)
H	Plate height	ν	Kinematic viscosity
k_1	Proportionality factor in sampling frequency	ρ	Ratio of tube diameter and particle diameter
L	Reactor length	σ_t^2	Variance of response curve (in time units)
m_t	Mean of response curve (in time units)	σ_V^2	Variance of response curve (in volume units)
n	Number of tanks	ϕ	Column resistance factor

TABLE 2

General flow equations

$\langle v \rangle$	=	$d^2 \Delta P / \phi \eta L$	(a)	L	=	$N h d$	(e)
t_v	=	$L/\langle v \rangle = N^2 h^2 \phi \eta / \Delta P$	(b)	d^2	=	$N h v \phi \eta D_m / \Delta P$	(f)
v	=	$\langle v \rangle d / D_m$	(c)	σ_V^0	=	$L A N^{-1/2}$	(g)
h	=	$f(v)$	(d)				

For dilute aqueous solutions, $\eta = 10^{-3}$ N s m^{-2} and $D_m = 10^{-9}$ m^2 s^{-1}.

The first equation in Table 2, Eqn. (a), relates the mean fluid velocity $\langle v \rangle$ and the pressure drop over the reactor ΔP. The column resistance factor ϕ depends on the type of reactor. The dynamic viscosity, η, for dilute aqueous solutions has the numerical value 10^{-3} (N s m^{-2}). The residence time (in h.p.l.c. the elution time for a component without retention) is given by Eqn. (b). It is convenient to use dimensionless quantities for the mean fluid velocity and for the plate height. The reduced velocity is defined in Eqn. (c) and can also be written as $v = Re\ Sc$. For dilute aqueous solutions, the kinematic viscosity, ν, is 10^{-6} (m^2 s^{-1}) and the molecular diffusion coefficient can be taken as 10^{-9} (m^2 s^{-1}). Therefore the Schmidt number, Sc, equals 1000. The Reynolds number, Re, is based on the appropriate characteristic length: $Re = \langle v \rangle d/\nu$. The reduced plate height h is defined as $h = H/d$. The reduced plate height is a function of the reduced velocity and the geometry of the reactor, whereas in chromatography often other contributions (e.g., mass transport between mobile and stationary phase) are also encountered. As there is no retention of the solute in f.i.a., the plate-height equations are simpler than those in h.p.l.c. The reactor length L is given by Eqn. (e). The correct value for the characteristic length d is given by Eqn. (f). In order to avoid additional peak broadening in the detector [6], the detector volume should not exceed one half of the volume variance of the peak σ_V^0. This parameter, which is not in common use in f.i.a., is defined as

$$\sigma_V^0 = \langle v \rangle A \sigma_t = f_v \sigma_t \tag{4}$$

where A is the free cross-area of the reactor and f_v is the volumetric flow rate (in m^3 s^{-1}). It should be noted that the parameter 4 σ_V^0 can be taken as an (optimistic) quantitative measure of reagent consumption per analysis. For open tubes and single bead string reactors (SBSR) [6], the free cross-area is entirely determined by d. For packed reactors with more particles per tube diameter, A can be adjusted by variation of the tube diameter. The equations in Table 2 are completely general, but not yet in a form suitable for calculations. Therefore more detailed relationships for different reactor types are presented in later tables.

OPTIMIZATION IN FLOW INJECTION ANALYSIS

The main goal of h.p.l.c. optimization studies is to minimize the separation time with a given plate number. In f.i.a. the plate number plays no role

on its own, because separation is not intended. The flow reactor has two functions: mixing of sample and reagent and providing a delay time for conversion of the analyte. From Eqn. (3), it can be seen that the sampling frequency is inversely proportional to the residence time: $f_{max} = k_1 t_v^{-1} N^{1/2}$. Therefore, in the case of chemical conversions, the optimization objective can be formulated as making N maximal, which is equivalent to making σ_t minimal, both at a fixed residence time, the value of which is dictated by the level of conversion which is aimed at. In the present treatment, the residence time is considered as a design parameter, the value of which is determined by the chemistry, temperature and concentration levels both of the analyte and the reagent solutions.

Inspection of plate-height equations reveals that in theory it is possible to obtain any plate number for instance by a decrease in characteristic length d. It is obvious that this approach leads to values of other experimental parameters, such as pressure drop and tube diameter, which are inacceptable from a practical, financial, measuring or other point of view. In the optimization procedure, one, more or all of these parameters may limit the performance of the flow system. It is emphasized here that the objective of maximizing the sampling frequency is not the only objective that can be optimized in a f.i.a. system. For instance, the object may be to minimize the reagent consumption per analysis or to minimize errors in the determination. In such cases, the sampling frequency can be treated as a constraint parameter which may not fall below a certain minimum value.

The intuitive approach to the objective of maximizing the sampling frequency is overall miniaturization of the system. Then at least two constraints are encountered: the pressure drop increases and the volume variance of the peak decreases, leading to impossibly small detector volumes. Intuition predicts that the optimal performance is expected at the highest available pressure drop and the lowest detector volume. In the following sections a detailed analysis is presented for different reactor types.

Straight open tubes

The relevant equations for straight open tubes are summarized in Table 3. The column resistance factor is 32 in this case. The plate-height equation is the familiar Aris—Taylor equation, which is valid [5] for $N > 30$ or when $t_v D_m / d^2 > 0.07$. An attractive feature of Eqn. (i) seems to be the occurrence of a minimum for h. However this minimum $h = 1/12^{1/2}$ at $v = (192)^{1/2}$ is

TABLE 3

Equations for straight open tubes

ϕ	=	32	(h)
h	=	$2/v + Cv$ (in f.i.a., $C = 1/96$)	(i)
h	=	Cv (large v)	(j)
d^2	=	$N h^2 \phi \eta D_m / C \Delta P$	(k)
$4 \sigma_V^0$	=	$\pi d^3 h N^{1/2}$	(l)

not of practical interest. In practical f.i.a. applications, high reduced velocities are used. In that case, the plate-height equation can be simplified. The correct tube diameter in this case is given by Eqn. (k). For an open tube, $A = \pi d^2/4$ and the volume variance σ_V^0 is given by Eqn. (l). In further derivations, the parameter $(4\ \sigma_V^0)$ will be used as a quantitative measure for the reagent consumption per analysis.

Following the analysis by Knox and Gilbert [3], equations for d, h, l and N can be derived which give each of these quantities as a function of the physical constants, the constraint parameters and (optionally) the design parameters. When h is eliminated between Eqns. (k) and (l) the tube diameter is obtained:

$$d = (\phi\eta\, D_m/\pi^2\,\Delta PC)^{1/8}\,(4\,\sigma_V^0)^{1/4} \tag{5}$$

From this equation the corresponding value for the reduced plate height is:

$$h = (C^3\,\Delta P/\pi^2\phi\eta D_m^3)^{1/4}\ (t_v)^{-1/2}(4\,\sigma_V^0)^{1/2} \tag{6}$$

From Eqn. (b), N is given by

$$N = (\pi^2 D_m{}^3\,\Delta P/C^3\phi\eta)^{1/4}(t_v)\,(4\,\sigma_V^0)^{-1/2} \tag{7}$$

The reactor length is found from Eqn. (e):

$$L = (D_m\,\Delta P^3/\pi^2 C\phi^3\eta^3)^{1/8}\,(t_v)^{1/2}\,(4\,\sigma_V^0)^{1/4} \tag{8}$$

The maximum sampling frequency is found from Eqns. (3) and (7):

$$f_{max} = k_1\ (t_v)^{-1/2}\ (\pi^2 D_m\Delta P/C^3\phi\eta)^{1/8}\,(4\,\sigma_V^0)^{-1/4} \tag{9}$$

From these design equations, important conclusions can be drawn. First, a high sampling frequency is favored by a small detector volume and also by high pressure drops. This supports the arguments for miniaturization, but the detector volume will soon be the constraint. For example, at a pressure drop of 1 bar the tube diameter is 145 μm for a detector volume of 1 μl, and it is 82 μm for a detector volume of 0.1 μl. The sampling frequency for the latter case is twice the sampling frequency for the larger detector. Secondly, short residence times allow for high sampling frequencies. A constraint is the requirement $N > 30$. Thirdly, as can be seen from Eqn. (9), high pressure drops are advantageous, although the sampling frequency is rather weakly dependent on the pressure drop. In f.i.a., the pressure drop should not exceed 1 bar (10^5N m^{-2}). However, in chromatography when the detector volume and the plate number are fixed, the only way to decrease analysis time is to increase the pressure drop as can be seen from Eqn. (9). Note that in this case a constraint can also be posed by the tube diameter (Eqn. 5).

Coiled tubes

In helically coiled tubes, both the pressure drop and the dispersion are influenced by the secondary flow phenomenon (Tijssen [7]). Equations for coiled tubes are given in Table 4. The Reynolds number is replaced by the Dean number Dn ($= Re/\lambda^{1/2}$; λ is the ratio of the helix diameter and the tube

TABLE 4

Equations for coiled tubes

ϕ	=	$32\,[1 + f(Dn)]$		(m)
h	=	$C\,\upsilon\,\kappa(\upsilon)$	(large υ)	(n)
κ	=	$5.6\,Sc^{1/3}\,\lambda^{1/3}\,\upsilon^{-2/3}$	(large υ)	(o)
h	=	$A_c\,d^{-1/3}\,\upsilon^{1/3}$		(p)
A_c	=	$5.6\,d_h^{1/3}\,Sc^{1/3}C$		(q)
d	=	$N h^4 \phi\,\eta\,D_m/\Delta P\,A_c^3$		(r)

diameter). For values of $Dn > 100$, the pressure drop is not different from its value in a straight tube at the same flow velocity ($f(Dn) \rightarrow 0$ in Eqn. m). The effect of the secondary flow on the reduced plate height can be described by a peak-width reduction coefficient κ (Eqn. o). An empirical correlation for κ as a function of $Dn\,Sc^{1/2}$ has been presented by Van den Berg et al. [8]. In the region $12.5 < Dn\,Sc^{1/2} < 200$, κ is given by $\kappa = 5.6\,(Dn\,Sc^{1/2})^{-0.67}$.

For lower values of the velocity, no secondary flow phenomena are observed in the dispersion. For values of $Dn\,Sc^{1/2}$ above 200, no reliable correlations for the dispersion are available as yet. Tijssen's correlations are probably too optimistic. Therefore, in this treatment, it will be assumed that only coils in the region described by the correlation of Van den Berg et al. [8] are taken into consideration. The results for lower velocities are presented above in the section on straight tubes.

A general strategy for the optimization of the coiled tubes is suggested by Eqn. (n). When C is replaced by $C\,\kappa(\upsilon)$ in Eqns. (5—9), then a trial-and-error procedure enables the design equations to be solved. By a little rearrangement, Eqns. (o—r) are the starting point for the design equations. In this treatment, the helix diameter d_h is considered to have a given value (e.g., 5 mm). Proceeding in an entirely analogous way as in the previous section, the following equations for d, h, N, L and f_{max} are obtained:

$$d = (\phi^2\eta^2 D_m/\pi^6 A_c{}^3\Delta P^2)^{1/19}(t_v)^{-1/19}\,(4\,\sigma_V^0)^{6/19} \tag{10}$$

$$h = (A_c^{36}\Delta P^5/\phi^5\eta^5\pi^4 D_m^{12})^{1/38}(t_v)^{-7/38}\,(4\,\sigma_V^0)^{2/19} \tag{11}$$

$$N = (\pi^2 D_m^6\Delta P^7/A_c^{18}\phi^7\eta^7)^{1/19}(t_v)^{13/19}\,(4\,\sigma_V^0)^{-2/19} \tag{12}$$

$$L = (D_m^2\Delta P^{15}/A_c^6\phi^{15}\eta^{15}\pi^{12})^{1/38}(t_v)^{17/38}\,(4\,\sigma_V^0)^{6/19} \tag{13}$$

$$f_{max} = k_1(t_v)^{-25/38}(A_c^{18}\eta^7\phi^7/\pi^2 D_m^6\Delta P^7)^{-1/38}\,(4\,\sigma_V^0)^{-1/19} \tag{14}$$

When Eqns. (10—14) are compared with their counterparts for straight tubes, it is seen that the optimal tube diameter is now a function of the residence time t_v. In practice, when only a limited number of tube diameters is available, the use of a non-optimal tube diameter will lead to a slightly increased reagent consumption or loss of maximum sampling frequency.

Packed reactors

To a first approximation, the general flow equation (a) (Table 2) for the pressure drop remains valid in the case of packed reactors. Values for the column resistance factor ϕ are given by Knox and Gilbert [3] as $\phi = 500$, by Guiochon [4] as $\phi = 500$—1000 and by Van den Berg et al. [8] as $\phi = 800$. In this section the value $\phi = 1000$ will be used. The product of constants η and ϕ then has the numerical value 1. The equations for packed reactors are summarized in Table 5. A packed reactor can be operated at the minimum of the h--v curve, because the volume variance of the peak can be adjusted by adjustment of the reactor diameter d_c (Eqn. w). The parameter ϵ is the void fraction of the packed reactor, which has the value 0.4 for a properly packed reactor. The minimum of the h—v curve is found as $h = 2$ at $v = 4$ (Knox and Gilbert [3]). The design equations now simplify considerably, although it should be kept in mind that a constraint parameter in the particle diameter d_p has been introduced deliberately here. This parameter can no longer be chosen freely, because it was decided to work at the minimum in the h—v curve.

The general time equation (b) is simplified to Eqn. (u), yielding the plate number N as $N = (t_v \Delta P/4)^{1/2}$. The corresponding sampling frequency is given by

$$f_{max} = k_1 (t_v)^{-3/4} (\Delta P/4)^{1/4} \tag{15}$$

The correct particle diameter is given by (Eqn. v)

$$d = (16\, t_v/\Delta P)^{1/4} (D_m)^{1/2} \tag{16}$$

The reactor length and the reagent consumption (from Eqn. w) are then

$$L = (16\, t_V^3 \Delta P D_m^2)^{1/4} \tag{17}$$

$$(4\, \sigma_V^0) = (\pi \epsilon\, d_c^2)\, (2 D_m\, t_v)^{1/2} \tag{18}$$

Two conclusions can be drawn from these design equations. First, when the pressure drop is made as high as possible in order to maximize the sampling frequency, the particle diameter will be a constraint, as shown by the fact that at 1 bar the particle diameters range from 3.5 to 20 μm when the residence time varies from 1 to 1000 s. Secondly, the reagent consumption equation (18) leaves two alternatives: either the reagent consumption may be kept constant for different residence times (case D′) so that the bed diameter must be optimized; or (case D) it can be decided to fix the bed

TABLE 5

Equations for packed reactors

ϕ	=	$1000; \phi\, \eta = 1$	(s)
h	=	2 (at the optimum; $v = 4$)	(t)
t_v	=	$4\, N^2/\Delta P$	(u)
d^2	=	$8\, N D_m/\Delta P$	(v)
$4\, \sigma_V$	=	$\pi\, \epsilon\, d_c^2\, 2\, d\, N^{1/2}$	(w)

diameter d_c, so that the reagent consumption is a function of the residence time.

Single bead string reactor

For the SBSR, the pressure drop relation (a) remains approximately valid, as experiments indicated. The column resistance factor was evaluated as approximately 500. Therefore, $\phi\eta$ is taken as 0.5 here. No rigorous plate-height equation for the SBSR is known yet. For the particular reactor described by Reijn et al. [5] the plate height h was found to be ≈ 10 for velocities from 3000 to 30 000. Later experiments confirmed this result for the same reactor geometry (d_p = 0.6 mm; d_c = 0.75 mm). This time h = 8 was found; the latter value of h will be taken here for the further deduction.

The equations for the SBSR are summarized in Table 6. In a similar way as before, design equations are obtained for the plate number and sampling frequency:

$$N = (\Delta P\, t_v/32)^{1/2} \tag{19}$$

$$f_{max} = k_1\, (t_v)^{-3/4}\, (\Delta P/32)^{1/4} \tag{20}$$

In contrast to the preceding case of the packed reactor operated at the optimum flow conditions, no constraints on the characteristic length d are imposed by the flow conditions for a SBSR, because the flow velocity can be varied over a wide range (Eqn. z).

However, the reagent consumption contains the characteristic length as a parameter. When the free cross-area for a SBSR is calculated as $(\pi\epsilon\rho^2 d^2)$ and the term $(\pi\epsilon\rho^2)$ is given the numerical value 2, then

$$4\sigma_V^0 = 16\, d^3 N^{1/2} = 16\, d^3\, (\Delta P\, t_v/32)^{1/4} \tag{21}$$

The role of the particle diameter in the SBSR can be compared with the role of the column diameter of the packed reactor.

From these design equations, the following conclusions can be drawn. First, the reactor should be operated at the highest possible pressure drop to obtain the maximal sampling frequency. Secondly, if operation with the reagent consumption as a constraint is desired (at the lowest acceptable value allowed by the detector volume), the particle diameter becomes a function of the residence time. This also influences the length of the reactor as $L = 8\,N\,d$. Finally, the reactor can be operated with a constant characteristic length, but the reagent consumption then becomes a function of the residence time.

TABLE 6

Equations for the SBSR

ϕ	=	$500; \phi\,\eta = 1/2$	(x)
t_v	=	$32\,N^2/\Delta P$	(y)
d^2	=	$4\,N\,v\,D_m/\Delta P$	(z)

DISCUSSION

The design equations presented above allow a comparison of the performance between the four reactor types considered. Some graphical illustrations are now given for the sake of clarity. As pointed out above, the performance of all reactor types with respect to sampling frequency is optimal at the highest pressure drop. This parameter is fixed at 1 bar. Figure 1 presents the results for open tubes (A straight, B coiled reactor) where an additional constraint is formed by the detector volume. This was chosen as 1 μl ($4\sigma_V^0$ is then 8 μl); yet another constraint for the open tubes is the condition for validity of the Taylor theory $N > 30$, or in the present examples, $t > 6$ (s). The packed reactors, i.e., the SBSR and the packed reactor operated at the optimum, are not subject to the detector volume constraint directly.

Figures 2 and 3 present the dimensions of the design. The characteristic length d in Fig. 2 corresponds to the tube diameter in cases A and B and to the particle diameter in cases C and D. The line C′ gives the required particle diameter for the SBSR operated at a constant reagent consumption; line D′ gives the bed diameter for the packed reactor in the same case.

The reagent consumption per analysis is given in Fig. 4. This parameter was taken as a constraint in cases A, B, C′, D′. It is seen that the design corresponding to D for residence times lower than 30 s is inacceptable from

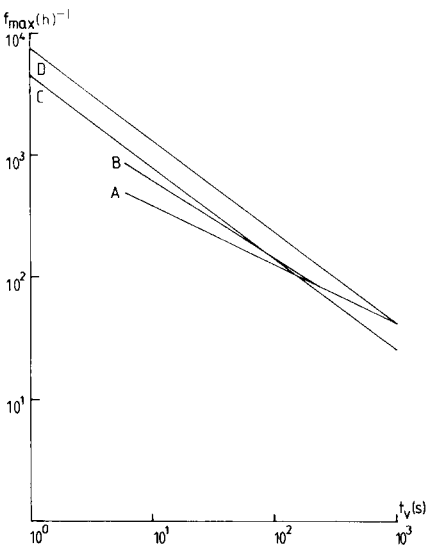

Fig. 1. Sampling frequency as a function of the residence time t_V. Pressure drop, 1 bar; reagent consumption, 8 μl for the open tubes. (A) Straight open tube; (B) coiled tube; (C) SBSR; (D) packed reactor operated at optimal conditions. Further design information is provided in Figs. 2 and 3.

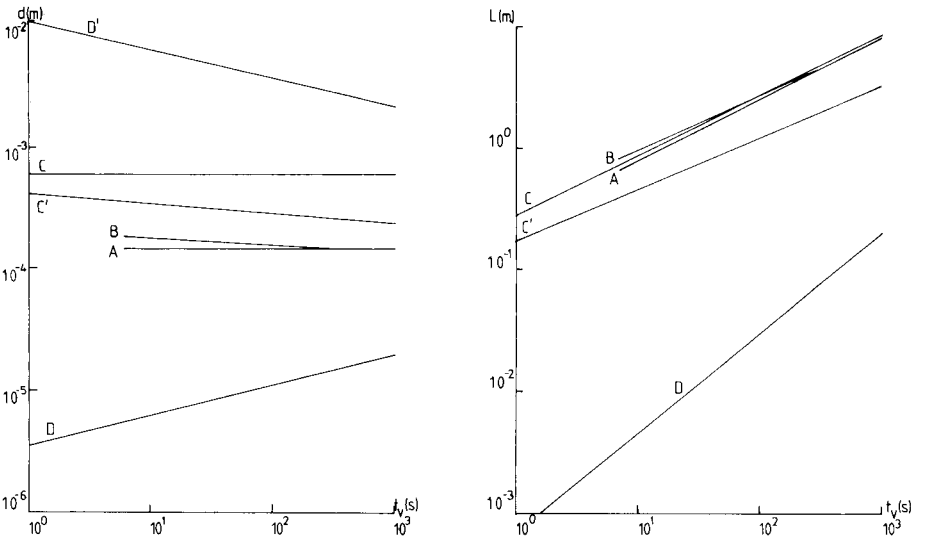

Fig. 2. Dimensions of the reactors as a function of the residence time t_v. Pressure drop, 1 bar. (A) Straight open tube; (B) coiled tube; (C') SBSR; all three reactors are operated at a constant reagent consumption of 8 μl. (D) Particle diameter for the packed reactors; (D') bed diameter for the packed reactor operated at a constant reagent consumption of 8 μl.

Fig. 3. Reactor length as a function of the residence time t_v. Pressure drop, 1 bar. (A) Straight open tube; (B) coiled tube; (C') SBSR; all three reactors are operated at a constant reagent consumption of 8 μl. (C) SBSR of a fixed geometry (see text); (D) packed reactor.

detector volume requirements. The SBSR with a constant geometry has the highest reagent consumption (case C). This comparison enables several conclusions to be drawn. Thus, all four reactor types allow for sampling frequencies over 100 h^{-1} at residence times of about 100 s and at a reagent consumption of 8 μl per analysis, at a pressure drop of 1 bar. The SBSR is characterized by a good performance at very favorable dimensions (e.g., design C). It is a worthwhile alternative in f.i.a. for the packed reactor operated at optimal flow conditions.

The performance of the f.i.a. reactors may be compared with the Auto-Analyzer approach. Snyder [9] states that, for the SMAC analyzer operated at a flow rate of 600 μl min^{-1} at a bubbling rate of 2 s^{-1}, the sampling frequency is 265 h^{-1} at a residence time of 500 s. This figure is higher than can be reached in f.i.a. with the present constraints, and the result is achieved at a reagent consumption of 150 μl per analysis.

Influence of the sample volume

When the parameter α is defined as the ratio of the sample volume, V_s and the reactor volume, V_r, it can be derived from earlier work [10] that for

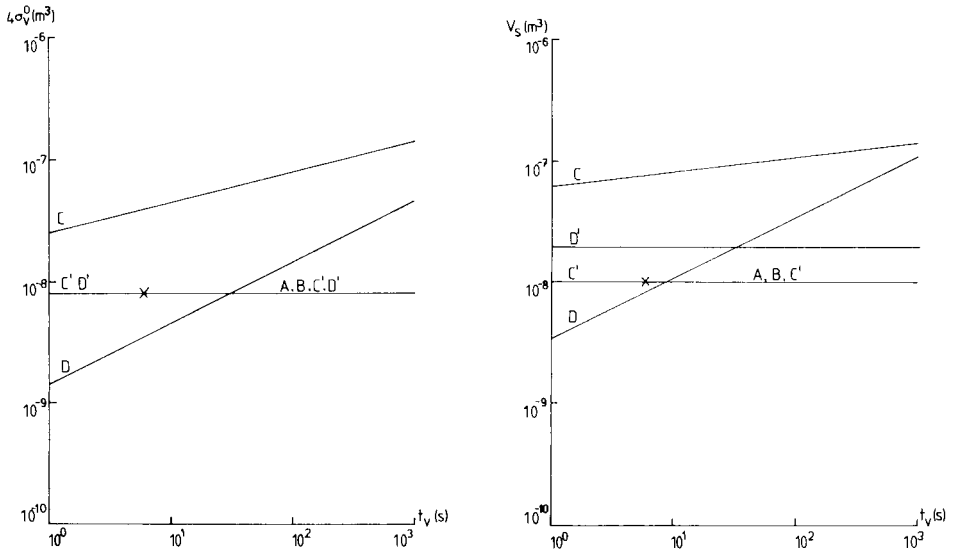

Fig. 4. Reagent consumption per analysis (4 σ_V^0) as a function of the residence time t_v. Pressure drop, 1 bar. (A) Straight open tube; (B) coiled tube; (C') SBSR; (D') packed reactor; all reactors were designed with this variable as a constraint parameter. (C) SBSR with a constant geometry; (D) packed reactor with a constant bed diameter (5 mm).

Fig. 5. Maximum allowable sample volume as a function of the residence time t_v. Pressure drop, 1 bar. (A) Straight open tube; (B) coiled tube; (C') SBSR; all three reactors are operated at a reagent consumption of 8 μl. (D') Packed reactor with the same reagent consumption as the other three reactors; (C) SBSR of constant geometry; (D) packed reactor with a fixed bed diameter (5 mm).

a non-reacting sample a dilution factor of 2 is obtained when $\alpha\, n^{1/2} = 2^{1/2}$. The time variance of the response curve in this case is $\sigma_t^2 = (1/n + \alpha^2/12)\, t_v^2 = (14/12\, n)\, t_v^2$. The sampling frequency is then given by

$$f_{max} = k_1\, (t_v)^{-1}\, N^{1/2}\, 0.93 \qquad (22)$$

It is seen that injection of a sample volume corresponding to $V_s = V_r\, 2^{1/2}/n^{1/2}$ results in a slight loss of maximal sampling frequency, while the reactor is operated at a dilution of only two. The influence of chemical kinetics has been investigated [11]. It was concluded from that work that, for first-order kinetics and adequate mixing of sample and reagent, it is useless to operate a f.i.a. reactor at residence times longer than needed to reach a conversion level of say 63% at sample volumes larger than corresponding to $\alpha\, n^{1/2} = 2^{1/2}$. Quite straightforward calculations indicate that for the cases A, B, C' and D' the maximum allowable sample volume is independent of the residence time. Figure 5 illustrates the result of these calculations for $\alpha\, n^{1/2} = 2^{1/2}$. The high sample volume that the SBSR can accommodate when operated at a constant particle diameter should be noted.

Conclusion

Complete design equations for flow injection systems are presented; the equations allow optimization of these systems. The equations are evaluated for the optimization objectives of maximal sampling frequency and minimal reagent consumption. Constraints in the optimization procedure are the pressure drop which should not exceed 1 bar in f.i.a. and the detector volume. It is concluded that reduction of the detector volume is the most promising way of improving the performance of (miniaturized) f.i.a. systems.

The authors thank Dr. R. J. Jonker for valuable discussions and for his suggestion to apply the analysis of Knox and Saleem to f.i.a.

REFERENCES

1 J. Růžička and E. H. Hansen, Flow Injection Analysis, Wiley, New York, 1981.
2 J. H. Knox and M. Saleem, J. Chromatogr. Sci., 7 (1969) 614.
3 J. H. Knox and M. T. Gilbert, J. Chromatogr., 186 (1979) 405.
4 G. Guiochon, Anal. Chem., 53 (1981) 1318.
5 J. M. Reijn, W. E. Van der Linden and H. Poppe, Anal. Chim. Acta, 126 (1981) 1.
6 H. Poppe, Anal. Chim. Acta, 114 (1980) 59.
7 R. Tijssen, Anal. Chim. Acta, 114 (1980) 71.
8 J. H. M. Van den Berg, R. S. Deelder and H. G. M. Egberink, Anal. Chim. Acta, 114 (1980) 91.
9 L. R. Snyder, Anal. Chim. Acta, 114 (1980) 3.
10 J. M. Reijn, W. E. Van der Linden and H. Poppe, Anal. Chim. Acta, 114 (1980) 105.
11 J. M. Reijn, W. E. Van der Linden and H. Poppe, Anal. Chem., submitted.

Analytica Chimica Acta, 145 (1983) 71—85
Elsevier Scientific Publishing Company, Amsterdam — Printed in The Netherlands

ENZYME REACTORS IN UNSEGMENTED FLOW INJECTION ANALYSIS

GILLIS JOHANSSON*, LARS ÖGREN[a] and BO OLSSON
Analytical Chemistry, University of Lund, P.O. Box 740, S-220 07 Lund (Sweden)
(Received 20th August 1982)

SUMMARY

The design of immobilized-enzyme reactors for use in flow injection analysis is discussed. The reactors should be optimized for a short residence time and a very high (>99.9%) conversion of substrate to products. Selection of carrier and immobilization method is important in order to increase the amount of active enzyme per unit volume. The efficiency of the reactor can be increased by decreasing the particle size in packed-bed reactors and the radius of open tubular reactors. The maximum inherent rate constant that can be obtained under optimal conditions is estimated for a number of enzymes of analytical interest; it is shown that with high rate constants and small particle diameters, residence times less than seconds can be obtained. Some applications of immobilized-enzyme reactors in flow systems are reviewed.

A combination of the flow injection technique described by Růžička and Hansen [1] and Stewart [2] with enzymatic methods of analysis should be able to produce useful solutions to a broad range of problems. It is advantageous to merge the speed and simplicity of flow injection analysis (f.i.a.) with the selectivity of the enzymatic methods, especially with immobilized-enzyme reactors optimized for the technique.

Reactor design has been studied in chemical engineering, both from theoretical [3, 4] and practical points of view. Enzyme reactors constitute a special case of a more general theory. Only liquid moving phases and solid unshrinkable, incompressible supports for the catalyst have to be considered. The reactions occur isothermally, because of the small reactor dimensions and the low substrate concentrations.

Analytical reactors should be able to process an impulse or a short plug of substrate with little dispersion and preferably with close to 100% conversion of substrate to products. The dispersion is normally of secondary importance in the bio-engineering field and high conversions are often avoided in order to improve production economy. The rate of conversion in a reactor depends on the rate of the chemical reaction as well as on the rate of the mass transfer. The chemical rate depends on the intrinsic kinetics of the immobilized enzyme and on the amount of catalyst. The dispersion can be reduced by appropriate reduction of reactor dimensions. It is thus necessary to con-

[a]Present address: AB Draco, P.O. Box 1707, S-221 01 Lund, Sweden.

0003-2670/83/0000-0000/$03.00

centrate the enzyme into a smaller volume or to increase the efficiency of mass transfer. With surface-bound enzymes, the amount of enzyme will depend on the total surface area and on the number of molecules per unit surface. Carr and Bowers [5] have recently reviewed the literature on analytical enzyme reactors and summed up the work in the field. The discussion in this paper will be restricted to packed-bed reactors with the enzyme immobilized in particles of porous support and to open tubular reactors with a thin enzyme layer on the walls.

SURFACE AREA PER UNIT VOLUME

A packed-bed reactor will develop dead volumes unless it is filled with a pressure-resistant support material. Porous glass seems to be one of the most suitable supports commonly used. It is available as chips of various sizes and pore diameters. The enzyme loading is to a first approximation proportional to the surface area [6], provided that the pore diameter is larger than the effective enzyme diameter. Table 1 shows how the surface area increases with a decreased pore diameter. The conclusion to be drawn at this stage is that the smallest possible pore diameter should be used in order to compound as much enzyme as possible into each unit volume.

The geometrical areas of open tubular reactors are several orders of magnitude less, compared on the basis of equal volumes (Table 1). Direct immobilization on the wall would give an enzyme loading of 0.1—1 mg m^{-2} and the amount of enzyme would thus be too low for analytical purposes even if the mass transfer were very fast. Some surface enlargement technique is therefore necessary in order to increase the enzyme loading. Nylon and other plastic tubings have been etched or hydrolyzed [7—14] or the enzyme has been immobilized in a porous silica layer or in a polyanionic gel on the tube wall [14, 15]. With the latter type, the inside area could be increased by irregularities in the coating, the "fuzzy wall" reactor, a design which enhanced the mass transfer. The surface area of glass capillaries can be enlarged very greatly by growing whiskers on the inside [16].

TABLE 1

Surface areas of some enzyme reactors all with a void volume of 100 μl (100 μl of CGP-10 ≃ 40 mg, total void fraction ≃ 0.8)

Packed-bed (CPG-10)		Open tubular		
Pore diameter (nm)	Area (m^2)	I.d. (mm)	Length (m)	Area (m^2)
24	5.5	0.1	12	0.004
35	3.8	0.2	3.2	0.002
50	2.5	0.5	0.5	0.0008
100	1.3	1.0	0.12	0.0004

ENZYME ACTIVITY PER UNIT SURFACE

A wealth of literature is available about methods for enzyme immobilization [17—19] and for each type of support material several possibilities have been worked out. Glass can be silylated giving alkylamino or arylamino derivatives to which enzyme can be bound by means of, e.g., glutaraldehyde, isothiocyanate, carbodiimide, triazine or azo coupling [5, 17, 19]. No one method is generally superior, for the loading and the stability will vary depending on the enzyme. For example, it was found that azo coupling is superior to glutaraldehyde coupling for immobilizing peroxidase [20, 21]. The opposite was true when lactate dehydrogenase was immobilized to the same type of support [22].

The type of linkage, the support material and the method of immobilization will influence the hydrophobicity and charge around the active center of the enzyme. Such factors may have pronounced effects on the substrate binding constant and the maximum rate of reaction, as well as on the pH optimum and sensitivity towards changes in ionic strength. The Michaelis constant may thus be altered by more than one order of magnitude [23].

Enzymes are normally not very pure as received and the impurities may interfere in several ways. They may be immobilized and thus compete with the active enzyme for sites on the support, and they may even be bound preferentially [21]. Impurities may deactivate the enzyme (proteolytic enzymes), and they may interfere with the reaction (catalase in reactions producing hydrogen peroxide) or lower the selectivity by forming products which are sensed by the detector.

An enzyme is bound to a support with many covalent bounds so that the stability towards shear forces becomes high [24]. Some of the enzyme remaining on the carrier after the immobilization is only physically adsorbed, however. Unless removed by thorough washing, it will desorb when the reactor is put into use and give rise to a fast initial loss of activity. Several other factors may contribute to a rapid deactivation with time. The most dramatic is bacterial growth which results in a sudden loss of activity. The sensitivity towards infection varies; e.g., peroxidase is almost immune, and even has a bactericidal effect [25]. Precautions include boiling of reagents, especially deionized water, dialysis or sterile filtration of samples, or addition of preservatives.

Heavy metals may be bound very tightly to an enzyme and inhibit its catalytic action. Metal contamination may occur during the immobilization or through the feed stream to the reactor [26]. Reactivation by treatment with a strong complex-former or on-line purification with a chelating resin may remove the metals [27]. Soluble chelating reagents will deactivate some enzymes [28].

In summary, it can be concluded that the activity of a preparation will vary widely depending on the immobilization. Half-life times of almost two years have been reported [29]. The new ceramic controlled-pore supports [30] may in many cases result in better stability than silica glass.

CONVERSION EFFICIENCY

Flow injection analysis is a dynamic method and the detector signal seldom reaches the steady-state level. It might therefore seem logical that enzyme reactors for f.i.a. should operate with incomplete conversion. There is a difference, however, in that the reactor performs a chemical conversion, whereas dispersion is a purely physical process. The success of the f.i.a. concept is due to the precise control of the mixing process and any chemical reactions have to be controlled to the same degree or the overall performance will be degraded.

A reactor capable of high conversion will provide a good immunity towards changes which affect the reaction rate. This is illustrated in Fig. 1 for two reactors having initial conversions of 99.9 and 30%, respectively. The effect of mass transfer was neglected in the calculations. The enzyme activity may be decreased by denaturation or losses of enzyme or binding of inhibitors, but also by changes in pH, ionic strength or sample composition (Fig. 1a). The more efficient reactor is only slightly affected whereas the conversion and therefore also the analytical signal are significantly reduced with the less efficient reactor. The next plot (Fig. 1b) shows that the more efficient

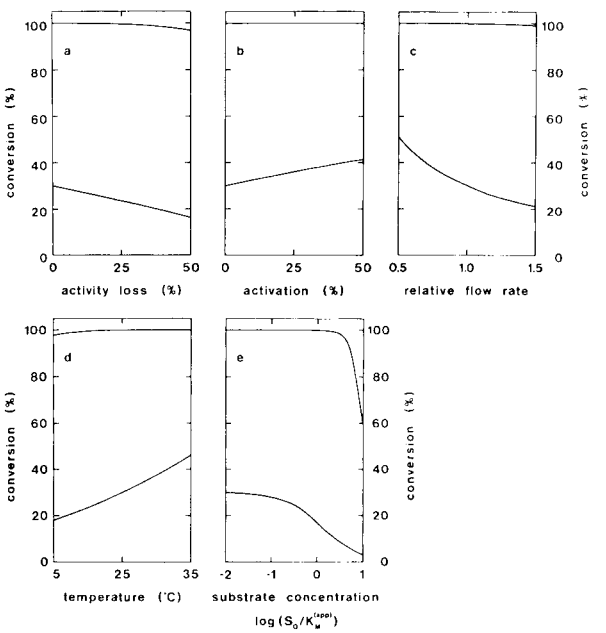

Fig. 1. Fractional conversion of substrate in reactors with negligible mass transfer resistance. The dependence on the parameters was calculated with first-order kinetic expressions except for the substrate concentration where Michaelis–Menten kinetics was assumed. The two reactors had initially a conversion of 99.9 (upper lines) and 30.0% (lower lines).

reactor is unaffected by factors which increase the activity. The effects of changes in flow rate and temperature are outlined in Fig. 1(c) and (d) and again are seen to be negligible for the more efficient reactor. The final plot (Fig. 1e), which assumes Michaelis–Menten kinetics, shows that the less efficient reactor will start to give non-linear calibration plots at substrate concentrations almost two orders of magnitude lower than the Michaelis constant.

With real reactors, there is also some mass transfer resistance which is a physical process and as such will be less affected by changes in the parameters mentioned above. When the mass transfer resistance becomes appreciable, the total reaction rate is controlled jointly by the physical and chemical processes and even an inefficient reactor will show an improved behaviour.

RATE OF REACTION IN A REACTOR

Kinetics

The Michaelis–Menten kinetics

$$S + E \rightleftharpoons ES \rightarrow P + E \tag{1}$$

expresses a mechanism by which the substrate, S, is bound reversibly to the enzyme, E, to form a substrate–enzyme complex, ES, which decomposes irreversibly to the product, P, and the enzyme. The rate of reaction is

$$-ds/dt = V_{max} S/(K_M + S) \tag{2}$$

where V_{max} is the maximum rate when $S \gg K_M$. K_M is the Michaelis constant with the dimension of concentration. If $S \ll K_M$, Eqn. (2) simplifies to a first-order expression.

Many enzymes show a much more complicated reaction scheme than that shown in Eqn. (1). For example, glucose oxidase requires oxygen as a cosubstrate, whereas alcohol dehydrogenase requires a coenzyme and also works reversibly. Nevertheless, the Michaelis–Menten kinetics has proved to be a very useful approximation when the cosubstrate or coenzyme is in excess. The further approximation with a first-order expression may at first seem to be less useful as the analytical concentrations quite often are larger than K_M (see Table 2). As discussed in detail by Goldstein [31], the effective substrate concentration in reactors with mass transfer resistance is less at the catalyst site than in the bulk. The reactor can therefore be represented by a first-order expression even at concentrations that are well above K_M of the soluble enzyme:

$$-ds/dt = K_{ps}^{(app)} S \tag{3}$$

with the apparent rate constant, $K_{ps}^{(app)}$, identical to $V_{max}/K_M^{(app)}$. Integration yields

$$-\ln [S_t/S_0] = K_{ps}^{(app)} \tau \tag{4}$$

TABLE 2

Estimated inherent rate constants, K, for some enzymes immobilized on porous glass

Enzyme	Pore diam. (nm)	IU mg^{-1}	K_M (M)	K (s^{-1})
Alcohol dehydrogenase	26	300	1.3×10^{-2}	2
L-Alanine dehydrogenase	29	30	1.7×10^{-3}	2
Asparginase	24	80	6×10^{-6}	1000
Carboxypeptidase A	15	35	1.9×10^{-3}	2
Creatine kinase	20	25	1.6×10^{-2}	0.2
Creatininase	30	70	3.3×10^{-2}	0.2
β-Galactose dehydrogenase	23	5	3.7×10^{-3}	0.1
β-Galactosidase	39	30	3.9×10^{-3}	0.7
Glucose oxidase	28	210	3.3×10^{-2}	0.6
Hexokinase	23	300	1×10^{-4}	300
Invertase	31	150	9×10^{-3}	2
Lactate dehydrogenase	25	550	6.7×10^{-3}	8
Malate dehydrogenase	19	1100	5.5×10^{-5}	2000
Peroxidase, horse radish	16	160	1.2×10^{-5}	1000
Urease	38	100	1.9×10^{-2}	0.5
Uricase	23	8	1.7×10^{-5}	50
Xanthine oxidase	31	0.4	1.3×10^{-6}	30

where S_0 and S_t are, respectively, the concentrations at the inlet and the outlet of the reactor and τ is the mean residence time

$$\tau = \pi R^2 L \epsilon_t / Q = L/F \tag{5}$$

where Q is the volumetric flow rate, R the radius, L the length of the reactor, ϵ_t the total void fraction and F the linear flow velocity.

If X is the fraction of substrate which has reacted during the transit ($X = 1 - S_t/S_0$) then

$$\tau = -[\ln(1-X)]/[K_{ps}^{(app)}] \tag{6}$$

This equation relates the two most important parameters in the design of analytical reactors, namely the fractional conversion and the mean residence time which in turn is related to the dispersion. If the apparent rate constant of the reactor can be increased sufficiently, the mean residence time can be kept low while almost complete conversion ($-\ln(1-X) = 6.9$ for 99.9% conversion) is still achieved.

Because of the chemical reaction there will be a depletion of substrate around as well as inside the enzyme support (see Fig. 2 [32]). At the limit when the catalyst becomes very efficient, the reaction will go to completion already at the surface and the enzyme in the interior will not be used at all. The utilization of the enzyme can be expressed by the effectiveness factor, η_t

$$\eta_t = \text{Rate with finite mass transfer/Rate with infinite mass transfer} \tag{7}$$

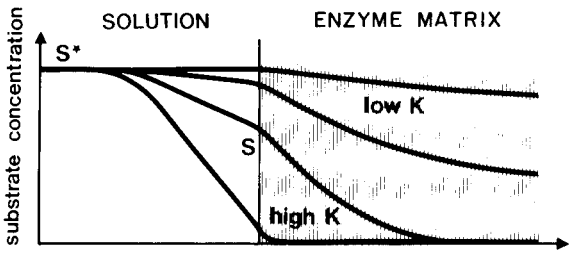

Fig. 2. Variation of the substrate concentration inside and outside a matrix with immobilized enzyme.

The total effectiveness factor, η_t, can be split up into effectiveness factors for external, η_e, and internal, η_i, mass transfer

$$\eta_e \, \eta_i = \eta_t \tag{8}$$

The effectiveness factors are given by the ratio of the rates which for first-order kinetics is equal to the ratio of the rate constants:

$$\eta_e = K_{ps}^{(app)}/K_{ps} \text{ and } \eta_i = K_{ps}/K \tag{9}$$

where K_{ps} is the rate constant in the absence of external mass transfer limitation and K the rate constant in the absence of all mass transfer resistances.

External mass transfer

The transport of substrate up to the enzyme bed is proportional to the concentration difference according to Fick's first law. At steady state, it will also be equal to the reaction rate

$$h(S^* - S) = K_{ps} S \tag{10}$$

where h is the transport coefficient and S^* and S are the substrate concentrations in the bulk and at the surface, respectively. The transport coefficient will take different forms depending on the flow pattern and the bed geometry [33]. An expression has been given [34] which has proved to be valid for reactors packed with porous glass [21, 35]

$$h = B F^{1/2} d_p^{-3/2} \tag{11}$$

where B is a constant, F the linear flow velocity and d_p the mean particle diameter. Because

$$K_{ps}^{(app)} S^* = K_{ps} S \tag{12}$$

the rate constants for packed-bed reactors will be related by

$$1/K_{ps}^{(app)} = (d_p^{3/2}/B F^{1/2}) + (1/K_{ps}) \tag{13}$$

Expressions for open tubular reactors have been derived by Kobayashi and Laidler [36] and tested experimentally on L-asparaginase attached to nylon tubing [37]. In the case of a diffusion-controlled reaction

$$h = B' F^{1/3} R^{-1/3} L^{-1/3} \tag{14}$$

where B' is another constant, R the radius and L the length of the tube. The dependence on L is a result of changes in concentration profile along the tube. Equation (14) is valid for a 2-m long tube (i.d. 1.0 mm) but not for very short or very long and thin tubes. The relations between $K_{ps}^{(app)}$ and K_{ps} take different forms depending on the conditions [36]. When the rate of reaction is low compared to the rate of mass transfer, the apparent rate constant will be equal to the inherent rate constant. The original paper [36] should be consulted for other cases.

Equations (11) and (14) show that the transfer of substrate will become more efficient as the linear flow velocity increases. This reflects the fact that the diffusion layers around the particles or at the tube wall become thinner. A decrease in particle size is very important for increased mass transfer in a packed-bed reactor. A reduction in radius is similarly of importance for improving the performance of tubular reactors although the precise mathematical form of the influence is unknown for small diameters.

Internal mass transfer

The internal mass transfer in a porous particle or in a layer can be expressed with the Thiele modulus, ϕ,

$$\phi = (\text{volume/external surface})\,(K/D_{eff})^{1/2} \tag{15}$$

where D_{eff} is the effective diffusivity in the pores. The volume/surface ratio becomes $d_p/6$ for a spherical particle and d, the thickness, for a layer on the inside of a tube ($d \ll R$). For a packed-bed reactor [4]

$$\eta_i = (1/\phi_s)\,[(1/\tanh 3\phi_s) - (1/3\phi_s)] \tag{16}$$

and for an open tubular reactor [3]

$$\eta_i = \tanh \phi_L / \phi_L \tag{17}$$

For large values of the Thiele modulus (i.e., large K and large d or d_p) the equations can be simplified to

$$\eta_i = (6/d_p)\,(D_{eff}/K)^{1/2} \text{ and } \eta_i = (1/d)\,(D_{eff}/K)^{1/2} \tag{18}$$

The equations state that η_i increases, i.e., the enzyme is utilized more efficiently, as d or d_p is decreased. A very large K results in a very small η_i and the enzyme in the interior will be little used (cf. Fig. 2). Equation (16) has been used to illustrate this in a quantitative way (see Fig. 3).

The compounded effect of internal and external mass transfer for packed-bed reactors can be calculated by means of Eqns. (8), (9), (13), and (16), as shown in Fig. 4. The apparent rate constant should be large in order to achieve a short residence time as well as a high fractional conversion (cf. Eqn. 6). The external mass transfer is the principal rate-limiting factor for large K values. It can be seen from the figure that a higher linear flow velocity will increase $K_{ps}^{(app)}$ but that the highest $K_{ps}^{(app)}$ values are attained only with very small particles.

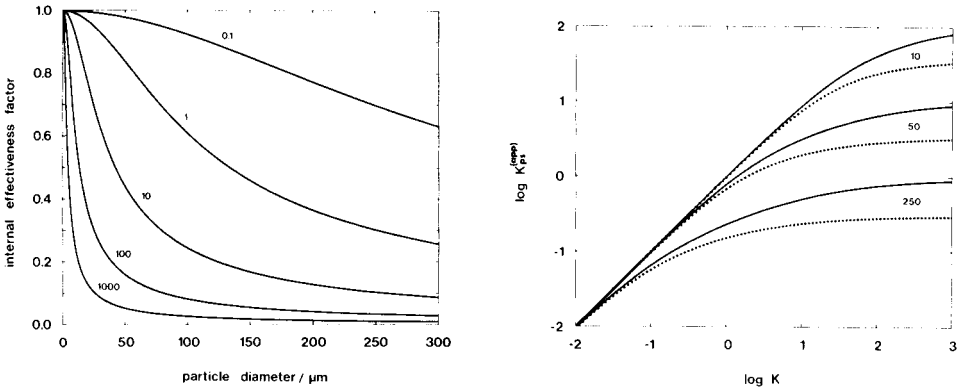

Fig. 3. The internal effectiveness factor as a function of the particle diameter, d_p, and the inherent rate constant, K, indicated on the curves. The calculation was made for spherical particles using Eqn. (16), with $D_{eff} = 2 \times 10^{-6}$ cm^2 s^{-1}.

Fig. 4. The apparent rate constant of packed-bed reactors plotted as a function of the inherent rate constant for particle diameters of 10, 50 and 250 μm and two linear flow velocities: (—) 1 cm s^{-1}; (---) 0.1 cm s^{-1}. $D_{eff} = 2 \times 10^{-6}$ cm^2 s^{-1}; $B = 3.8 \times 10^{-5}$ m s$^{-1/2}$.

Another paper from this laboratory [21] shows that the rate constants can be determined by varying the linear flow rate and the particle diameter. The above equations were found to describe the experiments quite well.

Michaelis—Menten kinetics

Enzyme preparations with K values of less than 1 s^{-1} are little influenced by mass transfer resistances. Integration of Eqn. (2) gives an expression for τ for reactions with Michaelis—Menten kinetics [38—40]:

$$\tau = [S_0 X/V_{max}] - [(K_M^{(app)}/V_{max}) \ln (1-X)] \quad (19)$$

with the same notations as above. If $S_0 \ll K_M^{(app)}$, the equation will simplify to Eqn. (6) and if $S \gg K_M^{(app)}$, the first term dominates and the reaction order becomes zero. Values of V_{max} and $K_M^{(app)}$ can be determined from the Lineweaver—Burke or Eadie—Hofstee plots [5], which are linear if the mass transfer influence can be neglected. The procedures for designing reactors when the constants are known has been discussed before [39].

A reactor with an appreciable mass transfer resistance shows an apparent Michaelis constant which becomes higher as the importance of mass transfer increases [41]. The validity of the first-order approximation will thus depend on the reactor design, but the Michaelis—Menten equation will have to be used sooner or later as S_0 is increased. Equations for reactors with mass transfer resistance and Michaelis—Menten kinetics are frequently difficult to solve in closed form.

A reactor operating with zero-order kinetics ($S_0 \gg K_M^{(app)}$) is obviously useless analytically because the amount of product is independent of the

substrate concentration. Even reactors operating in the Michaelis–Menten region ($S_0 \simeq K_M^{(app)}$) have disadvantages analytically because the output is a non-linear function of the input (cf. the lower curve in Fig. 1e). The linear range can be made to approach or even pass $K_M^{(app)}$ if the fractional conversion is made very high, $K_M^{(app)}$ can be increased by making the mass transfer resistance larger.

OPTIMIZATION

The inherent rate constant is a conditional constant and it can be increased by increasing the loading of enzyme on the surface and by increasing the surface area of the carrier. It is of interest to consider the magnitude of the inherent rate constant for various enzymes if an optimal enzyme packing is assumed. The intrinsic kinetic constants of an immobilized enzyme molecule will be affected by a number of factors [31]. For the purpose of this discussion, it will nevertheless be assumed that the K_M values of immobilized and soluble enzymes are equal; other assumptions are that the available surface area can be covered to 10% and that such a coverage can be obtained within pores which are twice as large as the diameter of the enzyme molecules. The specific activities (IU mg^{-1}) were taken from catalogues of commercially available chemicals and the purest product was selected. It was assumed that the impurities have the same molecular weight as the enzyme and are immobilized with the same probability. Table 2 shows the results of such calculations made for some enzymes of interest for applications of f.i.a. As a check the K value for peroxidase was also calculated for 72.9-nm pores, and was found to be 300 s^{-1}, which agrees fairly well with the value of 150 s^{-1} found experimentally [21] for aged reactors.

The results in Table 2 are informative about several aspects. With larger molecules, a larger pore size has to be selected which results in a smaller surface area per gram of glass (cf. Table 1). The result is that the supposed loading becomes close to 18 mg of enzyme per gram of glass irrespective of the molecular weight of the enzyme. The first-order rate constant equals the ratio of V_{max} and K_M. Urease has a high activity per mg of enzyme but its large K_M value will force the first-order rate constant to become low. Urease and glucose oxidase both have low rate constants but nevertheless both have performed well in flow injection systems [42–44]. Because the rate constants of most enzymes are larger than those mentioned, the prospects should be bright for making high-performance reactors for other applications. All diagrams in this paper were calculated using a diffusion coefficient of 0.7×10^{-5} cm^2 s^{-1}, which is an intermediate value for substrates of the enzymes listed in Table 2.

The residence time is a function of K as well as of the particle size (Fig. 5). The calculations were made for a reactor with a fractional conversion of 99.9%, a flow rate of 1 ml min^{-1} and a diameter of 2.0 mm. The length varies over several orders of magnitude; its size can be obtained from Eqn. (5)

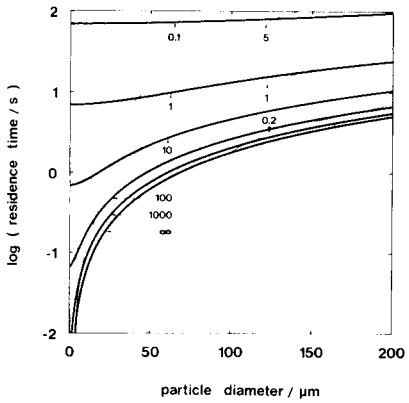

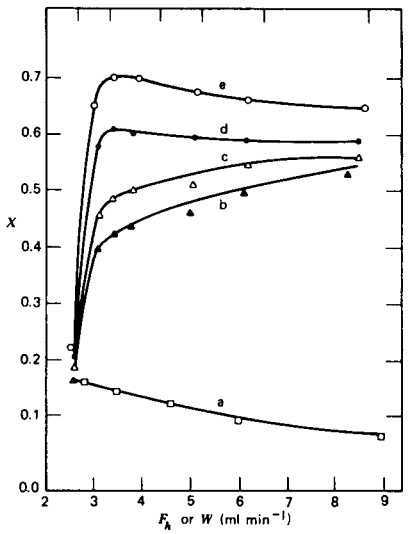

Fig. 5. The residence time, τ, in a packed-bed reactor (2.0 mm i.d., flow rate 1 ml min^{-1}, 99.9% conversion) plotted as a function of particle diameter for inherent rate constants between 0.1 and ∞ s^{-1}. The feint lines show where the pressure drop over the reactor equals 0.2, 1 and 5 atm. D_{eff} and B as in Fig. 4.

Fig. 6. Fractional conversion as a function of flow rate for an open tubular reactor: (a) straight tube, unsegmented flow; (b) straight tube, segmented flow; (c—e) coiled tubes, segmented flow. Reproduced, from Horvath et al. [46], with permission.

by inserting the τ value read from the figure. Figure 5 shows that the particle size is fairly unimportant for K values around 0.1 s^{-1}. The larger the rate constant, the greater the further decrease in mean residence time that can be obtained by decreasing d_p. In practice, there is little to be gained by increasing K much above 100 s^{-1}.

The pressure drop was also calculated by using Darcy's equation and various limits are marked in Fig. 5. With a small K value, the particle size can be increased above 200 μm in order to decrease the pressure drop with very little increase in residence time. Of course, the diameter can be increased to reduce the pressure drop further; the relative increase in dispersion will be small at first. A smaller conversion factor might have to be selected in order to decrease τ, but as the mass transfer resistance is negligible for small K values the full disadvantage of parameter dependence then has to be accepted (cf. Fig. 1).

Even if the smallest particle sizes must be excluded for practical reasons, quite a number of enzymes should be capable of giving reactors which convert 99.9% of the substrate to products in less than one second. The lengths of these reactors will approach the diameter used in the calculation. If the diameter had been decreased to say 1.0 mm, the linear flow velocity would

have increased, which in turn would have decreased τ further at the expense of an increased pressure drop. The striking conclusion is that it should be feasible to produce packed-bed reactors with volumes of a few microliters and with residence times in the millisecond range.

Such extremely short residence times may be of little practical interest at present. The system might therefore be optimized with some additional properties in mind. The plot in Fig. 1(a) shows that a reactor giving high conversion is little affected by activity losses. This property can be exaggerated by designing the reactor with say 99.9999% conversion efficiency. The length would only be twice as long but it could lose half of its activity before its performance decreased to that of a reactor giving 99.9% conversion.

It has been reported in several cases that enzyme stability improves for larger support particles. If the particle diameter is increased, the effectiveness factor will decrease, but as some enzyme is deactivated, the K value will decrease and the effectiveness factor will increase. Some of the enzyme in the center of the particles, which was little used at first, will thus be available as a reserve when the preparation ages. The conclusion is that, with enzymes which have high K values, the unnecessarily short residence times may be traded for an increased useful lifetime.

APPLICATIONS

Immobilized enzyme reactors have found numerous applications since their introduction almost twenty years ago [45]. They can easily be interfaced with almost any type of detector which can record the concentration of the substrate, a product, a cosubstrate or a coenzyme. Their utility can be increased by mounting different enzyme reactors in series or by co-immobilization of two or more enzymes. The detection methods used include spectrophotometry, chemiluminescence, fluorescence, amperometry, conductometry, thermometry and potentiometry with ion-selective electrodes or gas sensors.

Open tubular reactors are well suited for use in air-segmented analyzers. The tubes usually have a diameter of 1 mm and a length between 0.5 and 2 m. Air segmentation is very important for radial mixing. Further improvements result from the use of tight coiling, intermediate flow rates and short slug lengths, as shown in Fig. 6 [46]. When the same coils were operated with a homogeneous flow, the fractional conversion decreased drastically (curve a). The reactors are usually operated with intermediate fractional conversions. Carr and Bowers [5] estimated that the coil used by Hornby et al. [13] would have reached 99% conversion if it had been 210 cm long and operated with the shortest slug length of those studied. Typical operating conditions are illustrated in a recent paper with coiled 1-mm nylon tubes with immobilized creatininase [47]. The conversion was 23—28 and 53—60% for 0.5- and 1-m tubes, respectively, when the residence time was 30 s.

The open tubular reactors used so far are not well suited for flow injection applications. The sensitivity becomes too low and the dispersion too high with continuous flow, because of the large diameters of the tubes. Further development could result in more appropriate designs which might have advantages over packed-bed reactors for samples which could clog the latter.

Thermal detection methods require specially designed reactors in order to maximize the temperature transfer to the sensor [5, 48]. A thermistor can be placed in the effluent from a reactor or in the bed of immobilized enzyme. In order to increase the sensitivity, the heat capacity of the bed should be kept as low as possible if short pulses of substrate are to be measured. The maximum sensitivity will thus be obtained at less than complete conversion. The improved designs reported during the last few years have resulted in an increased sample throughput and a decreased sample volume. Danielsson et al. [49] injected 5—20 μl samples of serum directly into the buffer stream.

Cremonesi and Bovara [50] seem to have been the first to use immobilized enzymes together with a flow injection system. They reported on the determination of glucose, ethanol, and testosterone with enzymes immobilized on cellulose. They concluded that cellulose is to be preferred to, e.g., Sepharose because it is deformed less easily, but that further improvement in the matrix was desirable. Nevertheless, they obtained good linearity of response, high sensitivity and a sample capacity of 60 h^{-1} with h.p.l.c. equipment including a spectrophotometer which was not optimized for the purpose.

Glucose determinations have received much attention because of their clinical importance as can be seen by the list of references given by Carr and Bowers [5]. Watson et al. [42] developed a glucose analyzer for 2-μl sample injections, using a packed-bed reactor containing glucose oxidase immobilized on porous alumina. The mean residence time in the reactor was 15 s and the conversion was "100%". The detection was based on electrochemical oxidation of the hydrogen peroxide. In another flow injection method for glucose determinations [43], glucose oxidase and peroxidase were immobilized on porous glass and used in successive reactors with a photometric detector (555 nm); 45 samples per hour could be processed with negligible carry-over and with 25- or 100-μl samples depending on the desired range. This example also illustrated the use of an on-line dialyzer to keep the reactors free from large molecules, particles and bacteria. At a flow rate of 1 ml min^{-1} on both sides of the dialysis membrane, 16% of a test substance (catechol) passed across the membrane. Some sensitivity is thus lost in the dialyzer but it is still adequate for glucose determinations in both serum and urine.

Adams and Carr [51] observed serious adsorption in their flow injection system for urea determination. Proteins visibly coated the hydrophobic non-porous glass. The peak shape differed substantially when urea and

ammonia samples were injected. Gorton and Ögren [43] also used urease immobilized on porous glass; and employed an on-line dialyzer which passed 27% of the urea or ammonia into the buffer fed to the reactor. No interferences arose from adsorption, but a small difference was noted between the peak shapes produced by urea and ammonia samples. A dialyzer may thus reduce interferences from sample components, but will not remedy adsorption of products or dialyzable components. Such adsorption can be affected by changes in the immobilization method [21, 51].

REFERENCES

1 J. Růžička and E. H. Hansen, Anal. Chim. Acta, 78 (1975) 145.
2 K. K. Stewart, G. R. Beecher and P. E. Hare, Anal. Biochem., 70 (1976) 167.
3 O. Levenspiel, Chemical Reaction Engineering, 2nd edn., Wiley, New York, 1972.
4 C. N. Satterfield, Mass Transfer in Heterogeneous Catalysis, M.I.T. Press, Cambridge, 1970.
5 P. W. Carr and L. D. Bowers, Immobilized Enzymes in Analytical and Clinical Chemistry, Wiley, New York, 1980.
6 D. L. Eaton in D. E. Leyden and W. T. Collins (Eds.) Silylated Surfaces, Gordon and Breach, New York, 1980, p. 201.
7 W. E. Hornby and H. Filippuson, Biochim. Biophys. Acta, 220 (1970) 343.
8 H. Filippusson and W. E. Hornby, Biochem. J., 120 (1970) 215.
9 P. V. Sundaram and W. E. Hornby, FEBS Lett., 10 (1970) 325.
10 D. J. Inman and W. E. Hornby, Biochem. J., 129 (1972) 255.
11 J. P. Allison, L. Davidson, A. G. Hartman and G. B. Kitto, Biochem. Biophys. Res. Commun., 47 (1972) 66.
12 D. J. Inman and W. E. Hornby, Biochem. J., 137 (1974) 25.
13 W. E. Hornby, J. Campbell, D. J. Inman and D. L. Morris, in E. K. Pye and L. B. Wingard, Jr. (Eds.), Enzyme Engineering, Vol. 2, Plenum Press, New York, 1974, p. 401.
14 C. Horvath and B. A. Solomon in E. K. Pye and L. B. Wingard, Jr. (Eds.), Enzyme Engineering, Vol. 2, Plenum Press, New York, 1974, p. 259.
15 C. Horvath and B. A. Solomon, Biotechn. Bioeng., 14 (1972) 885.
16 H. A. Mottola, Anal. Chim. Acta, 145 (1983) 27.
17 K. Mosbach (Ed.), Methods in Enzymology, Vol. XLIV, Immobilized Enzymes, Academic Press, New York, 1976.
18 O. R. Zaborsky, Immobilized Enzymes, CRC Press, Cleveland, OH, 1973.
19 H. H. Weetall and S. Suzuki (Eds.), Immobilized Enzyme Technology, Plenum Press, New York, 1975.
20 P. Thibault, P. Monsan, O. C. Jouret, Sci. Aliment., 1 (1981) 55.
21 B. Olsson and L. Ögren, Anal. Chim. Acta, 145 (1983) 87.
22 J. E. Dixon, F. E. Stolzenbach, J. A. Berenson and N. O. Kaplan, Biochem. Biophys. Res. Commun., 52 (1973) 905.
23 L. Goldstein, Y. Levin and E. Katchalski, Biochemistry, 3 (1964) 1913.
24 H. H. Weetall, N. B. Havewala, H. M. Garfinkel, W. M. Buehl and G. Baum, Biotechn. Bioeng., 16 (1974) 169.
25 S. Henry, J. Koczan and T. Richardson, Biotechn. Bioeng., 16 (1974) 289.
26 R. P. Chambers, G. A. Swan, E. M. Walle, W. Cohen and W. H. Baricos, in H. H. Weetall and S. Suzuki (Eds.), Immobilized Enzyme Technology, Plenum Press, New York, 1979, p. 199.
27 L. Ögren and G. Johansson, Anal. Chim. Acta, 96 (1978) 1.
28 W. G. Bardsley, R. E. Childs and M. J. C. Crabbe, Biochem. J., 137 (1974) 61.

29 J. R. Ford and W. H. Pitcher, in H. H. Weetall and S. Suzuki (Eds.), Immobilized Enzyme Technology, Plenum Press, New York, 1975, p. 17.
30 H. H. Weetall in K. Mosbach (Ed.), Methods in Enzymology, Vol. XLIV, Immobilized Enzymes, Academic Press, New York, 1976, p. 134.
31 L. Goldstein in K. Mosbach (Ed.), Methods in Enzymology, Vol. XLIV, Immobilized Enzymes, Academic Press, New York, 1976, p. 397.
32 J. M. Engasser in P. Dunhill, A. Wiseman and N. Blakebrough (Eds.), Enzymic and Non-Enzymic Catalysis, Horwood, Chichester, 1978, p. 174.
33 A. J. Karabelos, T. H. Wegner and T. J. Hanratty, Chem. Eng. Sci., 26 (1971) 1581.
34 L. K. McCune and R. H. Wilhelm, Ind. Eng. Chem., 41 (1949) 1124.
35 B. J. Rovito and J. R. Kittrell, Biotechn. Bioeng., 15 (1973) 143.
36 T. Kobayashi and K. J. Laidler, Biotechn. Bioeng., 16 (1974) 99.
37 P. S. Bunting and K. J. Laidler, Biotechn. Bioeng., 16 (1974) 119.
38 L. Goldstein and E. Katchalski, Fresenius Z. Anal., Chem., 243 (1968) 375.
39 G. Johansson and L. Ögren, in E. Pungor and I. Buzas (Eds.), Ion Selective Electrodes, Akademiai Kiado, Budapest 1977, p. 93.
40 W. E. Morf, Mikrochim. Acta, (1980 II) 317.
41 T. Kobayashi and K. J. Laidler, Biotechn. Bioeng., 15 (1973) 47.
42 B. Watson, D. N. Stifel and F. E. Semersky, Anal. Chim. Acta, 106 (1979) 233.
43 L. Gorton and L. Ögren, Anal. Chim. Acta, 130 (1981) 45.
44 B. Olsson, L. Ögren and G. Johansson, Anal. Chim. Acta, 145 (1983) 101.
45 E. Reisel and E. Katchalski, J. Biol. Chem., 239 (1964) 1521.
46 C. Horvath, B. A. Solomon and J. M. Engasser, Ind. Eng. Fundam., 12 (1973) 431.
47 M. Mascini and G. Palleschi, Anal. Chim. Acta, 136 (1982) 69.
48 B. Danielsson, B. Mattiasson and K. Mosbach, Appl. Biochem. Bioeng., 3 (1981) 97.
49 B. Danielsson, K. Gadd, B. Mattiasson and K. Mosbach, Clin. Chim. Acta, 81 (1977) 163.
50 P. Cremonesi and R. Bovara, Biotechn. Bioeng., 16 (1976) 1487.
51 R. E. Adams and P. W. Carr, Anal. Chem., 50 (1978) 944.

Analytica Chimica Acta, 145 (1983) 87—99
Elsevier Scientific Publishing Company, Amsterdam — Printed in The Netherlands

OPTIMIZATION OF PEROXIDASE IMMOBILIZATION AND OF THE DESIGN OF PACKED-BED ENZYME REACTORS FOR FLOW INJECTION ANALYSIS

BO OLSSON* and LARS ÖGREN[a]

Department of Analytical Chemistry, University of Lund, P.O. Box 740, S-220 07 Lund (Sweden)

(Received 1st August, 1982)

SUMMARY

Packed-bed reactors containing horse radish peroxidase were optimized for use in flow injection systems. The most active and stable immobilizations were produced by azo linkage to porous glass. The influence of pore and particle diameter as well as pH of immobilization, number of coupling sites, and enzyme purity were studied. The reactor behaviour could be accurately described by a theory derived on the assumptions of first-order kinetics. The effects of internal and external mass transfer resistances were studied and the rate constants were evaluated. Design criteria for analytical reactors are discussed. A small particle diameter is shown to be of utmost importance in order to achieve low dispersion with fixed levels of back-pressure and conversion.

Although there are many theoretical treatments that can be applied to enzyme reactors in analytical flow systems, there are few relevant experimental data for the actual design. High conversion efficiency and low dispersion are of paramount importance analytically, in contrast to bioengineering where cost and productivity must be given the greatest weight. The design criteria thus differ considerably and it might be of interest to study in some detail how the variables should be selected for an analytical system. Packed-bed enzyme reactors have already been used in flow injection analysis [1, 2] and the success of the approach makes it interesting to work through an optimization in order to assess the importance of the physical parameters.

It is advantageous to convert essentially all the substrate to products [3, 4]. This can of course be accomplished by packing a sufficiently large reactor with the enzyme at hand. When low dispersion is essential for sensitivity and sample throughput, the dispersion can of course be decreased by using a smaller reactor and sacrificing some efficiency. The present study was undertaken to learn to what extent the dispersion (in practice, the mean residence time) can be decreased while 99.9% conversion is maintained. The strategy was to optimize the activity of the immobilized enzyme as well as the bed geometry.

---

[a]Present address: AB Draco, P.O. Box 1707, S-221 01 Lund (Sweden)

Peroxidase reactors are used in a method for determination of dissolved oxygen in a flow injection system [5] and for determination of β-D-glucose [1]. In both methods, hydrogen peroxide is produced on-line in another reactor containing immobilized glucose oxidase. The overall reaction between hydrogen peroxide, peroxidase and chromogens can be represented by

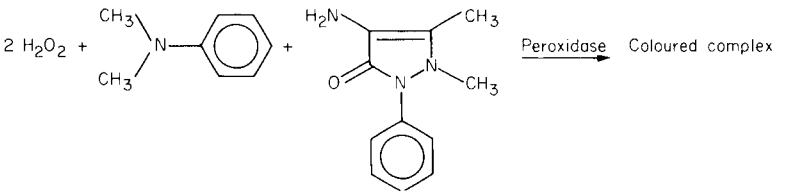

(1)

The peroxidase is first oxidized by hydrogen peroxide in a well-defined step [6]. The back-reduction takes place through an oxidative coupling of 4-aminophenazone and *N*,*N*-dimethylaniline. The reaction is only partly known [7, 8].

THEORY

Evaluation of the apparent rate constant of the immobilized enzyme

The overall kinetics of an enzyme immobilized within a porous support can be described by its apparent kinetic behaviour, which thus incorporates the resistance to mass transfer. Many enzymes with a complicated reaction scheme can be well approximated by Michaelis—Menten kinetics, which in turn can be replaced by a pseudo first-order expression, provided that the substrate concentration, S, is much smaller than the apparent Michaelis constant; thus for $S \ll K_M^{(app)}$,

$$-dS/dt = V_{max}^{(app)} S/(K_M^{(app)} + S) \rightarrow V_{max}^{(app)} S/K_M^{(app)} = K_{ps}^{(app)} S \quad (2)$$

$K_{ps}^{(app)}$ is the apparent rate constant (s^{-1}) of the pseudo first-order reaction. The integral expression is obtained in the usual way

$$-\ln (S_t/S_0) = K_{ps}^{(app)} t \quad (3)$$

where S_0 and S_t are the substrate concentrations at time 0 and t, respectively. For a reactor, the concentration at the inlet corresponds to S_0 and at the outlet to S_t, and, for steady-state measurements, the time coordinate corresponds to τ, the mean residence time (s). It is convenient to replace S_t/S_0 by $(1-X)$ where X is the fractional conversion in the reactor

$$K_{ps}^{(app)} = -[\ln (1-X)]/\tau \quad (4)$$

The mean residence time equals (reactor volume) × (total void fraction)/(volumetric flow rate). The fractional conversion, X, approaches unity as the reaction approaches completion. Reactors with fractional conversions in the range $X \approx 0.3$—0.7, give the most accurate values of $K_{ps}^{(app)}$.

It will be shown later that the first-order approximation is fully permissible for the peroxidase reactors.

Evaluation of the rate constant at zero external mass transfer resistance

The substrate concentration, S, at the (external) surface of a particle containing a catalyst will always be lower than the bulk concentration, S^*. The amount of depletion depends on the efficiency of the catalyst as well as on the thickness of the diffusion layer around the particles. It can be neglected for very slow reactions and very high linear flow velocities.

At steady state, the rate of transport to the particle surface will equal the rate of the reaction. For a (pseudo) first-order reaction

$$h\,(S^* - S) = K_{ps} S \tag{5}$$

where h is the transport coefficient (s^{-1}) and K_{ps} the rate constant (s^{-1}) at zero external mass transfer resistance. The rate can also be expressed by the apparent rate constant and the bulk concentration

$$K_{ps}^{(app)} S^* = K_{ps} S \tag{6}$$

Combination of Eqns. (5) and (6) and rearrangement gives

$$(K_{ps}^{(app)})^{-1} = h^{-1} + (K_{ps})^{-1} \tag{7}$$

Many expressions for h have been discussed by Karabelos et al. [9]. A correlation proposed by McCune and Wilhelm [10] and experimentally validated for porous glass by Rovito and Kittrell [11], can be rewritten in the form

$$h = 1.625\, a_m\, F\, (Sc)^{-2/3}\, (Re)^{-1/2} \tag{8}$$

where F is the linear flow velocity (m s^{-1}) and Sc and Re are the Schmidt and Reynold numbers. The constant is dimensionless. The external surface area per unit volume, a_m (m^{-1}), can be related to the particle size, d_p. For spherical geometry,

$$a_m = 6(1 - \epsilon_E)/d_p \tag{9}$$

where ϵ_E is the external void fraction. Substitution of Eqn. (9) into Eqn. (8) and insertion of expressions for Sc and Re gives

$$h = F^{1/2} d_p^{-3/2} B \tag{10}$$

$$\text{with } B = 9.75\, (1 - \epsilon_E)\, D_m^{2/3}\, \nu^{-1/6} \tag{11}$$

where D_m is the molecular diffusion coefficient ($m^2\ s^{-1}$) and ν the kinematic viscosity ($m^2\ s^{-1}$). Substitution of Eqn. (10) into Eqn. (7) gives

$$(K_{ps}^{(app)})^{-1} = d_p^{3/2}\, B^{-1}\, F^{-1/2} + (K_{ps})^{-1} \tag{12}$$

The final equation shows that K_{ps} can be evaluated from a series of $K_{ps}^{(app)}$ determined at various flow rates. Conversely, when K_{ps} is known, the effect of linear flow velocity on $K_{ps}^{(app)}$ can be predicted. $K_{ps}^{(app)}$ will increase as F increases, and at the limit, when the external mass transfer becomes infinitely fast, it will equal K_{ps}.

Evaluation of the inherent rate constant

Because of the limited rate of diffusion, there will be a gradual decrease of substrate concentration inwards towards the center of the particle, as the substrate is continually converted to products. The extent to which the reaction rate is lowered is expressed by the effectiveness factor, η_i, which for a (pseudo) first-order reaction is equal to the ratio of the rate constants

$$\eta_i = \text{external attainable rate/inherent rate} = K_{ps}/K \quad (13)$$

where K is the inherent rate constant (s^{-1}), free of all mass transfer resistance.

A full expression for η_i involves the appropriate differential equations for the rates. The solution [12] is

$$\eta_i = (1/\phi_s)\,[(1/\tanh 3\phi_s) - (1/3\phi_s)] \quad (14)$$

where the Thiele modulus for spherical geometry, ϕ_s, is

$$\phi_s = (d_p/6)\,(K/D_{eff})^{1/2} \quad (15)$$

with D_{eff} as the effective substrate diffusivity in the pores ($m^2\ s^{-1}$). K can be calculated from a series of K_{ps} values measured at various particle diameters.

A closer study of Eqns. (13—15) shows that for large values of ϕ_s (e.g., large d_p) the K_{ps} will be inversely proportional to d_p. For small ϕ_s (e.g., small d_p) K_{ps} will in the limit become independent of d_p. The internal mass transfer resistance is then negligible and a further reduction of d_p will not increase η_i, which already is close to unity.

EXPERIMENTAL

Immobilization of peroxidase

Horse radish peroxidase, EC 1.11.1.7. (Sigma, Type I, P-8125 and Type VI, P-8375) was immobilized on alkylamino- as well as arylamino-derivatized controlled-pore glass (CPG-10, Electro-Nucleonics, Fairfield, NJ, U.S.A.) by methods described by Weetall [13]. Different pore and particle sizes were used as well as different conditions for coupling (pH, enzyme purity, concentration of coupling sites).

Glutaraldehyde coupling to alkylamino glass. Acid-washed (boiling 5% nitric acid, 1 h) controlled-pore glass was treated (3 h, 75°C) with an aqueous 10% solution of 3-aminopropyltriethoxysilane (Merck, 821618) at pH 3.45. The preparation was dried overnight at 95°C to allow storage. A portion (0.5 ml) of glutaraldehyde solution (BDH Chemicals) 2.5% in 0.1 M phosphate buffer pH 7.0, was added to 50 mg of alkylamino glass. The reaction proceeded for 1 h at room temperature, initially at reduced pressure. Peroxidase (Type VI, 5.00 mg) in 0.25 ml of 0.1 M phosphate buffer pH 7.0, was added to the moist glass and the reaction was allowed to proceed overnight at 4°C. Each of the above steps was followed by extensive washing on a G3 glass filter.

Azo coupling to arylamino glass. The glass was aminated as described

above. A commercial organically aminated alkylamino glass was also used (Pierce, aminopropyl-CPG, 50-nm pore diameter, 80—120 mesh). The alkylamino glass was acylated by refluxing in a solution of 3% *p*-nitrobenzoyl chloride (analytical-reagent grade) in chloroform, also containing 5% triethylamine (Fluka, p.a.), for 4 h. The nitro group was reduced by boiling the glass in an aqueous 5% solution of sodium dithionite for 1 h. The arylamino glass was dried overnight at 95°C to allow storage. Diazotization was done at 0°C by mixing 50 mg of arylamino glass with 1 ml of 2 M HCl and adding 20 mg of solid sodium nitrite. The reaction was allowed to proceed for 30 min, initially at reduced pressure. Peroxidase (Type VI or Type I, 5.0 mg) in 0.25 ml of 0.1 M phosphate buffer pH 8.5 (alternatively pH 7.0 and 6.0) was added to the cold glass and the reaction was allowed to continue overnight at 4°C. Each of the above steps was followed by extensive washing on a G3 glass filter.

Characterization. The coupling yield was determined from the difference in optical absorbance before and after immobilization. The coupling yield of peroxidase was measured at 403 nm (ϵ = 91 cm^2 μmol^{-1} [14]) and of protein at 280 nm. Excess of reagent and the first washings were combined for the determinations of the yield.

Reagent

A phosphate buffer, 0.1 M, pH 6.0 was made 0.75 mM with respect to 4-aminophenazone (BDH Chemicals) and 2.5 mM with respect to *N,N*-dimethylaniline (99.5%; Riedel-de Haën). The substrate, hydrogen peroxide (Merck, Perhydrol), was also added to the solution (0.05 mM, except when otherwise stated).

Procedures

The combined reagent and substrate was pumped through the reactors with a peristaltic pump (Gilson, Minipuls 2) and the absorbance was measured at 555 nm with a flow-through spectrophotometer (Spectra Physics, model 770). The fractional conversion was taken as the absorbance ratio of the reactor under test compared to a 100-μl reactor known to give 100% conversion (no change in absorbance on a second pass). The reactors were mounted in the loop of a slide injector so that the reagent blank could be checked frequently. All measurements were made at 25.0°C.

The time stability was assessed by pumping combined reagent and substrate through 5-μl reactors continuously (3.0 ml h^{-1}) for 11 days. The fractional conversion was determined once every 24 h at a flow rate of 2 ml min^{-1}. The reactors were then stored for 22 days at 4°C and after that the fractional conversion was measured again.

The volumes of the reactors were 5 μl (1.25 mm i.d., length 4.1 mm), 20 μl (2.5 mm i.d., length 4.1 mm) and 84 μl (2.7 mm i.d., length 14.7 mm). The total and external void fractions were 0.82 and 0.48, respectively, as calculated from the densities of porous glass and silica, the specific

pore volume, and the packing density. The packing density was determined on a larger batch as 0.34 g ml^{-1}. The void fractions depend on packing and may differ from one reactor to another. The mean particle diameters were taken from the manufacturers data (see Table 3).

RESULTS AND DISCUSSION

Immobilization of peroxidase

Peroxidase has been immobilized on a variety of organic and inorganic materials. Coupling to porous glass has been accomplished with, e.g., glutaraldehyde [15], isothiocyanate [16], fluorodinitrobenzene [17], acrylic copolymers [18], and diazonium linkages [19]. Thibault et al. [15] reported on the optimization of glutaraldehyde coupling of peroxidase to porous glass. The activity and stability were found to be inferior to azo coupling.

The time stability of azo-bound peroxidase was measured on 5-μl reactors (Fig. 1). Corresponding measurements on glutaraldehyde-bound peroxidase are shown for comparison. It can be seen that the azo coupling gave a higher loading, was more active and had a better long-term stability. Preparations stored for six months in a refrigerator did not lose much activity.

All batches stabilized in the same way (Fig. 1) and measures of conversions cited in the following paragraphs relate to the stable values. Porous glass can be silylated in an aqueous or organic solvent. The latter method will introduce a larger amount of amino functional groups. Weetall [13] states that

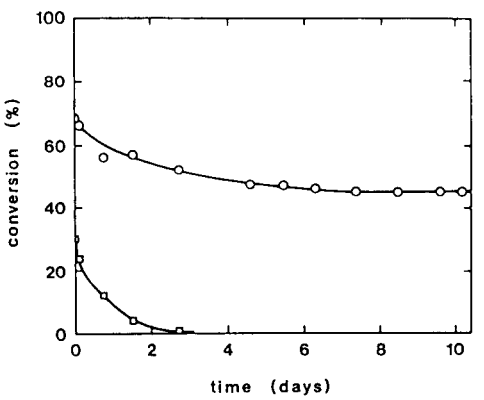

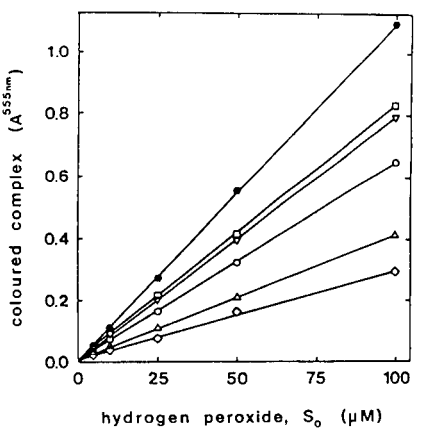

Fig. 1. Time stability of peroxidase (POD), immobilized to CPG (50 nm, 80—120 mesh): (○) azo-bound, 29 mg POD g^{-1} glass; (□) glutaraldehyde-bound, 3 mg POD g^{-1} glass.

Fig. 2. Product formation as a function of substrate concentration. (•) Complete conversion (100-μl reactor). Open symbols correspond to the 5-μl reactor with flow rates of: (□) 0.55, (▽) 1.0, (○) 2.0, (△) 4.4 and (◇) 7.5 ml min^{-1}.

the methods are of almost equal use but that the former results in a slightly more stable product. The present results (Table 1) conform essentially to earlier knowledge and aqueous silylation was used in the rest of the study. The pH during the immobilization was varied (Table 2) and it was found that more peroxidase was bound as the pH was increased. The activity is also superior for the batch made at pH 8.5.

Table 3 shows the effect of varying the pore size and the particle size of the glass, as well as the enzyme purity. It is well documented that the loading of enzyme increases with the surface area until the pores become too small for free entrance of the enzyme [20]. The coverage decreases slightly with

TABLE 1

Azo coupling of Type VI peroxidase to CPG (50 nm, 80—120 mesh). Effect of silylation technique

Silylation technique	Aqueous	Organic
POD yield (mg g^{-1})	29	26
Conversion (%)	45	50
$K_{ps}^{(app)}$ (s^{-1})	4.9	5.6

TABLE 2

Azo coupling of Type VI peroxidase to CPG (33 nm, 120—200 mesh). Effect of immobilization pH

pH of immobilization	6.0	7.0	8.5
POD yield (mg g^{-1})	22	35	58
Conversion (%)	70	71	76
$K_{ps}^{(app)}$ (s^{-1})	9.8	10.1	11.6

TABLE 3

Effect of enzyme purity, pore diameter, and particle size on the azo coupling of peroxidase to CPG

Enzyme purity	26% (Type I)			80% (Type VI)			80% (Type VI)
Mesh numbers	120—200			120—200			80—120
Mean part. diam. (μm)	←	100	→	←	100	→	150
Pore diam. (nm)	25	33	72.9	25	33	72.9	72.9
Area (m^2 g^{-1})	105	80	34	105	80	34	34
POD yield (%)	53	37	19	81	71	35	33
POD yield (mg g^{-1})	14	10	5	67	58	29	27
Protein yield (mg g^{-1})	70	71	66	68	62	35	30
Purity (% POD)	20	14	8	99	94	83	89
Coverage (mg POD m^{-2})	0.13	0.12	0.15	0.64	0.73	0.86	0.78
Conversion (%)	38	34	—	81	76	70	43
$K_{ps}^{(app)}$ (s^{-1})	3.9	3.4	—	13.5	11.6	9.8	4.6

increased area because of steric effects or a depletion of reagent. Thibault et al. [15] found the highest loading at a pore diameter of 15—25 nm.

The purity of the immobilized product was excellent with Type VI peroxidase but with Type I it was lower than that of the starting material. The preferential binding of impurities was even more marked for glutaraldehyde immobilization. Only 33% of the bound protein consisted of peroxidase, although Type VI enzyme was used. The purity of the preparation increased as the pore diameter decreased (Table 3), which indicates that some impurities are excluded from the pores. The results show that the enzyme purity has a profound influence on the peroxidase yield and activity.

Peroxidase has a molecular weight of 40 000 D which for a globular protein corresponds to an effective diameter of 8 nm, according to the Electro-Nucleonics data sheet. A full monolayer should then equal 1.2 mg protein m^{-2}. The initial coverage of peroxidase alone was found to be 0.8—0.9 mg m^{-2} at most (Table 3). As other proteins are also present, there should be very few empty sites on the surface. The activity, however, decreases with time and after one week only 5—10% active peroxidase remains. This can be estimated from the stability curves if the effects of mass transfer resistances are taken into account. $K_{ps}^{(app)}$ is a more direct measure of reactor activity than the conversion, because it is a linear rather than a logarithmic function. It is also independent of the reactor length in contrast to the conversion. The highest $K_{ps}^{(app)}$ is obtained (Table 3) with the purest enzyme, and the largest surface area. The smaller particles result in a slightly increased loading but in more than a doubled rate constant. To conclude, a reactor for an analytical system should be made through azo immobilization at pH 8.5 using Type VI peroxidase and a glass with 25-nm pore diameter with a small particle size. Such a reactor would give too high an activity for a study of bed geometry and the 72.9-nm glass was therefore used in the following study.

Tests of the validity of the mass transfer equations

Reaction order. The amount of product formed in a 5-μl peroxidase reactor was measured at various flow rates and substrate concentrations (Fig. 2). The linearity of the plots proves that the reaction follows first-order kinetics for substrate concentrations up to at least 0.1 mM. A mixed reaction order would have resulted in a downward curve of the plots, especially at high flow rates. The absorbance obtained with a 100-μl reactor known to give complete conversion is plotted in Fig. 2 for comparison.

The Michaelis constant for the soluble enzyme was determined spectrophotometrically as 12 μM. Enzyme reactors may thus show a pseudo first-order behavior at substrate concentrations which are large compared to the K_M of the soluble enzyme. Any of the lines in Fig. 2 could be a calibration graph for an analytical system and the linearity would then be a desirable property.

External mass transfer. Four different reactors varying in volume, diameter and particle size were studied. $K_{ps}^{(app)}$ was determined (from Eqn. 4) at

various linear flow velocities. The inverse $K_{ps}^{(app)}$ is plotted versus the (particle diameter)$^{3/2}$ × (linear flow velocity)$^{-1/2}$ in Fig. 3. Most of the points fall on two straight lines, one for each particle size. The slight difference in slope is most likely due to errors in d_p and ϵ_E. According to Eqn. (12) the slope should be B^{-1} and the intercept K_{ps}^{-1}. The linearity and the almost equal slopes validate Eqn. (12), at least for moderate flow velocities ($1 < Re < 20$).

A further test can be made by comparing the inverse slope, B, with a value calculated from physical constants according to Eqn. (11). With $\nu = 1 \times 10^{-6}$ m^2 s^{-1}, $D_m = 1.5 \times 10^{-9}$ m^2 s^{-1}, and $\epsilon_E = 0.48$, the constant B becomes 6.6×10^{-5}, compared to the experimental values which were 6.3 and 7.5×10^{-5}. The agreement is surprisingly good when all the uncertainties are taken into consideration.

The K_{ps} values found were 11.9 and 16.4 s^{-1} for the particle diameters 150 and 100 μm, respectively. The corresponding values of $K_{ps}^{(app)}$ for a 5-μl reactor at 1.0 ml min^{-1} were 3.3 and 6.1 s^{-1}. The external mass transfer resistance thus reduces the effectiveness of the reactor two to three times under these conditions.

The conversion efficiencies of some reactors are plotted versus the volumetric flow rate in Fig. 4. The solid lines are drawn from Eqn. (12) with the values of K_{ps} and B as found earlier. The theory describes the data well, except that the conversion at very low flow rates may be lower than predicted. This may be due to a peculiarity of the peroxidase reaction, to some neglected effect in the theory, or to systematic errors in the experiments.

Once the validity of Eqn. (12) has been proved and the K_{ps} and B values are known, the theory can be used to illustrate the effect of changing the

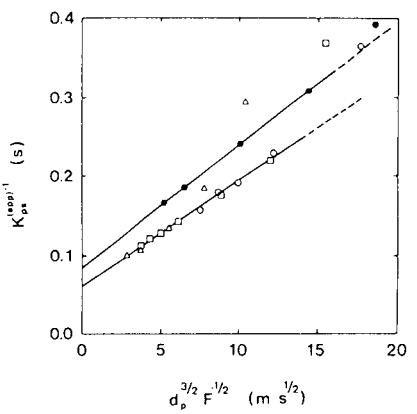

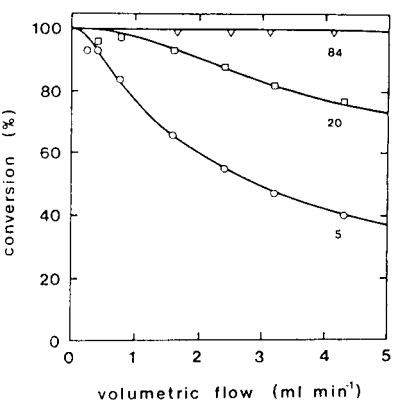

Fig. 3. Effect of linear flow velocity on the apparent rate constant: (•) 5-μl reactor, d_p = 150 μm, S_0 = 20 μM; (△) 5-μl reactor, d_p = 100 μm, S_0 = 25 μM; (□) 5-μl reactor, d_p = 100 μm, S_0 = 100 μM; (○) 20-μl reactor, d_p = 100 μm, S_0 = 100 μM.

Fig. 4. Percent conversion as a function of volumetric flow rate for reactor volumes of: (○) 5 μl, (□) 20 μl, (▽) 84 μl. The solid lines are calculated from Eqns. (4) and (12).

parameters in other ways. The fractional conversion was calculated as a function of the volumetric flow rate for some reactors all having the same volume but different diameters (Fig. 5). For a constant volumetric flow rate, the linear flow velocity will increase as the reactor diameter decreases. More substrate will then be transported into the particle and this will result in a higher conversion as shown in Fig. 5.

Internal mass transfer. The inherent rate constant, K, was calculated from Eqns. (13—15) using the K_{ps} values found (Table 4). The K values obtained with the two particle diameters agree within 15%. The Thiele modulus and the effectiveness factor are also given in the table. The small η_i values indicate that only a small fraction of the catalytic capacity of the enzyme is utilized. A total effectiveness factor including also the external mass transfer resistance would be even smaller.

The particle diameter is the most powerful variable for low effectiveness factors and there is an inverse relation between d_p and K_{ps}. The effect on

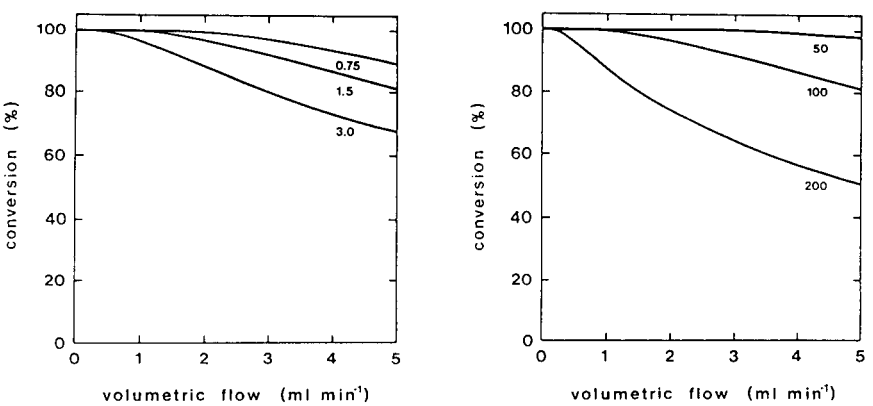

Fig. 5. Effect of reactor diameter on conversion calculated from Eqns. (4) and (12) with $K_{ps}^{(app)}$ = 16.4 s^{-1}, d_p = 100 μm, B = 7.5 × 10^{-5} m $s^{-1/2}$ for a reactor volume of 20 μl and reactor diameters of 0.75, 1.5 and 3.0 mm.

Fig. 6. Effect of particle diameter on conversion calculated from Eqns. (4) and (12—15) with K = 136 s^{-1}, B = 7.5 × 10^{-5} m $s^{-1/2}$, D_{eff} = 6 × 10^{-10} m^2 s^{-1} for a reactor volume of 20 μl and a reactor diameter of 1.5 mm. Particle diameters: 50, 100 and 200 μm.

TABLE 4

Inherent rate constant of peroxidase immobilized on CPG (72.9 nm pore diameter). D_{eff} estimated as 6 × 10^{-10} m^2 s^{-1}

d_p (μm)	K_{ps} (s^{-1})	K (s^{-1})	ϕ_s	η_i
100	16.4	136	8	0.12
150	11.9	156	13	0.08

conversion of changes in the particle diameters is illustrated in Fig. 6, where both internal and external mass transfer has been taken into account. The curves were calculated for reactors having the same physical form. The inherent rate constant, K, is free of all mass transfer limitations. It depends on the reagent and on the properties of the actual batch of immobilized enzyme. It is therefore a conditional rather than an intrinsic constant.

Optimization

One optimization objective for enzyme reactors in flow injection analysis, is to reach a certain level of conversion with a minimum of dispersion. The first step is to optimize the immobilization procedure in order to reach a high inherent activity. The utilization of the inherent activity should then be optimized in order to achieve a low residence time. The latter is related to low dispersion provided that some constraints on the dimensions are observed.

The residence time can be expressed in terms of the inherent rate constant, the degree of conversion, and some physical parameters, through Eqns. (4) and (12—14):

$$\tau = \left\{ [d_p^{3/2}/BF^{1/2}] + \left[\phi_s/K\left(\frac{1}{\tanh 3\phi_s} + \frac{1}{3\,\phi_s}\right)\right]\right\} [-\ln(1-X)] \qquad (16)$$

It can be seen that for a decreasing particle diameter (ϕ_s equals d_p multiplied by a constant (Eqn. 15)) and an increasing linear flow velocity, the residence time tends to a constant minimal value

$$\tau_{min} = K^{-1}\ [-\ln(1-X)] \qquad (17)$$

i.e., minimal dispersion is obtained when all resistance to mass transfer is absent.

Increased flow velocity and decreased particle size will both contribute to a larger pressure drop, ΔP (Nm^{-2}), over the reactor. An expression for ΔP is obtained by putting the relevant quantities into Darcy's equation, which then becomes

$$\Delta P = \tau\ F^2\ d_p^{-2}\ (\varphi\ \nu^*) \qquad (18)$$

(The product of the column resistance factor, φ, and the dynamic viscosity, ν^*, is approximately 1 N s m^{-2} [21] for irregular particle shapes and dilute aqueous solutions.)

With a limit set on the pressure drop, the relative importance of d_p and F on the residence time has to be assessed. It can be seen that in Eqn. (16) decreased particle size is of greater consequence than increased linear flow velocity, and that there will be no undue weighting for either of the parameters in Eqn. (18). It can therefore be concluded that in order to minimize the residence time, and hence the dispersion, the linear flow velocity should be sacrificed in favour of a reduced particle diameter.

The procedure to be followed in optimizing the bed geometry starts by

selecting the smallest practical particle size. The degree of conversion is then fixed. The next step involves a simultaneous computation of the residence time and the maximum linear flow velocity which fit the selected maximum value of ΔP. With the linear flow velocity fixed, the reactor diameter is adjusted to fit the desired volumetric flow rate. The reactor volume can then be determined from (residence time) × (volumetric flow)/(total void fraction).

To facilitate visualization of the relationships, two plots illustrating the dependence of reactor volume and back-pressure on the reactor diameter, are shown in Fig. 7. The plots are calculated for a particle diameter of 100 μm, with the assumptions that the conversion is 99.9%, the volumetric flow rate 1.0 ml min^{-1}, and the constants B and K as found experimentally. The dotted arrows illustrate how the selection of parameters proceeds; if the back-pressure of the reactor is chosen as 0.7 atm., the reactor diameter then should be 1 mm, which gives a required reactor volume of 20 μl. The steep rise in back-pressure below a certain reactor diameter is noteworthy.

The optimal residence time for three inherent rate constants, 10, 100 and 1000 s^{-1}, are plotted versus the particle diameter in Fig. 8. The curves are all calculated for a back-pressure of 1 atm at a fractional conversion of 99.9%. At the limit, when the particle diameter becomes very small, the

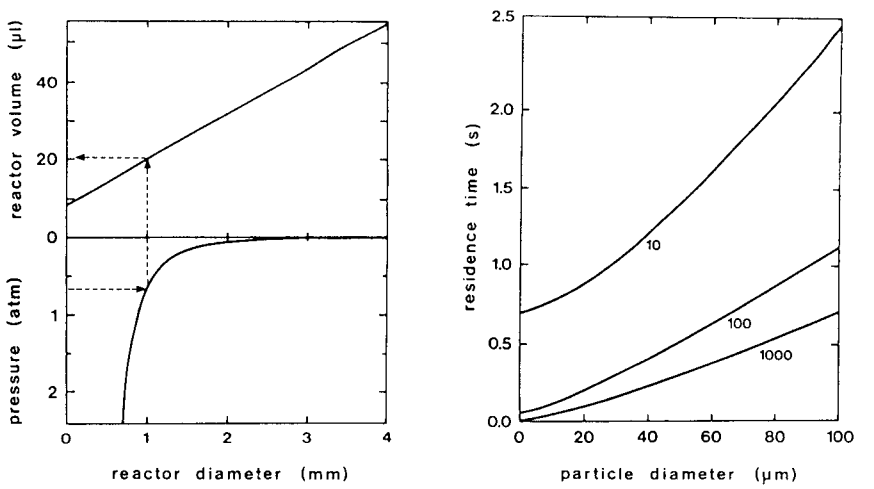

Fig. 7. Optimization of a peroxidase reactor. The dotted arrows show how the selection of parameters proceeds. Calculated from Eqns. (16) and (18) with K = 136 s^{-1}, d_p = 100 μm, $B = 7.5 \times 10^{-5}$ m $s^{-1/2}$. $D_{eff} = 6 \times 10^{-10}$ m^2 s^{-1}. $\varphi = 1 \times 10^3$, and $\nu^* = 1 \times 10^{-3}$ N s m^{-2} for a conversion of 99.9% and a flow rate of 1 ml min^{-1}.

Fig. 8. The residence time required for 99.9% conversion at a back-pressure of 1 atm as a function of the particle diameter. Calculated from Eqns. (16) and (18) with $B = 7.5 \times 10^{-5}$ $ms^{-1/2}$, $D_{eff} = 6 \times 10^{-10}$ m^2 s^{-1}. $\varphi = 1 \times 10^3$ and $\nu^* = 1 \times 10^{-3}$ Ns m^{-2} for the inherent rate constants: 10, 100 and 1000 s^{-1}.

apparent rate constant approaches the inherent rate constant. It can also be seen that for an active enzyme preparation ($K > 100\ s^{-1}$), the smallest possible particle diameter should be selected. For a less active preparation ($K < 10\ s^{-1}$), there is little to be gained from particle sizes smaller than 20–30 μm.

The authors are indebted to Professor Gillis Johansson for his stimulating interest and valuable discussions concerning this work.

REFERENCES

1 L. Gorton and L. Ögren, Anal. Chim. Acta, 130 (1981) 45.
2 A. Iob and H. A. Mottola, Anal. Chem., 52 (1980) 2332.
3 G. Johansson, Appl. Biochem. Biotech., 7 (1982) 99.
4 G. Johansson, L. Ögren and B. Olsson, Anal. Chim. Acta, 145 (1983) 71.
5 B. Olsson, L. Ögren and G. Johansson, Anal. Chim. Acta, 145 (1983) 101.
6 K. G. Paul, in P. D. Boyer, H. Lardy and K. Myrbäck (Eds.), The Enzymes, Vol. 8, 2nd ed., Academic Press, New York, 1963, p. 2.
7 B. W. Griffin and P. L. Ting, Biochem., 17 (1978) 2206.
8 F. T. Nayler and B. C. Saunders, J. Chem. Soc., (1950) 3519.
9 A. J. Karabelos, T. H. Wegner and T. J. Hanratty, Chem. Eng. Sci., 26 (1971) 1581.
10 L. K. McCune and R. H. Wilhelm, Ind. Eng. Chem., 41 (1949) 1124.
11 B. J. Rovito and J. R. Kittrell, Biotech. Bioeng., 15 (1973) 143.
12 C. N. Satterfield, Heterogeneous Catalysis, M.I.T. Press, Cambridge, 1970, p. 129.
13 H. H. Weetall, in K. Mosbach (Ed.), Methods in Enzymology, Vol. 44, Academic Press, New York, 1976, p. 134.
14 A. S. Brill, in M. Florkin and E. H. Stotz (Eds.), Comprehensive Biochemistry, Vol. 14, Elsevier, Amsterdam, 1973, p. 447.
15 P. Thibault, P. Monsan and C. Jouret, Sci. Aliment., 1 (1981) 55.
16 C. Flemming, A. Gabert and H. Wand, Acta Biol. Med. Ger., 32 (1974) 135.
17 Kikutake Junichiro, Jpn. Pat., Jpn. Kokai Tokkyo Koho, 78, 104, 789 (1978).
18 R. Epton, G. Marr and R. G. Ridley, Polymer, 20 (1979) 1447.
19 R. A. Messing and H. H. Weetall, U.S. Pat. 3, 519, 538 (1970).
20 D. L. Eaton, in D. E. Leyden and W. T. Collins (Eds.), Silylated Surfaces, Gordon and Breach, New York, 1980, p. 201.
21 J. M. Reijn, Flow Injection Analysis, Doctoral Thesis, Utrecht, 1982, p. 100.

Analytica Chimica Acta, 145 (1983) 101—108
Elsevier Scientific Publishing Company, Amsterdam — Printed in The Netherlands

AN ENZYMATIC FLOW INJECTION METHOD FOR THE DETERMINATION OF OXYGEN

BO OLSSON, LARS ÖGREN[a] and GILLIS JOHANSSON*

Department of Analytical Chemistry, University of Lund, P.O. Box 740, S-220 07 Lund (Sweden)

(Received 24th July 1982)

SUMMARY

An enzymatic flow injection method for the determination of dissolved oxygen is described. Oxygen from the sample is reduced quantitatively to hydrogen peroxide in a packed-bed reactor containing immobilized glucose oxidase. β-D-Glucose is used as a cosubstrate. The effluent is mixed with a stream containing chromogens and fed into a second reactor containing immobilized peroxidase. The coloured product formed is monitored spectrophotometrically. The response is linear from the detection limit (2—5 μM O_2) to air-saturated samples (0.3 mM O_2) when the peak areas are plotted versus the O_2 content in the samples (50 μl). The maximum speed for 1% carry-over is 60 samples per hour and the results are available 25 s after the start of sampling. Broadening of the peak is caused by adsorption of the coloured product in the peroxidase reactor.

Dissolved oxygen is an important co-substrate in many enzyme reactions. Usually the oxygen is in excess, e.g., when glucose oxidase is used for determination of β-D-glucose. The reaction works equally well when β-D-glucose is in excess and the dissolved oxygen is the limiting substrate. It should be possible to utilize any of a number of oxidoreductases for determination of dissolved oxygen. There appears to be only one earlier study in which oxygen was determined enzymatically [1].

The selectivity of glucose oxidase for the oxidant is high [2], the stability of the enzyme is also good and it is readily available in high purity at low cost. The reaction involves the coenzyme FAD (flavine adenine dinucleotide) which is permanently bound in the enzyme.

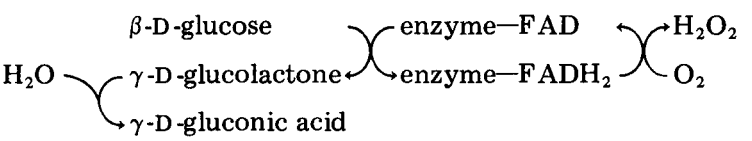

(1)

With β-D-glucose in excess, the flavine will be present in the reduced form, $FADH_2$. Reoxidation of $FADH_2$ with oxygen produces hydrogen peroxide quantitatively.

[a]Present address: AB Draco, P.O. Box 1707, S-221 01 Lund, Sweden.

Numerous methods are available for determination of hydrogen peroxide [3] and an electrochemical method has already been developed for flow injection analysis [4]. An enzymatic method was selected because of its high selectivity. Possible interferents are substances (e.g., phenolic compounds and some aromatic amines) which will react with or substitute the co-reactant. The enzymatic method involves peroxidase-catalyzed coupling of hydrogen peroxide with chromogens to a coloured product. Such reactions have been studied extensively because of their importance for determination of β-D-glucose and at least 35 reagents have been investigated more or less thoroughly. 4-Aminophenazone and *N*,*N*-dimethylaniline were selected for the present study

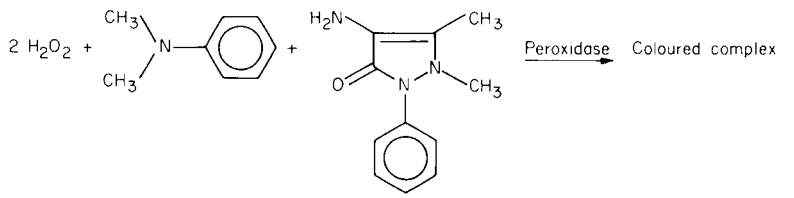

(2)

The detailed reaction mechanism is not known. It has been observed in this laboratory that the absorbance is somewhat less with immobilized peroxidase than with the soluble enzyme.

In the method described by Ghosh et al. [1] oxygen was reacted with a known excess of β-D-glucose as in Eqn. (1). The hydrogen peroxide was simultaneously destroyed by catalase which was present as an impurity. The enzymes were next destroyed by boiling. The remaining β-D-glucose was then determined spectrophotometrically with oxygen in excess in the usual way (Eqns. 1 and 2). In the method proposed here, the hydrogen peroxide formed in the reaction with glucose oxidase is determined directly on-line with the peroxidase-catalyzed colorimetric method (Eqn. 2). The glucose oxidase should be essentially free of catalase in order to prevent decomposition of the hydrogen peroxide.

EXPERIMENTAL

Flow injection system

A buffer containing β-D-glucose is pumped through the injector to a reactor with immobilized glucose oxidase as shown in Fig. 1. Chromogens are pumped in a second channel to a confluence point where the stream mixes with the sample stream. The colour-forming reaction takes place in a reactor with immobilized peroxidase and the product is monitored at 555 nm with a variable-wavelength flow-through spectrophotometer (LKB model 215). The sample is drawn into the sample loop (50 μl) by a second pump (LKB Vario-perpex) operated for 5 s at 3.0 ml min^{-1} for each sample. The slide injection valve (Cheminert SVA 8031) was operated by two pneumatic actuators controlled by a desk-top computer (ABC 800, Luxor, Sweden). The computer

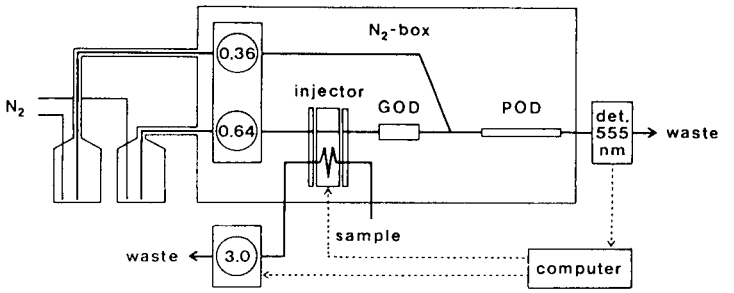

Fig. 1. Flow injection system for detection of oxygen. GOD, glucose oxidase reactor; POD, peroxidase reactor. For a detailed explanation, see text.

also controlled the sampling pump and collected absorbance values from the spectrophotometer. The computer evaluated the data and displayed the peak and operational parameters on the screen.

The reagents were contained in glass bottles which were connected to the pump tubings with 0.9 mm i.d. teflon for the liquid lines and coaxially with 2.5 mm i.d. nylon tubing for the gas line. The flow rates were 0.64 and 0.36 ml min^{-1} for the glucose and chromogen buffers, respectively. The connection to the spectrophotometer was through 0.3 mm i.d. teflon tubing.

The head of the reagent pump (Gilson, Minipuls 2) was fitted with a polycarbonate gas-tight box (volume 4 l) which also housed the injection valve and the enzyme reactors. Purified nitrogen (<10 ppm O_2), delivered by pressure regulators with steel membranes through steel and nylon tubing, was bubbled through the reagent bottles. The nitrogen passed into the gas-tight box via the coaxial connection and was vented through a safety valve in the box set for a slight overpressure. Oxygen exchange with the atmosphere has to be prevented up to the glucose oxidase reactor. After that it will not influence the results. The sample inlet tube was of thick-walled nylon (0.8 mm i.d., 2.5 mm o.d.). The permeation rate of oxygen through teflon and PVC is 250—500 times faster than through nylon-6. As there are no pump tubings available in oxygen-tight materials, it was necessary to resort to a gas-tight box for the pump head. The measures undertaken for the prevention of oxygen exchange and contamination were fully adequate.

Reagents

The injection line contained a 0.01 M phosphate buffer, pH 6.0, with 1 mM β-D-glucose (Pharmacia Fine Chemicals). The chromogen line contained a 0.14 M phosphate buffer, pH 6.0, with 2.14 mM 4-aminophenazone (BDH Chemicals), 6.92 mM *N,N*-dimethylaniline (99.5%; Riedel-de Haën) and 2.25% triethylamine (Fluka, p.a.). Selection of reagents is critical for the stability. Chemicals from some other manufacturers were not of sufficient purity. The chromogen buffer was renewed daily.

Enzyme reactors

Glucose oxidase from *Aspergillus niger* (EC 1.1.3.4) with less than 1.7% catalase activity (Serva) was azo-coupled to porous glass CPG-10 (Electro-nucleonics; pore diameter 72.9 nm, 120—200 mesh). A portion (0.25 ml) of 0.1 M phosphate buffer, pH 7.0, was added to 0.75 ml of enzyme solution (14 mg ml^{-1}); 0.9 ml of the resulting solution was added to 0.1 g of arylamino glass. The coupling gave a yield of 48%, i.e., 43 mg of glucose oxidase per g of glass. The enzyme-glass was wet-packed in a teflon reactor (2.7 mm i.d., 14.7 mm long, volume 84 μl).

Peroxidase from horse radish (EC 1.11.1.7; Sigma Type VI, P6140) was also azo-immobilized to porous glass [5] with the same pore and particle size. The immobilization gave a yield of 36%, i.e., 28 mg of peroxidase per g of glass. The enzyme-glass was wet-packed in a teflon tubing (1.0 mm i.d., 28 mm long, volume 22 μl). The packing was retained in the reactor by two nickel screens which were sealed against the flanged tube endings and held in place by Altex screw couplings.

Calibration

A three-necked 500-ml flask was fitted with an oxygen electrode (Beckman Monitor System 123305) in the center and a thermometer (±0.05° C) in one side port. The sampling line and tubings for air or nitrogen were fitted into the remaining port. The flask was filled with air-saturated 0.01 M phosphate buffer, pH 6.0. The oxygen electrode was calibrated by using the tables given by Hitchman [6]. The barometric pressure was read to ±1 mm Hg. Samples were also drawn into the sample loop and injected into the system described above. Other oxygen levels were produced by gas bubbling and determined with the oxygen electrode.

Hydrogen peroxide was standardized by visual titration with potassium permanganate.

RESULTS AND DISCUSSION

Properties of the method

Samples with various amounts of dissolved oxygen were injected into the system. The peak absorbances and peak integrals were plotted versus the sample oxygen concentration as determined by the electrode (Fig. 2). A straight line passing the origin is obtained when the peaks are integrated; peak height measurements resulted in a curved plot.

The colour-forming reaction in the peroxidase reactor can be tested separately if samples of hydrogen peroxide are injected. The β-D-glucose is of course excluded from the reagent pumped through the injection line during this test. The results are again plotted in Fig. 2. The peak absorbances fall exactly on the same line as those for the oxygen determination. This shows that the bend in the calibration is due to the colour-forming reaction and also that the reaction in the glucose oxidase reactor (Eqn. 1) is quantitative.

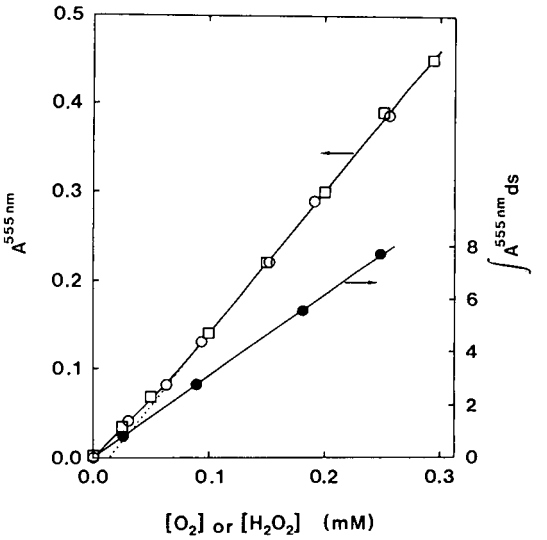

Fig. 2. Calibration curves for oxygen (○, ●) and hydrogen peroxide (□). Open symbols correspond to peak heights, and filled symbols to peak integrals.

Figure 3A shows the peak form when various amounts of dissolved oxygen were injected. There is a pronounced tailing in the peaks which is especially severe for small amounts of oxygen. A larger proportion of the coloured product is delayed in the system at low levels which explains the need to integrate the peaks in order to achieve a linear calibration plot.

In order to assess the physical dispersion of the system, catechol solution was used as a sample and monitored at 275 nm. Table 1 gives the peak widths at various heights for the catechol sample compared to an oxygen

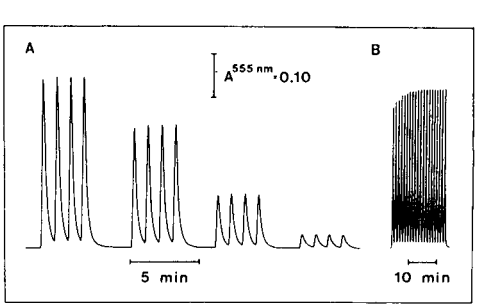

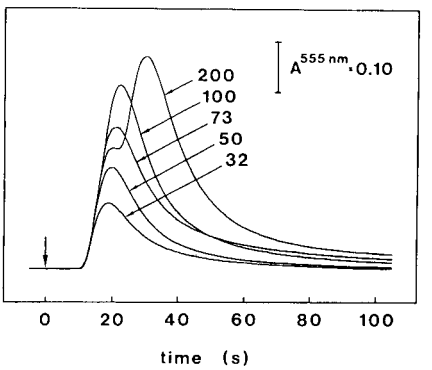

Fig. 3. Peak shapes. A, aged reactor with samples containing 0.248, 0.181, 0.089 and 0.026 mM O_2; B, new reactor, air-saturated samples.

Fig. 4. Variation in peak shape with sample volume (200, 100, 73, 50 and 32 μl) of air-saturated samples.

TABLE 1

Peak width(s) at half ($t_{w\,1/2}$), a tenth ($t_{w\,1/10}$), and hundredth ($t_{w\,1/100}$) of the peak height (Sample volume 50 μl, flow rate 1 ml min^{-1})

	Sample		
	Catechol	O_2 [a]	O_2
$t_{w\,1/2}$	5	13	25
$t_{w\,1/10}$	11	31	69
$t_{w\,1/100}$	18	60	>120

[a] With triethylamine added to the reagent solution.

sample. It can be concluded from the data that the peak broadening during oxygen determination is due to adsorption of the coloured product in the peroxidase reactor. An amine was therefore added to the final reagent in order to repress the adsorption and the effect of the addition can also be seen in Table 1. These data show that sixty oxygen samples can be processed per hour if a carry-over of 1% is acceptable. In the absence of adsorption, the system should have been able to process 200 samples per hour.

The colour of the peroxidase reactor can be seen through the teflon wall; it darkens permanently with use, probably because of polymerization and irreversible adsorption of the product. For a new reactor, the peak heights will increase with successive injections when a solution containing a high level of oxygen is sampled (Fig. 3B). The effect disappears completely with ageing of the reactor.

It is known that some of the available reagents for peroxidase-catalyzed colorimetric determination of hydrogen peroxide adsorb to porous glass [7, 8]. The present reagents were used before in this capacity without undue adsorption [8]. In the present study, peroxidase was azo-coupled to aryl-amino-glass whereas alkylamino-glass and glutaraldehyde coupling were used earlier. The reason for sticking to the former immobilization method in spite of its larger adsorption is that it gives a product with superior activity and stability [5].

The peak-to-peak noise corresponds to 0.001 absorbance unit. The detection limit, however, is set by the adsorption and is estimated as 2—5 μM oxygen. The peaks are evaluated relative to the base-line so that the background will be subtracted automatically. Nevertheless, the reagent blank should be reasonably low, otherwise the accuracy will be degraded. When the chromogen reagent was fresh, its absorbance was negligible (<0.001) but it increased during the day. The rate of increase varied from one batch of reagents to another.

The system was designed for a maximum oxygen level corresponding to 50 μl of air-saturated sample. The range may be adjusted, as usual in flow injection analysis, by adjusting the sample size. Oxygen-saturated solutions can be analyzed with 10-μl sample volumes.

Design of the flow injection system

The glucose oxidase reactor is the main dispersing element in the system if non-adsorbed compounds are considered. The actual peak shapes are determined mainly by adsorption in the peroxidase reactor and there is therefore little to be gained by attempting to reduce dispersion in the glucose oxidase reactor. The reactor size is large enough to convert essentially all the substrate to product, which is advantageous for an analytical system [9].

The optimization of peroxidase reactors is discussed separately [5]. Immobilization to 25-nm pore diameter glass was found to give the most active preparation. However, as the product adsorbs to the glass surface, it is here essential to optimize the activity with respect to surface area. A larger pore diameter will give a lower loading but with a better utilization of the enzyme. Although the volume of the reactor will be larger, the surface area will be lower, resulting in less adsorption. The reactor geometry was designed in accordance with the theory presented [5] to give 99.9% conversion with as small volume as possible.

In determining the size of the glucose-oxidase reactor, the difference between steady-state and f.i.a. measurements with large samples must be considered. When the β-D-glucose buffer was air-saturated and pumped through the reactor, the conversion of oxygen was essentially 100% up to 3.5 ml min^{-1}. The over-capacity seems to be 3.5 times (if the effect of increased mass transfer by increased linear flow is neglected). The dynamic properties of the reactor for various sample volumes are shown in Fig. 4. The peak height first increases with sample volume as usual, but at 200 μl a plateau is formed on the rising part of the curve. The level coincides with the amount of reduced coenzyme in the reactor (14 nmol equivalent to 60 μl of air-saturated sample). The amount was calculated from the known enzyme loading. The plateau appears because the sample plug is so long that the amount of β-D-glucose is insufficient in the middle. All the reduced $FADH_2$ in the reactor is then oxidized by oxygen and the sample then passes through without reaction.

A practical consequence of the limited capacity to reduce oxygen is that the amount of oxygen in large samples should not exceed 14 nmol. With small sample volume, β-D-glucose is mixed with the sample and more oxygen can be reduced.

Glucose oxidase was previously immobilized using glutaraldehyde coupling [8] whereas azo coupling was used in this study. Both methods yield active and stable reactors and no grounds for preference of one over the other have appeared so far.

Properties of the new method

The enzymatic method measures the amount of dissolved oxygen in the sample, in contrast to the oxygen electrode which measures the partial pressure. For standardized conditions like those used above, the information is independent of the principle but this is not so generally [6].

The injected sample volume is 50 μl but another 200 μl is required before the sample loop is completely flushed. Still, this is a moderate requirement compared to the usual oxygen methods. The result is available at the computer 25 s after the start at the sampling pump which again compares favourably with existing methods. If the glucose reactor has 100% conversion efficiency, the method can be calibrated with hydrogen peroxide samples. Some of the advantages are due to the f.i.a. principle and some to the chemical reaction scheme utilized.

The prospects for further development of the method seems to be good. If the peak broadening caused by adsorption could be remedied, the peak height and thus the sensitivity could be increased. The sample volume could then be reduced correspondingly or the detection limit could be decreased, and the sample throughput could be increased. Several routes are open for further work in order to reduce adsorption (e.g., different reagents, supports or immobilization method).

REFERENCES

1 A. Ghosh, V. Janic and H. A. Sloviter, Anal. Biochem., 38 (1970) 270.
2 M. Dixon, Biochim. Biophys. Acta, 226 (1971) 269.
3 G. G. Guilbault, Handbook of Enzymatic Methods of Analysis, Clinical and Biochemical Analysis Vol. 4, Dekker, New York, 1976.
4 H. Lundbäck, Anal. Chim. Acta, 145 (1983) 000.
5 B. Olsson and L. Ögren, Anal. Chim. Acta, 145 (1983) 000.
6 M. Hitchman, Measurement of Dissolved Oxygen, Wiley-Interscience, New York, 1978.
7 P. Thibault, P. Monsan and C. Jouret, Sci. Aliments, 1 (1981) 55.
8 L. Gorton and L. Ögren, Anal. Chim. Acta, 130 (1981) 45.
9 G. Johansson, L. Ögren and B. Olsson, Anal. Chim. Acta, 145 (1983) 71.

Analytica Chimica Acta, 145 (1983) 109—116
Elsevier Scientific Publishing Company, Amsterdam — Printed in The Netherlands

STUDIES OF DRUG—PROTEIN BINDING INTERACTIONS BY FLOW INJECTION ANALYSIS WITH FLUORIMETRIC DETECTION

G. L. ABDULLAHI, J. N. MILLER* and H. N. STURLEY[a]

Department of Chemistry, Loughborough University of Technology, Loughborough, Leicestershire, LE11 3TU (Gt. Britain)

J. W. BRIDGES

Robens Institute of Industrial and Environmental Health and Safety, University of Surrey, Guildford, Surrey, GU2 5XH (Gt. Britain)

(Received 9th August 1982)

SUMMARY

The applicability of single-channel and merging-zones flow injection systems with fluorimetric detection to the study of drug-protein binding interactions has been demonstrated. A study of the binding of the fluorescent probe 8-anilinonaphthalene-1-sulphonic acid (ANS) to human serum albumin by means of such systems gave results identical to those obtained by a static procedure, but the flow injection procedure was much more convenient. The flow injection methods were also used in pure albumin solution and in diluted serum to study the displacement of ANS by acidic drugs. The flow injection procedures were extended to investigate the binding of basic drugs to α_1-acid glycoprotein. A recent fluorescence probe derived from propanolol permitted calculations of the number and strength of the binding sites on this protein for propanolol and other drugs.

Drug—protein binding interactions are of great significance in analyses for drugs in biological samples. A very high proportion of a drug in blood serum, for example, may be bound to one or more serum proteins; it may then be necessary to ensure that an analytical procedure determines the total drug concentration, not just the concentration of the "free" (unbound) drug. Yet it is normally assumed that only the free drug is pharmacologically active, so that it may be desirable to determine the free drug only. Additionally, it frequently happens that two or more drugs or endogenous molecules compete for the same binding sites on a protein surface. Such competitive interactions can dramatically alter the activity of a drug. Drug—protein binding studies seek to establish two main points: the protein(s) in serum, tissues, etc., to which the drug is bound; and the number of binding sites present on a particular protein, with their relative strengths of binding (association constants).

[a]Present address: Amersham International Ltd., White Lion Road, Amersham, Great Britain.

Drug—protein binding studies in serum have largely concentrated on the binding of acidic drugs [1]. It is well established that such molecules normally bind to albumin, the most abundant serum protein. Several different physical methods have been used to investigate such interactions, but fluorescence methods are particularly attractive by virtue of their speed, sensitivity and large concentration range. Fluorimetric methods avoid the need for a physical separation of bound and unbound drug by observing changes in fluorescence intensity and/or wavelength that accompany binding; such changes may be undergone by the drug, the protein or a third (probe) molecule which competes with the drug for the protein-binding sites [2].

In contrast to the many studies of drug—protein interactions of acidic drugs, very much less is known about the behaviour of basic drugs. While some basic drugs may bind to albumin in pure solution [3], it is believed that in serum they bind preferentially to more acidic proteins [4]. Particularly important is α_1-acid glycoprotein (AAGP, also known as orosomucoid), a molecule of relative molecular mass ca. 44,000 containing some 40% carbohydrate, including 14 sialic acid residues [5]. Studies of protein binding with basic drugs have been inhibited by the lack of suitable fluorescent probes, but the recent synthesis of 1-{[2-(5-dimethylamino)naphthalene-1-sulphonylaminoethyl]-amino}-3-(1-naphthaleneoxy)-2-propanol (DAPN), a fluorescent probe derived from the basic drug propanolol [6], has permitted the extension of the fluorimetric approach in this area.

Flow injection analysis (f.i.a.) can readily be used with fluorimetric detectors [7, 8] and its rapidity and convenience, combined with its economy of samples and reagents, make it ideal for drug—protein binding studies. The present paper describes the application of f.i.a. to systems involving both acidic and basic drugs, showing for the first time the suitability of DAPN in the latter area. A brief preliminary account of that part of the work relating to acidic drugs has appeared elsewhere [9].

EXPERIMENTAL

The flow injection systems were built from polystyrene tubing of 0.57- or 0.75-mm internal diameter, the flowing carrier stream being propelled by a constant-head device (Mariotte flask) or by a peristaltic pump (Mini-S type, Ismatec, Zurich, Switzerland); flow rates were typically 2.5 ml min^{-1}. In single-channel experiments samples (ca. 20 μl) were injected through flap or septum injection valves. Merging-zone experiments utilised a double injection valve (Bifok, Sollentuna, Sweden) to inject similar volumes. Up to 100 cm of tubing separated the valve from the detector; the dispersion was $\geqslant 2.5$. Glass or silica flow cells (ca. 45 μl) were used in conjunction with Perkin-Elmer models 1000, 1000M, 2000 and MPF 44B fluorescence spectrometers as detectors. The same spectrometers were used in the static experiments (with 10-mm cuvettes) which were done for comparison purposes.

Human serum albumin, human AAGP, DAPN and 8-anilinonaphthalene-1-sulphonic acid (ANS) were products of Sigma. The AAGP was freed from traces of albumin by passing it through a short column of Blue Sepharose CL-6B (Pharmacia Ltd.) [10]. Buffer salts were of the highest grade commercially available and water was thrice-distilled from a silica still. Blood serum samples were volunteered by healthy laboratory workers.

Scatchard [11] plots were made by means of a computer program developed in this laboratory: the program corrects for inner filter effects [12] and for the background fluorescence of unbound fluorescent probe molecules.

RESULTS

In preliminary experiments, the binding of ANS to human serum albumin was studied, and the displacement of this probe was used to investigate the binding of other anionic species. It is well known [13] that ANS provides a very large enhancement of fluorescence on binding to albumin. In the present work the enhancement effect was observed when both single-channel and merging-zones flow injection systems were used. The merging zones furnished better mixing of sample and reagent, and utilised smaller volumes of both, and so this system was used routinely. An analysis of the results using the Scatchard [11] method is shown in Fig. 1. The f.i.a. data were obtained for flow rates of 3.0 ml min^{-1} in each channel. The buffer solution was 0.1 M tris(hydroxymethyl)-aminomethane hydrochloride, and the sample volume was 35 μl. Albumin and ANS solutions were maintained at 23 ± 0.5°C before injection. A short stopped-flow time (60 s) was sometimes used, but in the absence of competitive binding effects made little difference to the fluorescence observed. Fluorescence was observed at 460 nm (excitation wavelength 375 nm) with a spectral bandwidth of 20 nm. With a dispersion of 9.6, the coefficient of variation of replicate measurements was

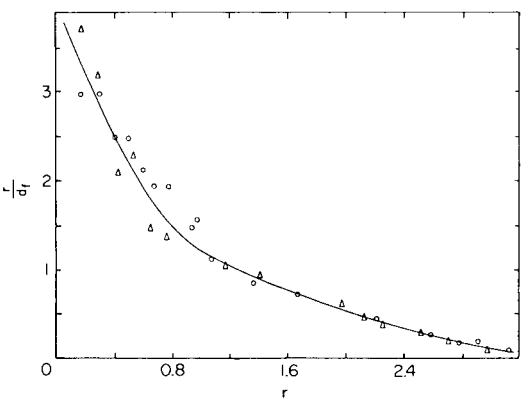

Fig. 1. Scatchard plot showing the binding of ANS to human serum albumin as determined by both static (○) and f.i.a. (△) fluorescence studies; r represents the number of moles of ANS bound per mole of protein, and d_f the concentration of the free ANS.

1.85%. In the experimental conditions used, inner filter effects and background signals arising from albumin and unbound ANS were negligible: intensity measurements could thus be converted directly to "bound ANS" concentrations. Figure 1 shows that the static and f.i.a. methods produced very similar results. Computer analysis of the data assumed a model with two types of binding site on the protein, with n_1 sites of the first type and n_2 of the second, the corresponding association constants being $(k_A)_1$ and $(k_A)_2$. The results of a best-fit analysis yielded $n_1 = 0.79$, $(k_A)_1 = 4.21 \times 10^6$ M; $n_2 = 2.72$, $(k_A)_2 = 0.23 \times 10^6$ M^{-1}.

Binding studies of acidic drugs

Table 1 shows the results of experiments in which ANS and acidic drugs competed for binding sites on the albumin molecule. These experiments were conducted in a merging-zones system, albumin being injected into one flowing stream of buffer, and a mixture of ANS and competing drug into

TABLE 1

Binding of acidic drugs to human serum albumin

Drug	Concentration (M)	% ANS displaced[a]	
		F.i.a.	Static
Sulphisomidine	10^{-4}	1.1	1.8
	10^{-5}	0.5	0.3
Sulphisoxazole	10^{-4}	4.7	3.6
	10^{-5}	1.8	1.0
	5×10^{-5}	(1.7)	(2.8)
Warfarin	10^{-4}	8.0	9.5
	10^{-5}	1.0	3.2
Phenylbutazone	10^{-4}	19.2	19.1
	10^{-5}	3.8	4.2
2-*p*-(Chlorophenoxy)-2-methylpropionic acid	10^{-4}	15.3	17.9
	10^{-5}	4.6	5.4
Ethacrynic acid	10^{-4}	30.8	37.6
	10^{-5}	16.4	13.7
	5×10^{-5}	(28.9)	(27.8)
Flufenamic acid	10^{-4}	46.7	53.8
	10^{-5}	19.7	16.1
	5×10^{-5}	(40.7)	(40.9)

[a]ANS concentration 5×10^{-6}—10^{-5} M. Numbers in parentheses show the results of experiments in which 50-fold diluted normal human serum was used as sample; in other cases the sample was 10^{-5} M human serum albumin.

the other. Again agreement between the f.i.a. and static methods is generally good, though some differences are apparent in the cases of flufenamic and ethacrynic acids. There was some evidence that such discrepancies might be ascribed to kinetic effects in the binding of ANS to albumin in the presence of competing molecules. Incorporation of a stopped-flow time of 60 s into the system produced substantial (ca. 30%) intensity changes in the case of flufenamic acid. In the competitive experiments utilising f.i.a., inner filter effects were again negligible in all cases except that of flufenamic acid, where a correction was needed. Table 1 also shows that the flow injection method can be used satisfactorily with serum samples: agreement between the static and f.i.a. approaches was excellent and at a dilution of 1:50 the background fluorescence of serum was negligible.

Binding studies of basic drugs

The drug—protein binding studies on basic drugs were facilitated by the fluorescence properties of DAPN. Preliminary experiments showed that the excitation and emission wavelengths of the molecule in free solution were 337 nm and 558 nm, respectively. On binding to AAGP, the fluorescence of DAPN increased approximately eight-fold and the excitation and emission wavelengths changed to 343 nm and 530 nm, respectively. After allowance had been made for the readily detectable fluorescence of unbound DAPN, graphical analysis showed that the protein has one strong binding site for DAPN ($k_A = 2 \times 10^6$ M^{-1}) and probably two weaker sites. In a single-channel flow injection system, injection of AAGP samples into a flowing stream containing DAPN (3.2 μg ml^{-1}) produced a linear increase in fluorescence over the AAGP concentration range 5—140 μg ml^{-1}. These and other experiments with DAPN utilised 0.05 M phosphate buffer, pH 7.0. Excitation and emission wavelengths were 346 nm and 525 nm, respectively.

The displacement of the bound DAPN by the "parent" drug propranolol was studied in two experiments. In the first (Fig. 2), samples containing AAGP and varying amounts of propranolol were injected into a DAPN stream. As the propranolol progressively displaced the probe from the protein, the signal intensity (measured against the constant fluorescence of the DAPN carrier stream) progressively decreased towards zero. Greater economy of sample and reagent was achieved when a merging-zones system was used: a DAPN/AAGP mixture was injected into one buffer stream and propranolol into the other. The results (Fig. 3) show that the fluorescence intensity of the merged zones decreased with increasing propranolol concentration until it corresponded to the fluorescence intensity of unbound DAPN. Similar studies showed that imipramine and chlorpromazine both displaced DAPN from the AAGP. In these cases the intrinsic fluorescence of the imipramine and (especially) chlorpromazine complicated the interpretation of the data, but the reduction in DAPN fluorescence could easily be detected at low concentrations of the drugs.

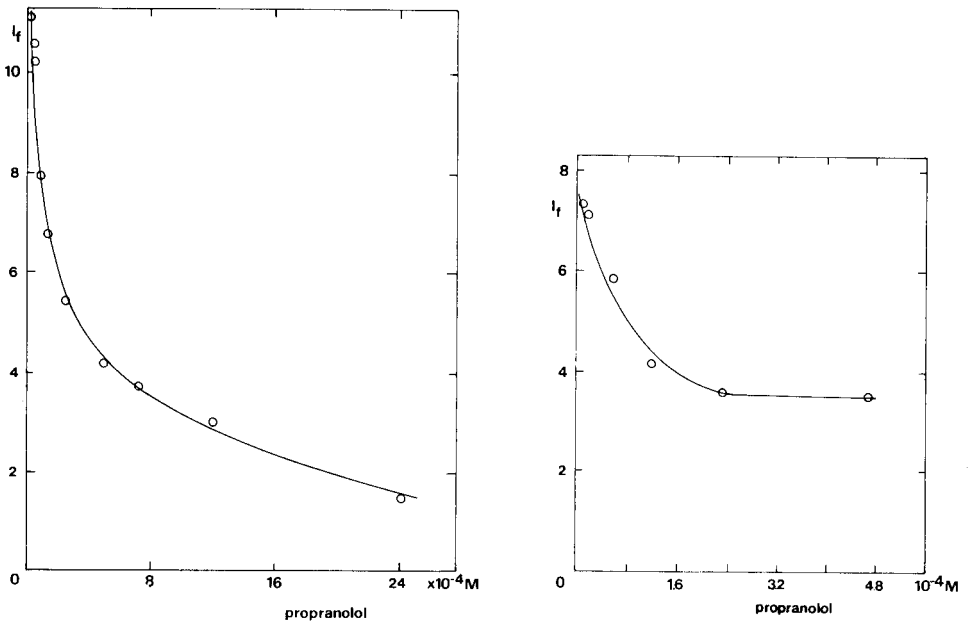

Fig. 2. Displacement of DAPN from AAGP by propranolol, determined by single-channel f.i.a. The vertical axis shows the intensity of fluorescence above the constant signal given by the flowing stream containing DAPN (3.4 μg ml^{-1}). Samples (20 μl) contained AAGP (0.16 mg ml^{-1}) and varying concentrations of propranolol.

Fig. 3. Displacement of DAPN from AAGP by propranolol, determined by merging-zones f.i.a. A mixture of DAPN (20 μg ml^{-1}) and AAGP (0.27 mg ml^{-1}) was injected into one stream and various concentrations of propranolol into the other.

DISCUSSION

The results obtained by f.i.a. in this work accord well with those reported by previous authors, and with the comparative measurements made in static systems. For example, it is well established that ANS binds to albumin at several sites, but preferentially at a site in the *N*-terminal domain of the protein: co-operative binding phenomena are probably involved [13, 14]. The computer model used in the present studies arbitrarily assumes two classes of non-interactive binding sites, and must be interpreted cautiously. Nonetheless, the existence of one strong binding site and several weaker ones is clearly shown. Investigations of the binding of various drugs to albumin, measured indirectly by using ANS displacement, were also in accord with earlier work (which has been reviewed [1]).

For the first time the fluorimetric method of studying drug binding to plasma proteins has been extended to basic drugs. The DAPN probe, the fluorescence properties of which were found to be similar to those described by Atlas and Levitzki [6], is not such a good probe as ANS, as it exhibits

substantial fluorescence in the unbound state, and the fluorescence enhancement effect, which can exceed 150-fold for ANS, is only about 8-fold for DAPN. Nonetheless, it is readily detected at micromolar concentrations and provides useful information on the number and distribution of binding sites on the AAGP molecule; details of this work will be reported at a later date. As the ANS probe method can readily be used in studies on diluted plasma, the binding of basic drugs to plasma can probably be studied by using DAPN, though a possible complication is that basic drugs apparently bind to many plasma fractions including AAGP [15]. DAPN will also be of value in investigations of the topography of the steroid-binding site [16] on AAGP: it is not certain whether this is the same site as that for basic drugs.

In summary, flow injection analysis brings to the study of drug—protein binding its usual advantages of convenience, speed, and sample economy; the use of fluorimetric detectors additionally provides sensitivity and a wide dynamic range. The flow injection procedures have the further advantages of facilitating kinetic studies (provided that reaction rates are not too high), and (in most cases) avoiding the problems arising from inner filter effects. Although no such attempt was made in the present work, it would be simple to interface the fluorimetric detector to a microcomputer programmed to calculate binding parameters, thus providing an almost completely automatic assessment of drug—protein binding interactions. In the authors' laboratory, further studies using DAPN and other fluorescent probes are continuing, and the results of this work, additional details of the computer calculations, and the fluorimetric characterisation of AAGP will be published elsewhere.

Part of this work was supported by a Project Grant from the Medical Research Council. G. L. A. thanks the University of Maiduguri, Nigeria, for financial support.

REFERENCES

1 J. W. Bridges and A. E. G. Wilson, in J. W. Bridges and L. F. Chasseaud (Eds.), Progress in Drug Metabolism, Vol. 1, Wiley, London, 1976, pp. 193—247.
2 C. F. Chignell in C. F. Chignell (Ed.), Methods in Pharmacology, Vol. 2, Appleton-Century-Crofts, New York, 1972, pp. 33—61.
3 J. Krieglstein, F. Lier and J. Michaelis, Arch. Pharmacol., 272 (1972) 121.
4 F. Andreasen, S. Husted, P. Jakobsen and E. B. Jensen, Acta Pharmacol. Toxicol., 46 (1980) 105.
5 K. Schmid, L. H. Chen, J. C. Occhino, J. A. Foster and K. Sperandio, Biochemistry, 15 (1976) 2245.
6 D. Atlas and A. Levitzki, Proc. Natl. Acad. Sci., U.S.A., 74 (1977) 5290.
7 J. I. Braithwaite and J. N. Miller, Anal. Chim. Acta, 106 (1979) 207.
8 C. S. Lim, J. N. Miller and J. W. Bridges, Anal. Chim. Acta, 114 (1980) 448.
9 J. N. Miller, Anal. Proc., 18 (1981) 227.
10 J. Travis, J. Bowen, D. Tewksbury, D. Johnson and R. Pannell, Biochem. J., 157 (1976) 301.

11 G. Scatchard, Ann. N.Y. Acad. Sci., 51 (1949) 660.
12 J. B. F. Lloyd, in J. N. Miller (Ed.), Standards in Fluorescence Spectrometry, Chapman and Hall, London, 1981, pp. 27—43.
13 G. Weber and D. J. R. Laurence, Biochem. J., 56 (1954) 31.
14 E. Daniel and G. Weber, Biochemistry, 5 (1966) 1893.
15 J.-P. Tillement, R. Zini, P. d'Athis and J. R. Boissier, J. Pharmacol. Clin., 4 (1974) 227.
16 M. F. Ryan and U. Westphal, J. Biol. Chem., 247 (1972) 4050.

Analytica Chimica Acta, 145 (1983) 117—124
Elsevier Scientific Publishing Company, Amsterdam — Printed in The Netherlands

THE BIO-ANALYTICAL POTENTIAL OF FLOW INJECTION ANALYSIS

P. J. WORSFOLD

Department of Chemistry, Sheffield City Polytechnic, Pond Street, Sheffield S1 1WB (Gt. Britain)

(Received 11th June 1982)

SUMMARY

The suitability of flow injection analysis for the study of biochemically specific interactions is discussed. The possibilities are illustrated by the analytical performance of two particular systems: a manifold incorporating an immobilized glucose oxidase coil for the determination of β-D-glucose in blood and a stopped-flow manifold used to monitor a model immunoprecipitin interaction between concanavalin A and yeast mannan.

Living organisms represent a complex and highly organised structure consisting of individual chemical compounds performing highly specialised roles. Of particular interest to the analytical chemist are those biomolecules that can be used as specific analytical reagents, such as enzymes and antibodies. These compounds are high-molecular-weight proteins that exhibit specificity in order to maximize the efficiency of their roles within the organism: enzymes to enhance their catalytic power, and antibodies to fulfil their immunological defence function.

The limiting factor in the analytical application of such reagents has been the problem of obtaining them in sufficient quantity and with the necessary activity for their usage in vitro. In the case of enzymes, recent technological advances regarding their immobilization on solid supports has, to a large extent, overcome these problems [1]. Correspondingly, ongoing research into the production of monoclonal antibodies should lead to their increased availability in a homogeneous form in the near future [2].

In order that such reagents can be most effectively utilised to cope with the escalating demand for specific analytical methods, suitable instrumentation, including a capacity for automation, is required. Centrifugal analysers and air-segmented continuous flow systems are currently the most popular instruments in routine use for automated enzyme and immune-based assays [3, 4] but both are relatively expensive and of complex design. The technique of flow injection analysis (f.i.a.) is based on the controlled and reproducible dispersion of a sample zone when introduced into an unsegmented continuously flowing carrier stream [5] and provides an attractive alternative for the study of biochemically specific interactions. The running costs are low and

the system is relatively easy to operate and maintain. A range of interactions that are suited to study by f.i.a. is shown in Table 1 and two particular applications are discussed in detail below.

The determination of blood glucose is one of the most frequently performed assays in a clinical laboratory. One approach is to use the reducing action of D-glucose in a colorimetric procedure, such as the reduction of hexacyanoferrate(III) ion in alkaline solution, but the method is liable to interference from other reducing agents. Enzymatic assays are therefore routinely used. When high accuracy is required, the hexokinase/glucose-6-phosphate dehydrogenase system is preferred but for routine use the glucose oxidase/peroxidase system is favoured [6]. This is a two-stage process based on the oxidation of β-D-glucose by glucose oxidase (GOD) to produce hydrogen peroxide followed by peroxidase-catalyzed oxidative coupling to give a coloured product:

$$\beta\text{-D-glucose} + H_2O + O_2 \xrightarrow{GOD} \delta\text{-gluconolactone} + H_2O_2 \quad (1)$$

$$2H_2O_2 + HBS + 4\text{-aminophenazone} \xrightarrow{POD} \text{quinoneimine dye} + H_2O \quad (2)$$

The quinoneimine dye can then be determined spectrophotometrically at 505 nm. This paper describes a flow injection system for the determination of blood glucose based on the above principle and incorporating a nylon tube immobilized glucose oxidase coil.

The selective complexation of polysaccharides and blood serum glycoproteins by concanavalin A, a globulin isolated from jack beans, is known closely to resemble the immunological response of living organisms [7] and is, therefore, of analytical interest. This paper also describes a stopped-flow system for monitoring the precipitin interaction between yeast mannan (the antigen) and concanavalin A (the antibody) by using a merging zones approach.

EXPERIMENTAL

Reagents

Glucose determination. The immobilized enzyme coil (Catalinks, Ames Division, Miles Laboratories) consisted of glucose oxidase (E.C.1.1.3.4) co-

TABLE 1

A range of biochemically specific interactions suited to study by f.i.a.

Type of assay	Analyte	Reagent	Mode of detection
Enzymatic	Substrate	Immobilized enzyme	U.v./visible[a]
Enzymatic	Substrate	Free enzyme	U.v./visible[b]
Enzymatic	Enzyme	Substrate	U.v./visible[b]
Immunoprecipitin	Antigen	Antibody	Turbidimetric[b]
Homogeneous immunoassay	Antigen	Labelled antigen + antibody	U.v./visible or fluorescer
Bioluminescence	ATP	Firefly luciferase	Visible[a]
Bioluminescence	NADH/NADPH	Photobacterium luciferase	Visible[a]

[a]Peak height. [b]Peak height or gradient.

valently bound to the inner surface of a nylon tube (25 cm in length; 1.0 mm i.d.) which was coiled into a cylindrical acrylic exoskeleton. When not in use the coil was filled with distilled water, capped and stored at 2—8° C. The reagents used were reconstituted with distilled water from kits supplied in conjunction with the coil. Glucose reagent one (GR1) contained potassium phosphate (pH 6.5; 0.2 M), EDTA-disodium salt (12.5 mM), 4-aminophenazone (1.2 mM) and peroxidase (E.C.1.11.1.7; >3000 U l^{-1}). Glucose reagent two (GR2) contained potassium phosphate (0.2 M), EDTA-disodium salt (12.5 mM) and 3,5-dichloro-2-hydroxybenzene sulphonic acid-disodium salt (HBS; 4.2 mM). Brij-35 was added to GR1 and GR2 (0.03% w/v) and the reagents were stable for six weeks when stored at 2—8° C. D-Glucose standards (see below for ranges) were prepared in saturated benzoic acid solution, at least 24 h before use to ensure attainment of mutarotation equilibrium, and were stored at 2—8° C.

Immunoprecipitin studies. An aqueous buffer solution containing sodium acetate (10 mM) and Brij-35 (0.3% w/v) was adjusted to pH 6.2 with acetic acid (1 M). Concanavalin A (antibody) was obtained as a lyophilized, salt-free, highly purified powder from *Canavalia ensiformis* (jack beans; Sigma) and dissolved in the above buffer solution (2 mg ml^{-1}). Yeast mannan (antigen; Sigma) standards were prepared in the above buffer solution over the range 0—10 mg ml^{-1}.

Apparatus and procedures

Glucose determination. The manifold used for the glucose determination is shown in Fig. 1. Unless otherwise stated, reagents were pumped at 1.4 ml min^{-1} (GR2) and 0.5 ml min^{-1} (GR1) using a peristaltic pump (Ismatec Mini S-840). Polyethylene tubing (0.5 mm i.d.) was used throughout the remainder of the system. Glucose standards (30 µl) were introduced into the system by means of a PTFE rotary valve and each sample was injected in triplicate. The absorbance signal was monitored at 505 nm by using a spectrophotometer (Varian VUV-50) equipped with a flow cell (7.9 µl volume; 10 mm path length) and a dual analog output. One output signal (1 mV full scale) was fed to a strip-chart recorder (Servograph REC 51) and the other (500 mV for 1.0 absorbance) to a digital multimeter (Hewlett-Packard 3438A; 3½ digit).

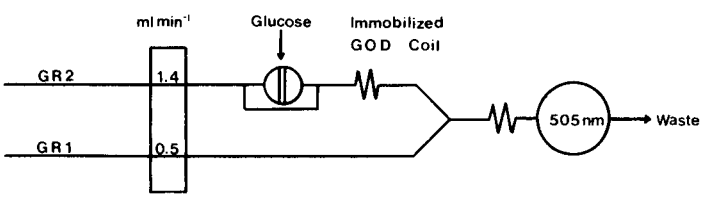

Fig. 1. Flow injection manifold for the enzymatic determination of glucose using an immobilized glucose oxidase (GOD) coil. Glucose standards (30 µl) are injected into a buffer stream (GR2) and peroxidase (POD) is added downstream (GR1). All tubing, 0.5 mm i.d.; total dispersion 8.5; distance from injection valve to GOD coil, 25 cm; distance from GOD coil to confluence point, 10 cm; distance from confluence point to detector, 90 cm.

Immunoprecipitin studies. The manifold for the immunoprecipitin studies is shown in Fig. 2. Two streams of the buffer were pumped at 0.5 ml min^{-1} using a peristaltic pump (Ismatec Mini S-840). Polyethylene tubing (0.5 mm i.d.) was used throughout the remainder of the system. Concanavalin A (30 μl) and yeast mannan (30 μl) were simultaneously introduced into separate buffer streams by means of a dual injection PTFE rotary valve. The system was operated in the stopped-flow mode by using an electronic pump timer [8] with a delay time of 5.5 s and a stop time of 60 s. The turbidity was monitored at 420 nm with the spectrophotometric system described above, and the output (1.0 V full scale) was recorded on the strip-chart recorder. Operation and data handling were controlled via a microcomputer as previously described [8]. The system was thermostatted at 25°C by means of a circulation bath.

RESULTS AND DISCUSSION

Glucose determination

The air-segmented continuous-flow method for the determination of blood glucose using an immobilized glucose oxidase coil (Catalinks, Miles Laboratories) was readily adapted to the flow injection system. For routine clinical applications, the preferred sample matrix is whole blood, because this obviates the need for sample pretreatment, and a dialysis unit is normally incorporated into the system to reduce background interference. In these studies, however, aqueous glucose standards were used in place of whole blood samples and, therefore, a dialysis unit was not included. In preliminary studies, aqueous glucose standards covering the normal clinical range (0—25 mM) were measured by direct injection into the manifold shown in Fig. 1. The non-linearity of the resultant calibration curve can be explained by the fact that the Michaelis constant (K_M) for glucose oxidase is in the region of 30—110 mM glucose [9] and the probability that substrate concentrations in the enzyme coil approached this level in the absence of a dialysis unit.

The effect of varying the flow rate of the substrate through the immobilized enzyme coil was, therefore, studied for a more dilute series of standards (0—2.5 mM). The results, shown in Table 2, indicate that whilst the response

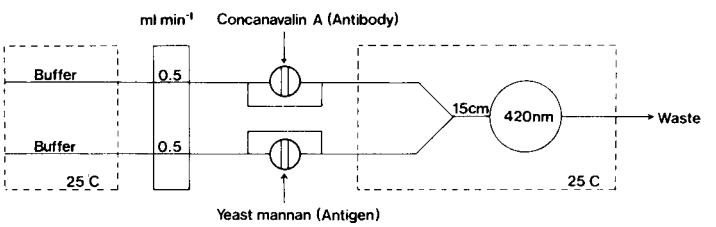

Fig. 2. Flow injection manifold for the study of the immunoprecipitin interaction between concanavalin A (antibody) and yeast mannan (antigen) using a stopped-flow merging zones technique. Delay time 5.5 s; stop time 60 s. Distance from injection valve to confluence point, 6 cm; distance from confluence point to detector, 15 cm.

TABLE 2

The effect of substrate (glucose) flow rate through the enzyme coil on signal intensity for a series of glucose standards (0—2.5 mM)

Concentration (mM)	Signal intensity (absorbance)					
	At 1.4 ml min^{-1}			At 2.0 ml min^{-1}		
	Mean[a]	SD	RSD (%)	Mean[a]	SD	RSD (%)
0.5	0.0554	0.0012	4.3	0.0500	0.0010	2.0
1.0	0.1083	0.0024	2.2	0.0900	0.0010	1.1
1.5	0.1497	0.0012	0.8	0.1173	0.0006	0.5
2.0	0.1795	0.0022	1.2	0.1320	0.0017	1.3
2.5	0.2009	0.0032	1.6	0.1457	0.0038	2.6

[a]All results are means of six experiments.

is still non-linear over the range 0—2.5 mM glucose, the sensitivity is much enhanced by using a lower flow rate. This is due to the fact that the glucose oxidase coil operates at less than 100% efficiency under the conditions described, and substrate conversion is therefore inversely proportional to flow rate [10].

The precision of the technique was assessed after a further dilution of the standards (0—0.25 mM); the lower flow rate (1.4 ml min^{-1}) was used for glucose reagent 2, and each standard was measured six times. Table 3 shows the within-batch precision found on two separate occasions within a three-week period. The correlation coefficients for the calibration graphs were 0.9990 for the first run and 0.9993 for the second run. Between-batch correlation can be described by the equation $x = 1.0537y - 0.0005$ with a correlation coefficient of 0.9997, x corresponding to run 1 and y to run 2. The recorder output for a series of standards from the first run, injected in

TABLE 3

Within-batch precision for a series of glucose standards (0—0.25 mM)

Concentration (mM)	Signal intensity (absorbance)					
	Run 1			Run 2		
	Mean[a]	SD	RSD (%)	Mean[a]	SD	RSD (%)
0.05	0.0057	0.0001	1.8	0.0056	0.0002	3.6
0.10	0.0119	0.0005	4.2	0.0118	0.0007	5.9
0.15	0.0172	0.0001	0.6	0.0175	0.0003	0.2
0.20	0.0220	0.0003	1.4	0.0230	0.0005	2.2
0.25	0.0273	0.0004	2.7	0.0281	0.0008	2.8

[a]All results are means of six experiments.

triplicate, are shown in Fig. 3. The results indicate that tube-immobilized enzymes, incorporated within a flow injection manifold, provide a system that has a number of analytically and economically attractive features. These include a high sample throughput (80—90 samples/hour), almost immediate availability of the analytical result and an acceptable precision for clinical purposes. Furthermore, the long-term stability of the enzyme coil (illustrated by between-batch precision) eliminates the problems associated with free enzyme methods.

Future work will involve the analysis of whole blood samples, by the incorporation of a dialysis unit into the manifold, with a view to implementing the technique for routine analysis at a local hospital. It should be noted that an alternative approach for the analysis of real samples is a stopped-flow system [8, 11], an application of which is discussed below.

Immunoprecipitin studies

When an immunoprecipitin assay is done on real samples the two major analytical constraints are the time required for the determination and the need for a sufficiently active antiserum, which is expensive. These constraints can, however, be minimized by the use of a flow injection system with merging zones [12]. In these studies the problem of obtaining antiserum was overcome by using a model system. Preliminary studies with concanavalin A and yeast mannan showed that the turbidity resulting from interactions occurring in a continuous-flow manifold gave a limited detector response. The sensitivity was therefore increased by using a stopped-flow approach, in which the merged antibody and antigen zones were stopped between the confluence point and the detector 5.5 s after injection for a period of 60.0 s

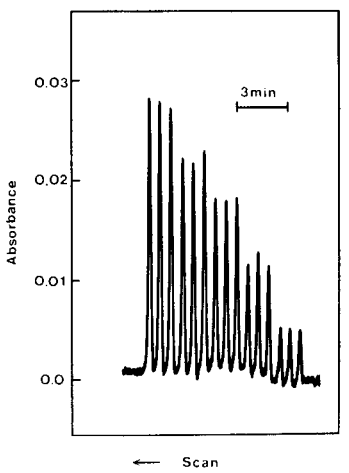

Fig. 3. Enzymatic determination of glucose showing triplicate injections of a series of standards (0—0.25 mM).

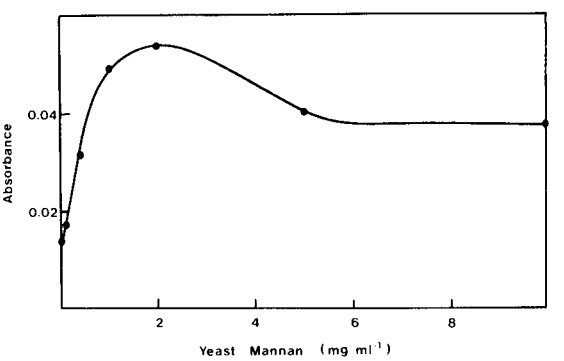

Fig. 4. The relationship between yeast mannan (antigen) concentration and turbidity.

to allow the immunological interaction to develop. Thereafter the sample zone was swept through the flow cell by reactivating the peristaltic pump and the transient turbidity was recorded. Table 4 shows the turbidity resulting from the interaction of yeast mannan (0—10.0 mg ml^{-1}) with concanavalin A (2 mg ml^{-1}) under the above stopped-flow conditions.

This stopped-flow technique therefore provides a cheap analytical method for immunoprecipitin studies with the analytical result available 1 min after sample injection as compared with 10 min for the comparable manual procedure [13]. The precision and the range of the technique also compare favourably with those of the manual procedure for the determination of yeast mannan and by modifying the experimental conditions the range could be extended or the technique applied to other polysaccharide determinations. Furthermore, for a more sensitive measurement of antibody—antigen complexes in general, a laser nephelometric detector could be used. The relationship between yeast mannan concentration and turbidity is represented graphically in Fig. 4 and the zone of equivalence of the interaction ($\approx$2 mg ml^{-1} yeast mannan) is clearly indicated. For routine clinical applications, the antibody would be in excess and the concentration of antigen would be interpolated from the linear region of the calibration curve below the equivalence point.

Future work will involve the utilization of the concentration gradients generated in flow injection systems [11] to develop immunoprecipitin assays for clinical samples using both continuous-flow and stopped-flow merging zones techniques. Such systems will also allow studies of both the quantitative and kinetic aspects of various homogeneous immunoassay procedures.

The author thanks the Ames Division of Miles Laboratories for the provision of Catalinks immobilized glucose oxidase coils and glucose reagent kits, Prof. J. Růžička and Dr. E. H. Hansen for initial help and encouragement, and The Royal Society for the award of a Fellowship at The Technical University of Denmark for part of this work.

TABLE 4

Relationship between antigen (yeast mannan) concentration and turbidity

Antigen conc. (mg ml^{-1})	Absorbance[a]		RSD (%)	Antigen conc. (mg ml^{-1})	Absorbance[a]		RSD (%)
	Mean	SD			Mean	SD	
0	0.0132	0.0007	5.3	2.0	0.0535	0.0012	2.2
0.1	0.0167	0.0005	3.0	5.0	0.0403	0.0011	2.7
0.5	0.0301	0.0011	3.6	10.0	0.0371	0.0003	0.8
1.0	0.0499	0.0011	2.2				

[a]All results are means of five experiments.

REFERENCES

1 G. G. Guilbault and M. H. Sadar, Acc. Chem. Res., 12 (1979) 344.
2 J. N. Miller, Chem. Brit., 17 (1981) 62.
3 C. P. Price and K. Spencer (Eds.), Centrifugal Analysers in Clinical Analysis, Vol. 1, Praeger, New York, 1980.
4 Technicon AutoAnalyzer Bibliography 1957/1967, Technicon Corporation, Tarrytown, New York, 1967.
5 J. Růžička and E. H. Hansen, Flow Injection Analysis, Wiley-Interscience, New York, 1981.
6 H. U. Bergmeyer and E. Bernt, in H. U. Bergmeyer (Ed.), Methods of Enzymatic Analysis, Vol. 3, Academic Press, London, 1974, p. 1205.
7 I. J. Goldstein, C. E. Hollermann and J. M. Merrick, Biochem. Biophys. Acta, 97 (1965) 68.
8 P. J. Worsfold, J. Růžička and E. H. Hansen, Analyst, 106 (1981) 1309.
9 B. E. P. Swoboda and V. Massey, J. Biol. Chem., 240 (1965) 2209.
10 L. Gorton and L. Ogren, Anal. Chim. Acta, 130 (1981) 45.
11 S. Olsen, J. Růžička and E. H. Hansen, Anal. Chim. Acta, 136 (1982) 101.
12 J. Růžička and E. H. Hansen, Anal. Chim. Acta, 106 (1979) 207.
13 J. A. Cifonelli and F. Smith, Anal. Chem., 27 (1955) 1639.

Analytica Chimica Acta, 145 (1983) 125—133
Elsevier Scientific Publishing Company, Amsterdam — Printed in The Netherlands

KINETIC DETERMINATION OF MAGNESIUM AND CALCIUM BY STOPPED-FLOW INJECTION ANALYSIS

HENRIK KAGENOW[a] and ARNE JENSEN*

Department of Chemistry AD, The Royal Danish School of Pharmacy, 2 Universitetsparken, DK-2100 Copenhagen Ø (Denmark)

(Received 4th May 1982)

SUMMARY

A kinetic method for the simultaneous determination of magnesium and calcium ions in solution is described. The method is based on the dissociation reactions of cryptand (2.2.2) complexes; a stopped-flow injection technique is used with spectrophotometric monitoring of the phthalein complexone complexes of the released metal ions. Analyses were done at a rate of 80 h^{-1}, with injected sample volumes of 80 µl. A microcomputer system for data acquisition and control of the system is described.

Flow injection systems, particularly when operated in the stopped-flow mode, have proven very suitable for kinetic types of chemical analysis [1]. Alkaline earth metal ion complexes of polyether diamine-type ligands, cryptands [2], show well-defined dissociation patterns when exposed to suitable scavenger ions [3]. The pseudo first-order dissociation reaction has a rate constant characteristic of the metal ion in question, thus allowing differential kinetic analysis to be applied [4, 5]. The unusual kinetic and thermodynamic

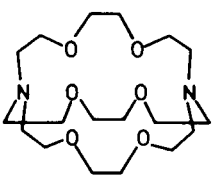

Cryptand (2.2.2)

properties of the cryptand (2.2.2) complexes of magnesium and calcium form the basis of the simultaneous determination of the two metal ions by stopped-flow injection analysis. The magnesium complex dissociates very quickly, whereas the calcium complex dissociates relatively slowly (k_{diss} = 0.15 s^{-1}) when potassium ions are used as scavenger.

---

[a]Present address: Radiometer A/S, 72 Emdrupvej, DK-2400 Copenhagen, Denmark.

EXPERIMENTAL

Reagents

All chemicals used were of analytical-reagent grade and redistilled degassed water was used throughout.

Calcium carbonate and magnesium metal were dissolved in concentrated hydrochloric acid and the solutions diluted with water to make up the metal ion standard solutions. The cryptand (2.2.2) was used as received (Merck) and stable 0.01 M stock solutions were prepared [5]. The colour-forming reagent consisted of 2×10^{-4} M phthalein complexone (*o*-cresolphthalein complexone), 0.02 M potassium nitrate and 0.05 M triethylamine, the pH being adjusted to 10.5 with nitric acid. The carrier solution was 0.05 M triethylamine and was also adjusted to pH 10.5 with nitric acid.

Prior to injection all metal standards and mixtures were made 0.05 M in triethylamine and 4×10^{-4} M in cryptand (2.2.2). Final metal ion concentrations were in the range $4—20 \times 10^{-5}$ M (see Tables).

Apparatus

The flow system used is shown in Fig. 1. The pump used was an Ismatec Mini-S-840 equipped with pump tubing to give a flow rate of 2 ml min^{-1} in each channel. The injection valve was a teflon/perspex bi-layer sandwich loop type [1] operated by the action of a micro-switch controlled electromotor via a friction clutch. A sampling system (not shown in Fig. 1), used for filling the sample loop automatically, was connected to the injection valve [1]. The system consisted of a peristaltic pump (Ismatec Mini-S-840) and an LKB 7000 Ultrorac fraction collector equipped with an electromotor-activated vertically moving stainless steel probe. The flow system (mixing coil etc.) was described previously [4—6], and dimensions are shown in Fig. 1. The cuvette compartment and mixing coil were thermostated at 25°C.

A modified Hitachi-Perkin Elmer 124 spectrophotometer equipped with an 18 μl flow-through cuvette was used as detector. The analog output of the spectrophotometer was simultaneously fed to the microcomputer system

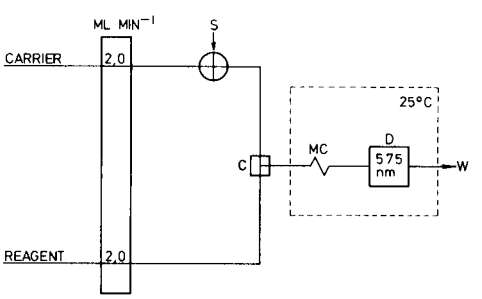

Fig. 1. Flow injection manifold. (S) Point of injection (80 μl sample volume); (C) confluence point, micromixing chamber, 3 μl; (MC) mixing coil, 30 cm, 0.5 mm i.d.; (D) detection, 18 μl flow cell, 575 nm. All tubing 0.5 mm i.d.

described below and a Radiometer REC 61 recorder with an REA 112 high-sensitivity unit.

Microcomputer system

A microcomputer was linked to the flow injection system in order to facilitate data acquisition and control [1, 7, 8]. A block diagram of the microcomputer-controlled flow injection system is shown in Fig. 2. The microcomputer was a Hewlett-Packard 9825 T desktop computer with built-in tape cartridge drive, equipped with an HP-98035A real-time clock interface and an HP-98034A HP-IB interface to which an HP-3438A digital multimeter, an HP-59306A relay actuator, an Anadex matrix printer and an HP-7225A plotter were connected. The analytical signal of the spectrophotometer was presented to the microcomputer via the multimeter (2.7—4.7 conversions/second, dual slope, 100 ms integration).

The state of six two-state power relays could be selected from the microcomputer via the relay actuator. These relays controlled the status of the injection valve ("fill" or "inject" position), the pump ("start" or "stop") and the sampling system (shift and wash functions).

Measuring procedures

The injected sample solution, containing the magnesium and calcium ions complexed by an excess of cryptand (2.2.2), meets the reagent in the confluence point (C in Fig. 1). As the reagent contains a relatively high concen-

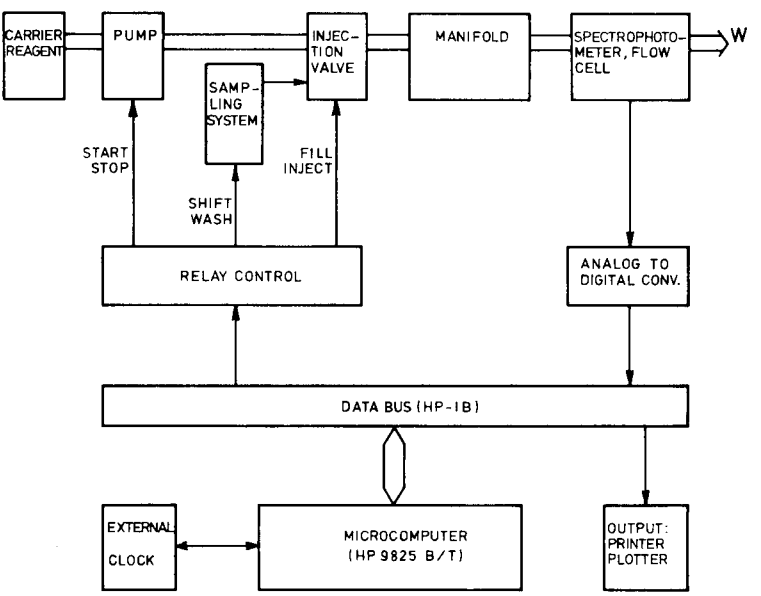

Fig. 2. Microcomputer system and interfacing to flow injection system. (For details, see text.)

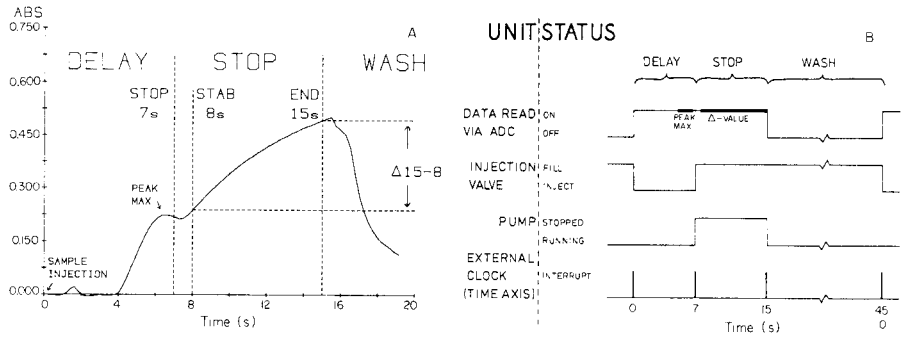

Fig. 3. Stopped-flow timing. A, Timing, related to actual response curve (for details, see text). B, Simplified scheme of events occurring during one cycle.

tration of potassium ion (scavenger), dissociation of the cryptand complexes begins at this point and proceeds while the sample zone moves forward through the mixing coil (MC) to the flow cell. The reagent also contains a metal indicator, phthalein complexone, which instantly reacts with liberated magnesium and calcium ions to yield colored complexes with maximum absorbance at 575 nm.

The magnesium—cryptand complex is weak and dissociates quickly, so that all magnesium ions are liberated before the sample reaches the flow cell. The calcium complex, however, dissociates relatively slowly, and, as the potassium ion concentration can be considered constant, follows pseudo first-order kinetics. A constant fraction, preferably small, of the total calcium initially present is, therefore, liberated together with all of the magnesium at a given time after the sample has entered the flow cell. When the flow is stopped with the sample in the flow cell, the pseudo first-order dissociation reaction proceeds, and the concentration of free calcium ions will, therefore, increase while that of magnesium remains constant. Thus, the initial value measured spectrophotometrically at any given point of the normal flow injection curve, conveniently chosen as the peak maximum value for easy location, will represent the sum of total magnesium plus a constant fraction of the calcium originally present in the sample. A measurement of the increase in absorbance over a constant time interval after the stop of the flow, will be proportional exclusively to the calcium ion concentration.

The whole procedure is visualized in Fig. 3A, where an original response curve, output to the digital plotter after storage in computer memory, is shown with indication of the peak maximum value (peak max) and the absorbance increase over a constant time interval, $\Delta(15-8)$. Figure 3A also shows a small stabilization period (1 s), which is used when the Δ value is calculated from the measured absorbance values. A schematic timing diagram, with sampling system timing omitted to avoid confusion, is shown in Fig. 3B. This diagram shows the status of the various units during the delay, stop and wash periods of one cycle. All events were controlled by the

microcomputer, and all time-critical events, e.g., stopping the pump after a precise delay, were handled according to an external time axis-interrupt scheme, set up via the programmable clock. The timing values given in Fig. 3A are those used in the final system, i.e., delay time 7 s, stabilization time 1 s, absorbance measurement 7 s, wash-time 30 s, and a total cycle time of 45 s.

Data, i.e., absorbance outputs from the spectrophotometer, read via the multimeter, together with corresponding "milliseconds-from-injection" values, read from the programmable clock, were treated with simple algorithms, similar to those described earlier [9], to reveal the peak max and Δ values as indicated above. This was done either between successive readings (real time, during wash cycles) on the complete set of data for a single injected sample stored in computer memory, or at the end of a complete analytical run on all complete sets of data stored on magnetic tape. Standard data and sample contents were calculated from the peak maximum and Δ values according to various regression models (see below), again either in real time or at the end of a complete run, and the results were output to the printer and eventually to the plotter.

RESULTS AND DISCUSSION

Flow system

A confluence configuration was chosen in order to establish uniform conditions over the entire sample plug throughout the system. A micro-mixing chamber at the confluence point served to mix sample and reagent efficiently without the need of a very long mixing coil; the shorter the mixing coil, the lower the fraction of dissociated calcium—cryptand complex at the peak maximum and the higher the sensitivity for both metal ions.

Sensitivity was further improved by keeping contributions to dispersion, apart from the 1:1 dilution in the confluence point, as low as possible.

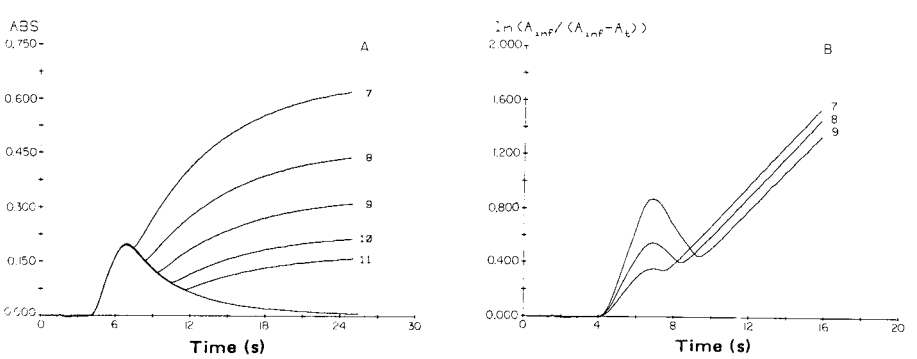

Fig. 4. Variation of the delay time. A, Responses of a 12 × 10^{-5} M calcium standard when stopped in the flow-cell 7, 8, 9, 10 and 11 s after injection. B, Collected data from three of the experiments shown in A plotted according to first-order kinetics.

Overall dispersion values, as normally defined in f.i.a. and calculated from experiments with bromothymol blue and sodium tetraborate solutions [1], were 3.1 at the peak maximum and 3.3 at the 7-s stop-gradient point, respectively. (It should be noted that the observed peak maximum referred to above and throughout the text appears a little later than the time when the actual "most concentrated part of the sample plug" passes through the flow cell, cf. the flow injection peak profile in relation to the rate constants involved here).

The establishment of uniform pseudo first-order conditions within the flow system appears from Fig. 4B, for which absorbance/time data (Fig. 4A) from three experiments with the same calcium standard and varying delay times (7—9 s) were output to the digital plotter (after initial storage on magnetic tape) and subsequently transformed logarithmically according to first-order kinetics. A linear relationship holds for all delay times and the slope, 0.15 s^{-1}, is the same as the dissociation rate constant found in homogeneous solution (with identical chemical composition and measured spectrophotometrically by a manual method).

Microcomputer system

The versatile microcomputer-controlled flow injection system described has proven very well suited for the total automation of the stopped-flow technique as well as for a number of other flow injection techniques. It is based on the system described by Olsen et al. [8]. Although the microcomputer used for this work is very powerful indeed, and allows all control operations, calculations and outputs of results to be performed in real time when intensive interrupt control is used as described, this approach is of interest mainly for routine work. For development purposes, it is often more convenient to collect raw data and store them (here on magnetic tape) for later processing and inspection, as was, for instance, demonstrated in Fig. 4A, where data from five experiments were superimposed for easy comparison.

The discussion and the standard deviation data given below prove that the conversion rate and mode of operation of the analog-to-digital converter used here are satisfactory with respect to resolution of the analytical signal. If, however, the rates of the monitored reactions are even faster than here, or if for instance high-speed titrations [7] are to be done with the system, better resolution is required. For such work, a 30 Hz non-integrating analog-to-digital conversion system, communicating with the computer via a BCD-interface, is used.

Timing

The timing sequence and actual time intervals (cf. Fig. 3) were chosen so as to give a high absorbance increase during a reasonably short constant interval of time after the flow had been stopped. Figure 4A clearly demonstrates the possibility of altering this value by varying the delay time. A 7-s delay after injection and then measurement for 7 s from the 8th to the 15th

second, the $\Delta(15 - 8)$ value, gave satisfactory results. The inclusion of a 1-s stabilization time between stopping the pump and starting the measurement of the absorbance increase, greatly improves reproducibility, as noise caused by irregularities in the flow pattern immediately after the pump stops, is discarded. The approach of using a fixed delay time from injection to stopping the flow was preferred to stopping the flow a fixed time after location of the peak maximum, because it is simpler and yields equally reproducible results.

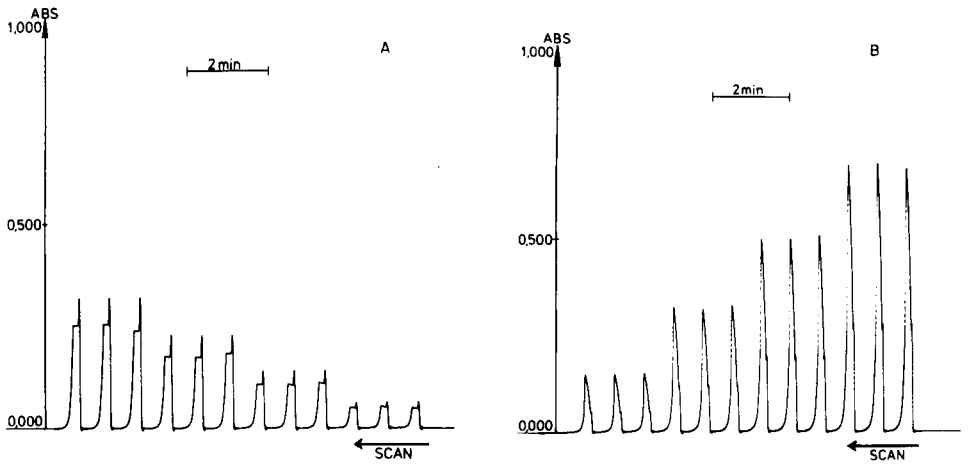

Fig. 5. Response for magnesium and calcium (direct recorder trace): A, four magnesium standards (4, 8, 12 and 16 × 10^{-5} M in scan direction); B, four calcium standards (16, 12, 8 and 4 × 10^{-5} M in scan direction). All injected in triplicate at a sampling rate of 80 h^{-1}.

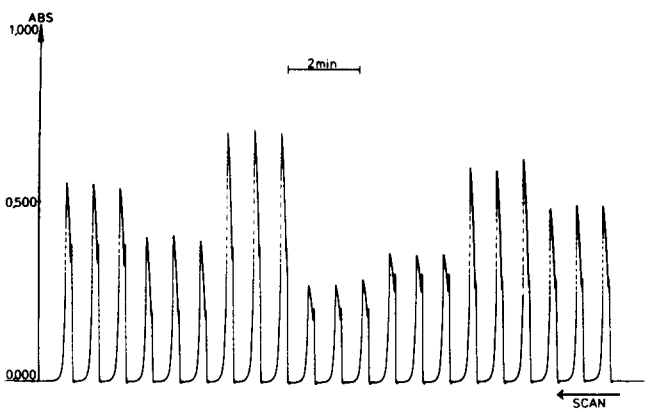

Fig. 6. Response (direct recorder trace) for seven calcium/magnesium mixtures injected in triplicate at a sampling rate of 80 h^{-1}. Concentrations (in scan direction) as in the table.

TABLE 1

Analysis of mixtures of calcium and magnesium, with results calculated directly from separate magnesium and calcium standard solutions and from mixed calcium/magnesium standards

$[Mg^{2+}] + [Ca^{2+}]$ taken ($\times 10^{-5}$ M)	$[Mg^{2+}]$ found ($\times 10^{-5}$ M)	Rel. Error (%)	$[Ca^{2+}]$ found ($\times 10^{-5}$ M)	Rel. Error (%)
Calculation based on separate standards				
8.00 + 8.00	8.14	1.8	8.70	8.8
4.00 + 12.00	4.20	5.0	12.87	7.3
12.00 + 4.00	12.68	5.7	4.33	8.3
8.00 + 4.00	8.37	4.6	4.16	4.0
8.00 + 12.00	7.91	−1.1	13.55	12.9
4.00 + 8.00	4.42	10.5	8.21	2.6
12.00 + 8.00	12.82	6.8	8.49	6.1
Calculation based on mixed standards				
8.00 + 8.00	7.80	−2.5	8.06	0.8
4.00 + 12.00	4.21	5.3	11.78	−1.8
12.00 + 4.00	11.93	−0.6	4.16	4.1
8.00 + 4.00	7.95	−0.6	4.01	0.3
8.00 + 12.00	7.64	−4.5	12.39	3.3
4.00 + 8.00	4.36	9.1	7.63	−4.7
12.00 + 8.00	12.10	0.8	7.87	−1.6

Determination of magnesium and calcium

Examples of the analytical responses appearing on the analog recorder, are given in Figs. 5 and 6. It is clear that in the case of magnesium ions alone (Fig. 5A), no further color develops after the flow has stopped; thus a peak maximum value is the sole analytical signal. Both a peak maximum and an absorbance increase, after the flow has stopped, are apparent for calcium ions (Fig. 5B). It can, by direct comparison, be perceived from the run of seven magnesium/calcium mixtures (Fig. 6) that they represent a linear combination of the former two situations.

The reproducibility of the method is very good, considering the high analytical throughput (80 samples per hour) and the mechanical requirements (pump, tubing) of the stopped-flow approach. Standard deviations, calculated from ten repeated injections of the same mixed standard (8×10^{-5} M magnesium with 8×10^{-5} M calcium), were found to be 0.3% for the peak maximum value and 0.6% for the $\Delta(15-8)$ value.

Table 1 shows the results of determination of a set of magnesium/calcium mixtures. These results were calculated from standard data obtained for separate magnesium and calcium standard series, and from standard data for mixed standards, the latter being calculated by multiple linear regression. The use of mixed standards for calibration improves the results, when compared to the clearly over-estimated concentrations found when separate

standard series were used for calibration. This is partly due to the fact that the indicator used, phthalein complexone, has different affinity for, and tends as well to form dinuclear complexes with, the two metal ions [10].

In conclusion, it is therefore recommended to use a mixed standard scheme for these types of analyses, and this approach has been taken in developing methods for the simultaneous determinations of magnesium and calcium in water samples, serum samples, etc. The method described above demonstrates not only the reproducibility, the high frequency and the low sample volume needed, but also a combination of the stopped-flow injection technique and a rather complicated kinetic analysis.

REFERENCES

1 J. Růžička and E. H. Hansen, Flow Injection Analysis, Wiley-Interscience, New York, 1981.
2 J. M. Lehn and J. P. Sauvage, J. Am. Chem. Soc., 97 (1975) 6700.
3 B. G. Cox and H. Schneider, J. Am. Chem. Soc., 99 (1977) 2809.
4 D. Espersen and A. Jensen, Anal. Chim. Acta, 108 (1979) 241.
5 H. Kagenow and A. Jensen, Anal. Chim. Acta, 114 (1980) 227.
6 J. H. Dahl, D. Espersen and A. Jensen, Anal. Chim. Acta, 105 (1979) 327.
7 A. U. Ramsing, J. Růžička and E. H. Hansen, Anal. Chim. Acta, 129 (1981) 1.
8 S. Olsen, J. Růžička and E. H. Hansen, Anal. Chim. Acta, 136 (1982) 101.
9 P. J. Worsfold, J. Růžička and E. H. Hansen, Analyst, 106 (1981) 1309.
10 F. Gaizer, M. Mátè, and J. Lázàr, Talanta, 28 (1981) 127.

Analytica Chimica Acta, 145 (1983) 135—141
Elsevier Scientific Publishing Company, Amsterdam — Printed in The Netherlands

SPECTROPHOTOMETRIC DETERMINATION OF CALCIUM WITH A FLOW INJECTION SYSTEM

G. NAKAGAWA*, H. WADA and C. WEI

Laboratory of Analytical Chemistry, Nagoya Institute of Technology, Showa-ku, Nagoya 466 (Japan)

(Received 28th April 1982)

SUMMARY

The indirect spectrophotometric determination of 0.8—7.2 ppm calcium in the presence of magnesium, phosphate and sulphate by flow injection analysis (f.i.a.) is described. The method is based on the exchange reaction between the calcium and the zinc complex of ethylene glycol-bis(2-aminoethylether)tetraacetic acid (EGTA) in the presence of 4-(2-pyridylazo)resorcinol (PAR): Ca + Zn(EGTA) + 2 PAR ⇌ $Zn(PAR)_2$ + Ca(EGTA). A home-made and a commercial flow injection system with a sampling rate of 80 h^{-1}, are compared. Results for water samples are in good agreement with those obtained by atomic absorption spectrometry.

Recently, several methods for the determination of calcium by flow injection analysis (f.i.a.) have been proposed. They are based on atomic absorption spectrometry [1], potentiometry with an ion-selective electrode [2] and spectrophotometry using *o*-cresolphthalein complexone [2—5] or glyoxal bis(2-hydroxyanil) [6] as chromogenic reagents. The reaction of calcium with the former reagent is influenced by magnesium, and the latter reagent has a low water solubility.

The indirect determination of calcium in the presence of magnesium by polarography or spectrophotometry based on the exchange reaction (omitting charges for simplicity) Ca + M(EGTA) + nA ⇌ Ca(EGTA) + MA_n has been reported [7, 8]. In these methods, the large difference between the stability constants of the ethylene glycol-bis(2-aminoethylether)tetraacetic acid (EGTA) complexes with calcium and magnesium was utilized. Calcium can be determined by measuring the concentration of MA_n. For favorable conditions, the conditional equilibrium constant of the above exchange reaction should be sufficiently large, and the conditional equilibrium constant of the reaction M(EGTA) + nA ⇌ MA_n + EGTA should be sufficiently small, because MA_n produced by the second reaction determines the blank value [9]. In the spectrophotometric method, a chromogenic reagent A reacts with metal ion M released from its EGTA complex by the formation of the Ca(EGTA) complex, but should not react with calcium. 2-Carboxy-2′-hydroxy-5′-sulfoformazylbenzene (zincon) or 1-(2-pyridylazo)-2-naphthol

(PAN) have been used as chromogenic reagents with zinc or manganese(II) as the metal M [8].

In the present study, calcium (0.8—7.2 ppm) was determined by f.i.a. in a similar way. Zinc and 4-(2-pyridylazo)resorcinol (PAR) were employed.

EXPERIMENTAL

Apparatus

A home-made flow injection manifold was used. The flow diagram is shown in Fig. 1. A chromogenic reagent solution containing Zn—EGTA and PAR, and a buffer solution were delivered each at 0.64 ml min^{-1} with a reciprocating pump (Kyowa Seimitsu, KHU W-52). The sample was injected into the stream of the buffer solution via a rotary valve to which a loop of given volume was attached. Sample and the reagent were mixed in the 200-cm coil. A flow cell (Nippon Bunko; 0.3-mm light path, 0.3 μl volume) situated in a spectrophotometer (Nippon Bunko UVIDEC-100-IIW), and a recorder (Yokokawa Denki; type 3066) were used for recording the absorbance.

During this study, a commercial flow injection analyzer (FICS; Denki Kagaku Keiki Co., Japan) became available. The results obtained by the use of this FICS are also described.

Reagents and solutions

For the EGTA solution, 9.5090 g of the reagent was dissolved in 30 ml of 1 M sodium hydroxide, and the solution was diluted to 250 ml and standardized against a cadmium solution using Eriochrome Black T as indicator. Zinc metal (purity 99.99%, 1.6343 g) was dissolved in a small amount of hydrochloric acid. The excess of acid was removed by evaporation and the residue was diluted to 250 ml with water. 4-(2-Pyridylazo)resorcinol (0.1075 g) was dissolved in a little sodium hydroxide solution and the solution was diluted to 100 ml. Calcium carbonate (0.2502 g) was dissolved in a small amount of hydrochloric acid. The excess of acid was removed by evaporation and the residue was diluted to 250 ml with water. Working standard calcium solutions in the range 2.0×10^{-5}—2.0×10^{-4} M were prepared by dilution of the stock solution with water. Sodium tetraborate decahydrate (borax, 63.0 g) was dissolved in hot water and the solution was diluted to 1.0 l. All other chemicals used were of analytical-reagent grade. The water used was redistilled in a hard-glass vessel.

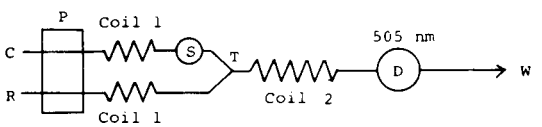

Fig. 1. Flow diagram of the home-made manifold: (P) reciprocating pump; (C) buffer solution; (R) chromogenic reagent solution; (S) sample injector (40 μl); (T) confluence point; (D) spectrophotometer; (W) waste. Coils 1, for damping (1.0 mm i.d., 500 cm); coil 2 (0.5 mm i.d., 200 cm).

For the chromogenic reagent solution, 50 ml of the EGTA solution and 50.5—52.0 ml of zinc solution were mixed, and diluted to 500 ml to give a 1.0×10^{-2} M Zn—EGTA solution containing a slight excess of zinc. Portions (10 ml) of this solution and the PAR solution were mixed, and 50 ml of borax solution was added. The solution was adjusted to pH 7.9 with hydrochloric acid and diluted to 500 ml. Borax solution (50 ml) was diluted to 500 ml whilst the pH was adjusted to 7.5.

Procedure for the home-made system

Sample solution containing 0.8—8.0 ppm of calcium was injected into the stream of buffer solution (C) by the rotary valve, the sample size being 40 μl. The stream met the reagent stream (R) at point T. After passage through reaction coil (2), the absorbance at 505 nm was measured. The concentration of calcium was obtained from the peak height by comparison with a calibration graph.

RESULTS AND DISCUSSION

Effects of reaction conditions

The concentrations of Zn—EGTA and PAR in the reagent solution affected the peak height. The highest peak was obtained with 2.0×10^{-4} M Zn—EGTA and 5.0×10^{-5} M PAR. However, at this PAR concentration, the linear response range for calcium was narrow, so 1.0×10^{-4} M PAR was used.

Zinc forms various chelates with PAR in the pH range 7.5—10: Zn(PAR), Zn(HPAR) (PAR) and $Zn(PAR)_2$. These chelates have different molar absorptivities. Moreover, the conditional equilibrium constants of the exchange

TABLE 1

The influence of other cations on the determination of calcium

Ca taken ($\times 10^{-5}$ M)	Other ion ($\times 10^{-4}$ M)	Ca found ($\times 10^{-5}$ M)	Other ion ($\times 10^{-4}$ M)	Ca found ($\times 10^{-5}$ M)
	Mg 1.0	4.0	Fe 0.1	4.0
	5.0	4.0	0.5	4.0
4.0	10.0	4.1	5.0	4.0
	Al 0.5	4.0		
	5.0	4.0		
	Mg 5.0	10.0	Fe 5.0	10.0
10.0	10.0	10.0	Cu 0.2	11.5
	Al 5.0	10.0	Zn 0.2	11.7
			Mn 0.2	11.5
	Mg 5.0	16.0	Fe 0.5	16.0
16.0	10.0	16.2	5.0	16.0
	Al 5.0	16.1		

TABLE 2

Determination of calcium in water samples

Sample	Calcium found (ppm)	
	F.i.a.	A.a.s.
Pond water (1)	8.28	8.21
Pond water (2)	8.50	8.36
Tap water (1)	8.00	8.08
Tap water (2)	7.00	—

reactions change with pH, so the peak height and the blank value are seriously affected by the pH. Therefore, the pH of the chromogenic reagent solution and buffer must be adjusted accurately. The peak height was greatest at pH 7.5—8.0.

The effects of changing sample volume, flow rate, reaction coil length and temperature were examined. Although the peak height decreased as the sample volume was increased from 30 to 45 μl, a 40-μl loop was used for sample injection because injection of smaller volumes was not reproducible. The peak heights decreased by only 10% when the separate flow rates were increased from 0.64 to 1.92 ml min^{-1}. Increase in the reaction coil length from 200 to 400 cm almost halved the peak heights. When the temperature was increased from 25° C to 50° C, the peak height increased by about 20%, probably because of acceleration of the exchange reaction. Room temperature, however, was employed for simplicity of operation.

Under these optimum conditions, the calibration graph was linear for 0.8—7.2 ppm Ca. About 80 samples could be determined in 1 h.

Effects of other ions

The influence of magnesium, copper(II), zinc, manganese(II), iron(III) and aluminum was examined by measuring the peak height responses. The

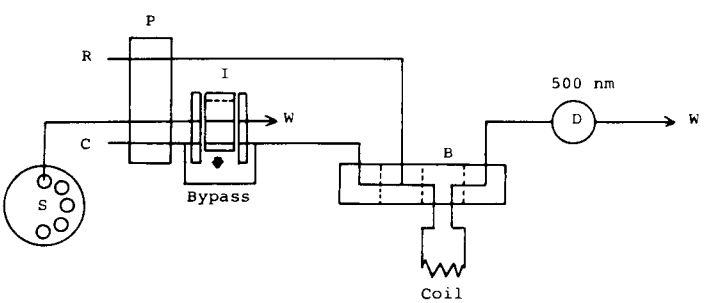

Fig. 2. Flow diagram of the FICS analyzer: (S) autosampler; (I) rotary sample injector; (P) peristaltic pump; (R) chromogenic reagent solution; (C) buffer solution or redistilled water; (B) connecting blocks for mixing and reaction coils (1 mm i.d., 100 cm); (D) spectrophotometer, (W) waste.

results are given in Table 1. Magnesium did not interfere at least up to 24 ppm. Aluminum ($\leqslant$13 ppm) and iron ($\leqslant$28 ppm) did not interfere if the pH of the sample solution was adjusted previously to 8 and the supernatant liquid was injected. Copper(II), zinc and manganese(II) interfered seriously. These interferences could be eliminated by prior extraction with 8-quinolinol, by adding to the sample solution (10 ml) 1 ml of 1 M perchloric acid and 2 ml of 1% (w/v) 8-quinolinol solution in acetic acid, adjusting the pH to 8, and shaking with 10 ml of benzene. The aqueous phase was injected into the flow injection system. When present in a solution of 1.0×10^{-4} M each of Cu, Zn, Mn, Fe(III) and Al, 5.0×10^{-5} M and 12.0×10^{-5} M calcium gave recoveries of 102 and 100%. Phosphate and sulfate (each 10^{-3} M) did not interfere in the determination of $4—16 \times 10^{-5}$ M calcium.

Determination of calcium in water

The flow injection method was applied to the analysis of water samples, and the results were compared with those obtained by atomic absorption spectrometry (a.a.s.). The water samples were diluted and the interfering metals removed by extraction with 8-quinolinol if necessary. The results given in Table 2 are in good agreement with those by a.a.s.

In flow injection analysis the optimum conditions are changed by the manifold used. In the following section the results obtained with FICS is described.

Results with the FICS analyzer

The FICS manifold is described in Fig. 2. A flow-through cuvette with a 10-mm light path and 8-μl volume is situated in the spectrophotometer D.

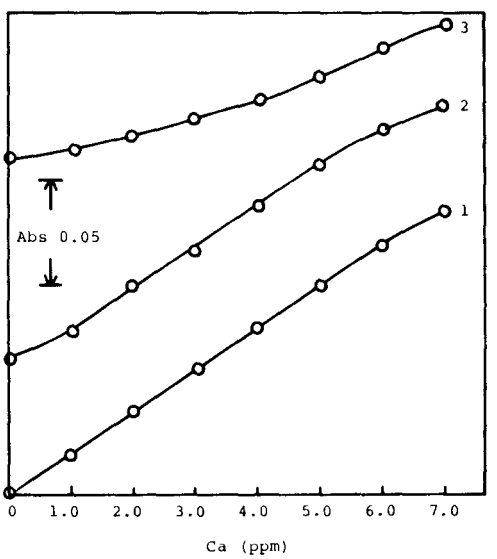

Fig. 3. Calibration graphs for calcium using the FICS analyzer: (1) pH 7.5; (2) pH 8.5; (3) pH 9.5. (8×10^{-5} M Zn—EGTA, 1% excess of Zn, 4.0×10^{-5} M PAR).

The chromogenic reagent solution and the buffer solution or redistilled water were each delivered at 1.25 ml min^{-1}. The sample (20 μl) was injected into the carrier stream by using the autosampler S and the sample injector I. Mixing occurred in a 100-cm (1 mm i.d.) coil. The absorbance of the $Zn(PAR)_2$ chelate was measured via a 500-nm filter.

Effect of experimental conditions. The concentrations of zinc—EGTA ($0.2—2.0 \times 10^{-4}$ M) and PAR ($0.1—1.0 \times 10^{-4}$ M) were reexamined. Best results were obtained with 8.0×10^{-5} M Zn—EGTA and 4.0×10^{-5} M PAR. The excess of zinc affected the height of the baseline and the determinable concentration range of calcium. When the excess was large, the baseline was too high to be backed off. A 1—4% excess of zinc gave good results. Each flow rate was varied between 0.8 and 1.75 ml min^{-1}. The higher the flow rate, the higher was the peak, but the reproducibility was poor when either flow rate was faster than 1.5 ml min^{-1}. Thus, 1.20—1.30 ml min^{-1} was used for each flow.

As was the case with the home-made apparatus, the peak was highest in the pH range 7.5—8.0 and the linear calibration range was wider than at pH 8.5—9.5. The value of the blank again increased with increasing pH. Calibration graphs for calcium at pH 7.5, 8.5 and 9.5 are shown in Fig. 3. As can be seen in Fig. 4, 1—6 ppm calcium can be determined at pH 7.5—8.0. With the FICS analyzer 80 samples can be determined per hour. Magnesium (10^{-3} M) appears to have a slight enhancing effect (Fig. 4).

Zincon was also examined as the color-forming reagent. In this case, the sensitivity was low; the linear calibration range was 4—32 ppm calcium.

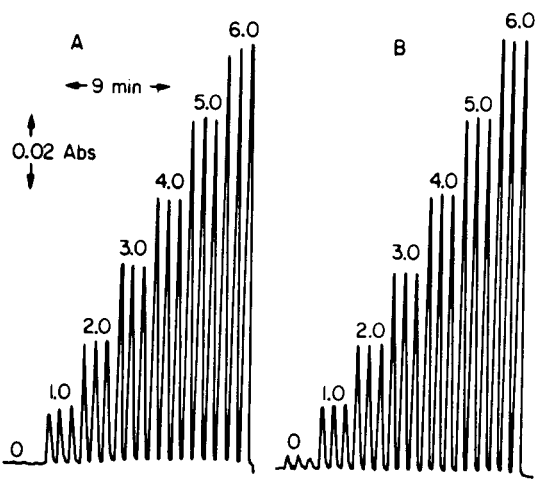

Fig. 4. Charts obtained with calcium standards: (A) alone; (B) containing 10^{-3} M (24 ppm) magnesium (8×10^{-5} M Zn—EGTA, 1% excess of Zn, 4.0×10^{-5} M PAR, pH 7.5). The numbers on the peaks correspond to ppm calcium.

This study was supported by a Grant-in-Aid for Scientific Research (No. 554169) from the Ministry of Education, Science and Culture (Japan).

REFERENCES

1 E. A. G. Zagatto, F. J. Krug, H. Bergamin F°, S. S. Jørgensen and B. F. Reis, Anal. Chim. Acta, 104 (1979) 279.
2 E. H. Hansen, J. Růžička and A. K. Ghose, Anal. Chim. Acta, 100 (1978) 151.
3 W. D. Basson and J. F. van Staden, Analyst, 103 (1978) 296.
4 W. D. Basson and J. F. van Staden, Analyst, 104 (1979) 419.
5 H. Kagenow and A. Jensen, Anal. Chim. Acta, 114 (1980) 227.
6 A. O. Jacintho, E. A. G. Zagatto, B. F. Reis, L. C. R. Pessenda and F. J. Krug, Anal. Chim. Acta, 130 (1981) 361.
7 G. Nakagawa and M. Tanaka, Talanta, 9 (1962) 847.
8 G. Nakagawa, I. Namiki and M. Tanaka, Talanta, 13 (1966) 1135.
9 G. Nakagawa and M. Tanaka, Talanta, 9 (1962) 917.

Analytica Chimica Acta, 145 (1983) 143—150
Elsevier Scientific Publishing Company, Amsterdam — Printed in The Netherlands

DETERMINATION OF MOLYBDENUM AT $\mu g\ l^{-1}$ LEVELS BY CATALYTIC SPECTROPHOTOMETRIC FLOW INJECTION ANALYSIS

FANG ZHAO-LUN* and XU SHU-KUN

Institute of Forestry and Soil Science, Academia Sinica, Shenyang (People's Republic of China)

(Received 3rd June 1982)

SUMMARY

A flow injection analytical method based on the catalytic action of molybdenum on the oxidation of iodide by hydrogen peroxide in acidic medium is proposed. The triiodide formed is measured spectrophotometrically at 350 nm. Molybdenum is determined in natural water samples without preconcentration at a sampling rate of 90 h^{-1} with 200-μl sample injections. The detection limit is 0.7 $\mu g\ l^{-1}$ and the calibration curve is linear over the range 1—1000 $\mu g\ l^{-1}$. The relative standard deviation is 0.83% for 50 $\mu g\ l^{-1}$ molybdenum and 1.9% for 13 $\mu g\ l^{-1}$ molybdenum.

Several kinetic methods for the determination of molybdenum based on the molybdenum-catalyzed oxidation of iodide by hydrogen peroxide in acidic medium to form the triiodide ion have been developed since the original proposal by Yatsimirskii and Afanas'eva [1]. Spectrophotometric [1—3], enthalpimetric [4], and ion-selective electrode [5] methods have been used for measurement of the reaction rates, and extremely low detection limits for molybdenum in the $\mu g\ l^{-1}$ range have been achieved. However, manual procedures for kinetic measurements are tedious and difficult to control, and automation of the reaction-rate measurement has been attempted [2, 6, 7]. Fuge [6] developed an automated colorimetric method based on the catalytic reaction, using a Technicon AutoAnalyzer. Trace amounts of molybdenum were determined in waters, geological and biological samples. However, owing to excessive carryover in the system, the sampling rate was limited to 10 h^{-1}. Later, Bradfield and Stickland [7] were able to increase the sampling rate to 40 h^{-1} in the analysis of plants with the AutoAnalyzer, but the precision was inferior.

In the present work, conditions for both the catalyzed and uncatalyzed reactions were studied and optimized in order to adapt the reaction to a flow injection system. The flow injection technique developed by Růžička and Hansen [8] lends itself readily to the critical control of all parameters associated with reaction-rate kinetic measurements. A detection limit of 0.7 $\mu g\ l^{-1}$ and a sampling rate of 90 h^{-1} were achieved in the determination of molybdenum in natural waters.

EXPERIMENTAL

Apparatus and reagents

A Carlo Erba 8-channel peristaltic pump was used with Tygon pump tubes. The single-channel rotary sampling valve was similar to the one described by Růžička and Hansen [8], controlled manually. The reaction coil was 0.5 mm i.d. Tygon tubing 200 cm in length. Thermostatting was not used (see below); the ambient temperature was approximately 20°C during the experiments. The absorbance was measured at 350 nm with a Pye-Unicam SP8-100 recording spectrophotometer equipped with a 70-μl flow cell.

All chemicals were of reagent grade and deionized water was used throughout. A molybdenum standard stock solution (100 μg ml^{-1}) was prepared by dissolving 150 mg of MoO_3 in 10 ml of (1 + 1) ammonia liquor and diluting to 1 l with water. Working standards in the range 20—120 μg l^{-1} were prepared by suitable dilution of the stock solution. The peroxide reagent was prepared daily from 3% hydrogen peroxide and 1 M hydrochloric acid by dilution with water. The optimum concentration of the reagent was 0.03% hydrogen peroxide in 0.2 M HCl. A 2% (w/v) potassium iodide solution was prepared by dissolving 2 g of potassium iodide in water and diluting to 100 ml; 0.1% (w/v) EDTA was added to the solution when necessary to minimize interferences.

Procedure

The flow injection system and experimental parameters are shown in Fig. 1. Samples were pumped into the 200-μl sample loop for 20 s and then

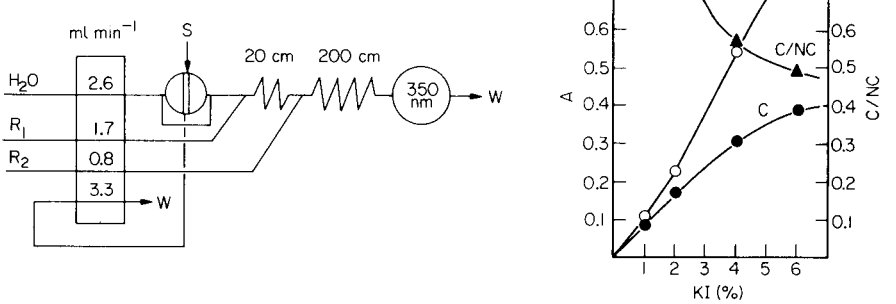

Fig. 1. Flow injection system for the catalytic spectrophotometric determination of molybdenum. S, sample injection (200 μl); R_1, 2% potassium iodide solution; R_2, 0.03% hydrogen peroxide in 0.2 M hydrochloric acid; W, waste.

Fig. 2. Effects of potassium iodide concentration on the catalyzed and uncatalyzed reactions. Conditions: 0.03% hydrogen peroxide in 0.2 M hydrochloric acid; 200 μl of 50 μg l^{-1} molybdenum injected; residence time, 25 s. C, catalyzed reaction (peak height absorbance); NC, uncatalyzed reaction (baseline absorbance); C/NC, catalyzed to uncatalyzed reaction rate ratio.

injected into the water carrier stream by turning the valve manually. After another 20 s, the valve was returned to its original position, and the next sample was pumped into the sample loop. The potassium iodide and peroxide reagents were added to the carrier stream at confluence points downstream. The reaction proceeded in the 200-cm long reaction coil and the absorbance was recorded at 350 nm.

Water samples were filtered before analysis.

RESULTS AND DISCUSSION

Fixed-time kinetic measurements

In a flow injection system, the apparent reaction rate may be readily determined by measurement of the peak height, because the time of reaction from injection of sample or confluence of reagent (whichever starts the final reaction) to the appearance of the peak is constant. The stopped-flow technique has been recommended for reaction-rate measurements [8]. However, some preliminary studies with the stopped-flow method showed that it was unsuitable for this particular reaction because the uncatalyzed oxidation of iodide by peroxide in the absence of molybdenum is pronounced, and large blank values were recorded. In the conventional mode of flow injection analysis, this uncatalyzed reaction forms the baseline of the output, and careful optimization of reaction conditions produced a relatively steady baseline allowing precise peak measurements.

Optimization of reagent concentrations

Two basic considerations were kept in mind. The first was that, whilst in manual kinetic measurements the reaction rate should be slow enough to permit accurate measurement of absorbances and time intervals, and in air-segmented continuous flow systems the rate should be slow enough to allow steady-state signals to be obtained with acceptable baselines, it is beneficial to work at higher reaction rates in flow injection systems. Fast reactions are most suitable for flow injection systems because the sample residence times are short (except in the stopped-flow mode), and high sampling rates can be obtained. The second consideration was that the oxidation of iodide by hydrogen peroxide in acidic medium is catalyzed by molybdenum, but also proceeds uncatalyzed; the absorbance of the triiodide ion produced in the uncatalyzed reaction forms the baseline of the flow injection recorder output. The aim was therefore to find the reaction conditions which would optimize the ratio of the catalyzed reaction to the uncatalyzed reaction (C/NC), i.e., the signal-to-noise ratio.

The effects of potassium iodide concentration on the catalyzed and uncatalyzed reaction rates are shown in Fig. 2. The catalyzed reaction was measured by peak height whilst the uncatalyzed reaction was estimated by measuring the baseline absorbance against deionized water. The uncatalyzed reaction rate increases almost linearly with iodide concentration to over

6% KI, whereas for the catalyzed reaction the relationship is linear up to 2%, increasing more gradually at higher concentrations, and so decreasing the C/NC ratio. Although better sensitivities were obtained with higher potassium iodide concentrations, the baseline absorbance and noise were also higher, with no real advantage in detection limits. As a compromise between sensitivity and C/NC ratio, the concentration selected was 2% (w/v) potassium iodide, which provided a reasonable detection limit and sensitivity with short residence times. This concentration is one to two orders higher than those used in manual or air-segmented systems. The high reaction rate thus obtained is the main reason for the high sampling rate in the flow injection procedure.

The effects of hydrogen peroxide concentration over the range 0.01—0.125% on the uncatalyzed and catalyzed reactions were studied similarly. The pattern was analogous to that shown in Fig. 2 for iodide. The relationship between the peroxide concentration and the uncatalyzed reaction rate was perfectly linear over the whole range studied whereas the catalyzed reaction was virtually unaffected by increase in the peroxide concentration over 0.03%. This concentration was therefore chosen for its high C/NC ratio and relatively high sensitivity. The effect of changing the hydrochloric acid concentration is shown in Fig. 3. The relationships between acid concentration and absorbance are not linear for either the uncatalyzed or catalyzed reaction, and the C/NC ratio reaches a maximum at 0.1—0.2 M HCl (approximately 0.015—0.03 M in the final flow stream); 0.2 M HCl was chosen for its favourable C/NC ratio and higher sensitivity.

Study of the flow system

Direct determinations of molybdenum in natural waters require sensitivity at $\mu g\ l^{-1}$ levels. After some preliminary studies, the highly sensitive flow injection system [9] shown in Fig. 1 was adopted with a large 200-μl sample injected into a carrier stream of water. Because the reaction involved is sensitive to changes in reagent concentrations (see above), using the reagent as a carrier stream would lead to false peak heights, double peaks and even negative peaks arising from changes of the uncatalyzed reaction rate at different reagent concentrations.

The flow rates of the carrier stream and reagents, and their ratios, were chosen so that sample injection would be reasonably rapid, and the residence time adequate to ensure relatively high sensitivity at a reaction coil length of 200 cm. The use of a 20-s injection period, which left a small amount of sample in the sample loop (this was flushed out by the next sample) provided a sampling rate of 90 h^{-1}. Adequate mixing of the merging streams was achieved in the proposed system; a "mixing point" consisting of a 90° turn inserted after the last confluence point made no difference to peak heights.

Interferences. The interferences of many ions and the effects of ionic concentration have been studied frequently [1—3, 6, 7]. As the reaction conditions are somewhat different in the flow injection system, the effects of the

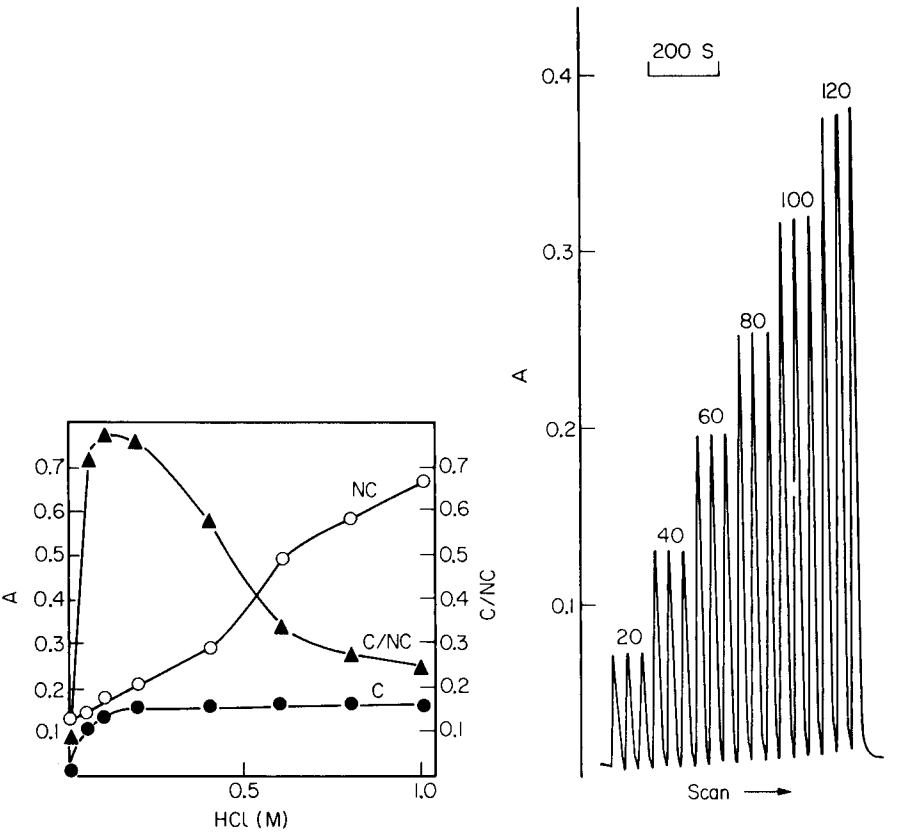

Fig. 3. Effects of acidity on catalyzed and uncatalyzed reaction rates. Conditions as for Fig. 2, except for 2% KI.

Fig. 4. Continuous signals recorded with the f.i.a. system in Fig. 1 obtained by injecting triplicate molybdenum standards in the range 20—120 $\mu g\ l^{-1}$; sampling rate, 90 h^{-1}; chart speed, 100 s cm^{-1}.

ions most likely to cause interferences in natural water samples were investigated. From the results (Table 1), ions present in natural waters in normal concentrations are unlikely to interfere. The tungstate and chromate ions might pose a problem at concentrations similar to molybdenum but this rarely happens. The interference of tungstate can be minimized by adding 0.1% EDTA [3] to the potassium iodide solution, but the sensitivity of the determination is then lowered by 30%. Chromate interference was best eliminated by reduction to chromium(III) by adding hydrogen peroxide to the acidified sample and evaporating to dryness [6]. Interference from Fe^{3+} in the AutoAnalyzer method has been reported [6, 7], 200 mg l^{-1} iron showing an apparent molybdenum content of 1 mg l^{-1}. In this study, when the pH of the solution was adjusted to the range of most natural waters (i.e., pH 5—9), a 2 mg l^{-1} Fe^{3+} solution was yellowish, presumably from hydrated

TABLE 1

The effect of various ions on the determination of molybdenum (50 $\mu g\ l^{-1}$)

Ion	Conc. added ($mg\ l^{-1}$)	Mo found ($\mu g\ l^{-1}$)	Ion	Conc. added ($mg\ l^{-1}$)	Mo found ($\mu g\ l^{-1}$)
V(V)	0.2	51	Mg^{2+}	100	49
W(VI)	0.1	60	Al^{3+}	10	50
W(VI)[a]	0.1	51	NO_3^-	500	50
Cr(VI)	0.1	58	SO_4^{2-}	500	50
Fe^{3+}(pH 8)	2.0	49[b]	PO_4^{3-}	30	51
Ca^{2+}	100	48	SiO_3^{2-}	40	50

[a]With 0.1% EDTA added.
[b]Absorbance caused by coloration corrected.

iron(III) oxide; such solutions produced no interference other than their colour. The interference could be corrected by injecting a second aliquot of the sample into the flow injection system with the potassium iodide solution replaced by water, measuring the peak absorbance, and subtracting it from the total absorbance. Although the final reaction mixture had an acidity of 0.03 M HCl, the coloration did not change during the short residence time, which suggests that the iron remained in the hydrolyzed form and did not participate in the catalytic reaction. Thus, interferences from Fe^{3+} will not be expected in the pH range of most natural waters. Samples with low pH and high Fe^{3+} concentrations (a few mg l^{-1}) may be processed by adjusting to pH 8 and correcting for the colour of the hydrolyzed iron.

Fuge [6] observed a marked effect on the reaction rates from changes in ionic strength in an air-segmented system; 3.5% sodium chloride caused a drop in molybdenum peak height of 35%. Both the catalyzed and uncatalyzed reactions were affected and negative peaks were obtained for blanks. Bradfield and Stickland [7] reported a 20% depression from 3.3% calcium chloride. These serious interferences were not encountered in the flow injection system; 3% sodium chloride in the sample caused a depression of less than 4% in the peak height. This improvement might be due to the higher reagent concentrations used in the flow injection system. It seemed at first that direct analysis of undiluted sea water using standards prepared in distilled water might be feasible. However, further studies showed that undiluted sea water gave rise to interfering negative peaks at low molybdenum concentrations, presumably owing to large differences in refractive index between carrier and sample. Such interferences can be overcome by suitable dilution of the sea water. When standards were prepared in water, a 1:1 dilution of sea water samples with deionized water prior to analysis proved satisfactory; alternatively, the carrier stream could be changed to 3% sodium chloride, with 3% sodium chloride added to all standards, which provided better sensitivity for sea water.

Effect of reaction temperature. When the ambient temperature of the reaction coil was changed from 16°C to 35°C, the peak height for a 100 $\mu g\ l^{-1}$ molybdenum sample as well as the baseline increased by 6%, which corresponds to a 0.3% deviation for a 1°C fluctuation. As the room temperature can be readily controlled within ±1°C during a 2-h run, no further attempt was made to control the ambient temperature by using a water bath.

Precision and accuracy. The precision of the method was tested by injecting 20 samples and recording the peak absorbances. Relative standard deviations were 0.83% for 50 $\mu g\ l^{-1}$ Mo, and 1.9% for 13 $\mu g\ l^{-1}$ Mo. The precision of the AutoAnalyzer method was 2.3% for a 10 $\mu g\ l^{-1}$ sample [6]. The precision achieved is well illustrated by the continuous trace recorded for a series of samples and shown in Fig. 4; carry-over is less than 1% at a 90 h^{-1} sampling rate. Although the calibration range shown is 20—120 $\mu g\ l^{-1}$ Mo, the graph is linear up to 1000 $\mu g\ l^{-1}$ with absorbance readings of over 3. The detection limit of the method, calculated as three times the standard deviation of a 13 $\mu g\ l^{-1}$ molybdenum standard, is 0.7 ppb.

The recoveries obtained by adding 50 ppb Mo to water samples with no pretreatment other than filtering and diluting when necessary were generally satisfactory, as shown in Table 2.

In the analysis of samples with low molybdenum concentrations, errors may arise from false peaks originating from rotation of the sampling valve. As the baseline signal of the proposed method is produced by the significant uncatalyzed reaction, it is rather sensitive to small variations in flow rate. Thus, peak heights equivalent to 3 $\mu g\ l^{-1}$ Mo were sometimes detected, but the problem did not arise with samples having higher molybdenum concentrations. Recordings at high chart speed showed that these false peaks do not coincide with the sample peak, and no corrections need be made as long as the two peaks can be differentiated. Nevertheless, peaks of samples with molybdenum contents below 3 $\mu g\ l^{-1}$ require some experience for interpretation, and it is recommended that 3 $\mu g\ l^{-1}$ molybdenum be added to samples which are suspected to have such low molybdenum contents.

TABLE 2

Recovery of molybdenum added to natural waters

Water sample	Amount of Mo in water ($\mu g\ l^{-1}$)	Amount found after addition of 50 $\mu g\ l^{-1}$ Mo	Recovery (%)
Tap water	5.5	56.0	101
River water	15.5	65.5	100
River water	2.5	53.0	101
Well water	1.5	51.0	99
Sea water	5.0	55.0	100
Sea water	4.5	54.0	99
River water	27.0	78.5	103

Further applications

The method was tested for further possible applications. Extracts with 0.1 M NaOH of soils low in organic matter can be analyzed directly after neutralization of the extract with 0.1 M HCl. Sodium hydroxide extracts of soils high in organic matter produced considerable absorbance at the wavelength used, but when the organic content is low it can be corrected for by injecting the sample into the f.i.a. system with the potassium iodide reagent replaced by water, and subtracting the absorbance recorded. Further work on the application of the method to plant ashes is in progress. As plant ashes or residues from plant digests are taken up in acid solutions, the method must be modified by omitting the acid in the peroxide reagent and replacing the carrier stream of water by 0.05 M hydrochloric acid, so that the final acidity in the reaction mixture was not altered compared to the original method.

REFERENCES

1 K. B. Yatsimirskii and L. P. Afanas'eva, Zh. Anal. Khim., 11 (1956) 319.
2 T. P. Hadjiioanou, Anal. Chim. Acta, 36 (1966) 360.
3 Cui Wan-cang and Yuan Xiu-shun, Fenxi Huaxue (Analytical Chemistry), 9 (1981) 461.
4 R. Feys, J. Devynck and B. Trémillon, Talanta, 22 (1975) 17.
5 A. Altinata and B. Pekin, Anal. Lett., 6 (1973) 667.
6 R. Fuge, Analyst, 95 (1970) 171.
7 E. G. Bradfield and J. F. Stickland, Analyst, 100 (1975) 1.
8 J. Růžička and E. H. Hansen, Anal. Chim. Acta, 114 (1980) 19.
9 J. Růžička and E. H. Hansen, Flow Injection Analysis, Wiley-Interscience, New York, 1981, p. 58.

Analytica Chimica Acta, 145 (1983) 151—158
Elsevier Scientific Publishing Company, Amsterdam — Printed in The Netherlands

SAMPLE PRECONCENTRATION BY CONTINUOUS FLOW EXTRACTION WITH A FLOW INJECTION ATOMIC ABSORPTION DETECTION SYSTEM

LAGE NORD

Department of Analytical Chemistry, Royal Institute of Technology, S-100 44 Stockholm (Sweden)

BO KARLBERG*

Bifok AB, Box 124, S-191 22 Sollentuna (Sweden)

(Received 19th June 1982)

SUMMARY

The flow manifold described allows automatic extraction of metal ions in aqueous samples into 4-methyl-2-pentanone with ammonium pyrrolidinedithiocarbamate as an extracting agent. The organic extract is led into the loop of an injector situated in an integrated feed system of an atomic absorption spectrometer. No dispersion of the injected organic extract plug, 110 μl, occurs in the aqueous feed stream and the resulting signal from the spectrometer is a peak. An increase in sensitivity of 15—20 is achieved for copper, nickel, lead and zinc in comparison with direct aspiration of the aqueous samples. The sampling frequency is 40 h^{-1} and the consumption of 4-methyl-2-pentanone is typically 0.3 ml min^{-1}. The detection limit for copper is about 1 $\mu g\ l^{-1}$.

Liquid—liquid extraction of metal ions from aqueous samples into an organic solvent is frequently used in connection with flame atomic absorption spectrometry (a.a.s.) [1]. It is used both as a preconcentration method and for separation of the analyte from an interfering matrix. The degree of concentration (concentration ratio) in an extraction is equal to the ratio of the aqueous and organic phase volumes, provided that 100% extraction of the analyte can be achieved.

Most commercial atomic absorption instruments are designed for sample feed rates in the range 4—10 ml min^{-1}. Below 4 ml min^{-1} the sensitivity drops rapidly. In the development of a continuous, on-line extraction system for a.a.s., this is definitely a limitation. A concentration ratio of 10 would require a minimum sample flow rate of 40 ml min^{-1} in order to keep the organic flow rate above 4 ml min^{-1}. In composing an extraction system out of standard parts commonly used for flow injection analysis, the total flow rate cannot be allowed to exceed 20 ml min^{-1} for technical and practical reasons. Consequently, the direct, continuous feeding of the nebulizer with organic extract must be abandoned if a concentration ratio of more than about 4 is aimed at while the sensitivity in the detection step is maintained.

In a previous paper [2], a method for integrating a low flow-rate extraction system with a high flow-rate nebulizer feed system for atomic absorption spectrometry was presented. This integration could be achieved without any significant loss in the sensitivity of the detection. The total flow rate in the extraction system was typically 5.6 ml min^{-1}. The organic solvent extract stream, with a flow rate less than 1 ml min^{-1}, was interconnected to a loop of an injector. The injector was situated in the aqueous feed stream to the a.a.s. instrument. The feed rate was kept at 4—5 ml min^{-1} so that the conditions for optimum performance of the a.a.s. instrument were guaranteed. On activation of the injector, a defined portion (100—200 μl) of the organic extract was introduced into the aqueous carrier. Neither back-extraction nor dispersion of the organic plug occurred. In a separate experiment, the results from continuous aspiration of organic extract were compared with the results from flow injection introduction into an aqueous feed stream. No drop in sensitivity was found when the injected volumes were above 100 μl.

This paper describes the further development and refinement of this extraction system integrated with a flow-injection atomic absorption detection system. The limiting factors for the extraction have been investigated and the maximum attainable sensitivity increase has been explored for a number of metal ions.

EXPERIMENTAL

Reagents

Working standards in the range 1 μg l^{-1} to 1 mg l^{-1} Cu, Zn, Pb and Ni were prepared from 1000 mg l^{-1} certified standard solutions. All metal standard solutions were acidified with nitric acid. 4-Methyl-2-pentanone (methyl isobutylketone; MIBK; reagent-grade) was used without further purification. A solution (1 g/100 ml) of reagent-grade ammonium pyrrolidinedithiocarbamate (APDC) and 1 M acetic acid/acetate buffer was prepared each day and extracted twice with MIBK to remove any metal ions present.

Apparatus

A Varian AA6 atomic absorption spectrometer equipped with background correction and an adjustable nebulizer with a glass bead was used throughout. Instrument settings and adjustments of the air/acetylene flame and the nebulizer glass bead were according to recommended procedures.

The flow system comprised three peristaltic pumps (FIA 08), two flow injection analyzers (FIA 05, Bifok, Sollentuna, Sweden) provided with a variable volume injector and a two-way valve, respectively, an extraction manifold with a membrane phase separator [3] and displacement bottles for pumping of MIBK as described previously [2]. The phase separator was specially designed for streams where the aqueous/organic flow rate ratio is high. The separator groove for the segmented stream had a large volume, 1600 μl, while the recipient groove volume was 36 μl. This design gives the

segmented stream a low linear flow velocity in the groove, thus allowing the organic phase stream to approach the membrane.

A microcomputer (SDK 85, Intel, Santa Clara, CA) was used for the timing of the two-way valve and the injector.

Manifold design

Figure 1 shows a flow diagram of the connected extraction and a.a.s. systems. The sample S is pumped into the extraction system via a two-way valve I1 mounted on an FIA 05. Water for rinsing, A3, is continuously pumped to the valve and by microcomputer control of the valve (I1) a reproducible sample/rinse cycle is obtained. The sample solution can be changed during the rinsing period without introduction of air into the extraction system. A stream of buffered APDC, R, is merged with the sample/rinse stream just before the segmentor C. A stream of MIBK is obtained by pumping water (A2) into a displacement bottle B1 filled with MIBK. The extraction takes place in extraction coil D and a controlled fraction of the extract is separated in the phase separator E. The flow rate of the separated extract, A4, is controlled by pumping via a displacement bottle B2. The aqueous phase and the remaining MIBK are led to waste via a short restrictor. The separated extract fills the loop of the injector, I2. At a delay time equal to the residence time of the sample in the extraction system, the injector is actuated by the microcomputer. The extract is injected into the stream of water A1 and transported as an undispersed plug to the nebulizer of the a.a.s. Three peristaltic pumps were used to control fully all individual flow rates.

The flow rates of the streams S, R, A2, and A3 given are those measured before the pump. When the aqueous and organic streams equilibrate in the extraction coil, the flow rates will change. This means that the actual aqueous/organic phase ratio differs slightly from the calculated flow ratio.

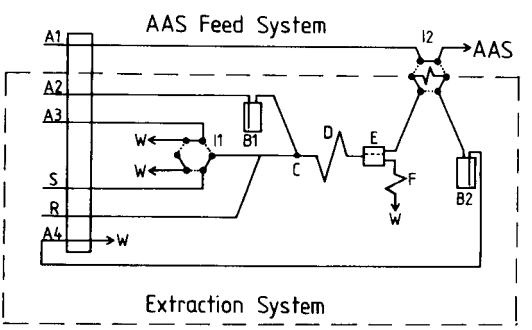

Fig. 1. Extraction manifold. Flow streams: A1, the aqueous a.a.s. carrier; A2, water feed to displacement bottle B1 providing a stream of MIBK; A3, wash water used in the sampling cycle; S, sample; R, the APDC reagent; A4, water back-feed from displacement bottle B2. C, Phase segmentor; D, extraction coil; E, phase separator; F, restrictor (0.5 m, 0.5 mm i.d. teflon); W, waste. I1, the sample inlet valve in the (—) sample and (·····) wash positions; I2, the injector, volume 110 μl, in the (—) filling and (·····) inject positions.

RESULTS AND DISCUSSION

Flow rates in the extraction system

The f.i.a.—a.a.s. manifold shown in Fig. 1 has a rather complex flow pattern. Because several of the flows can be varied individually, the number of flow combinations is vast. However, a systematic investigation is necessary in order to find optimum conditions for the extraction so that a high concentration ratio of the sample can be achieved with a good repeatability.

Figure 2 shows the effect of varying the sample flow rate while the organic flow rate is kept constant. The upper scale shows the flow ratio of sample/organic phase, and the lower scale the sample flow rate. The ordinate is the absorbance of the injected extract plugs, reflecting the concentration ratio. As expected, the absorbance increases when the flow ratio of sample to organic phase increases but a maximum is attained at a value of 15 corresponding to a sample flow rate of 6.5 ml min^{-1}. This is true for all the three different coils used, which means that the total flow rate seems to be the cause of the drop in the extraction efficiency rather than the coil volume and diameter.

At high flow rates it is impossible to observe visually any deviation in the flow pattern in the extraction coil but there is a definite risk that the small

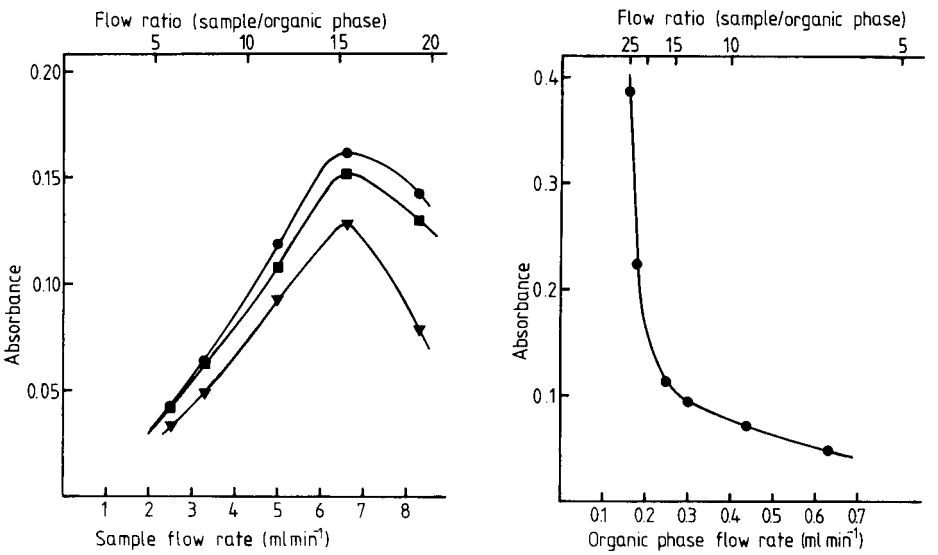

Fig. 2. Absorbance as a function of sample flow rate for a 50 $\mu g\ l^{-1}$ Cu standard, using the manifold in Fig. 1. Extraction coils (teflon): (•) 3 m, 0.7 mm i.d.; (▪) 2 m, 1.0 mm i.d.; (▾) 1 m, 2.0 mm i.d. Flows (see Fig. 1): A1, 6.0 ml min^{-1}; A2, 0.43 ml min^{-1}; R is kept at 0.13 × S.

Fig. 3. Absorbance as a function of the flow rate of the organic phase for a 50 $\mu g\ l^{-1}$ Cu standard. Flows (see Fig. 1): A1, 6.0 ml min^{-1}; A3 = S = 4.0 ml min^{-1}; R, 0.5 ml min^{-1}. Extraction coil: 3 m, 0.7 mm i.d. teflon.

organic segments are disrupted so that an irregular segmentation pattern results. This might lead to an inferior contact between the two phases and as a result the extraction efficiency will decrease. The physical disruption of organic segments was not assured experimentally. Nevertheless, the conditions for this event should be discussed because it might be the cause of the deviation in Fig. 2. The ability of a segment to resist disruption should depend on the length of the segment. The force that tends to disrupt the segment is proportional to the linear flow velocity. Both the segment length and the linear flow velocity are inversely proportional to the cross-section area of the extraction tube. This means that the conditions for segment disruption will depend only on the total flow rate and the flow ratio, and not on the tube diameter. This might be the explanation for the simultaneously appearing maximum values for the different coils in Fig. 2. A consequence of these results is that the concentration ratio cannot be increased indefinitely just by increasing the sample flow rate.

Figure 3 shows the absorbance as a function of the flow rate of the organic phase. The flow rates of the aqueous streams are kept constant, which means that the total flow rate is nearly constant. Thus, it is possible to change the flow ratio of the sample to organic phase over a large range and still keep the total flow rate almost constant. As expected, the absorbance increases when the organic flow rate decreases. The flow rate and flow ratio values refer to the ingoing streams. As MIBK is slightly soluble in water, the actual phase-volume ratio (aqueous/organic) in the extraction coil will be higher than the corresponding flow ratio when the two phases equilibrate. This explains why the absorbance is not proportional to the flow ratio. Although there is no sign of decreased extraction efficiency at low flow rates of the organic phase, the r.s.d. of the signal increases strongly, up to 10% at 0.15 ml min^{-1} compared with 2% at 0.3 ml min^{-1}. Therefore, the maximum flow ratio is 15—20, if a relatively good repeatability is to be maintained.

Figure 4 shows a situation where the flow ratio of sample to organic phase is kept constant while the total flow rate is varied. This makes it possible to isolate the effect of the total flow rate. At a total flow rate of 4.8 ml min^{-1}, the extraction efficiency starts to decrease.

The three experiments presented in Figs. 2—4 show that the flow ratio of the sample to the organic phase is limited to about 15. Too high sample and total flow rates will decrease the extraction efficiency and too low an organic flow rate will induce a high standard deviation. Furthermore, at very low organic flow rates, the sample throughput is reduced because a certain volume of extract is needed to rinse and fill the injector in the a.a.s. feed stream. For analytical purposes, a sample flow rate of 4 ml min^{-1} and an organic phase flow rate of 0.3 ml min^{-1} were found to be a suitable combination taking repeatability, concentration ratio and sample throughput into consideration.

Residence time in the extraction system

When the total flow rate changes the residence time in the extraction coil will also change. The effect of the residence time can be studied by changing

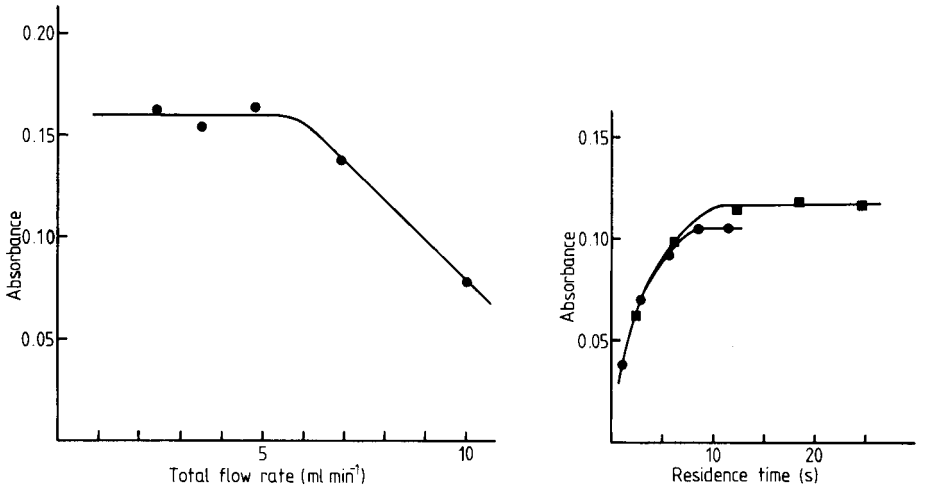

Fig. 4. Absorbance as a function of the total flow rate for a 50 $\mu g\ l^{-1}$ Cu standard. Flows (see Fig. 1): A1, 5.8 ml min^{-1}; A2 + S + R is the total flow rate; S/A2 = 14 ± 1; R/S = 0.14. Extraction coil: 3 m, 0.7 mm i.d. teflon.

Fig. 5. Absorbance as a function of the residence time for a 50 $\mu g\ l^{-1}$ Cu standard. Flows (see Fig. 1): A1, 6.2 ml min^{-1}; A2 + S + R, 3.9 ml min^{-1} (▪) and 8.3 ml min^{-1} (•); S/A2 = 12; R/S = 0.13. Extraction coils: 0.4, 1.0, 2.0, 3.0 and 4.0 m, 0.7 mm i.d. teflon.

the coil length while the flow rates are kept constant. The results of such an experiment are shown in Fig. 5. Two different total flow rates with the same flow ratio were tested. The two curves coincide to a large extent and a residence time about 8 s is sufficient to give maximum extraction. The corresponding coil lengths were 1.5 m and 3 m, respectively.

Some conclusions regarding the influence of the residence time on the extraction efficiency can be drawn from the results in Fig. 2 (3 m × 0.7 mm i.d.) and Fig. 4. The decrease in extraction efficiency starts at residence times of 11 and 13 s, respectively. These values are well above the 8-s value found in the experiment shown in Fig. 5. This observation may be taken as an indication that the decrease in extraction efficiency is caused by other factors than insufficient residence time.

Analytical performance of the system

The concentration ratio and the sample throughput are the two most important factors in an automatic extraction system of this kind. A sample throughput of 40 h^{-1} without any carry-over was aimed at for the manifold in Fig. 1. The source of carry-over can be traced to four parts of the system, namely, the sample introduction system, the extraction coil, the phase separator, and the injector for introduction of extract into the a.a.s. feed system. For the flow rates actually used, a slight carry-over occurred. This was found to originate in the extract injector (I2 in Fig. 1). This carry-over

could be eliminated by making a second injection of extract at some time after the analytical injection, see Fig. 6A. Two peaks will then result for each sample. Solutions with copper concentrations of 50 and 0 $\mu g\ l^{-1}$ were alternately introduced at a sample rate of 40 h^{-1}. The analytical peaks are marked. Figure 6B shows repeated introduction of standards containing 0—50 $\mu g\ l^{-1}$ copper into the system using the principle described above. The analytical peaks are marked for the second run of the set.

In addition to copper, tests were also made with nickel, lead and zinc; Table 1 summarizes some results. If the sensitivities in Table 1 are compared to those measured by direct aspiration of aqueous sample the increase is 19 times for Cu, 16 for Zn, 23 for Pb, and 18 for Ni. The increase in sensitivity is substantially larger than the flow ratio of the sample to the organic phase. This may be explained by the higher a.a.s. sensitivity for MIBK solutions. Furthermore, the dissolution of organic phase into the aqueous phase makes the real concentration degree higher than the flow ratio.

Background correction was used throughout and a background peak was detected only for zinc. This did not present any problem because the height of the peak was constant over a relatively long period of time. The noise was estimated in three different ways. For copper, MIBK solvent free from copper, was injected into the a.a.s. feed system and the standard deviation of the corresponding part of the baseline was measured. For zinc, the noise

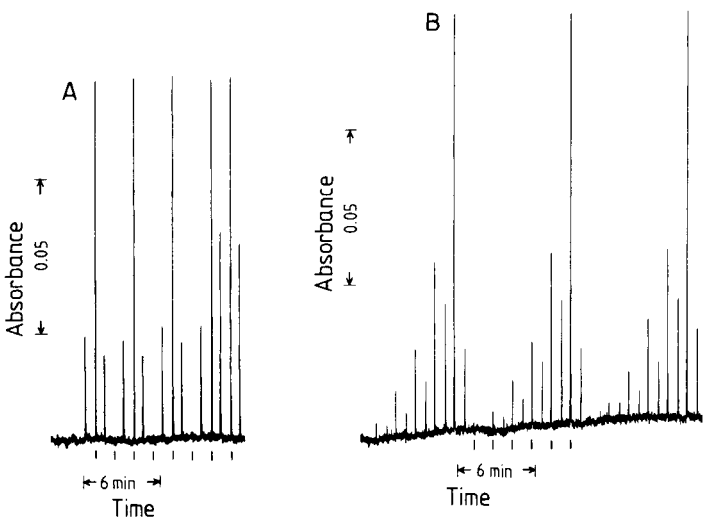

Fig. 6. Analytical performance for copper solutions. A, from the left: 50, 0, 50, 0, 50, 0, 50, 50 $\mu g\ l^{-1}$ Cu; analytical peaks are indicated by bars below the baseline. Sampling cycle: 60 s sample introduction and 30 s wash. Flows (see Fig. 1): S = A3 = 4.1 ml min^{-1}; S/A2 = 12.8. Extraction coil: 3 m, 0.7 mm i.d. teflon. B, three sets of copper standards, 0, 2, 5, 10, 20, and 50 $\mu g\ l^{-1}$ Cu; analytical peaks are denoted for second set. Flows (see Fig. 1): A1, 5.8 ml min^{-1}; A2, 0.3 ml min^{-1}; S = A3 = 4.0 ml min^{-1}; R, 0.3 ml min^{-1}; S/A2 = 13.2.

TABLE 1

Analytical performance of the manifold for some metals

Element	Sensitivity (Abs./mg l^{-1})	R.s.d. (%)[a]	Background absorbance	Noise[b]	Flow ratio of sample/organic phase
Cu	2.7	1(50)	0	0.0008	13
Zn	10.2	6(10)	0.033	0.0016	10
Pb	1.1	4(100)	0	0.002	12
Ni	1.3	4(50)	0	0.004	10

[a]For the concentration, in $\mu g\ l^{-1}$, given in parentheses. [b]Standard deviation of the background absorbance.

was estimated from the standard deviation of the background peaks and for lead and nickel directly from the baseline.

The APDC is a non-selective extracting agent and thus capable of extracting a great number of metals. The results in Table 1 indicate that multimetal extraction is possible with the flow manifold even at a high sampling frequency and with a high concentration ratio. The flow manifold should then be advantageous in combination with emission techniques such as inductively-coupled plasma and atomic emission spectrometry.

This work was supported by the Swedish National Board for Technical Development.

REFERENCES

1 M. S. Cresser, Solvent Extraction in Flame Spectroscopic Analysis. Butterworths, London, 1978.
2 L. Nord and B. Karlberg, Anal. Chim. Acta, 125 (1981) 199.
3 L. Nord and B. Karlberg, Anal. Chim. Acta, 118 (1980) 285.

Analytica Chimica Acta, 145 (1983) 159—168
Elsevier Scientific Publishing Company, Amsterdam — Printed in The Netherlands

FLOW INJECTION CALIBRATION METHODS FOR ATOMIC ABSORPTION SPECTROMETRY

J. F. TYSON*, J. M. H. APPLETON and A. B. IDRIS

Department of Chemistry, Loughborough University of Technology, Loughborough, Leicestershire LE11 3TU (Gt. Britain)

(Received 8th June 1982)

SUMMARY

The use of an atomic absorption spectrometer as a detector in flow injection analysis is briefly reviewed. A new simplified model is described for the dispersion effects observed with such systems; the model is based on considering the dispersion to be due to a single hypothetical mixing chamber located immediately prior to the measurement stage. The utility of this approach is demonstrated for two methods of calibration commonly used in atomic absorption spectrometry, and it is shown that flow injection sample and standard handling techniques are comparable to manipulation with volumetric apparatus. The flow injection method has a number of advantages for the analogue of the standard addition method. The use of an exponential concentration gradient is proposed as a novel method of calibration using a single concentrated standard. Results are presented for the determination of chromium in standard steels.

Since 1975, when flow injection analysis (f.i.a.), as the term is generally understood, was described by Růžička and Hansen [1], there has been considerable interest in applying the elegant simplicity of the basic idea to a wide range of analytical methods. Most of these applications have utilized the chemistries of existing analytical techniques and considerable ingenuity has been used in adapting some of these techniques to continuously flowing systems. The essence of f.i.a. is to allow reproducible dispersion between a plug of sample solution injected into a carrier stream and a reagent in, or added to, the carrier stream so that the extent of the reaction may be monitored by a downstream detector. Thus most applications of f.i.a. have used a system comprising a detector appropriate to monitoring the chemical reaction and spectroscopic (mainly molecular absorption spectrophotometry) and electrochemical (mainly potentiometric) techniques have been prominent. In addition to the great varieties of chemistries adapted for f.i.a., the high precision of which enables some of the stringent kinetic requirements of reactions of analytical utility to be relaxed, it has not been overlooked that the rapid through-put of samples possible with f.i.a. (one of its attractive features as a fully automated system) means that f.i.a. can be used for analytical measurements where no chemistry is required, merely rapid, reproducible transport of sample solution to detector. For such analyses, a low

dispersion system is required so that unnecessary dilution does not occur, or the dispersion can be designed so that solutions which are "off-range" can be suitably diluted.

There is a tendency for the through-put of a flow injection system to be described in terms of so many samples per hour, although this figure is not synonymous with so many determinations per hour. As current practice favours injection of samples in triplicate, and as allowance must be made for similar injection of the range of calibration standards, a more realistic figure might be obtained by dividing the samples-per-hour figure by three (or more) and calling it determinations per hour. Such a calculation still does not allow for the time spent in obtaining the sample or for any pretreatment it may need to get it into a form suitable for injection.

The use of atomic absorption spectrometry (a.a.s.) as the detection method in f.i.a. has been reported on only about ten occasions. Thus a.a.s. has not excited much interest as a detector system for f.i.a.; indeed, most of the applications would be better described as using flow injection simply as a sample introduction system. Nearly all the applications described use the limited dispersion flow injection mode described above, so that the sample handling system could be considered as an automated "discrete nebulization" [2] or "micro-sampling nebulization" [3] accessory. The advantages of flow injection for sample introduction are exemplified by Wolf and Stewart who report [4] on the excellent precision (hence low detection limits) obtainable for zinc and copper and the improvement in nebulizer performance achieved when the flow rate of carrier is controlled by a suitable pump rather than by the oxidant flow rate.

Nebulizer performance was also considered by Yoza et al. [5] who, in determining magnesium, used a compensating flow of either air or solution to match the manifold flow rate to the optimum flow rate of the nebulizer. The enhancing effects of organic solvents were utilized by Fukamachi and Ishibashi [6] who injected aqueous solutions of a number of metals into a carrier stream of an immiscible solvent (either n-butyl acetate or methyl isobutyl ketone) propelled solely by the "suction" of the nebulizer. Bergamin and co-workers [7—9] have demonstrated the feasibility of their zone-sampling injection technique as well as the use of the merging-zone technique for the addition of lanthanum to a calcium solution. The simultaneous use of both dual-channel atomic absorption and dual-channel atomic emission spectrometers enabled Basson and van Staden [10] to analyse water samples for four elements simultaneously by splitting the stream between the two instruments. Mindel and Karlberg [11] have outlined some of the advantageous features of using flow injection as a sample introduction system and suggested that solvent extraction could be carried out in the flowing stream. Tyson and Idris [12, 13] have discussed the characteristics of the instrument response curve and demonstrated the feasibility of the flow injection analogue of the standard addition method; they proposed the use of a concentration gradient generated by flow injection as the basis of a single-standard calibra-

tion method. Greenfield [14] has demonstrated that these ideas are also workable with an inductively-coupled plasma instrument whose use has also been described by Jacintho et al. [15]. Recently, the hydride generation reaction has been adapted to a flow injection manifold by Åström [16], for the determination of bismuth.

Model for dispersion behaviour

The extent to which a sample plug disperses during its passage through a narrow tube under conditions of laminar flow has been the subject of numerous studies. Exact solution of the appropriate equations appears difficult and various numerical methods have been based on introduction of reduced units to make the system of equations dimensionless. The relevance of these to the conditions normally encountered in flow injection manifolds has recently been critically evaluated [17] and it has been suggested that these numerical solutions are more useful than the solutions obtainable when either convection or diffusion is regarded as the predominant mechanism. The latter solutions have been used as a basis for explaining the dispersion phenomena encountered in f.i.a. and for providing a number of guidelines for the design of manifolds [18].

In an atomic absorption spectrometer, several physical and chemical processes occur in converting the solution flowing into the nebulizer to a population of free atoms. The resultant absorbance—time relationship is, to a good approximation, exponential and thus the atomic absorption instrument behaves as though it contained a single well-stirred mixing chamber. The concentration (C)—time (t) relationship when a step change in concentration from 0 to C_m occurs in a stream flowing with volume flow rate u, just prior to a mixing chamber of volume V is given by

$$C = C_m\,[1-\exp(-ut/V)] \tag{1}$$

If it is assumed that absorbance (A) is directly proportional to concentration, then the shape of the corresponding A—t curve is given by

$$A = A_m\,[1-\exp(-ut/V)] \tag{2}$$

(All symbols used are explained in Table 1.) The curve shape can be analyzed to obtain a value of V if A_m and u are known. A plot of $\ln [A_m/(A_m - A)]$ vs. t has a slope of u/V. For typical flow rates, compatible with optimum nebulizer performance, V ranges between 60 and 100 μl. Thus the flow injection equivalent of the basic a.a.s. manifold is as shown in Fig. 1. It was observed that increasing the length of the connecting tubing, L, up to 200 cm still produced exponentially-shaped peak profiles. Thus it is proposed that a convenient way of describing the total dispersion effects (caused by injection, flow system and detector) is to consider them as due to a hypothetical single mixing chamber located immediately prior to a detector with an instantaneous response. In this model, pure plug flow is considered to occur between the point of injection and the mixing chamber.

TABLE 1

List of symbols

A	Absorbance
A_m	Steady-state absorbance (or infinite volume absorbance)
A_P	Peak absorbance
C	Concentration
C_m	Steady-state concentration
C_P	Peak concentration
C^R	Concentration of reagent in carrier stream
C^S	Concentration of standard injected
C_t^S	Concentration of top standard in calibration sequence
C_x	Concentration of sample
D	Dispersion based on concentration of injected solution, $D = C_m/C_p$
D^R	Dispersion based on concentration of carrier stream solution, $D^R = C_m^R/C_p^R$
L	Tube length between injector and nebulizer
$R_{i/a}$	Minimum mass ratio of interferent to analyte species necessary to achieve maximum interference effect
t	Time
u	Pumping rate, i.e., volume flow rate
V	Volume of hypothetical mixing chamber
V_i	Volume injected

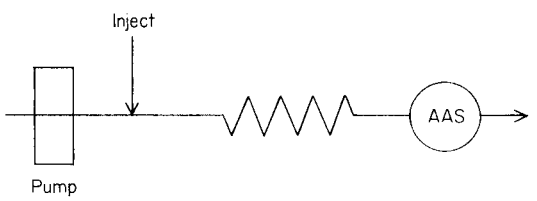

Fig. 1. Flow injection manifold with atomic absorption detector. The pumping rate, u, is about 6 ml min^{-1}; connecting tube dimensions are 0.58 mm i.d. and lengths, L, between 3 and 200 cm; the apparent detector volume is 100 μl.

The use of this model in the design of a flow injection manifold for performing reagent addition and standard addition is described in this paper. Furthermore, it is proposed that the inclusion of a real mixing chamber into the flow system, whose volume is large compared with the hypothetical volume, could provide concentration—time profiles useful for calibration purposes.

EXPERIMENTAL

Apparatus

A Gilson Minipuls-2 peristaltic pump, together with an Altex type 201-25 8-port injection valve (having two external sample loops) and 0.58 mm i.d. tubing formed the basis of the flow injection manifold. A Shandon Southern A3300 atomic absorption spectrometer was used for the studies on reagent

and standard addition methods and a Perkin-Elmer 290B spectrometer was used for the studies of the concentration profiles for calibration. The spectrometer outputs were monitored either by a chart recorder or a Baird Atomic Datacomp microprocessor data handling accessory.

The flow injection manifold was as shown in Fig. 1. A variety of injection loop volumes ranging from 13 to 500 μl and connecting tube lengths from 3 to 200 cm were used.

Samples, standards and reagents

The iron samples were prepared by dissolution in hydrochloric acid, as described by Nall et al. [19]. The chromium and magnesium standards were prepared by dilution of stock 1000 mg l^{-1} solutions (BDH Chemicals). Iron(III) solution (10,000 mg l^{-1}) was prepared by dissolving the appropriate amount of high-purity iron granules (BCS 149/3) in hydrochloric and nitric acids.

Procedures

Preliminary experiments. The variation of dispersion as a function of pumping rate, tube length, and volume injected was investigated. The precision of the procedure was evaluated by replicate injections of the standard solution.

Reagent addition method. A carrier stream of iron(III) was used and various volumes of sample and standards were injected. The length of connecting tubing was also varied. For the steel analysis, the tube length was 200 cm and the volume injected was 50 μl.

Standard addition method. The samples were used as the carrier stream and various volumes of the standards were injected. Various lengths of connecting tube were investigated. A tube length of 200 cm and an injection volume of 50 μl were used in the analysis of steel samples.

Exponential dilution flask calibration method. A cylindrical glass mixing chamber of volume 8.5 ml was incorporated into the flow line. The inlet was located on a base diameter and the outlet axially at the top [18]. A stream switching method was used to produce a sharp boundary between tri-distilled water and a 2.5 mg l^{-1} magnesium standard solution. The mixing chamber was stirred by a magnetic follower.

RESULTS AND DISCUSSION

As the quantitative parameter used in these studies was peak height, the dispersion, D, of the system was considered to be the ratio of the steady-state concentration, C_m, to the concentration at the peak, C_p. This designation of dispersion follows the accepted practice of previous flow injection publications. Thus $D = C_m/C_p$. The value of V, the volume of the hypothetical mixing chamber, was calculated for various values of L from the variation of D with V_i for each particular value of L. On the basis of the

proposed model, the peak maximum is achieved as the rear boundary of the plug of sample just enters the mixing chamber. This occurs at time $t_m = V_i/V$. Substitution in Eqn. (1) gives

$$C_p = C_m\ [1-\exp(-V_i/V)] \tag{3}$$

$$\text{Thus } D = [1-\exp(-V_i/V)]^{-1} \tag{4}$$

Thus $\ln(1-1/D) = -V_i/V$ and $\ln[D/(D-1)] = V_i/V$.

Thus a plot of $\ln[D/(D-1)]$, which in practice is calculated as $\ln[A_m/(A_m - A_p)]$, vs. V_i has a slope of $1/V$. For L equal to 200 cm, a least-squares fit of the regression line to the points produced the equation

$$\ln[A_m/(A_m - A_p)] = 0.00488\ V_i - 0.0143$$

The correlation coefficient was 0.999 and the value of V was 205 μl. Replicate injection of standards had a precision of 0.8% relative standard deviation based on peak height.

Analysis of the curve shape according to Eqn. (2) produced when a step change in concentration was made close to the nebulizer, gave a virtually constant value of V of 61 μl for flow rates between 3.7 and 9.5 ml min^{-1}. This is due to the mode of operation of the nebulizer which will give a steady-state response signal which is a function of flow rate.

Reagent addition method

If the carrier stream contains a reagent of concentration C_m^R then as the sample plug passes through the "mixing chamber", the reagent concentration varies according to $C^R = C_m^R \exp(-ut/V)$. Thus, at the peak maximum,

$$C_P^R = C_m^R \exp(-V_i/V) \tag{5}$$

and, by analogy with the dispersion of the sample (Eqn. 4), the reagent dispersion, D^R, is given by

$$D^R = C_m^R/C_P^R = \exp(-V/V_i) \tag{6}$$

Thus, combining Eqns. (4) and (6)

$$D^R = D/(D-1) \tag{7}$$

In the determination of chromium in steel, it is known that the iron exerts a depressive effect on the chromium absorbance. It was found in this study that the depressive effect was constant, provided that the iron-to-chromium mass ratio was greater than 30:1. If the most concentrated standard (C_t^S) used in the calibration was 20 mg l^{-1} Cr, then the relation between dispersion and peak concentration enables the minimum iron concentration at the peak to be calculated. Thus from Eqns. (6) and (7), the minimum concentration of iron in the carrier stream can be calculated as $C_m^{Fe} = 20 \times 30/(D-1)$. This equation can be generalized to give

$$C_m^R = C_t^S \times R_{i/a}/(D-1) \tag{8}$$

In this study, a dispersion of 4 was used and thus the concentration of iron added to the carrier was 200 mg l^{-1} or greater. The results obtained under these conditions for the analysis of some British Chemical Standard steels are given in Table 2.

Standard addition method

The sample carrier stream contains the analyte at concentration C_x and thus the concentration at peak maximum when a standard of concentration C^S is injected is obtained by combining Eqns. (3) and (5) to give

$$C_p = C^S [1 - \exp(-V_i/V)] + C_x \exp(-V_i/V) \quad (9)$$

The change in concentration, ΔC, which occurs at the peak maximum, $C_p - C_x$, is given by

$$\Delta C = C^S [1 - \exp(-V_i/V)] + C_x \exp(-V_i/V) - C_x$$

Thus $\Delta C = (C^S - C_x) [1 - \exp(-V_i/V)]$ and from Eqn. (4), $\Delta C = D^{-1} (C^S - C_x)$. Thus a plot of ΔC vs. C^S would intercept the C^S axis at C_x. Assuming absorbance to be a linear function of concentration then

$$\Delta A = (k/D)(C^S - C_x) \quad (10)$$

where ΔA is the observed change in absorbance and k is the proportionality constant relating absorbance and concentration. The method is illustrated in Fig. 2 in which the concentration of the carrier stream was 9.0 mg l^{-1}. The normal use of the standard addition method in a.a.s. is to compensate for interference effects in the samples. For this flow injection method to function likewise, the dispersion must be designed so that interference effects in the sample stream operate to the appropriate extent on the injected standards. This can be done in a manner similar to that outlined in the previous section for the reagent addition method.

From Eqns. (6), (7) and (9),

$$C_p = (C_t^S/D) + C_x (D - 1)/D$$

Thus the concentration of interferent C_p^R at the peak must be

$$C_p^R = R_{i/a} [(C_t^S/D) + C_x (D - 1)/D]$$

TABLE 2

Results of reagent addition and standard addition calibration methods

Sample	Chromium found (%)		Certified value (%)
	Reagent addition	Standard addition	
BCS 220/2	5.12 ± 0.06	5.13 ± 0.02	5.12
BCS 241/2	5.34 ± 0.02	5.34 ± 0.02	5.35
BCS 261/1	17.3 ± 0.1	17.4 ± 0.1	17.4

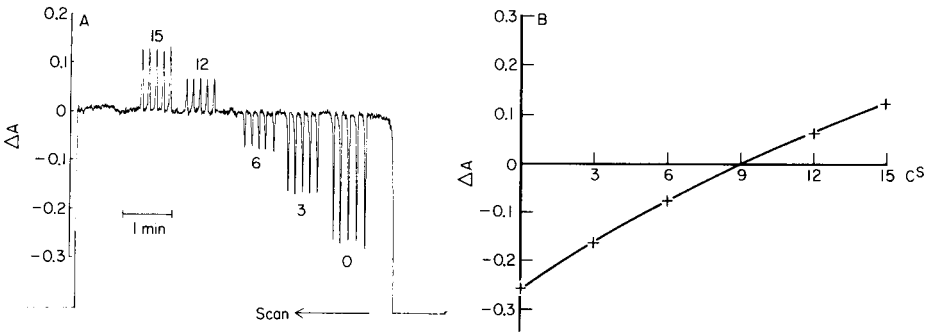

Fig. 2. (A) Chart recording of response for standard addition method. The "sample" was the carrier stream (9 mg l^{-1} Cr) and the peaks correspond to the injection of solutions containing 0, 3, 6, 12 and 15 mg l^{-1} Cr. (B) Plot of results from Fig. 2. A as ΔA (difference between peak absorbance and carrier stream absorbance) vs. concentration of standard. When $\Delta A = 0$, then the concentration corresponds to that in the carrier stream (see Eqn. 10).

and, from Eqns. (6) and (7), the minimum concentration of iron in the carrier stream must be

$$C_m^R = R_{i/a}\,[C_t^S/(D-1) + C_x] \qquad (11)$$

Equation (11) is thus the general equation for the standard addition method analogous to Eqn. (8) for the reagent addition method.

The conditions used in the experiments described here were $D = 4$, $C_t^S = 20$ mg l^{-1}, $R_{i/a}$ (Fe:Cr) = 30. Thus for a sample containing 10 mg l^{-1} Cr, the minimum concentration of the interferent, iron, had to be 500 mg l^{-1}. As the samples did not contain the appropriate iron to chromium concentration ratio, sufficient iron was added so that the sample carrier streams contained at least 500 mg l^{-1} iron. The results obtained by this method for the BCS steels are shown in Table 2.

Exponential dilution flask calibration method

The concentration—time profile generated by a real mixing chamber of volume V_m is given from Eqn. (1): $C = C_m\,[1 - \exp(-ut/V_m)]$. An analysis of the curve shape, produced at a flow rate, u, of 5.1 ml min^{-1}, showed that the mixing chamber behaved as though V_m were 7.2 ml. This value was used in subsequent calculations. The curve produced by the instrument when the concentration was stepped from zero to 2.5 mg l^{-1} is shown in Fig. 3; the steady-state signal for this concentration corresponded to 16.6 cm on the chart paper. The curve obtained from

$$A = 16.6\,[1 - \exp(-5.1\,t/60 \times 7.2)] \qquad (12)$$

is also shown in the Fig. 3. The good agreement which is obtained shows that the dispersion of the real mixing chamber completely dominates all other sources of dispersion in the system. Thus, if a sample solution is introduced

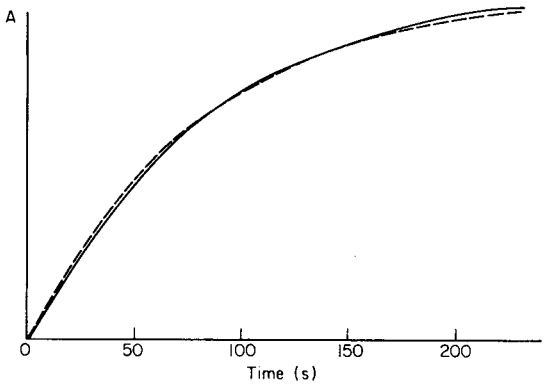

Fig. 3. Absorbance—time relationships: (—) produced when a step change in concentration occurred just prior to the mixing chamber; (---) calculated according to Eqn. (12).

into the instrument at the same flow rate as the exponential concentration profile was produced, a characteristic time value may be obtained from the A—t plot which can then be converted to a concentration by substitution into Eqn. (1). The results of some preliminary experiments with magnesium as the test element are given in Table 3.

CONCLUSIONS

In addition to the advantages of using flow injection sample introduction methods for atomic absorption spectrometry, which have already been described in the literature, the results of the present study indicate that the precise dispersion characteristics of flow injection manifolds can be used as a substitute for volumetric manipulation and that flow injection analogues of "reagent" addition (matching standards to samples) and standard addition methods of calibration may be devised. This standard addition method, in particular, has two advantages: (a) the same standard solutions are used for a range of samples, thus considerably reducing the amount of volumetric manipulation necessary; and (b) an interpolative procedure is provided for obtaining unknown concentrations, which is more accurate than the normal extrapolative method.

Although it has been shown that the simplified model for the dispersion effects observed proposed here (the single hypothetical mixing chamber) is lyte. In the g.s.a.m. calculations, these factors may be considered as a pseudo-applicable to flow injection manifolds coupled to atomic absorption spec-

TABLE 3

Results for exponential dilution flask calibration method

Real conc. (mg l^{-1})	0.125	0.25	0.5	1.0	1.5	2.0
Conc. found (mg l^{-1})	0.128	0.255	0.52	1.04	1.55	2.07
Error (%)	+2	+2	+4	+4	+3	+4

trometers, it may be that this is due to the flow rates and detector behaviour peculiar to a.a.s., and that the model may not have general applicability. It is difficult to examine previously published data to see if this model fits other flow injection systems, as very few publications give sufficient information concerning peak shape, dispersion, etc. However, a preliminary examination of some of Růžička's and Hansen's results [18] (particularly when Figs. 10, 11 and 12 of ref. 18 are examined) for a solution spectrophotometric system with detector volume 18 μl, pumping rates 0.5 and 1.5 ml min^{-1}, and tube lengths (0.5 mm i.d.) up to 200 cm, is very encouraging in this respect.

It is hoped to provide further details of the new model, including consideration of some of the relevant time parameters of peaks, and of the exponential dilution flask calibration method as well as examination of other flow injection-based methods of generating concentration gradients that could be utilized for calibration purposes, in future publications. It has recently been reported [20] that the tail section of a single injection can be used empirically in this way to provide a method of "electronically" reconstructing a calibration curve. Thus, "it is hoped that the present outline will inspire further thoughts about the undiscovered possibilities which f.i.a. gradient techniques have to offer" [20].

A. B. Idris and J. M. H. Appleton gratefully acknowledge financial support from the National University of Malaysia and the Zimbabwe Government Department of Manpower Training and Social Services, respectively.

REFERENCES

1 J. Růžička and E. H. Hansen, Anal. Chim. Acta, 78 (1975) 145.
2 T. Uchida, I. Kojima and C. Iida, Anal. Chim. Acta, 116 (1980) 205.
3 R. C. Fry, S. J. Northway and M. B. Denton, Anal. Chem., 50 (1978) 1719.
4 W. R. Wolf and K. K. Stewart, Anal. Chem., 51 (1979) 1201.
5 N. Yoza, Y. Aoyagi, S. Ohashi and A. Tateda, Anal. Chim. Acta, 111 (1979) 163.
6 K. Fukamachi and N. Ishibashi, Anal. Chim. Acta, 119 (1980) 383.
7 E. A. G. Zagatto, F. J. Krug, H. Bergamin F°, S. S. Jørgensen and B. F. Reis, Anal. Chim. Acta, 104 (1979) 279.
8 B. F. Reis, A. O. Jacintho, J. Mortatti, F. J. Krug, E. A. G. Zagatto, H. Bergamin F° and L. C. R. Pessenda, Anal. Chim. Acta, 123 (1981) 221.
9 E. A. G. Zagatto, A. O. Jacintho, L. C. R. Pessenda, F. J. Krug, B. F. Reis and H. Bergamin F°, Anal. Chim. Acta, 125 (1981) 37.
10 W. D. Basson and J. F. van Staden, Fresenius Z. Anal. Chem., 302 (1980) 370.
11 B. D. Mindel and B. Karlberg, Lab. Pract., July (1981) 719.
12 J. F. Tyson, Anal. Proc., 18 (1981) 542.
13 J. F. Tyson and A. B. Idris, Analyst, 106 (1981) 1125.
14 S. Greenfield, Ind. Res. Dev., August (1981) 140.
15 A. O. Jacintho, E. A. G. Zagatto, H. Bergamin F°, F. J. Krug, B. F. Reis, R. E. Bruns and B. R. Kowalski, Anal. Chim. Acta, 130 (1981) 243.
16 O. Åström, Anal. Chem., 54 (1982) 190.
17 J. T. Vanderslice, K. K. Stewart, A. G. Rosenfeld and D. J. Higgs, Talanta, 28 (1981) 11.
18 J. Růžička and E. H. Hansen, Anal. Chim. Acta, 99 (1978) 37.
19 W. R. Nall, D. Brumhead and R. Whitham, Analyst, 100 (1975) 555.
20 S. Olsen, J. Růžička and E. H. Hansen, Anal. Chim. Acta, 136 (1982) 101.

Analytica Chimica Acta, 145 (1983) 169—178
Elsevier Scientific Publishing Company — Printed in The Netherlands

FLOW INJECTION SYSTEMS WITH INDUCTIVELY-COUPLED ARGON PLASMA ATOMIC EMISSION SPECTROMETRY
Part 2. The Generalized Standard Addition Method

E. A. G. ZAGATTO*, A. O. JACINTHO, F. J. KRUG and B. F. REIS
Centro de Energia Nuclear na Agricultura. USP, 13400 Piracicaba, S.P. (Brasil)
R. E. BRUNS and M. C. U. ARAÚJO
Instituto de Química, Universidade Estadual de Campinas, 13100 Campinas, S.P. (Brasil)
(Received 25th June 1982)

SUMMARY

In multicomponent analysis by inductively-coupled argon plasma emission spectrometry, the generalized standard addition method is useful in overcoming matrix and/or spectral interferences. As this method requires many standard additions, it becomes cumbersome when done manually if many elements are to be determined. By using a flow injection system, the standard addition manipulations required can be significantly simplified and completed within a shorter period of time with much less sample material. A flow injection system with merging zones is used to demonstrate the method for analyses of a Ni/Cu/Zn standard and of alloys. The reproducibility of measurements of the injected sample, with or without additions of standards is always better than 99%. The results obtained compare well with those obtained by the manual procedure and also with those obtained by atomic absorption spectrometry.

The increasing interest in flow injection analysis (f.i.a.) [1] is due to its characteristics of simplicity, versatility, cost, precision, and high sampling rate. This high sampling frequency makes f.i.a. particularly suitable for long runs of samples, e.g., in hydrological, biomedical, agronomic and geological work [1]. A successful combination of f.i.a. with inductively-coupled argon plasma emission spectrometry (i.c.p.e.s.) was described earlier [2], and, the good performance of such systems has been emphasized [3]. A main advantage is that losses in accuracy caused by variations in the sample matrix, mainly sample viscosity, can be decreased by the provision of a more constant sample flow rate to the nebulizer of the spectrometer. In i.c.p.e.s., for some types of samples, however, spectral interferences are often the limiting factor on the accuracy as well as the sensitivity of determinations [4].

Recently, the generalized standard addition method (g.s.a.m.) [5, 6] has been proposed as an expansion of the well known standard addition method. Its success in overcoming both matrix effects and spectral interferences in i.c.p.e.s. has been reported [7]. This method requires a number of additions of standard solutions to the sample in order to measure mutual interferences

and also the matrix effect, allowing accurate simultaneous determinations of several analytes. In addition, complete characterization of the instrument is attained [7]. The concepts and related calculations are described elsewhere [5, 7, 8]. The application of this method in routine large-scale analysis is cumbersome if the many standard additions required are done manually. The large number of measurements required for each sample drastically reduces the sampling rate and increases the sample volume needed.

The good performance of flow injection systems with i.c.p.e.s., and the feasibility of standard additions in these systems, make it attractive to include the g.s.a.m. for the analysis of materials where spectral interferences and/or matrix effects impair accuracy. This paper reports the development of such a flow injection system for the routine analysis of copper-nickel alloys by i.c.p.e.s.

EXPERIMENTAL

Reagents, standards and samples

Freshly distilled-deionized water was used. The acids were analytical grade and high-purity argon was employed. The stock standard solutions were prepared from spectrographically pure substances (Johnson-Matthey; Specpure). Working standards for the application of the g.s.a.m. (20.0 ppm Cu, 40.0 ppm Cu, 60.0 ppm Cu, 20.0 ppm Ni, 40.0 ppm Ni, 60.0 ppm Ni, 1.00 ppm Zn, 2.00 ppm Zn, 3.00 ppm Zn and the blank) were prepared in 4% (w/v) nitric acid. For comparison, the same synthetic sample (40.0 ppm Cu + 40.0 ppm Ni + 2.00 ppm Zn, in 4% w/v nitric acid) as used in the earlier manual procedure [7] was prepared. The blank solution, used as carrier streams and as standard, was a 4% (w/v) nitric acid solution.

The alloys (250 mg) were dissolved in 10 ml of aqua regia (3:1 hydrochloric acid and nitric acid), the final volume being completed to 100.0 ml with water. Before measurement, the samples were diluted manually 25-fold with water. This dilution, which may also be done in the flow injection system by using a smaller injected volume [1, 2], is necessary to match the mean analyte concentrations in the samples with the i.c.p. linear ranges.

Apparatus

A Jarrell-Ash model 975 ICAP AtomComp spectrometer with a cross-flow nebulizer was employed. The wavelength for nickel measurements was 243.7 nm; the other operating conditions were as specified in Part 1 [2]. The standard software furnished by the manufacturer in the PDP-8 computer was maintained with no background correction applied. The integration period was fixed at 10 s and the pre-burn time at 13 s. The calibration for the usual measurements was based on a two-point standardization, from the blank and standard concentrations of 40.0 ppm Cu, 40.0 ppm Ni and 2.00 ppm Zn. Mixed standards were not employed to avoid any effects of spectral interferences. For the g.s.a.m., no previous calibration was required

and the responses measured after each addition were those of intensities from the channel for each element ratioed to a constant current source. The intensities related to the blank were measured from time to time; very small variations relative to the analytical responses were observed. As the standard addition method requires the analytical response to be zero in the absence of the analyte [9, 10], the net intensity values were obtained by subtracting the small blank values from the measured intensities.

The proportional injector, manifold tubing and connectors were the same as used earlier [2]. Alternatively, a Technicon AAII peristaltic pump furnished with tygon pumping tubes was used. The flow injection system and the spectrometer were coupled as already described [2].

Flow system

The system used for the analysis of alloys utilizes successive injections of the sample, each one accompanied by the injection of a different standard, the additions being achieved by the merging zones approach [11]. This system therefore does the manual part of the partition generalized standard addition method [5, 7, 8], because the successive sample zones can be considered as aliquots for which the volume does not vary after the different additions.

The flow diagram of the system is shown in Fig. 1. When the proportional injector (I) rests in the sampling position, as indicated, both sample (S) and standard solution to be added (A) are pumped to fill the corresponding loops (L_S and L_a) before going to waste (W). After the sampling period, the central sliding part of the injector is moved to the alternative position so that the selected volumes of sample and standard are introduced into their corresponding carrier streams (C_s and C_a) as well defined, reproducible zones [1]. The zones merge at confluence point *y*, and mixing is improved inside the following mixing coil (M_C) before the processed sample zone reaches the nebulizer. After measurement, the sample zone is discarded. The standard solution pumped is replaced by another, the sample is kept and the injector

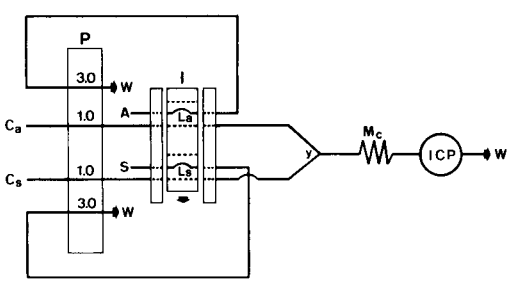

Fig. 1. Flow diagram of the proposed system. P is the peristaltic pump with indication of flow rates (ml min^{-1}); I is the proportional injector shown in the sampling position. The sample (S) and standard (A) solutions fill loops L_S and L_a which are the volumes introduced into the carrier streams (4% w/v nitric acid). M_C is the mixing coil (70 cm).

is switched back to the position specified in Fig. 1, starting a new cycle. After successive measurements involving all standards, including the blank (without addition), the g.s.a.m. data have been obtained and next sample can be processed.

Application of the generalized standard addition method

The amounts of added standards can be expressed either in quantity or concentration units, because the volume of the processed sample zone is the same regardless of the additions involved. Concentration units (ppm) are preferred here. These concentration values could be processed without correction in a perfectly symmetrical flow injection system [11], where both the sample and the standard solutions undergo the same degree of dispersion. However, the construction of a perfectly symmetrical flow injection system is very difficult.

In this study, any effect of system asymmetry can be corrected by multiplying the added concentration values (ΔC, Table 1) by the f_A/f_S ratio, where

TABLE 1

Input file for the f.i.a.—g.s.a.m. application to the synthetic sample

Input file			Comment
FIA—ICP—GSAM for Zn, Cu, Ni			Title
4 9 3 0			TDC computational method, number of additions, number of analytes, no scaling
0.	0.	1.	
0.	0.	2.	
0.	0.	3.	
20.	0.	0.	
40.	0.	0.	C Matrix of concentrations (ppm)
60.	0.	0.	
0.	20.	0.	
0.	40.	0.	
0.	60.	0.	
24477.	15759	9299.	R_0 Matrix of the responses related to the situation without addition
24155.	15724.	13281.	
24339.	15737.	17385.	
24514.	15805.	21805.	
37901.	16242.	9836.	
50954.	15859.	9877.	R Matrix of responses related to C
62722.	15407.	9927.	
23546.	23900.	9096.	
23762.	33072.	9682.	
24725.	40639.	9978.	

f_A and f_S are the dispersion factors related to standard and sample, respectively. This is demonstrated by considering a single-analyte solution which is injected into the f.i.a.—i.c.p.e.s. system to simulate first the sample and then the standard. If linearity of the response plot can be assumed, responses R_S and R_A are related to the analyte concentration (C) by the equations $R_S = \alpha_S C$ and $R_A = \alpha_A C$. Here, α_S and α_A are the global response constants of the whole system for the analyte present in the sample and standard, respectively. Thus $R_S/R_A = \alpha_S/\alpha_A$.

The α values depend both on the flow injection system and on the i.c.p. spectrometer, being regarded as the product of the dispersion factors (f_A or f_S) and the response constant of the detection unit. For a given analyte, this constant is the same for both sample and standard, and the above equation reduces to $R_S/R_A = f_S/f_A$. In symmetrical systems, $f_S = f_A$ and no correction is needed because $R_S = R_A$. In asymmetrical systems, the added concentrations must be multiplied by f_A/f_S so that $R_S = R_A$ for a given analyte. In the g.s.a.m. calculations, these factors may be considered as a pseudo-matrix effect which alters the slope of an hypothetical calibration curve and is eliminated by the g.s.a.m.

Calculations

All calculations were done by a PDP-10 computer, the g.s.a.m. program written in Fortran IV (Infometrix, Seattle, WA) being used with small modifications. Table 1 shows one of the input data files which contains information about the sequence of additions, amounts of added standards, responses measured initially and after each addition, and dispersion factors. The final results of initial amounts of analytes are given in ppm.

The g.s.a.m. solves the overdetermined system of equations $\Delta\mathbf{CK} = \Delta\mathbf{R}$, where $\Delta\mathbf{C}$ and $\Delta\mathbf{R}$ are matrices representing changes in concentrations and analytical responses caused by the additions of the analytes. Matrix **K** contains the coefficients relating the contribution of each of the analytes to the different responses. The dimensions of these matrices are discussed elsewhere [5] and for this application, $\Delta\mathbf{C}$ and $\Delta\mathbf{R}$ are 9×3 (i.e., nine standard additions and three analytes to be determined). The 3×3 **K** matrix is determined from the eqn. [5]

$$\mathbf{K} = (\Delta\mathbf{C}^t\,\Delta\mathbf{C})^{-1}\,\Delta\mathbf{C}^t\,\Delta\mathbf{R}$$

and indicates the sensitivities of all sensors to all analytes for the system studied. The initial analyte concentrations C_0 are obtained [5] from

$$C_0 = [\mathbf{R}(\Delta\mathbf{C}^t\,\Delta\mathbf{R})^{-1}\,\Delta\mathbf{C}^t - \mathbf{I}]\,\Delta\mathbf{C}$$

Here, **R** is the matrix of responses, related to the concentration matrix **C** (Table 1).

Procedures

Prior to system dimensioning, it was necessary to investigate the effect of the emergent flow rate on the Cu, Ni and Zn measurements. The solutions (blank, 10.0 ppm Cu, 10.0 ppm Ni or 10.0 ppm Zn in 4% (w/v) nitric acid) were pumped continuously at different flow rates (0.5—6.3 ml min^{-1}) and measured with a 10-s integration period. For three pumping rates (1.5, 3.0 and 4.5 ml min^{-1}), relative standard deviations of ten measurements were calculated. These tests showed that a flow rate of 2.0 ml min^{-1} was optimal; this means 1.0 ml min^{-1} for each of the merging carrier streams C_S and C_A (Fig. 1) in a symmetrical flow system. The effect of the length of the M_C mixing coil on reproducibility was investigated with 40, 70 or 110 cm coils. Finally, injected volumes of the sample and standard solutions, compatible with the integration period and the other system dimensions, were chosen.

The pre-burn time was then fixed by analysing the measured peak shape of the sample zone. These tests involved a ΔI scan [2], an integration period of only 1 s and the utilization of 10.0 ppm standards of Cu, Ni or Zn. Later, the dispersion factors related to sample and standards (f_S and f_A) were determined for Cu, Ni and Zn as already described [2]. The same standards as used for the i.c.p. calibration were employed.

Before the g.s.a.m. was applied, the linearities of the calibration plots for Cu and Ni were checked by measuring 0.0, 25.0, 50.0, 75.0 and 100.0 ppm standards prepared in 4% (w/v) nitric acid. This procedure was not applied for zinc because of the expected small zinc concentrations in the alloys and the low concentration levels of the zinc additions.

The flow injection system (Fig. 1) was then employed for the analysis of the synthetic sample and of the alloys by using the g.s.a.m. The standards were added in the following order: blank, 1.00 ppm Zn, 2.00 ppm Zn, 3.00 ppm Zn, 20.0 ppm Cu, 40.0 ppm Cu, 60.0 ppm Cu, 20.0 ppm Ni, 40.0 ppm Ni and 60.0 ppm Ni. For some samples, the entire procedure was applied in triplicate so that the precision of results could be assessed.

Finally, the samples were analysed by a manual procedure with the g.s.a.m. Equal volumes (15.0 ml) of the sample and the standards (the same as specified above) were mixed and measured in the i.c.p. with pneumatic sample aspiration.

RESULTS AND DISCUSSION

Changes in flow rate within the interval studied here caused small variations in the measured signal for both sample and blank solutions (Fig. 2), and the reproducibility of measurements was also affected, as was noted previously [2]. Reproducibility also deteriorated when the flow rate was 6.3 ml min^{-1}, probably because higher flow rate affected the plasma stability [2]. These results are general, and similar effects were observed for 30 other metals under different acidity conditions. All these data, useful for designing other f.i.a.—i.c.p.e.s. systems, are available on request. For the

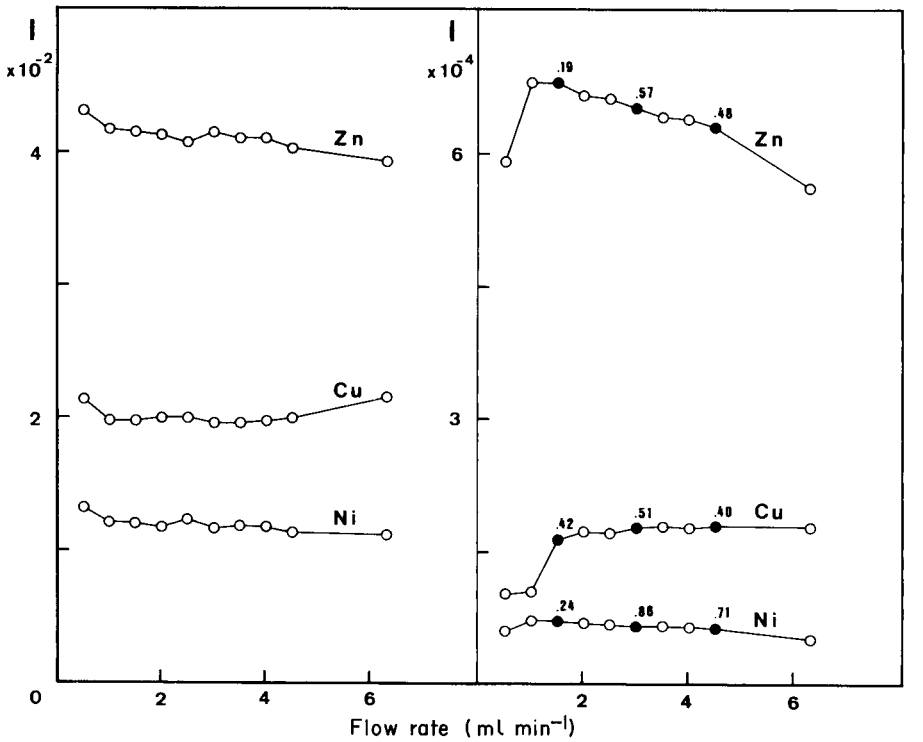

Fig. 2. Effect of the sample flow rate towards the inlet of the plasma on the signal (I). The left-hand curves refer to the blank and the right-hand curves to 10.0 ppm Zn, Cu and Ni standards. The numbers near the filled points indicate the relative standard deviations (%) of the corresponding measurements calculated after ten measurements.

present system, in which Cu, Ni and Zn concentrations were to be determined simultaneously, a 2.0 ml min^{-1} flow rate was chosen as the best compromise between reproducibility, sampling rate and plasma stability.

The relative standard deviations of the measurements were almost unaffected by variations in the length of the M_C mixing coil (Fig. 1), which therefore does not play an important role in the precision of measurement, in contrast to most flow injection systems. As there is no chemical reaction within the mixing coil, and the signal is averaged over the integration period, the mean signal is less dependent than usual on the mixing conditions. The coil length was, therefore, kept as small as possible while still allowing some mixing as well as attachment of the Y-connector (Fig. 1) to the inlet of the i.c.p. nebulizer. The short coil also enhanced the possible sampling rates [1].

The injected volumes were 500 μl, which corresponds to L_S and L_a loops of 100 cm. These large volumes are necessary to permit an integration period of 10 s without significant decrease in dispersion factors which leads to loss

in sensitivity. Analysis of the measured peak profiles showed that a pre-burn time of 13 s is sufficient to permit initiation of the i.c.p. operation and sample injection to be simultaneous ($\Delta I = 0$) [2]. Also, with the large peak width, the integration period can be located in the central part of the sample zone, where there is a more constant concentration than at the ends of the zone. Under such conditions, small differences in injection and measurement starting times are not significant, and the internal standard technique used earlier [2] becomes unnecessary. Parallel experiments confirmed that the precision of measurements without an internal standard was always somewhat better than the precision obtained in measurements based on ratios involving cadmium as internal standard.

After system dimensioning, the f_S and f_A dispersion factors were determined for Cu, Ni and Zn (Table 1). The differences between f_S and f_A reflect the system asymmetry. The small but significant differences observed for dispersion factors corresponding to different metals indicate that although the measured peak shape depends basically on the flow injection system [2], the i.c.p. spectrometer also has some influence on peak shape.

The linearity of the i.c.p. responses for copper and nickel were considered adequate for this application, as the linear regression coefficients were 0.99984 and 0.99988, respectively ($n = 5$). Linear responses were noticed also with regard to the other involved sensors. The relative standard deviations of measurements of the injected sample (40.0 ppm Cu + 40.0 ppm Ni + 2.00 ppm Zn, in 4% w/v nitric acid) were estimated after ten repetitions as 0.9, 0.3 and 1.4%, respectively. As the physical sample dispersion inside the flow injection system is the same for all metals, the differences in precision must be due to the i.c.p. system.

The proposed system for the application of g.s.a.m. requires about 10 min for each sample, which is significantly shorter than the time necessary to perform the equivalent manual procedure. Also the f.i.a.—g.s.a.m. combination offers the advantage of requiring only one set of standards for all samples.

After experimental measurements for all the standard additions to the synthetic sample, initial analyte concentrations of 39.2 ppm Cu, 40.3 ppm Ni and 2.23 ppm Zn were calculated by using the g.s.a.m. computer program in the TDC calculating mode [7]. The values based on the IDC computational method [7] were almost identical. The deviations from the true values are probably due to the inherent extrapolation of the standard addition method which decreases precision [9]. In fact, after a triplicate application of the g.s.a.m., relative standard deviations of 4.7, 2.5 and 9.3% were calculated for Cu, Ni and Zn, respectively.

The results obtained by applying the g.s.a.m. to the alloys are shown in Table 2 which also presents the results obtained by the manual procedure, by conventional i.c.p.e.s. based on calibration curves, and by atomic absorption spectrometry (a.a.s.) [12]. The same standards as used for the g.s.a.m. were employed for the a.a.s. calibration, after suitable manual dilutions of the samples and standards. Of particular interest are the erroneously high

TABLE 2

Results obtained by the proposed method (a), by the manual i.c.p.—g.s.a.m. procedure (b), by conventional i.c.p.e.s. (c) and by atomic absorption spectrometry (d)
(The concentrations are given as ppm of the element in the diluted sample. Values related to conventional i.c.p.e.s. and a.a.s. are based on three measurements.)

Alloy	Method	[Cu]	[Ni]	[Zn]
1	a	44.1	17.1	~0.09
	b	45.3	17.3	~0.01
	c	48.4	18.4	0.26
	d	44.7	17.5	0.03
2	a	59.0	24.5	~0.12
	b	60.5	23.5	~0.04
	c	62.8	24.9	0.36
	d	62.8	23.5	0.05
3	a	33.0	60.3	~0.08
	b	32.4	59.5	~—0.01
	c	32.9	61.5	0.67
	d	32.5	58.3	0.01

zinc concentrations obtained by conventional i.c.p.e.s., which can be explained by spectral interferences from copper and nickel (cf. Table 3). The g.s.a.m. results indicate that this interference is overcome as the zinc results are scattered around zero concentration, i.e., zinc measurements are limited by the noise from the zinc channel. The g.s.a.m. results for zinc are in agreement with those obtained by a.a.s., where interferences from copper and nickel are negligible [12].

The K matrix related to alloy 1 is shown in Table 3 which indicates the contribution of the three metal concentrations to the three sensors. The data related to spectral interferences between copper and nickel are characterized by uncertainties of about 20%, as was shown by successive measurements of alloy 1.

By comparing the K-matrices obtained for the other alloys, small variations in the diagonal values, in general less than 3% per 4 hours of ICP operation, were verified. This indicates the absence of both a pronounced matrix effect and instrumental drift. These variations did not affect the g.s.a.m.

TABLE 3

K matrix related to alloy 1

Element	Analytical channel		
	Cu	Ni	Zn
Cu	1360	≈5	32.8
Ni	≈56	878.2	21.2
Zn	—	—	4203

results but, in the conventional procedure, would require successive ICP recalibrations.

Conclusions

The feasibility of applying the generalized standard addition method in a flow injection system connected to a multielement detector has been demonstrated for a simple quasi-symmetrical flow injection system and inductively-coupled plasma emission spectrometry. The equivalent manual procedure is significantly simplified. The proposed system should, however, be regarded as only a step in the development of new technology. Present limitations include the relatively low sampling rate and the necessity of preparing a series of standards. The latter disadvantage might be overcome by using the zone-sampling approach [13], which permits controlled dilution of a given standard before its injection into the final standard carrier stream. Studies concerning this point are in progress.

Partial support of this research by the Conselho Nacional de Desenvolvimento Científico e Tecnológico, the Financiadora de Estudos e Projetos, and a United Nations Development Program is greatly appreciated. The authors thank B. R. Kowalski, O. M. Matsumoto, M. F. Giné and O. Bahia F°, for critical comments, and the Comissão Nacional de Energia Nuclear for travel grants.

REFERENCES

1 J. Růžička and E. H. Hansen, Flow Injection Analysis, Wiley-Interscience, New York, 1981.
2 A. O. Jacintho, E. A. G. Zagatto, H. Bergamin F°, F. J. Krug, B. F. Reis, R. E. Bruns and B. R. Kowalski, Anal. Chim. Acta, 130 (1981) 243.
3 S. Greenfield, Ind. Res. Development, August 1981, 140.
4 S. Greenfield, Pure Appl. Chem., 52 (1980) 2509.
5 B. E. H. Saxberg and B. R. Kowalski, Anal. Chem., 51 (1979) 1031.
6 C. Jochum, P. Jochum and B. R. Kowalski, Anal. Chem., 53 (1981) 85.
7 J. H. Kalivas and B. R. Kowalski, Anal. Chem., 53 (1981) 2207.
8 R. W. Gerlach and B. R. Kowalski, Anal. Chim. Acta, 134 (1982) 119.
9 J. Kragten, Talanta, 28 (1981) 901.
10 I. L. Larsen, N. A. Hartmann and J. J. Wagner, Anal. Chem., 45 (1973) 1511.
11 H. Bergamin F°, E. A. G. Zagatto, B. F. Reis and F. J. Krug, Anal. Chim. Acta, 101 (1978) 17.
12 M. Pinta, Atomic Absorption Spectrometry, Adam Hilger, London, 1975.
13 B. F. Reis, A. O. Jacintho, J. Mortatti, F. J. Krug, E. A. G. Zagatto, H. Bergamin F° and L. C. R. Pessenda, Anal. Chim. Acta, 123 (1981) 221.

Analytica Chimica Acta, 145 (1983) 179—187
Elsevier Scientific Publishing Company, Amsterdam — Printed in The Netherlands

TURBIDIMETRIC DETERMINATION OF SULPHATE IN PLANT DIGESTS AND NATURAL WATERS BY FLOW INJECTION ANALYSIS WITH ALTERNATING STREAMS

F. J. KRUG*, E. A. G. ZAGATTO, B. F. REIS, O. BAHIA F^{Q} and A. O. JACINTHO

Centro de Energia Nuclear na Agricultura — USP, Caixa Postal 96, 13400 Piracicaba, Sao Paulo (Brasil)

S. S. JØRGENSEN

Royal Veterinary and Agricultural University, 40 Thorvaldsenvej, 1871 Copenhagen V (Denmark)

(Received 23rd April 1982)

SUMMARY

An improved flow injection system with alternating streams of reagents is described for the turbidimetric determination of sulphate. Samples are injected into an inert carrier stream which is mixed with barium chloride to form a barium sulphate suspension. The range of the method can be extended to low concentrations by continuously adding sulphate to the sample carrier stream. System performance is improved by automatic alternate pumping of the reagent stream and an alkaline EDTA solution at high flow rate. All operations are controlled by an electronically-operated proportional injector-commutator. Even after routine analysis of 3000 samples of natural waters and plant digests, baseline drift was not observed. The proposed method is suitable for 120 samples per hour with a relative standard deviation less than 1% for sulphate concentrations in the range 1—30 ppm (waters) or 5—200 ppm (plant digests). The results compare well with those obtained by standard manual procedures.

The determination of sulphate in plant digests and natural waters by flow injection analysis (f.i.a.) [1] based on the measurement of the turbidity of a barium sulphate suspension has been described [2]. However, routine use of this method since 1976 produced occasional problems caused by accumulation of the barium sulphate precipitate in the flow-through cuvette, leading to drifting baselines. The build-up of a precipitate in the analytical path was also noted by Baban et al. [3] who used an alkaline barium chloride—EDTA solution in combination with acidified samples in order to remove precipitated barium sulphate by dissolution into alkaline EDTA. Although the exploitation of pH gradients and the masking properties of EDTA offer interesting possibilities, the procedure suggested [3] requires a preliminary manual pH adjustment which makes it less suitable for large-scale routine use.

This paper reports a modified flow injection system for sulphate determinations in plant digests and natural waters, in which the baseline stability, analytical precision and sampling rate are improved, by rinsing the analytical

path through intermittent replacement of the reagent stream by an alkaline EDTA solution. Both sample injection and the sequence of the alternating streams are controlled by an electronically operated injector-commutator [4, 5].

When the original procedure [2] was used, nearly the same non-zero signal caused by "schlieren" effects was obtained at all sulphate concentrations below 10 ppm. With a confluence configuration [6], this non-zero signal almost vanished but sensitivity was not significantly improved, probably because at the low concentrations the barium sulphate is formed too slowly to produce a concentration-dependent turbidity within the mean residence time in the analytical line.

In the system proposed here, this problem is overcome by continuously adding sulphate to the sample carrier stream and to the sample zone so that sulphate concentrations below 10 ppm can be measured under good conditions. The use of alternating streams prevents any drift in baseline caused by this continuous sulphate addition, so that a very sensitive method results.

EXPERIMENTAL

Samples, standards and reagents

All chemicals were of analytical grade except the poly(vinyl alcohol) (Elvanol 71-30; DuPont). Freshly distilled-deionized water was used.

Natural water samples were collected, filtered through a 0.45-μm membrane filter and soon analyzed without further pretreatment. Plant samples were digested with nitric and perchloric acids [2]. Titration of a representative number of plant digests with a standard sodium hydroxide solution showed [7] that the digests were about 0.25 M in perchloric acid. The standards for plant analysis, in the range 0.0—100.0 ppm sulphate, were therefore made 0.25 M in perchloric acid. The standards for water analysis ranged from 0.0 to 25.0 ppm sulphate.

The R_1 reagent (Fig. 1) was a 5% (w/v) barium chloride dihydrate solution in 0.05% (w/v) poly(vinyl alcohol) solution, prepared daily [2]. The R_2 reagent was 0.3% (w/v) in EDTA (disodium salt) and 0.2 M in sodium hydroxide. The R_3 reagent was either a 300 ppm sulphate solution prepared in water for plant analysis, or a 100 ppm sulphate solution also 0.5 M in nitric acid for water analysis. The sample carrier stream C_S was 0.25 M perchloric acid for plant analysis or water for water analysis, to minimize pH gradients in the sample zone.

Apparatus and flow diagram

The peristaltic pump and spectrophotometer with flow cell and recorder were the same as used earlier [2]. Alternatively, an Ismatec mp 13 peristaltic pump was used with a 634 Varian spectrophotometer and a REC 61 recorder with a REA 112 high-sensitivity unit (Radiometer). The wavelength was set at 410 nm.

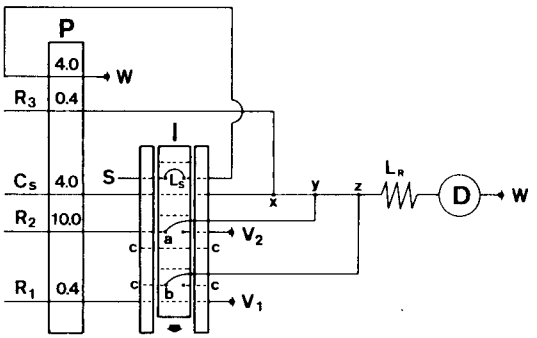

Fig. 1. Flow diagram of the systems proposed for plant and water analysis. Flow rates given are in ml min^{-1}. Lines xy = yz = 5 cm and bz = 20 cm are made from 0.8 mm i.d. tubing; ay = 20 cm is made from 0.5 mm i.d. tubing. L_R is the reaction coil (100 cm). Further details are given in the text.

The manifold was made from 0.8 mm i.d. polyethylene tubing, except where mentioned otherwise. The connectors were made from perspex and the reaction coils and sample loops were built by winding the polyethylene tubes around PVC tubes (5 cm long, 2 cm diameter). The injector commutator [8] had three 2:3:2 commutation sections and was operated electronically [4, 5].

The flow diagram of the system used for the sulphate determinations is shown in Fig. 1 which indicates the injector commutator (I) in the sampling position, closed lines being denoted by c. The sample (S) is pumped (P) to fill the sample loop (L_S), which is 100 cm long and defines exactly the volume to be injected, the excess of sample going to waste. Meantime, the barium chloride reagent (R_1) is directed towards its recovery vessel (V_1) while the alkaline EDTA reagent (R_2) pumped at high speed washes the analytical path. Commutation of the injector to the injection position introduces the selected sample volume into the sample carrier stream (C_S), and simultaneously switches the streams R_1 and R_2, so that R_2 is pumped to its recovery vessel (V_2) and reagent R_1 is directed to the analytical path. At confluence point x (Fig. 1), sulphate is added to the sample zone to permit determinations of <10 ppm sulphate. At confluence point y, leakage of R_1 to the analytical path is insignificant. Reagent R_2 is added at point z, and the precipitation reaction occurs in the L_R coil. The sample zone then reaches the detection unit (D) where the turbidity is measured at 410 nm and recorded. The sample then goes to waste (W) and the injector commutator is switched back to the position indicated in Fig. 1, starting a new cycle. Thus the R_2 wash removes completely any residual precipitate which might act as a primary precipitation nucleus or clog the system.

The system can be simplified to use only two commutation sections of the injector-commutator, by pumping R_1 and R_2 alternately through the same line ay. Line ay must, however, be very short (<4 cm in this case) to

prevent delays in switching the streams at y. Further, washing of the system became less efficient and the pH of the sample zone in coil L_S was more difficult to control than in the recommended system.

The dimensions of the system shown in Fig. 1 were selected on the basis of the following considerations. The ratio between the flow rates of the sample carrier stream C_S and the sum of the flow rates of R_1 and R_3 should be as high as possible, to minimize dilution of the sample zone at the confluence points x and z. The pumping rates of C_S, R_1 and R_3 were chosen to achieve a sampling rate of not less than 100 samples per hour even when the reaction coil length (L_R) was 100 cm and 1-ml samples were injected. The R_2 flow rate was fixed as discussed later. A 100-cm reaction coil provided good mixing conditions and so a relatively noise-free baseline and good precision. When this length was only 25 cm, the baseline was noisy and reproducibility was poor. With the 100-cm coil, the available reaction time is around 7 s (see below). The sample aspiration rate is not critical provided that it is adequate to fill the sample loop within the allowed cycle. The transmission lines xy and yz must be as short as possible.

RESULTS AND DISCUSSION

Sample volume, acidity and reaction rate

Both peak height and peak width increase with increasing sample volume [1], and the sample volume selected for a given analytical path must be a compromise between sampling rate and analytical sensitivity. As 100 cm of the manifold tubing has an inner volume of about 500 μl, sample volumes of 250—1000 μl of aqueous 20.0, 60.0, 100.0 and 160.0 ppm sulphate standards were tested; the system of Fig. 1 was used, but the R_3 line held water and the R_2 reagent was not used. A sample volume of 500 μl, which corresponds to a sample loop of 100 cm, was chosen for the analysis of samples containing up to about 100 ppm of sulphate. For these dimensions, the sample dispersion factor [8] was measured as 0.8. For the analysis of more concentrated samples (60—160 ppm sulphate), a sample loop of 30 cm is recommended.

The influence of acidity on the rate of formation of the barium sulphate suspension and thus, on sensitivity, was studied with the flow injection system of Fig. 1, without the alkaline EDTA solution. Sulphate standards (20.0—100.0 ppm) were prepared in water, and the R_3 reagent was successively 0.1, 0.3, 1.0 and 3.0 M nitric or perchloric acid. For each acidity, calibration graphs were obtained by injecting (500 μl) the standards in triplicate. It was found that increasing acidity decreases peak heights and detection limits, for both acids. When the perchloric acid concentration in the R_3 reagent was varied from 0.1 to 3.0 M, the absorbances related to the 60.0 ppm standard decreased from 0.24 to 0.15, while for 20.0 ppm, the absorbance (0.04) corresponding to the lowest acidity almost vanished when the acidity was changed to 3.0 M. The decreases in detection limit and peak

height were much more pronounced (about three times) when nitric acid was used. These results are due mainly to the effect of the acidity on the kinetics of formation of the barium sulphate suspension. The possibility of increased solubilization of barium sulphate at stronger acidity [9] is not relevant here. This was demonstrated by pumping a 60.0 ppm sulphate standard instead of the sample carrier stream C_S. When the maximum signal corresponding to a steady-state situation was reached, the pump was stopped and the increase in turbidity was followed as a function of time. With 0.1 M perchloric acid in the R_3 line, the maximum signal was attained within 7 s (the usual mean sample residence time inside the reaction coil R_L), whereas with 3.0 M perchloric acid, complete reaction was achieved only after about 4 min and only 70% reaction was obtained within 7 s. This effect was more pronounced for lower sulphate concentrations. Similar but more pronounced trends were found with nitric acid.

On the basis of these experiments, and given the acidity in the sample digests (about 0.25 M in perchloric acid [7] which would correspond to an acidity of about 2.5 M in the R_3 reagent), it was decided not to add acid via this reagent in the system for plant analysis. If the acidities of the plant digests differ, sodium acetate can be added to the R_3 reagent to form some pH buffering in the reaction coil. For water analysis, the R_3 reagent should be 0.5 M in nitric acid to provide enough acidity to overcome the hydrogencarbonate interference. If the water samples have been preserved by acid addition, this acidity must be taken into account and the R_3 acidity reduced accordingly.

System washing

Several procedures were investigated to eliminate the baseline drift caused by the build-up of barium sulphate on the inner walls of the reaction coil and flow cell. Initially, the continuous barium chloride addition used in the earlier procedure [2] was changed to pulsed addition with a merging zones configuration [10]. Sequential addition of an alkaline EDTA wash solution injected simultaneously with the sample into the same carrier stream, but via another injection port, was also tested. However, baseline drift persisted for all these conditions, and the need for a new system design became evident. The performance of an alkaline EDTA solution at high speed was therefore investigated. Its addition via an alternating stream configuration was necessary to permit suitable acidity during the formation of the barium sulphate suspension and suitable alkalinity during the wash period.

The flow injection system proposed for plant analysis (Fig. 1) was used because the different acidities of the sample and sample carrier stream caused the baseline drift problem to be rather critical with simpler manifolds. The R_3 line initially contained water, the standards ranging from 0.0 to 100.0 ppm sulphate were prepared in 0.25 M perchloric acid and the alkaline EDTA solution, pumped at 10 ml min^{-1}, was 0.2 M in sodium hydroxide, which sufficed to neutralize the perchloric acid and to provide an

alkaline pH inside the reaction coil during the wash period. Parallel tests indicated that higher alkali concentrations, up to 0.5 M, did not affect the washing performance. Concentrations of 0.03, 0.1, 0.3, 1.0 and 3.0% (w/v) EDTA in the R_2 reagent were tested. The result was somewhat unexpected, as the recorded peak shapes were almost unaffected by variations of the EDTA concentration, indicating the unimportance of the R_2 reagent composition in the wash performance. It must be emphasized also that when the R_2 solution was 0.25 M perchloric acid, washing of the system was still adequate. This leads to the important conclusion that efficient washing owes more to the sudden surge in flow rate than to chemical reaction of the alkaline EDTA and any residual barium sulphate, i.e., washing out the system depends strongly on mass transport. The higher EDTA concentrations, however, caused a slight increase in the blank signal because of the "schlieren" effect. Yet, it was decided to keep the EDTA in the R_2 reagent, first because of its favourable complexing properties [3] and also because long-term use showed that without EDTA and with the sulphate addition, there was a slight increase in baseline even when alternating streams were used. The EDTA concentration finally chosen was 0.3% (w/v) in 0.2 M sodium hydroxide.

The effect of the R_2 reagent flow rate was studied with the same flow injection system for a 100.0 ppm sulphate standard, prepared in 0.25 M perchloric acid. The alkalinity and EDTA content of the R_2 reagent were changed for each investigated pumping rate, in order to keep the concentrations of EDTA and sodium hydroxide inside the reaction coil L_R (Fig. 1) unaffected by variations in the R_2 solution flow rate. Thus, when this reagent flowed at 10, 5 or 2.5 ml min^{-1}, the sodium hydroxide concentration was 0.2, 0.4 or 0.8 M and the EDTA concentration was 0.3, 0.6 or 1.2% (w/v), respectively. The situation without a washing solution (R_2 pumping rate = 0) was also investigated. The results are shown in Fig. 2, which indicates that the flow rate of the R_2 solution has a marked effect on the recorded peak shape and so on the wash efficiency and sampling rate. This confirms that this process is much more dependent on mass transport than on the involved chemistry. A flow rate of 10 ml min^{-1} was chosen because the wash time [1] was then only a few seconds (Fig. 2) and because very high flow rates should be avoided to prevent excessive hydrodynamic pressure [1].

After the R_2 flow rate had been defined, the injector-commutator timing was fixed at 15 s in the sampling position, and 13 s in the injection position. This provided a carry-over of less than 0.5%, and a sampling frequency of about 128 samples per hour.

Sulphate addition

The effect of the sulphate addition was studied by incorporating sulphate in the R_3 reagent in the system proposed for water analysis (Fig. 1). Although it was shown that this addition could be used in a merging zones configuration [10], this possibility was not used in the final system, which was kept

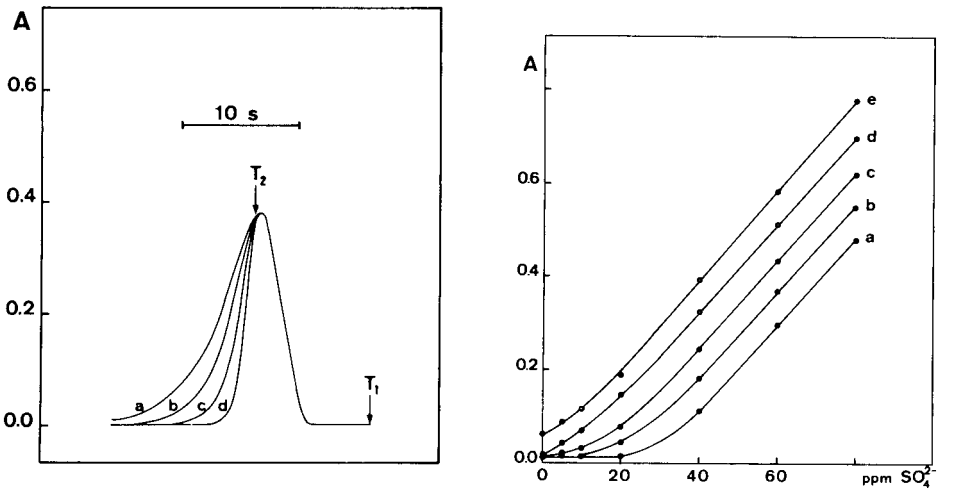

Fig. 2. Effect of the flow rate of the R_2 solution on the recorded peak shape. A 100.0 ppm sulphate standard (in 0.25 M $HClO_4$) was injected at T_1. T_2 corresponds to the moment of switching streams. Peaks *a*, *b*, *c* and *d* correspond to wash solution flow rates of 0, 2.5, 5 and 10 ml min^{-1}, respectively.

Fig. 3. Effect of sulphate addition. Curves *a*, *b*, *c*, *d* and *e* correspond to 0, 100, 200, 300 and 400 ppm sulphate in the R_3 reagent. Results refer to the plant system.

as simple as possible for routine use. Standards in the range 0.0—50.0 ppm sulphate were prepared in water, and sulphate concentrations of 0—200 ppm in the R_3 reagent, also 0.5 M in nitric acid, were tested. The calibration graphs thus prepared showed that, when the sulphate concentration in the R_3 reagent was 100 ppm, which corresponds to an effective sample concentration about 10 ppm higher than that of the injected sample, linearity was good and the detection limit was improved to about 1 ppm sulphate. This concentration, therefore, was usually employed for water analysis. However, in routine large-scale water analysis, it is often possible to have batches with higher acidities because of the different procedures used for water preservation after sample collection. When sample acidities were high, the sulphate concentration in the R_3 reagent was increased.

In experiments concerned with plant analysis, standards (0.0—80.0 ppm sulphate) were prepared in 0.25 M perchloric acid, and sulphate concentrations of 0—400 ppm (prepared in water) were tested in the R_3 line. The need for higher additions is due to the higher sample acidity, which reduces the rate of formation of the barium sulphate suspension, as discussed above. The resulting calibration graphs (Fig. 3) indicated that a suitable sulphate concentration in the R_3 reagent was 300 ppm. Good linearity was observed and the detection limit was about 2 ppm sulphate.

Analytical characteristics

Figure 4 shows a portion of the recording of a routine run for the determination of sulphate in water samples. After 1200 determinations, no baseline drift was noticed and changes in the slope of the calibration curves were very small (less than 5%) indicating good long-term stability. Also, relative standard deviations of measurements were in general $<0.5\%$ both for water and plant systems, when the sulphate content exceeded 10 ppm.

When 500 ppm of calcium (as calcium chloride), hydrogencarbonate (as sodium hydrogencarbonate) or magnesium (as magnesium chloride) was added to the sulphate standards, no interference was detected for the water or plant analysis systems. Also, recoveries ranging from 97 to 102% were assessed for the water system; interference from organic matter thus seems unlikely. It can be seen from Table 1 that the results obtained by the pro-

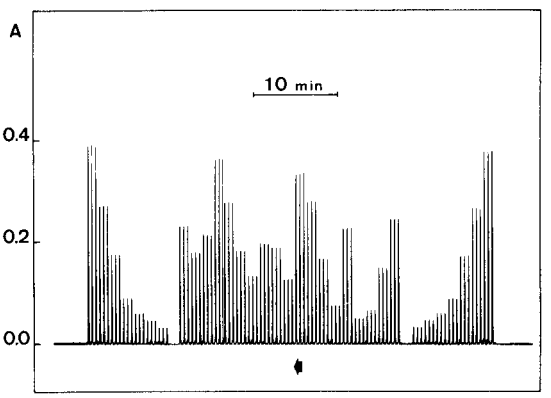

Fig. 4. Routine analysis of water samples recorded with the manifold shown in Fig. 1. From right to left: a series of sulphate standards (25.0, 20.0, 15.0, 10.0, 5.0, 2.5 and 0.0 ppm) followed by 19 samples and a second set of standards, all of them injected in triplicate.

TABLE 1

Comparison of procedures for the determination of sulphate in plant digests and natural waters

Plant sample	% S (dry matter)		Water sample	ppm SO_4^{2-}	
	F.i.a.	Manual gravimetric method [11]		F.i.a.	Manual turbidimetric method [12]
01	0.30	0.25	109	11	10
12	0.25	0.24	114	18	18
16	0.32	0.29	122	25	23
22	0.30	0.27	125	21	23
36	0.26	0.26	134	16	15
79	0.46	0.46	192	32	29

posed methods compare well with those obtained by the standard gravimetric procedure for plant digests [11] and the turbidimetric procedure for water samples [12]. It should be stressed that in water analysis, colour interference can be corrected by running blanks, if necessary; this is easily done in the flow injection system by withdrawing the barium chloride from the R_1 reagent.

Support of this research by DANIDA (Danish Development Agency) and CNPq (Conselho Nacional de Desenvolvimento Científico e Tecnológico) is greatly appreciated. The authors thank J. Růžička and E. H. Hansen for critical comments, E. Derbyshire for editing the original manuscript, the International Atomic Energy Agency for support to S. S. J., and the Comissão Nacional de Energia Nuclear for funding travel.

REFERENCES

1 J. Růžička and E. H. Hansen, Flow Injection Analysis, Wiley-Interscience, New York, 1981, p. 207.
2 F. J. Krug, H. Bergamin F°, E. A. G. Zagatto and S. S. Jørgensen, Analyst, 102 (1977) 503.
3 S. Baban, D. Beetlestone, D. Betteridge and P. Sweet, Anal. Chim. Acta, 114 (1980) 319.
4 H. Bergamin F°, B. F. Reis, A. O. Jacintho and E. A. G. Zagatto, Anal. Chim. Acta, 117 (1980) 81.
5 B. F. Reis, A. O. Jacintho, J. Mortatti, F. J. Krug, E. A. G. Zagatto, H. Bergamin F° and L. C. R. Pessenda, Anal. Chim. Acta, 123 (1981) 221.
6 H. Bergamin F°, B. F. Reis and E. A. G. Zagatto, Anal. Chim. Acta, 97 (1978) 427.
7 B. F. Reis, H. Bergamin F°, E. A. G. Zagatto and F. J. Krug, Anal. Chim. Acta, 107 (1979) 309.
8 A. O. Jacintho, E. A. G. Zagatto, H. Bergamin F°, F. J. Krug and B. F. Reis, Anal. Chim. Acta, 130 (1981) 243.
9 J. S. Fritz and G. H. Schenk, Quantitative Analytical Chemistry, 3rd edn., Allyn and Bacon, Boston, 1974, p. 59.
10 H. Bergamin F°, E. A. G. Zagatto, F. J. Krug and B. F. Reis, Anal. Chim. Acta, 101 (1978) 17.
11 W. Horwitz (Ed.), Official Methods of Analysis of the Association of Official Analytical Chemists, 13th edn., AOAC, Washington, 1980, pp. 38—39.
12 American Public Health Association, American Water Works Association and Water Pollution Control Federation, Standard Methods for the Examination of Water and Wastewater, 14th edn., American Public Health Association, New York, 1975, p. 496.

Analytica Chimica Acta, 145 (1983) 189—196
Elsevier Scientific Publishing Company, Amsterdam — Printed in The Netherlands

AMPEROMETRIC DETERMINATION OF HYDROGEN PEROXIDE IN PICKLING BATHS FOR COPPER AND COPPER ALLOYS BY FLOW INJECTION ANALYSIS

HANS LUNDBÄCK

Analytical Chemistry, University of Lund, P.O. Box 740, S-220 07 Lund (Sweden)

(Received 12th May 1982)

SUMMARY

The hydrogen peroxide is oxidized at +1.5 V vs. SCE at a glassy carbon electrode of the wall-jet type. The samples are diluted about 100 times in a dispersion coil before entering the amperometric detector. The calibration curve is linear from 10^{-4} to 1 M H_2O_2, when 5-μl samples are used. With 50-μl samples the detection limit decreases to 10^{-6} M H_2O_2. Neither metal ions (Cu^{2+}, Zn^{2+}, Ni^{2+}, Al^{3+}) up to 0.5 M nor changes in the sulfuric acid concentration of the samples between 0.1 and 1 M interfere with the hydrogen peroxide determination. About 75 samples can be analyzed per hour.

An automated method is needed for monitoring of hydrogen peroxide in pickling baths in the metal-working industry, because better control of bath composition ensures better quality of the finished product. Precise control will also prevent waste of chemicals and thus improve the process economy. Hydrogen peroxide has become used more extensively, mainly because of its environmental advantages over chromates. A typical bath for copper pickling contains 0.5—2 M sulfuric acid and 0.1—0.6 M highly stabilized hydrogen peroxide. The metal ion concentration increases with time up to approximately 0.5 M.

Few methods except electrochemical ones are well suited for the intended application. A patent has been granted [1] for an amperometric method based on a platinum electrode. A linear-sweep method with a glassy carbon electrode has previously been developed in this laboratory [2], but instrumental methods do not necessarily provide a sufficient degree of automation for industrial use. Even a simple manual operation such as dilution may require the involvement of laboratory personnel in the operation of the instrument. Flow injection analysis (f.i.a.) provides a simple means for complete automation [3] and this approach was therefore selected in developing an automatic analyzer for hydrogen peroxide in pickling baths.

EXPERIMENTAL

Equipment

Samples were introduced with a slide injector (Chromatronix; 0.8 mm i.d. channels, 5 μl, Kel-F) into a stream of 1 M H_2SO_4 (Fig. 1). The carrier flow rate was normally 1.5 ml min^{-1} and the connecting tubings (0.9 mm i.d.) were made of teflon. The length recommended for the dilution coil (b) is 1.4 m (see below). A coil (0.3 mm i.d., 100 cm long) was inserted between the peristaltic pump (Gilson, Minipuls 2) and the detector in order to damp the flow pulsations.

The working electrode was made of glassy carbon (Le Carbone, Lorraine, type V.10); the exposed circular surface had a diameter of 0.6 mm. The glassy carbon was glued into a glass tube with an epoxy resin. The electrode was mounted horizontally in a Plexiglas cell so that it could be pushed towards the inlet nozzle. The distance between the electrode and the nozzle was not critical but was kept around 0.5 mm. Theory [4] predicts that the response of a wall jet electrode of this type should be rather insensitive to variations in the distance to the nozzle. The reference was a saturated calomel electrode (Radiometer, K701) and the auxiliary electrode was a platinum wire. A suction tube was mounted close to the cell wall to keep the liquid level constant. The working electrode was ground with a fine emery paper, polished with alumina 1 and 0.25 μm (Struers, Copenhagen); and cleaned in an ultrasonic bath. The electrode was pretreated by keeping it at +1.5 V in 20 mM H_2O_2 and 1 M H_2SO_4 until the current became constant. This pretreatment seemed to last indefinitely with the analytical procedure used. The electrode was kept at the desired potential all the time because a stabilization period of at least one hour was required every time the apparatus was switched off.

Measurements were made with a polarographic analyzer (PAR, model 174) and a strip-chart recorder. The working electrode potential was +1.50 V vs. SCE unless otherwise stated.

Solutions and samples

Standard solutions were made from hydrogen peroxide (Perhydrol, p.a.; Merck) and standardized by visual titration with potassium permanganate which had been standardized against oxalate. Samples were prepared from a technical stabilized hydrogen peroxide (Hy-Brite, FMC Corp., U.S.A.). The effects of an auxiliary stabilizer were evaluated by using MS402 (EKA, Bohus, Sweden). Pickling baths were obtained from Gränges Metallverken, Sweden, and the tests reported here were made on a bath with the composition 0.1 M Hy-Brite H_2O_2, 0.65 M Cu^{2+}, 0.24 M Zn^{2+} and 2 mM Fe^{3+}.

RESULTS AND DISCUSSION

Optimization of the flow injection system

The samples were diluted in coil (b) (see Fig. 1) between the injector and the detector. Three lengths, 0.7, 1.4 and 2.8 m (0.9 mm i.d., coil diameter 26 mm) were tested. Figure 2 shows the peak shapes obtained with 5-μl

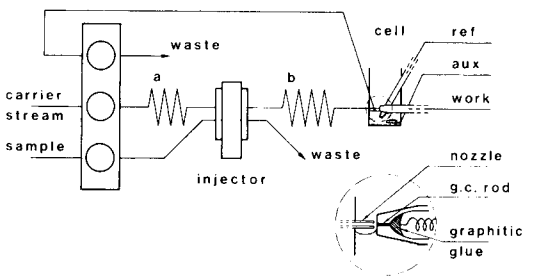

Fig. 1. Flow injection system for the determination of hydrogen peroxide in pickling baths. (a) Pulse flow damping coil; (b) dispersing coil. For further details, see text.

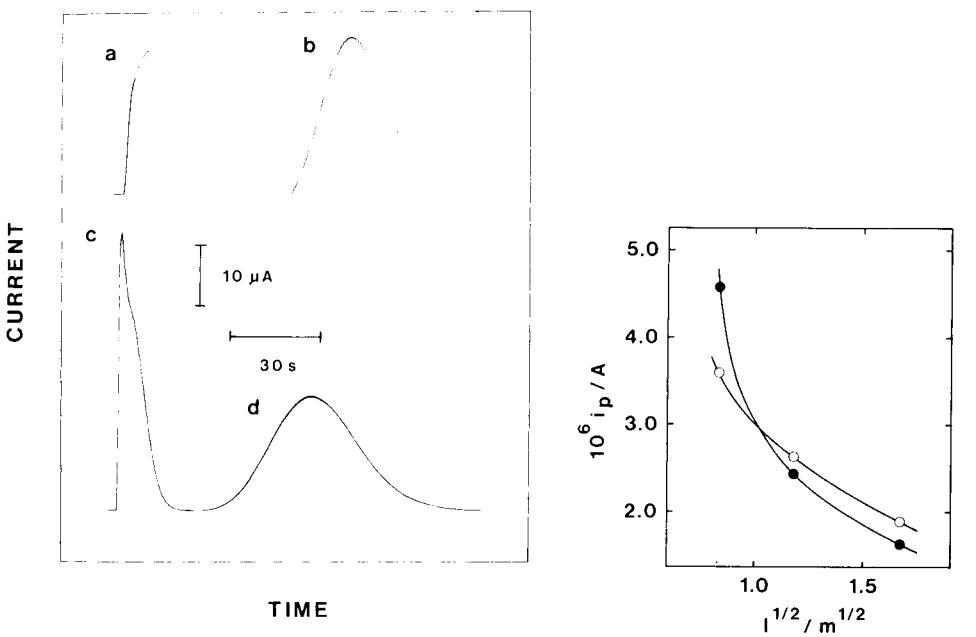

Fig. 2. Variation in peak shape when the length of the dispersing coil and the flow rate are changed: (a) 1.4 m, 2.19 ml min^{-1}; (b) 1.4 m, 1.06 ml min^{-1}; (c) 0.7 m, 2.19 ml min^{-1}; (d) 2.8 m, 1.06 ml min^{-1}.

Fig. 3. Variation of the peak height with the squared length of the dispersion coil. Samples were 0.1 M H_2O_2 in 1 M H_2SO_4. Flow rate: (○) 1.06 ml min^{-1}; (●) 2.19 ml min^{-1}.

samples. Comparison of peaks (a) and (b) shows that a high flow rate causes peak distortion, which becomes even worse with shorter coils (peak c). The peak shape improves (peak d) with longer coils and moderate flow rates. Dilution may produce double peaks because of the combined effect of Taylor and convective dispersion [5]; double peaks or severe distortion result in poor reproducibility of peak-height measurements. Small samples and a large inner diameter of the tubings are necessary for large dispersion, i.e., for high sample dilution in the flow stream. This high dilution and a reasonably high flow rate are required for proper detector performance. The remaining means to reduce peak distortion is to increase the tube length.

Figure 3 illustrates how the peak height varies with tube length for two different flow rates. The effect of changes in the flow rate is very small for the two larger coils because of the combined effects of dispersion and detector. After taking into account both the peak shape (Fig. 2) and the effect of flow rate and tube length (Fig. 3), a flow rate of 1.5 ml min^{-1} and a tube length of 1.4 m were selected. The 2.8 m coil could, of course, also have been chosen at the expense of a somewhat lower sample throughput and a slightly reduced sensitivity.

Electrochemical detection

Hydrogen peroxide can be oxidized electrochemically to oxygen and hydrogen ions [6, 7]. It also decomposes catalytically to oxygen and water in a non-electrolytic step. Carbon, if used as electrode material, can be oxidized to carbon dioxide either chemically by hydrogen peroxide or electrochemically at high potentials [8]. Reduction of hydrogen peroxide as a basis for an analytical method is out of the question for samples containing reducible metal ions.

Platinum catalyzes the non-electrolytic decomposition of hydrogen peroxide very efficiently even in the presence of high concentrations of technical stabilizers. This side-reaction contributes to oxygen bubble interference at the electrode. Gold does not cause any significant catalytic decomposition in solutions containing sulfate ions, but the oxidation is more irreversible and requires a more positive voltage. The oxidation is partly under kinetic control for all electrode materials and the reproducibility of the surface state is poor for platinum and even worse for gold. The surface properties of glassy carbon electrodes are reproducible when the electrode has attained a steady state [2]. Sample dilution improves the precision by reducing the surface oxidation of the electrode material. Because of a changed oxidation mechanism above 0.15 M H_2O_2, dilution is also necessary to obtain linear calibration curves.

Figure 4 shows the steady-state total current, the background current and the net current of the amperometric detector based on a glassy carbon electrode. The background current increases around + 1.4 V and becomes a significant fraction of the total current at higher potentials. The relation between the total current and the background current varies with the sample

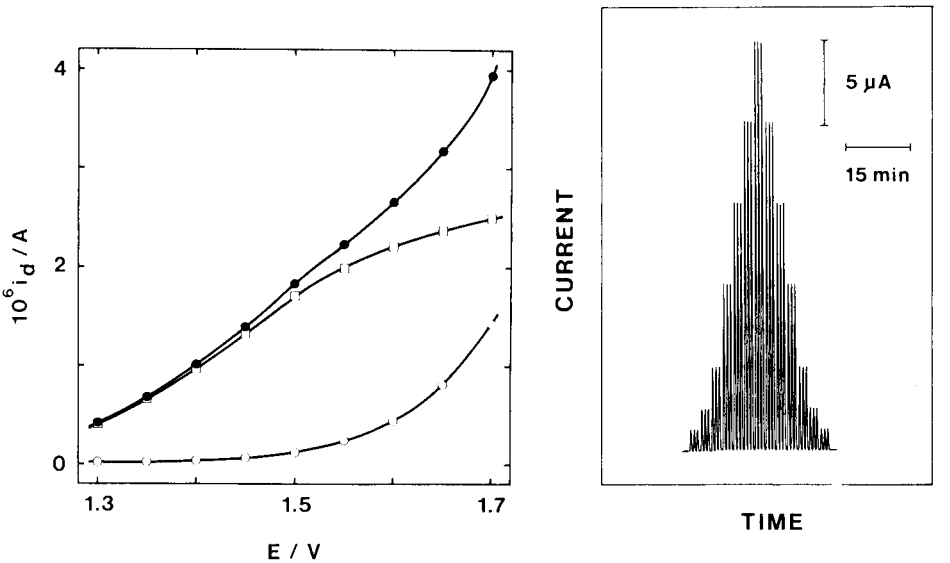

Fig. 4. Working electrode current (i_d) plotted versus the applied potential (E) measured vs. SCE, at a flow rate of 1.5 ml min^{-1}. (•) Total current with a steady supply of 1 mM H_2O_2 in 1 M H_2SO_4; (○) background current obtained with 1 M H_2SO_4; (□) net current after subtraction of the background.

Fig. 5. Calibration record for triplicate injections (5 μl) in each direction of samples containing 0.050, 0.100, 0.200, 0.400, 0.600, 0.800 and 1.00 M H_2O_2 in 1 M H_2SO_4. Flow rate 1.5 ml min^{-1}.

composition. The conditions in Fig. 4 correspond to the peak of an injected sample with a concentration of 0.1 M H_2O_2. A potential of +1.5 V was selected because it provides good sensitivity and tolerable background current.

The response of the detector depends on the rate of mass transfer, i.e., flow rate, geometry and viscosity. Doubling the flow rate increased the response by 11%, which is less than the increase expected from theory [4]. When the viscosity was varied, by varying the sulfuric acid concentration between 0.1 and 1 M, the response followed theory, i.e., it decreased with the viscosity to the power of −1.08. The fact that the detector shows less flow dependence than expected, but still follows theory when the viscosity is varied, may be explained by a partial kinetic control of the oxidation current. The net current in Fig. 4 does not reach a plateau, which supports this explanation.

Oxygen bubble formation constitutes the main experimental obstacle in making measurements in hydrogen peroxide solutions. The bubbles block part of the electrode surface and interfere with mass transfer. Thus, signals are excessively noisy at higher concentrations of hydrogen peroxide. The difficulties can be largely overcome by sample dilution and an elec-

trode arrangement in which a rapid liquid flow displaces the bubbles, but the selection of surrounding materials is also of importance. Teflon should be avoided because the oxygen bubbles grow and accumulate on the surface, and break away causing disruption of the steady-state mass transfer. Very fast measurements are less affected as only small amounts of oxygen are produced. The use of pulse or fast sweep methods [2] with vigorous stirring between the sweeps or pulses, reduces the interference from oxygen bubbles; but the background currents were large and less well defined, restricting the range to relatively concentrated peroxide solutions. Under these conditions the peak position will vary with sample composition and surface state of the electrode. With the wall-jet electrode used in this work, bubbles are removed much more efficiently, and measurements can be made amperometrically at the constant potential. The background current then becomes much lower and more stable so that the range can be extended downward. The samples can therefore be diluted more, which further improves electrode stability and decreases interferences. The f.i.a. method provides another advantage, i.e., that the background current can be compensated automatically if peak height over the base line is measured.

Hydrogen peroxide determination

The amperometric detector was used for hydrogen peroxide determination using the flow injection scheme of Fig. 1. The 5-μl samples were diluted about 100 times with 1 M H_2SO_4 in the 1.4-m dispersion coil. A typical calibration record is shown in Fig. 5. A strictly linear calibration curve (r = 0.99997) was obtained from the detection limit, 2×10^{-5} M, to 1 M H_2O_2. The repeatability of successive measurements was better than 0.5% and the relative precision for repeated measurements during one day was 1% for the upper part of the range. The accuracy of the determinations was better than 0.5% when measurements and standardizations were done in rapid succession. The response was equal for samples made from p.a. hydrogen peroxide and from the technical product.

There was an increasing negative deviation when the sample concentrations were above 1 M H_2O_2. This is due both to the IR drop in the solution and to partial oxygen coverage of the electrode. The range can of course be adjusted upward by increasing the size of the dilution coil or by decreasing the sample volume. The use of 1-μl samples increased the linear response to 5 M H_2O_2. The range can be adjusted downwards most simply by increasing the sample volume, which will decrease the dispersion and provide less dilution. A detection limit of 10^{-6} M H_2O_2 was obtained with 50-μl samples introduced by a pneumatic loop injector. The peak current at the detection limit was 0.5 nA and the drift in the background current was 1.5 nA h^{-1}. The background current and the drift can be reduced by selecting a lower electrode potential.

Interferences

Variations in the acidity (0.1—1 M H_2SO_4) or metal ion content (0—0.5 M Cu^{2+}, Zn^{2+}, Ni^{2+} or Al^{3+}) of the sample did not affect the peak height. Increasing the acidity to 3 M H_2SO_4 reduced the peak height by about 1%. Iron(III) did not interfere as such, but the hydrogen peroxide decomposed very quickly in the presence of 0.5 M Fe^{3+}. Addition of extra stabilizer, up to 5% v/v, did not affect the peak height.

Standard additions were made to samples taken from an alloy pickling line. Correct recoveries, within 1% of calculated values, were obtained. Thus, hydrogen peroxide can be determined in pickling baths of the specified composition without interference. The errors produced by higher amounts of peroxide are small and can be eliminated by reducing the sample size.

Several advantageous circumstances contribute to the absence of interferences. Samples with high acidity or high metal ion concentration produced changes in the shape of the rising part of the f.i.a. peak, because the changed viscosity altered the dispersion profile. The peak height was not affected, however, and the viscosity changes therefore had no influence on the analytical signal.

The selected carrier electrolyte, 1 M H_2SO_4, was used because it matched most of the samples with respect to viscosity. Less concentrated acid, 0.1 M H_2SO_4, resulted in negative interference from metal ions, whereas 3 M H_2SO_4, attacked the electrode chemically, so that the sensitivity of the electrode decreased with time.

Most of the improvements compared with the earlier method [2] are due to the greater dilution and the physical arrangement of the detector. The short exposure of the electrode surface to the sample is also of importance for the suppression of interferences from the stabilizer. The signal decreased with time when a solution containing a high concentration of peroxide and stabilizer was fed continuously to the detector. The height of the initial rise, however, was the same whether or not stabilizer was present. This behaviour can be explained by assuming that the stabilizer is adsorbed slowly at the electrode surface. In the f.i.a. method, the peak passes so quickly that the adsorption is slight, and desorption of the stabilizer is fast enough to ensure that a clean electrode is available for the next sample.

About 75 samples can be analyzed per hour which is much more than needed for the present purpose. Further development, based on building a dedicated instrument with pneumatic samplers, seems to be straightforward and is under way in this laboratory.

Financial support from Jernkontoret and helpful discussions with members of Committee 607/77 are gratefully acknowledged. Grateful acknowledgement is made to Professor Gillis Johansson for valuable discussions concerning this work.

REFERENCES

1 T. Ikuta, K. Ishii, I. Ikeya and T. Hayakawa, Mitsubishi Gas Chemical Co. Inc., Japan Kokai 7874.098 (CL. GO1N27/42), 0, 1 Jul. 1978, Appl. 76/150.009, 14 Dec. 1976.
2 H. Lundbäck and G. Johansson, Anal. Chim. Acta, 128 (1981) 141.
3 J. Růžička and E. H. Hansen, Flow Injection Analysis, Wiley, New York, 1981.
4 J. Yamada and H. Matsuda, J. Electroanal. Chem., 44 (1973) 189.
5 J. M. Reijn, W. E. van der Linden and H. Poppe, Anal. Chim. Acta, 126 (1981) 1.
6 J. J. Lingane and P. J. Lingane, J. Electroanal. Chem., 5 (1963) 411.
7 A. Hickling and W. H. Wilson, J. Electrochem. Soc., 98 (1951) 425.
8 G. I. Zakharkin, M. R. Tarasevich and R. Kh. Burshtein, Elektrokhimiya, 10 (1974) 1811.

Analytica Chimica Acta, 145 (1983) 197—201
Elsevier Scientific Publishing Company, Amsterdam — Printed in The Netherlands

Short Communication

THE APPLICATION OF STRONGLY REDUCING AGENTS IN FLOW INJECTION ANALYSIS
Part 1. Chromium(II) and Vanadium(II)

R. C. SCHOTHORST*, J. M. REIJN, H. POPPE and G. DEN BOEF

Laboratory for Analytical Chemistry, University of Amsterdam, Nieuwe Achtergracht 166, Amsterdam (The Netherlands)

(Received 21st April 1982)

Summary. Many reagents cannot easily be applied in quantitative analysis, because of their instability under atmospheric conditions. When such reagents are prepared in a flowing stream, their applicability is very promising; for example, in flow injection analysis, a reagent need be stable only for 20—30 s. The application of chromium(II) and vanadium(II) in flow injection analysis is described. Nitrate and nitrite can be determined in the concentration range 5×10^{-5}—5×10^{-3}. Calibration graphs show good linearity.

The application of strongly reducing agents in analytical chemistry, although very well known for nearly a century, has remained limited because of the need to work under oxygen-free conditions, which makes the storage of standard solutions rather difficult. The introduction of flow injection analysis provides a new future for these as well as for other unstable reagents. When it is possible to prepare an unstable reagent in a flowing stream, the only requirement for analytical applicability is that its decomposition is negligible during the time necessary for a reaction in a flowing system, which is often only 20—30 s.

The quantitative reduction in acidic solution of vanadium(IV) and vanadium(V) to vanadium(II) and of chromium(III) to chromium(II) has been described by Stone and Hume [1]. Both reactions are possible in a Jones reductor. In the case of vanadium, the conditions are not very critical, but for chromium it is necessary to use the green chromium chloride as the starting material. Both vanadium(II) and chromium(II) are powerful reducing agents. Typical values for normal redox potentials in acid solution are

$$Cr^{3+} + e \rightleftharpoons Cr^{2+} \qquad E^0 = -0.41 \text{ V}$$

$$VO^{2+} + 2H^+ + e \rightleftharpoons V^{3+} + H_2O \qquad E^0 = +0.36 \text{ V}$$

$$V^{3+} + e \rightleftharpoons V^{2+} \qquad E^0 = -0.26 \text{ V}$$

In order to achieve quantitative reactions by means of these reagents in other than acidic solutions, complexing agents have to be added to the solutions,

as such additions influence the formal potentials of these redox couples. The reducing ability of the complexed compounds often depends on the pH.

In the case or chromium(II), the influence of pH and EDTA on the reducing properties has been extensively described by Pecsok et al. [2] and by Groeneveld and den Boef [3]. The pH region between 7 and 10 is particularly suitable for quantitative analysis. Above pH 10, the reactions of chromium(II)—EDTA with reducible substances are rather slow, whereas below pH 7 the instability of chromium(II)—EDTA towards water causes difficulties. Flow injection determinations with chromium(II)—EDTA can be monitored spectrophotometrically at 600 nm, the wavelength of maximum absorption of the reaction product chromium(III)—EDTA.

In the case of vanadium(II), the pH at which reductions are possible is less critical. The redox potentials of half-reactions involving vanadium(II) in the presence of EDTA have been investigated by Pecsok and Juvet [4]. The formal potentials in the pH region between 7 and 10 are about the same as for the half-reaction chromium(III)/chromium(II). Flow injection determinations with vanadium(II) can also be monitored spectrophotometrically, at 350 nm where vanadium(II)—EDTA absorbs.

Three test substances were used: firstly iodate because it was expected that this compound would react instantaneously with both vanadium(II) and chromium(II); and secondly nitrate and nitrite because their determination may be of practical importance.

Experimental

The flow system. The system is schematically shown in Fig. 1. The reagent stream, which contains either chromium(III) of vanadium(IV) species, is sucked through the reductor and a debubbling device (DB). This debubbler is necessary for removal of the hydrogen produced in the reductor. The somewhat unusual position of the reductor and debubbler, upstream of the peristaltic pump, was found to be the most suitable position in practice. After the peristaltic pump (Gilson), the reagent stream, which now contains chromium(II) or vanadium(II), is merged in a Y-piece with a buffer solution containing EDTA. The mixing of the two streams is stimulated in single bead string reactor (SBSR) 1 [5]. This reactor has a length of 0.20 m and a tube diameter of 1 mm and is packed with 0.6-mm glass beads. The tube material is nylon, because such tubing has the lowest permeability for oxygen [6].

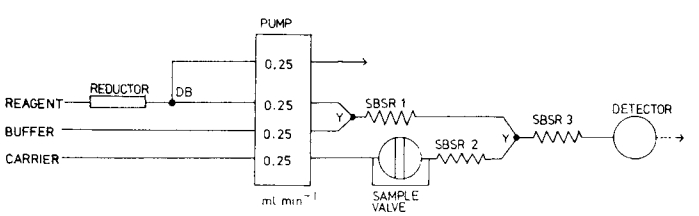

Fig. 1. Flow diagram.

The sample solution is introduced with the aid of an injection valve (Rheodyne) with a loop volume of 32 μl. The sample is introduced in a carrier stream consisting of distilled water. The sampling valve is connected by means of SBSR 2 (identical to SBSR 1 and intended to control dispersion of the sample zone) to a second Y-piece, where the carrier stream merges with the combined reagent—buffer stream. Immediately after the confluence point, there is a third SBSR 3 with a length of 0.40 m and with the same geometry as the other two. In this SBSR the mixing of sample and reagent is achieved and the chemical conversion of the analyte takes place [5]. A home-made flow-through cell (optical path length 10 mm, volume 8 μl) is used with a spectrophotometer with variable wavelength (Zeiss PMQ II with a digital readout device).

The flow rates in each stream are indicated in Fig. 1. No attempts were made to optimize the flow system yet [7], as the main goal of this work was to illustrate the feasibility of the use of instable reagents in f.i.a.

Determinations with chromium(II)—EDTA as a reducing reagent. The Jones reductor [1] was prepared in the following way. The solid zinc particles (Merck, for reductor preparation) are sieved and from the fraction with a particle diameter <0.6 mm, 5 g is taken and rinsed with 1 M HCl. The zinc is amalgamated in a solution which contains 0.3385 g of mercury(II) chloride in 10 ml of 0.1 M HCl. The amalgamation process takes 15 min. After a rinse with distilled water, the amalgamated zinc particles are packed in a glass tube (length 140 mm, inner diameter 4 mm). The reductor is then ready for use.

The reagent stream contains 10^{-2} mol of chromium(III) chloride in 1 l of 0.1 M HCl. The buffer solution contains 0.3 mol of Tris and 0.033 mol of EDTA per litre and the pH is adjusted to 8.6 with hydrochloric acid. The sample solutions contained the test substances potassium iodate, sodium nitrate and sodium nitrite, all of analytical-reagent grade. All solutions are carefully deaereated by bubbling nitrogen gas through them, because oxygen interferes in the determinations. The detection is done at 600 nm.

Determinations with vanadium(II)—EDTA as a reducing reagent. The reductor was prepared in a similar way as for the case of the chromium reagent, except for the mercury(II) solution, which now contains 0.0685 g of mercury(II) chloride in 10 ml of 0.1 M HCl, yielding a degree of amalgamation of 1% [1].

The buffer solution again contains 0.3 mol of Tris and 0.033 mol of EDTA per litre, but now the pH is adjusted to 8.6 with sulphuric acid. The sample solutions contained the same test substances. In the case of vanadium, two different concentration ranges can be accommodated, because of the relatively high molecular absorptivity of vanadium(II)—EDTA. The reagent solution for the higher concentration range contains 10^{-2} mol of vanadyl sulphate and 6×10^{-2} mol of sulphuric acid per litre, while the reagent solution for the lower concentration range contains 10^{-3} mol of vanadyl sulphate and 6×10^{-2} mol of sulphuric acid per litre. Detection is done at 350 nm.

Results and discussion

Three test substances were used to establish the performance of the flow system. The results of calibration of the flow system are summarized in Table 1. The correlations for the absorbance (A) as a function of the concentration of the analyte in the sample solution, C_{in}, show good linearity. From the moments of a peak resulting from the injection of 1.66×10^{-3} M KIO_3 with 10^{-2} M chromium(II)—EDTA as a reducing reagent, the number of tanks to which the flow system corresponds is calculated. The mean equals 50 s and the variance is 121 s^2, therefore the number of tanks is about 20.

The dilution factor of the system was determined in the following way: all solutions were replaced with distilled water and the peak resulting from the injection of 10^{-2} M chromium(III)—EDTA was recorded. The height of this peak is called $C_{out,max}$. Then, the carrier solution was replaced by the 10^{-2} M chromium(III)—EDTA solution and the steady-state absorbance was recorded $C_{in,steady}$. The dilution is then found from $D = C_{out,max}/C_{in,steady} = 0.21$.

The conversion in the case of chromium can be obtained in the following way: the reference point is chromium(III)—EDTA, and the conversion corresponds to the ratio of the peak height obtained for each of the test substances to the peak height obtained after injection of an equivalent amount of chromium(III)—EDTA. The conversions found in this way were 100% for iodate, 66% for nitrate and 58% for nitrite (with respect to reduction of nitrate and nitrite to ammonia). In the case of vanadium, for the high vanadium concentrations, the conversion of iodate was assumed to be 100%. Then, the conversions for nitrate and nitrite were 44% and 71%, respectively. For the lower vanadium concentrations, the conversion of iodate falls to 88%, for nitrite to 46% and for nitrate no signal was observed.

The apparently strange conversion behaviour towards nitrate and nitrite is

TABLE 1

Calibration lines for the flow injection systems

Analyte	Reagent conc. (M)	Sample concentration range (M)	Regression line	Regression coefficient, r
Vanadium(II)—EDTA as reagent				
KIO_3	10^{-2}	1.66×10^{-4}—1.66×10^{-3}	$A = (1100 \pm 4)\, C_{in}$	0.9999
	10^{-3}	1.66×10^{-5}—1.66×10^{-4}	$A = (970 \pm 10)\, C_{in}$	0.9989
$NaNO_3$	10^{-2}	1.25×10^{-4}—1.25×10^{-3}	$A = (483 \pm 5)\, C_{in}$	0.9989
	10^{-3}	1.25×10^{-5}—1.25×10^{-4}	no signal	
$NaNO_2$	10^{-2}	1.66×10^{-4}—1.66×10^{-3}	$A = (783 \pm 9)\, C_{in}$	0.9987
	10^{-3}	3.33×10^{-5}—1.66×10^{-4}	$A = (508 \pm 8)\, C_{in}$	0.9983
Chromium(II)—EDTA as reagent				
KIO_3	10^{-2}	1.66×10^{-4}—1.66×10^{-3}	$A = (140 \pm 0.5)\, C_{in}$	0.9999
$NaNO_3$	10^{-2}	1.25×10^{-4}—1.25×10^{-3}	$A = (122.5 \pm 0.5)\, C_{in}$	0.9998
$NaNO_2$	10^{-2}	1.66×10^{-4}—1.66×10^{-3}	$A = (82 \pm 0.6)\, C_{in}$	0.9994

at present being investigated in more detail. It is known, however, from batch experiments that both species are fully converted into ammonia when chromium(II) is the reducing reagent. An attempt to detect ammonia with the aid of a gas-diffusion membrane was not successful.

The authors thank Mr. W. Ozinga for experimental aid.

REFERENCES

1 H. W. Stone and D. N. Hume, Ind. Eng. Chem. Anal. Ed., 11 (1939) 598.
2 R. L. Pecsok, L. D. Shields and W. P. Schaefer, Inorg. Chem., 3 (1964) 114.
3 E. R. Groeneveld and G. den Boef, Fresenius Z. Anal. Chem., 237 (1968) 85.
4 R. L. Pecsok and R. S. Juvet, J. Am. Chem. Soc., 75 (1953) 1202.
5 J. M. Reijn, W. E. van der Linden and H. Poppe, Anal. Chim. Acta, 123 (1981) 229.
6 R. G. Gerritse, J. Chromatogr., 77 (1973) 406.
7 J. M. Reijn, H. Poppe and W. E. van der Linden, Anal. Chim. Acta, 145 (1983) 59.

Analytica Chimica Acta, 145 (1983) 203—206
Elsevier Scientific Publishing Company, Amsterdam — Printed in The Netherlands

Short Communication

FLOW INJECTION ANALYSIS WITH CHEMILUMINESCENCE DETECTION IN THE DETERMINATION OF FLUORESCEIN- AND FLUORESCAMINE-LABELLED SPECIES

V. K. MAHANT, J. N. MILLER* and H. THAKRAR

Department of Chemistry, Loughborough University of Technology, Loughborough, Leicestershire, LE11 3TU (Gt. Britain)

(Received 15th August 1982)

Summary. Many fluorescence immunoassays have indifferent limits of detection because of the background signals from biological samples. Scattered light contributes to this background, but can be eliminated by exciting conventional fluorescent labels via chemiluminescence reactions involving bis(2,4,6-trichlorophenyl)oxalate. This reaction, whose rate can be controlled, is conveniently used in a flow injection system with a luminometer as a detector. Such a system is applied to study fluorescein- and fluorescamine-labelled species at concentrations as low as 10^{-11} M (ca. 0.5 pg in a 100 μl sample). The effects of antibodies on the luminescence signals from labelled antigens are discussed.

It has been demonstrated [1, 2] that fluorimetry is a suitable detection technique for flow injection analysis (f.i.a.), and several authors have taken the logical step of combining f.i.a. with chemiluminescence detectors [3—6]. Chemiluminescence detection and f.i.a. are well matched. Both are cheap, compact and simple technically, and f.i.a. can provide the extreme reproducibility of sample and reagent mixing that is so essential for precise chemiluminescence studies yet is frequently lacking in static procedures. Combinations of f.i.a. and chemiluminescence detectors have been applied to several systems, including the determination of peroxide using luminol [3], the benzoyl peroxide oxidation of amines [5], and the fluorescein-sensitised oxidation of sulphide by sodium hypochlorite [6]. A further important type of chemiluminescent reaction, that involving peroxyoxalate [7, 8] has apparently not been studied by using f.i.a., though it has been used to detect dansylated amino acids separated by high-performance liquid chromatography [9]. An oxalate [bis(2,4,6-trichlorophenyl)oxalate, TCPO, is the most commonly used] reacts with hydrogen peroxide in the presence of a fluorophor: intense emission from the fluorophor is seen, probably via a high-energy dioxetane intermediate. This reaction is of great potential value in biochemical systems where fluorescent labels are readily bound to analytes, e.g., fluorescence immunoassay. Such labels can be excited and detected with higher sensitivity and simpler equipment than in conventional fluorimetry, and the substantial background signal caused by scattering of the external light source in a

fluorimeter does not arise in chemiluminescence measurements. The principal disadvantage of the peroxyoxalate system is that the oxalate esters which are most useful as sources of chemiluminescence are not soluble in water, so that mixed solvent systems will normally be necessary in biochemical studies where a mainly aqueous environment must be maintained. This communication describes the application of f.i.a. to the study of peroxyoxalate chemiluminescence, and illustrates the potential of the method, and its problems, for new immunoassay methods.

Experimental

In the single-channel flow injection experiments, the tubing used was of 0.76-mm internal diameter, and the flowing stream was propelled by a miniature peristaltic pump (Model 840 Ismatec, Zurich, Switzerland). Two types of detector were used. One was a fluorimeter (Fluorimet, Baird-Atomic, Braintree, Essex) modified by removal of its light source, incorporation of a silica flow cell (100 μl volume), and a new sample compartment lid incorporating a septum injector; samples could thus be injected directly into the flowing stream close to the detector. Samples (100 μl) were injected from disposable syringes. Extreme precautions were necessary to ensure that the sample compartment was light-tight, in view of the high instrument gain settings used. In other experiments, a luminometer (LKB Model 1250) was used. This instrument is provided with a holder for a cylindrical sample tube; a flow cell was constructed by winding the plastic tubing (0.76 mm i.d.) around such a tube. A gelatin filter with maximum transmission at 500 nm was placed between the flow cell and the photomultiplier tube. Samples were injected from a 6-port Rheodyne valve, with a sample loop volume of 100 μl. With this system, the portion of the flow tubing ($\leqslant$50 cm) between the injection point and the detector was covered with black insulating tape, to prevent a "fibre optic" effect introducing stray light into the detector.

Fluorescamine (Fluram, Roche Diagnostics, Welwyn Garden City, U.K.) derivatives of thyroxine and 3,5,3'-tri-iodothyronine (Sigma, Poole, U.K.) were prepared by conventional means [10]. TCPO was prepared as previously described [8] and fresh solutions in acetone were made up hourly. Hydrogen peroxide, 0.5 M, was prepared in triply distilled water and stored in a teflon container. All other reagents were of the highest grade commercially available.

Results and discussion

Preliminary experiments with the modified fluorimeter as detector clearly showed the high sensitivity of the technique. When 10^{-11} M fluorescein (in 0.01 M phosphate buffer, pH 7.4) was mixed with 5 mM TCPO and injected into a flowing stream (flow rate 4.5 ml min^{-1}) of 0.5 M peroxide, as little as 10^{-14} mol of fluorescein could be detected (background plus two standard deviations). In photoluminescence analysis only an instrument of the highest quality or specialised design could achieve such limits of detection. However,

even when extreme care was taken to ensure reproducibility (e.g., accurate timing between the pre-mixing of TCPO and sample and injection, see below) the coefficient of variation was always at least 3.5% and often worse. Fluorescein-labelled albumin showed much less intense emission (fluorescein: albumin ratio of ca. 4:1), perhaps because of the protein-quenching effect described below. Fluorescamine-labelled thyroxine and tri-iodothyronine could be detected at 2 ng ml^{-1} levels in the luminometer system; this is again at least as good as the detection limits obtained on the best fluorescence spectrometers (Fig. 1). In all these experiments, maximum light intensity was reached within a few seconds of injection; the kinetics of peroxyoxalate emission can be affected by alterations in solvent [11], but this was not examined here because of the need for dilute, near-neutral buffers in immunoassays.

Further investigation revealed two important effects which would limit the applicability of the assay in biological samples. Firstly, it was apparent that pre-mixing of the sample and TCPO could lead to a decrease in the signal. A fluorescamine—thyroxine conjugate, mixed with TCPO solution ten minutes before injection, yielded a signal indistinguishable from the background emission; the hydrolysis of TCPO in aqueous media may explain this result. The precise timing needed to eliminate this effect could of course be achieved by the use of a more sophisticated merging-zones system for f.i.a. It was also observed that addition of TCPO (in acetone) to the phosphate buffer produced a turbid solution with a high absorbance; a mixture containing 5 mM TCPO in a buffer—acetone (93:7) solvent had an absorb-

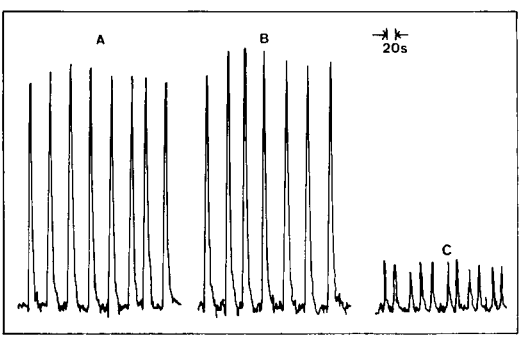

Fig. 1. Analysis of fluorescamine-labelled tri-iodothyronine (A) and thyroxine (B) by TCPO (5 mM) excitation. Samples contained 25 ng ml^{-1} of the analytes and, after mixing with TCPO solution, 7% by volume of acetone. The blank signal is shown in C.

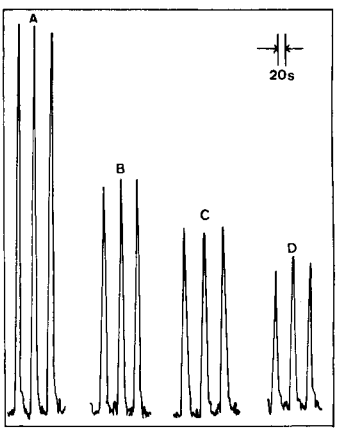

Fig. 2. Quenching of TCPO-excited luminescence of fluorescamine—thyroxine by proteins. Effects of addition to 25 ng ml^{-1} fluorescamine thyroxine (A) of 0.1 μg ml^{-1} human serum albumin (B), anti-human albumin serum diluted 1:200 (C), and normal human serum diluted 1:100 (D).

ance of ca. 0.70 at 500 nm. Such an effect might account for the poor precision of the experiments. It might also produce substantial light losses via the chemiluminescence analogue [12] of the inner filter effect familiar in fluorescence spectroscopy. Only 1:1 (v/v) acetone—water mixtures, which would be unacceptable in immunoassays, would eliminate this effect.

It is well established that addition of anti-thyroxine antisera to fluorescein and fluorescamine derivatives of thyroxine produces a substantial increase in the fluorescence of these conjugates (though the mechanism is not the same in these two examples) [10, 13]. Attempts were made to reproduce this effect in the present work, using peroxyoxalate excitation of the fluorophor. It was found, however, that the enhancement effect was replaced by a non-specific quenching phenomenon that apparently occurs in all protein-containing solutions. Examples of this effect are given in Fig. 2. Recent work has shown that the effect increases with the relative molecular mass of the protein, being negligible in the case of insulin ($M_r \approx 5{,}700$) and maximal when the relative molecular mass exceeds ca. 100,000.

This work thus demonstrates the potentially great sensitivity of combining peroxyoxalate reactions with flow injection systems for the determination of these fluorescent derivatives. The chemiluminescence signal is, however, subject to non-specific quenching, as has been reported for other systems [14]. Preliminary studies have indicated that such effects, and the problems caused by the poor solubility of TCPO in aqueous systems, can be minimised by a careful choice of buffer systems; homogeneous immunoassays utilising fluorescence enhancement effects can then be successfully developed.

H. T. was supported by a Research Studentship from the Science and Engineering Research Council.

REFERENCES

1 K. Kina, K. Shiraishi and N. Ishibashi, Talanta, 25 (1978) 654.
2 J. I. Braithwaite and J. N. Miller, Anal. Chim. Acta, 106 (1979) 395.
3 G. Rule and W. R. Seitz, Clin. Chem., 25 (1979) 1635.
4 J. L. Burguera and A. Townshend, Proc. Anal. Div. Chem. Soc., 16 (1979) 263.
5 J. L. Burguera and A. Townshend, Talanta, 26 (1979) 795.
6 J. L. Burguera, A. Townshend and S. Greenfield, Anal. Chim. Acta, 114 (1980) 209.
7 M. M. Rauhut, Acc. Chem. Res., 2 (1969) 80.
8 A. G. Mohan and N. J. Turro, J. Chem. Ed., 51 (1974) 528.
9 S. Kobayashi and K. Imai, Anal. Chem., 52 (1980) 424.
10 G. Handley, J. N. Miller and J. W. Bridges, Proc. Chem. Soc. Anal. Div., 16 (1979) 26.
11 M. L. Grayeski and W. R. Seitz, Abstract No. 712, 1982, Pittsburgh Conference and Exposition on Analytical Chemistry and Applied Spectroscopy.
12 E. Ratzlaff and S. R. Crouch, Abstract No. 713, 1982, Pittsburgh Conference and Exposition on Analytical Chemistry and Spectroscopy.
13 D. S. Smith, FEBS Lett., 77 (1977) 25.
14 A. Thore, Science Tools, 26 (1979) 30.

Analytica Chimica Acta, 145 (1983) 207—212
Elsevier Scientific Publishing Company, Amsterdam — Printed in The Netherlands

Short Communication

PERFORMANCE AND CHARACTERISTICS OF THE FLUORIDE-SELECTIVE ELECTRODE IN A FLOW INJECTION SYSTEM

P. VAN DEN WINKEL* and G. DE BACKER

Eenheid Aktiveringsanalyse, Vrije Universiteit Brussel (Belgium)

M. VANDEPUTTE, N. MERTENS, L. DRYON and D. L. MASSART

Farmaceutisch Instituut, Vrije Universiteit Brussel, Laarbeeklaan 103, B-1090 Brussel (Belgium)

(Received 18th June 1982)

Summary. A simple, inexpensive home-made timer for coupling cam-controlled samplers to injectors for flow injection analysis is presented. Experimental conditions and a flow diagram are described for the determination of fluoride by means of a fluoride-selective electrode in the concentration range 0.3—10 ppm, with a sample rate up to 120 h^{-1}.

The equipment of clinical and analytical laboratories often includes continuous automatic analysis systems of the older generation. This generally means that sample rate and sample-to-wash ratio are controlled by cams. Apart from their price, these electromechanical devices show the disadvantages of poor flexibility and limited sample rate and reproducibility. In view of the application of samplers of this type to flow injection analysis (f.i.a.) with high rates, a simple and inexpensive home-made timing device for coupling cam-controlled samplers to injector units was developed and applied for the automated determination of fluoride by means of a fluoride-selective electrode.

Description and operation of the timer

Wiring diagram. The wiring diagram is shown in Fig. 1. The use of commercially available impulse counters T_1 and T_2 (Hengstler, Type 0.78-251-M6) with built-in oscillators of 100 Hz and internal relays (r_1 and r'_1; r_2 and r'_2), in combination with an external, current impulse-triggered electromagnetic memory switch R_1 (Siemens, Type F104-V-23003-B0037) yields a bistable circuit which allows control of sample rate, sample-to-wash ratio (S/W) and sample injection control. The output (6′) of the oscillator of T_2 is fed into the input (1′) of either T_1 or T_2 via S_2 (cycle start) and the external contacts (11-13-14) of the magnetic switch. The preset cycle start mode (S = sampling interval, preset and counted on T_1; W = washing interval, preset and counted on T_2) is established by means of switch S_3 and the push-button S_4. By short-circuiting the latter, a current impulse actuates one of the

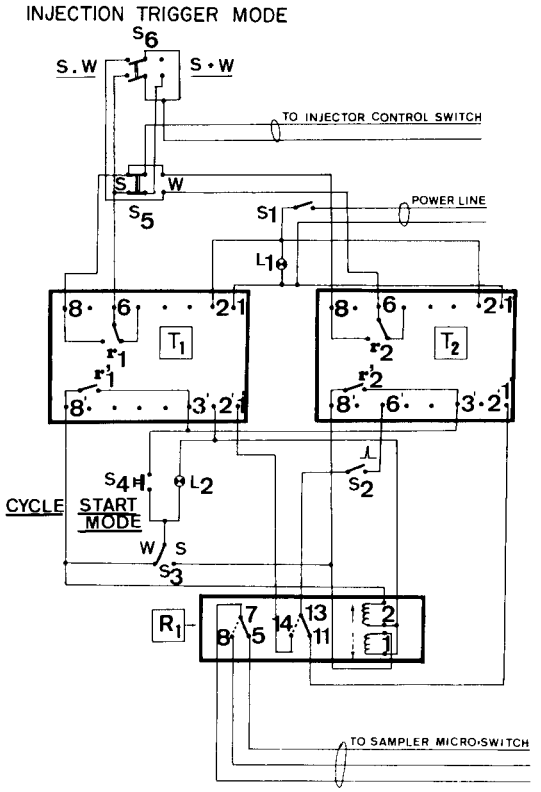

Fig. 1. Wiring diagram for AKTA timer. T_1 and T_2 are impulse counters; R_1 is the electromagnetic memory switch.

coils (R_1-1 or -2) of the magnetic switch, forcing contact 13 into the appropriate position (R_1-1 = S mode start; R_1-2 = W mode start). A duty cycle (S + W) is started by closing S_2 after the sample (t_s on T_1) and wash (t_w on T_2) interval times have been preset and after the memory and display of both counters have been reset manually. After time t_s (or t_w) the normally open (NO) contact r'_1 of T_1 (or r'_2 of T_2) temporarily closes, thus actuating R_1-2 (or -1) which results in the oscillator frequency being fed into the other counter. At the end of each sample (or wash) interval, the counter involved automatically resets its memory and display. Thus a cycle once started will repeat indefinitely.

Sample rate and sample-to-wash ratio control. The sample-wash cycle of the sampler is controlled by removing its cam and then connecting the contacts of the associated micro-switch to the second set of contacts (5, 7 and 8) of R_1 in an appropriate way. As contacts 5, 7 and 8 also actuate the cycle start MODE contacts, perfect synchronization is obtained between the sampler needle movement (and its position) and the sample or wash interval start (and lapse) on T_1 and T_2. The sample-to-wash ratio is then given by

t_s/t_w; the sample rate is $3600/(t_s + t_w)$, and the cycle time t_c is $t_s + t_w$. In order to allow operation with either cam control or external-timer control, the sampler is fitted with a change-over switch (external-internal time control) and a three-pin plug-in connector.

Injection trigger and synchronization of sampling and injection. Injection of the sample into the carrier stream with an FIA 05 control unit (Bifok, Sweden) is done by means of a push-button on the front panel of the apparatus while the injection time (t_i) is set by prior adjustment of the time potentiometer. External triggering can be done by connecting the parallel contacts on the rear panel of the apparatus to an appropriate short-circuiting device. This is achieved by means of the change-over switch combination S_5—S_6 and the NO relay contacts r_1 and r_2 which are briefly actuated after lapses of t_s and t_w, respectively. Switch S_6 allows the choice of injection triggering at the end of t_s and t_w (S·W) or at the end of t_s or t_w (S + W). In the latter case, the position of S_5 determines whether injection occurs at the end of t_s (S) or of t_w (W).

Because of the delay in pumping tubes and manifold, the sample concentration profile at the sample needle and at the injection point may be out of phase. This is shown in Fig. 2. In Fig. 2A, sample pick-up and injection are in phase, i.e., sample is injected when sample has been picked-up; in Fig. 2B,

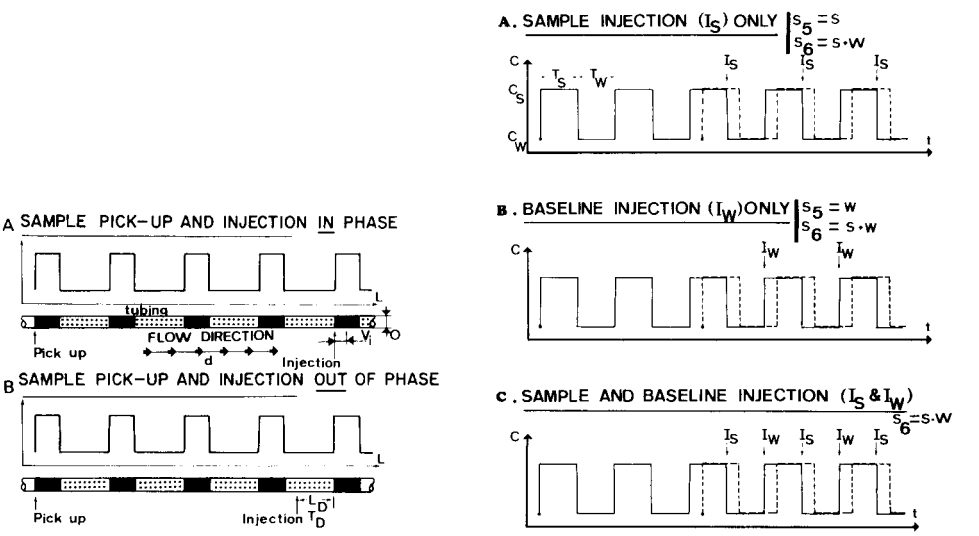

Fig. 2. Sample pick-up and injection phase shift. A and B show the sample pick-up and injection in phase and out of phase, respectively. T_D, delay time; L_D, delay line length; O, tube cross section area; d, flow rate; V_i, injected volume; $T_D = L_D\ O/d$.

Fig. 3. Injection modes. S_5 and S_6, change-over switches; S, sample injection only; W, base-line injection only; S + W, sample or base-line injection; S·W = sample and base-line injection; C, fluoride concentration of sample (C_S) and base-line (C_W); T_S, sample interval; T_W, wash interval, t, time. Concentration profiles: (—) at sample needle and (---) at the injector.

the phase shift is eliminated by inserting a delay line of appropriate length L_D in the sample stream. Though a drawback at first sight, the adjustment of the phase shift (T_D) by means of additional delay lines allows correct sample (and/or base-line) injection at the trigger points of the counters. Appropriate choice of sample rate, flow rate, injection volume and time then allows either baseline or sample, or baseline and sample injection in the carrier stream at optimal points of the concentration versus time curve. This is shown in Fig. 3, where the cycles for sample only, wash only or sample and wash are illustrated. By means of a delay line, sample pick-up and injection are shifted over $t_s/3$, while 2/3 of a sample or wash interval is used for flushing and filling of the injection valve.

Flow diagram and experimental conditions for potentiometric fluoride determination

The flow diagram for automatic potentiometric determination of fluoride involving the modified sampler is shown in Fig. 4. By means of a pump (Gilson Minipuls, calibrated for flow rate), samples (or base-line) and base-line are mixed with the conventional total ionic strength adjustment buffer (TISAB) in a 1:1 ratio and fed into a potentiometric cell (Bifok) fitted with an F1052 fluoride electrode and a K401 saturated calomel electrode (both Radiometer) via a variable volume valve (Bifok L100-1). Sampler and injector control unit (Bifok 05) are both triggered by the AKTA timer as described above. The potential difference is measured by means of an Orion 601 millivoltmeter coupled to a recorder (model BD9, Kipp en Zonen). To examine and eliminate any errors from mechanical inertia or pen overshoot of

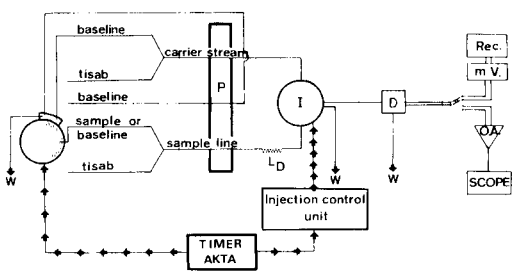

Fig. 4. Flow diagram for potentiometric fluoride determinations. P, pump; D, detector, I, variable volume valve; L_D, delay line; W, waste.

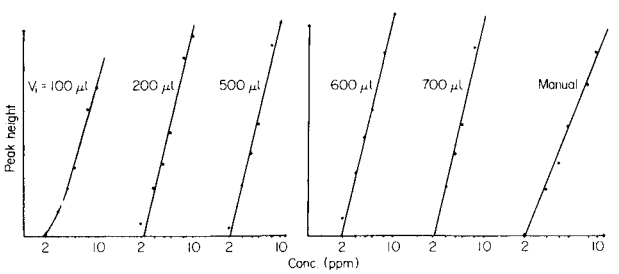

Fig. 5. Influence of the injector loop volume (V_i) on the response.

the recorder, preliminary experiments were done with an operational amplifier (Tektronix AH501) operated in a 1:1 inverting configuration coupled to a memory oscilloscope (model 7613, Tektronix).

The experimental conditions are summarized in Table 1. Assuming a sample rate of 120 h^{-1} with S/W = 1 and a sample cup volume of 1.5 ml yields a maximum flow rate of 6 ml min^{-1}. As quantitative pick-up of the samples from the cups is impossible, a value of 5.5 ml min^{-1} is applied for the sample (d_s) and carrier (d_c) streams. This high flow rate gives the required jet over the sensor surface and electrolytic contact with the reference electrode. As the injector must be filled and emptied twice in one cycle ($t_s + t_w$), the injection time for equal flow rate in sample and carrier stream must be $t_i \leqslant t_c/4 = (t_s + t_w)/4$. With S/W = 1, this yields $t_i \leqslant t_s/2 = 7.5$ s. The maximum injector loop volume is then given by $V_i = d_s\, t_i = 0.7$ ml. To reduce carry-over to a minimum, the first quarter of each sample is used to flush the injector. An acceptable phase shift between sample pick-up and the injection is therefore $t_d = 0.25\, t_s \approx 4$ s. Finally, as carrier stream and base-line solution are identical (0.3 or 1.0 ppm F^- as NaF in water), the timer is operated in the S injection mode only.

Results and discussion

Influence of the injector volume and sample rate on the response (1—10 ppm range). In preliminary experiments, sample rates of 60, 90 and 120 h^{-1} and a S/W ratio of 1 were tested for the concentration range 1—10 ppm. When 30-μl samples were injected, the calibration plots were non-linear, with serious loss of sensitivity at 1 ppm, and there was trouble from sloping base-lines. Increasing the injected sample volume by using an injector with external loop resulted in increasing improvement of the linearity of the calibration plots (Fig. 5). However, even with large injected volumes, the indicator electrode still operates under non-equilibrium conditions, as can be seen in Table 2. The results show that the percentage of equilibrium reached increases with increasing concentration, which is in agreement with earlier findings [1]; and that for a particular concentration jump, the percentage of equilibrium reached increases linearly with the injector volume up to 700 μl (for a sample rate of 120 h^{-1}), as was demonstrated by application of a statistical linearity test [2] to the experimental data.

TABLE 1

Preset of experimental conditions for automatic fluoride determination

	Preset condition
Sample rate = 120 h^{-1}; S/W = 1	$t_s = t_w = 15$ s
Sample volume = 1.5 ml[a]	$d_s = d_c \leqslant 5.5$ ml min^{-1}
Injector filled and emptied twice per cycle; $t_s = t_w = 15$ s	$t_i \leqslant 7.5$ s
$d_s = d_c = 5.5$ ml min^{-1}; $t_i = 7.5$ s	$V_i \leqslant 0.7$ ml
Use 1/4 of a "sample" for flushing; $t_s = 15$ s	$t_d \simeq 0.4$ s

[a]Quantitative pick-up impossible.

TABLE 2

Influence of the injector volume on the % equilibrium reached in the flow injection system.

Concn. jump (ppm)	Percent equilibrium for injector volumes (μl) of				
	130	273	582	712	852
1→5	36.8	51.4	54.0	60.1	63.5
1→7.5	46.9	62.1	65.6	70.4	71.7
1→10	46.7	61.0	64.6	69.7	71.1

Study of carry-over. Carry-over or sample—sample interaction was studied by successive injections of three 10 ppm samples (A_1, A_2, A_3) immediately followed by three 2 ppm samples (B_1, B_2, B_3) and measurement of the resulting peak heights (a_1, a_2, a_3; b_1, b_2, b_3) at 120 h^{-1} and S/W = 1. As proposed by Broughton et al. [3], carry-over can be evaluated as $C = (b_1 - b_3)/(a_3 - b_3)$, when the magnitude of the measured signal is directly proportional to the actual concentration. For potentiometric analysis, however, this equation must be written as $C = (10^{-E_{B1}/S} - 10^{-E_{B3}/S})/(10^{-E_{A3}/S} - 10^{-E_{B3}/S})$ where E_X is the potential difference measured for X (A_1, B_1, etc.) with regard to that of the base-line concentration and S is the slope of the calibration plot in the concentration range studied. Application of an extended non-parametric sign test [4] on the experimental data proved that there was no statistically significant carry-over.

Application at lower concentration. In order to apply the system for the analysis of urine and potable water samples, its behaviour in the concentration range 0.1—5 ppm was investigated. For concentrations above 0.3 ppm, linear calibration plots were obtained at sample rates up to 60 h^{-1} and S/W = 1. No carry-over occurred and the precision is of the order of 5%, as can be expected for automated potentiometric procedures.

Conclusions

A simple, inexpensive home-made timer enables samplers of the older generation to be coupled to modules for flow injection analysis, to provide a system in which sample rate, sample-to-wash ratio, delay time and injection can be controlled perfectly. The experimental set-up was applied successfully for the determination of fluoride by means of an ion-selective electrode operated at a maximum sample rate of 120 h^{-1} for a S/W ratio of one.

The authors thank Dr. B. Karlberg (Bifok AB, Sollentuna, Sweden) for providing the variable volume valve used.

REFERENCES

1 J. Mertens, P. Van den Winkel and D. L. Massart, Anal. Chem., 48 (1976) 272.
2 B. E. Cooper, Statistics for Experimentalists, Pergamon Press, Oxford, 1969.
3 P. M. G. Broughton, M. A. Buttorph, A. H. Gowenlock, D. W. Neill and R. G. Skentelberry, J. Clin. Pathol., 22 (1969) 278.
4 M. Vandeputte, Ph.D. Thesis, Vrije Universiteit Brussel, 1982.

Analytica Chimica Acta, 145 (1983) 213—217
Elsevier Scientific Publishing Company, Amsterdam — Printed in The Netherlands

Short Communication

A FLOW-THROUGH DETECTOR FOR SIMULTANEOUS DETERMINATIONS OF GLUCOSE AND UREA IN SERUM SAMPLES

MARCO MASCINI* and GIUSEPPE PALLESCHI
Istituto di Chimica Analitica, Università di Roma, Rome (Italy)
(Received 27th July 1982)

Summary. Glucose and urea electrodes are prepared by immobilizing glucose oxidase and urease on nylon net and fixing the nets on oxygen and ammonia gas sensors. Both enzyme electrodes are fixed in a single flow cell (40 μl volume). Serum is diluted tenfold with 0.1 M Tris buffer (pH 8.3) to fit the calibration graphs for both sensors. Samples are pumped for 1 min, with wash periods of 2 min for recovery to the baseline. Results on serum samples are in good agreement with the results obtained by conventional spectrophotometry.

Determinations of the glucose and urea concentrations in serum samples are often required for clinical diagnosis and evaluation of several diseases in both urgent and in routine situations [1]. In recent years, various methods for these determinations have been based on the use of gas probes with enzyme-containing membranes [2—15], which have become a realistic alternative to the classical colorimetric measurements. In this communication are reported the results obtained with a prototype in which the glucose and urea sensors are assembled in a single cell and the two determinations are done simultaneously on the same sample.

Enzyme sensors have been prepared by immobilizing enzymes on nylon nets [16]. These sensors provide good analytical performance and unusual mechanical ruggedness. One of the prerequisites for an enzyme sensor to be used in a flow system is that the membrane itself should be strong. It is common practice to remove the sensors from the cell for inspection or for storage at low temperature when not in use; in the initial sensor assembly and in removal from the cell, the enzyme layer must not be damaged in any way. Most procedures for immobilizing enzyme for electrode construction [2—11] result in fragile membranes, and the mechanical integrity of the enzyme-containing membrane becomes impaired after a short period of use even though the enzyme activity may last longer. The preparation based on immobilization on nylon nets is superior.

Experimental

Materials. Glucose oxidase and urease (Sigma) have activities of 125 U mg^{-1} and 54 U mg^{-1}, respectively. All other reagents were of analytical

purity. The nylon net used (A. Bozzone, Appiano Gentile, Italy) had a mesh of 120 cm^{-2} with a thickness of 100 μm and a free surface of 35%. Serum reconstituted in the pathological and normal range were obtained from Boeringher (Mannheim).

Procedures. The chemical procedure for immobilizing enzymes on nylon net was derived from the method of Hornby and Morris [17] and details have been reported [16]. The oxygen probe was a pO_2 electrode (Instrumentation Laboratory; 0.1 M KCl internal solution, 0.5-mil teflon membrane, platinum cathode and silver anode). The ammonia probe was a pCO_2 electrode (Instrumentation Laboratory) modified with an internal solution of 0.1 M ammonium chloride and a polypropylene membrane.

The nylon nets were secured with O-rings together with the plastic membrane of the gas probes (teflon and polypropylene) so that the geometry of the assembled sensors for urea and glucose was the same as that of the gas probes. The flow cell shown in Fig. 1 was modified from an IL model 213 cell intended for measurements of pCO_2 and pO_2 in blood; the cell volume is estimated to be 40 μl.

Results and discussion

The activity of the enzymes immobilized on nylon nets was measured as described by Bertrand et al. [18]; the immobilized material was placed in a solution containing the substrate in excess, the concentration of the product was monitored, and the specific immobilized activity was calculated in nmol min^{-1} cm^{-2}. Figure 2 shows the variation of the specific activity with pH. To measure the enzyme activity of urease at the different pH values, it was necessary first to prepare a calibration graph for ammonia at each pH value

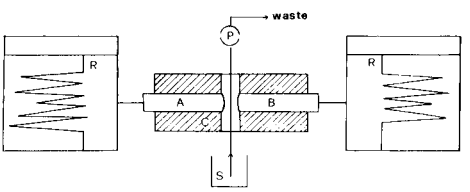

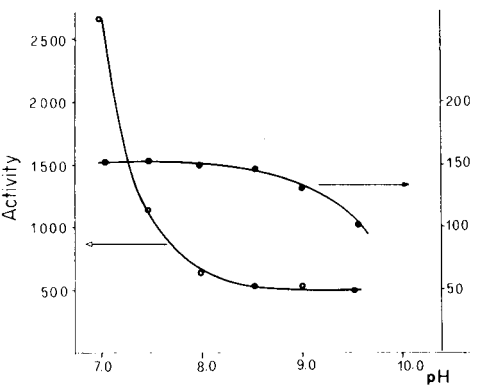

Fig. 1. Flow cell for the glucose and urea sensors: A, glucose electrode; B, urea electrode; C, thermostated cell; P, peristaltic pump; R, recorder; S, sample. The flow rate was 1.8 ml min^{-1}. Samples were changed manually.

Fig. 2. Specific activity (in nmol min^{-1} cm^{-2}) of glucose oxidase and urease immobilized on nylon net as a function of pH: (○) urease; (●) glucose oxidase.

in the presence of 0.1 M urea. Then for each pH, the amount of ammonia obtained when a piece of nylon net (2 cm^2) was placed in 20 ml of 0.1 M urea was recorded and the specific immobilized activity was calculated from the calibration curve. The enzyme activity was found to decrease from pH 7 to 8 and then remained constant for both enzymes (Fig. 2). However, as is well known, the response time of the ammonia probe decreases from pH 7.0 to 9.5.

Table 1 shows the variation of the response time of the urea sensor in the flow cell as a function of pH, for an increase in urea concentration from 10^{-4} to 10^{-3} M, which is the range suitable for serum samples after tenfold dilution. The response time was calculated according to IUPAC recommendations [19]. From the results reported in Fig. 2 and Table 1, and from other results on the lifetime of the enzyme membranes kept in various pH buffers, it was decided to dilute the samples tenfold with a 0.1 M Tris buffer at pH 8.3.

The ranges of concentration of glucose and urea in the diluted sera are, respectively, 6.5—10.5 mg dl^{-1} and 2—4.5 mg dl^{-1}. The glucose sensor gave a linear calibration plot for the range 1—20 mg dl^{-1} with a correlation coefficient (r) of 0.9997; the urea sensor provided linear response for the range 0.2—10 mg dl^{-1} (r = 0.9996). The lifetimes for both sensors exceeded 6 months even when the sensors were left at room temperature, provided that they were kept wet.

The samples were pumped at a flow rate of 1.8 ml min^{-1} for 1-min intervals, with 2-min wash periods with the buffer. Figure 3 shows typical recordings for standards and samples when urea and glucose were measured simultaneously. It can be seen that the maximum value is not approached for either sensor, and that return to the baseline is observed even for ammonia probe [12]. The sample rate is only 20 h^{-1} but could be increased by improving the washing step.

Clinical results (Table 2) show reasonable agreement with the spectrophotometric results. The mean accuracy (±4%) is worse than the standard deviations on standards which were about 2% for both urea and glucose.

Conclusion

The measurement with enzyme electrodes, i.e., with enzyme immobilized on the electrode surface, offers an alternative approach to open tube or packed column reactors with immobilized enzymes in flow analysis. The

TABLE 1

Response time (90%) of the urea sensor as a function of pH for changes in the urea concentration from 10^{-4} to 10^{-3} M (Buffer: 0.1 M phosphate for pH 7.0—8.0 and 0.1 M Tris for pH'8.5—9.5.)

pH	7.0	7.5	8.0	8.5	9.0	9.5
Time(s)	38	34	31	24	26	26

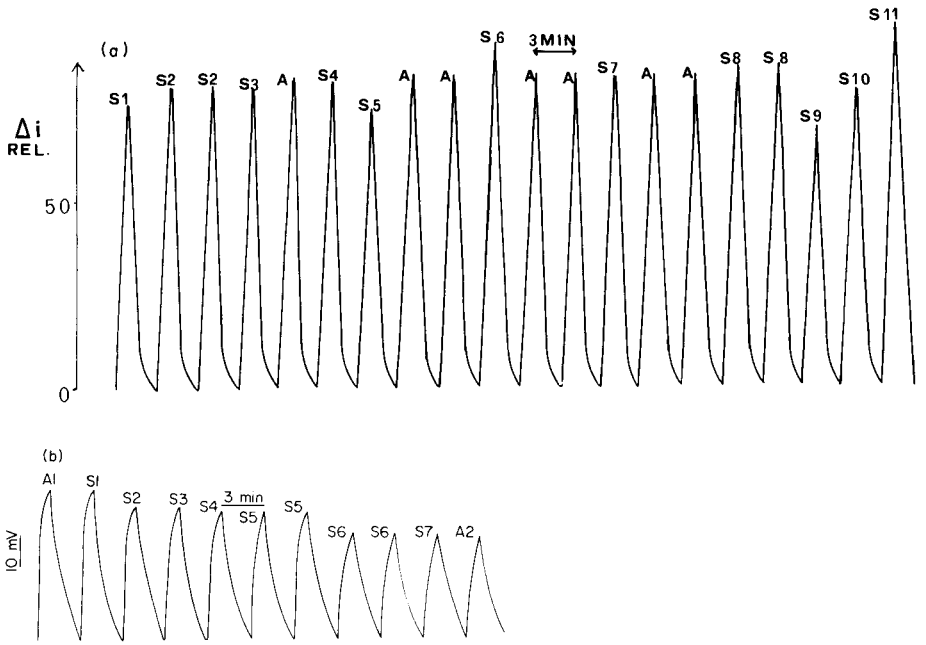

Fig. 3. Typical recordings for glucose and urea in serum samples and standards in continuous operation: (a) glucose determinations with a 100 mg dl^{-1} standard (A) in serum samples (S_1—S_{11}); (b) urea determinations with two standards (A_1 = 60 mg dl^{-1} and A_2 = 30 mg dl^{-1}) in serum samples (S_1—S_7).

TABLE 2

Analysis of serum samples

Serum	Spectrophotometry		Proposed method		Error (%)	
	Glucose (mg dl^{-1})	Urea (mg dl^{-1})	Glucose (mg dl^{-1})	Urea (mg dl^{-1})	Glucose	Urea
1	130	30	133	30	0.8	0
2	307	31	308	31	0.3	0
3	84	40	86	38	2	5
4	92	62	96	60	4	3
5	66	26	68	24	3	8
6	90	38	94	36	4	6
7	88	38	81	37	8	5
8	103	37	104	35	1	6
9	105	22	106	24	1	8
10	105	24	103	24	2	0
11	100	42	102	40	2	5
12	88	34	86	33	2	3
13	91	51	94	57	3	12
14	89	39	89	37	0	5
15	102	24	105	34	3	41

TABLE 2 (continued)

16	94	50	101	48	7	4
17	135	48	149	41	10	14.5
18	140	42	156	37	11	12
19	64	38	67	31	5	18
20	80	35	85	34	6	3

enzyme electrodes can be more practical when the percentage conversion need not be 100%, i.e., when the substrate concentration in the sample is far higher than the limit of detection of the detector probe. This is the case for glucose and urea in serum samples. The reliability of such measurements with the new immobilization method on nylon net has been confirmed.

REFERENCES

1 Handbook of Clinical Laboratory Data, 2nd edn. The Chemical Rubber Co. Cleveland, Ohio, 1968.
2 S. J. Updike and G. P. Hicks, Nature, 214 (1967) 986.
3 J. Havas, E. Porjesz, G. Nagy and E. Pungor, Hung. Sci. Instrum., 49 (1980) 53.
4 L. Sokol, C. Garber, M. Shults and S. Updike, Clin. Chem., 26 (1980) 89.
5 J. L. Romette, B. Froment and D. Thomas, Clin. Chim. Acta, 95 (1979) 249.
6 M. Koyama, Y. Sato, M. Aizawa and S. Suzuki, Anal. Chim. Acta, 116 (1980) 307.
7 H. B. J. Makin, P. J. Warren and J. D. Edridge, Clin. Chim. Acta, 84 (1978) 137.
8 S. J. Updike, M. C. Shults and M. Busby, J. Lab. Clin. Med., 93 (1979) 518.
9 M. Niwa, K. Itoh, A. Nagata and H. Osawa, Tokai J. Exp. Clin. Med., 6 (1981) 403.
10 M. Koyama, J. Koezuka and Y. Sato, Toshiba Rev., 132 (1981) 2.
11 M. Mascini and G. G. Guilbault, Anal. Chem., 49 (1977) 795.
12 L. Gorton and L. Ogren, Anal. Chim. Acta, 130 (1981) 45.
13 G. G. Guilbault in H. H. Weetall (Ed.), Immobilized Enzymes, Antigens, Antibodies and Peptides, M. Dekker, New York, 1975 p. 293.
14 M. E. Meyerhoff and Y. M. Fraticelli, Anal. Chem., 54 (1982) 27R.
15 P. M. Vadgama, K. G. M. Alberti and A. K. Covington, Anal. Chim. Acta, 136 (1982) 403.
16 M. Mascini, M. Iannello and G. Palleschi, Anal. Chim. Acta, in press.
17 W. E. Hornby and D. L. Morris, in H. H. Weetall (Ed.), Immobilized Enzymes, Antigens, Antibodies and Peptides, M. Dekker, New York, 1975.
18 C. Bertrand, P. R. Coulet and D. G. Gautheron, Anal. Chim. Acta, 126 (1981) 23.
19 G. G. Guilbault, Ion Selective Elect. Rev., 1 (1979) 139.

Analytica Chimica Acta, 145 (1983) 219—223
Elsevier Scientific Publishing Company, Amsterdam — Printed in The Netherlands

Short Communication

A MICROPROCESSOR-CONTROLLED FLOW INJECTION ANALYSER FOR THE DETERMINATION OF TERBUTALINE SULPHATE

MATS STRANDBERG* and SIDSEL THELANDER

Astra Pharmaceutical Production AB, Analytical Control, S-151 85 Södertälje (Sweden)

(Received 23rd April 1982)

Summary. The determination is based on the reaction with 4-aminoantipyrine and potassium hexacyanoferrate(III). The system is automatic with a microcomputer controlling the sampler and injection valve, reading the output from the spectrophotometer and evaluating the result. The system is intended for drug analysis, and the matrix viscosity can vary considerably between different formulations without affecting peak area measurements.

Phenolic compounds are easily determined by reaction with 4-aminoantipyrine and potassium hexacyanoferrate(III) [1—5]. The detection of the reaction product is done spectrophotometrically. The reaction between 4-aminoantipyrine and phenol and the structure of terbutaline sulphate are shown below.

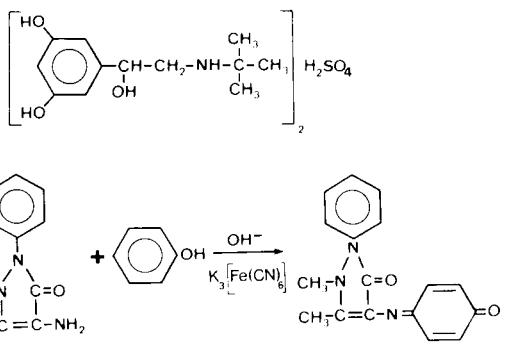

Terbutaline sulphate, the active substance in drugs for the treatment of asthma, is a phenolic compound that fulfils the requirements [1] for reacting with 4-aminoantipyrine and the reaction product has maximum absorbance at 550 nm. However, the coloured compound formed is not stable, so the measurements have to be carefully timed.

Automation of a spectrophotometric determination is most easily done with a continuous flow system. Because of the high sample capacity, the use of flow injection analysis (f.i.a.) to automate the terbutaline determination was investigated. The problem of measuring after a fixed time is readily over-

come with an f.i.a. system as the time when the sample is introduced to the spectrophotometer is controlled by the pumping rate and the length of the tubing, which are kept constant. Evaluation of the results from a chart recorder is time-consuming and error-prone, and is preferably transferred to a computer. Therefore it was decided to construct a dedicated f.i.a. system controlled by a microcomputer, which could, with minor changes in hardware and software, be adapted to other flow systems. The integration of a microcomputer with the system can be done either by buying a complete computer or by putting together boards needed for the system. As the experience as well as the development system required for writing programs were available, it was decided to follow the latter course. Program development is by far the most time-consuming part in the development. When the system is built from individual boards, it is possible to tailor the system according to the exact needs. Unnecessary components can be excluded, but the system can still be expanded when required.

Experimental

Microcomputer. The microcomputer is built around an INTEL board SBC 80/24 comprising a 8085A-2 CPU. This board contains all necessary RAM, EPROM and IO apart from the analog/digital converter (ADC), which is a multibus-compatible board from DATEL (ST-711). The ADC board contains a 12-bit ADC, a programmable amplifier with gains of 1, 2, 4 and 8 times, a sample-and-hold and an analog multiplexer with 16 input channels. The human interface consists of a cathode ray tube (CRT) terminal and a small line-printer. The f.i.a. system is based on commercial equipment; a HATI A40 sampler, a Gilson Minipuls 2 peristaltic pump, a BIFOK FIA-05 injection valve and manifold, and a LDC Spectromonitor II spectrophotometer with an 8-μl flow cell (Fig. 1). The sampler and injection valve are interfaced to the microcomputer with two relays so that they can be controlled remotely.

Flow injection system. The flow system used is described in Fig. 2. Designing the flow system in order to achieve suitable sensitivity and reproducibility requires testing of different lengths of mixing coils and flow

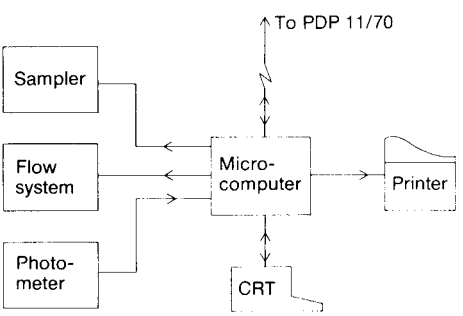

Fig. 1. Block diagram of the system.

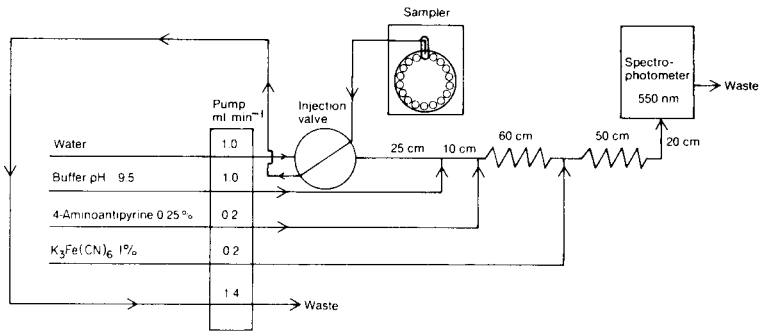

Fig. 2. The flow system. Tygon pump tubing was used with 0.7 mm i.d. polypropylene tubing for the manifold.

rates of the different streams. The system is intended for quality control of all the different tablets, solutions and syrups which contain the active substance, and thus the matrix varies considerably in ionic strength and viscosity. It is essential that the reagents and the sample are mixed together well and that this process is not too dependent on the viscosity and the ionic strength. Consequently, buffer and reagents are added to the main stream as sidestreams and so the mixing is independent of the dispersion of the sample.

The system is optimized for a concentration in the samples of 0.1 mg ml^{-1}, which will result in a peak absorbance of about 0.6. All samples are diluted to this nominal concentration with the exception of samples from the tablet dissolution test which have a concentration range of 12—150 μg ml^{-1}. The reagents are dissolved in water. For the sample concentration given, the excess of 4-aminoantipyrine (4-AAP) is about 10 times and the 4-AAP—hexacyanoferrate(III) ratio is 1:3. This is close to the figures recommended by Svobodova and Gasparic [5].

The sensitivity does not increase with an increase in concentration of either or both of the reagents, but when reagent concentrations are doubled, a precipitate starts to form. The buffer strength is 0.3 M. It is possible to redesign the flow system to gain simplicity but that involves some trade-offs. For example, injecting the sample into the buffer stream will result in the buffer having minimum capacity where the sample has maximum concentration. To overcome this problem either the sample dispersion or the strength of the buffer has to be increased. Increasing the concentration of the buffer might affect the mixing with the sample and probably an extra mixing coil would have to be included, which would increase the dispersion and decrease the sensitivity. It is also possible to mix the buffer and the 4-AAP beforehand without sacrificing sensitivity, but the 4-AAP solution cannot be stored, unlike the buffer, so it was decided to keep all solutions separate and make fresh solutions of the 4-AAP and hexacyanoferrate every day. The buffer is prepared once every two weeks.

Software. The program is written in PL/M, a high-level language for microprocessors, with the exception of some minor parts in assembly language. It occupies about 12 kbyte. The essential parts of the program are initialization, controlling the analysis and data collection, calculating final results and printing a report. The initialization consists of a dialogue between the operator and the computer to load the correct parameters concerning the run. The computer checks validity and rejects unreasonable inputs and it also monitors baseline stability before samples are injected.

The sample run starts by advancing the sampler and washing the injection valve for 35 s before injecting. Data collection starts and the computer reads the ADC 10 times per second and calculates a moving average of five successive readings which are stored in a ring buffer of nine elements. These are used to calculate the first derivative, and based on its value the program determines the start, the peak and the end of the sample. The baseline is read before and after the injection, and the height and integral of the peaks are compensated for baseline drift during the injection. A second injection of the same sample is made and the program returns the mean result for the two injections. Each series of samples is preceded and succeeded by three standards. When all samples have been injected, the program evaluates the concentrations based on a linear least-squares fit and prints a report of the calculated results together with the equation of the line, the regression coefficient and the sample number.

Results and discussion

To evaluate the reproducibility and accuracy of the system, tests were run on five separate occasions. On each occasion, 10 different tablets were analyzed twice. Also, 10 separate analyses were done on a homogenized sample of 100 tablets. The concentration measured had a total relative standard deviation of 0.55%. Of this, 26% arose from within-series errors, and the remainder equally from between-series and between-occasions errors. These results are more than adequate and the system is reliable and easy to maintain. The start-up time is about 30 min which is shorter than the time needed for sample preparation, and thus is not significant.

One of the goals was to be able to run all different pharmaceutical formulations on the same system. To judge this possibility, measurements of peak height versus peak area were evaluated. Peak height values were too small for all samples where the viscosity of the sample was higher than that of the standard. Thus the dispersion of the sample is influenced by the viscosity and the peaks will be smaller but broader as the viscosity increases. In Fig. 3 the relationship between viscosity and peak height and peak area is shown. The influence on peak height is quite strong while the peak area is almost constant. This is to be expected because the amount injected is constant and the area should only be influenced by the flow rate. Thus, if the flow rate is constant, integration of the peaks is to be preferred. Experience showed also that integration is less susceptible to random noise or microbubbles passing through the cuvette.

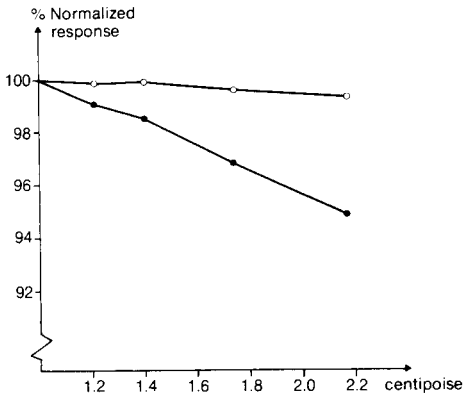

Fig. 3. The influence of viscosity on: (•) peak height and (○) peak area. (Test made with the set-up shown in Fig. 2 but pumping water in all lines and injecting terbutaline sulphate mixed with various amounts of glycerol and measuring the u.v. absorption. Viscosity was measured with an Ostwald viscosimeter.)

In the present determination, however, the reaction product is not stable but decomposes slowly. This means that the absorbance decreases by around 1% during detection, which will introduce an error in the area as well as in the peak height when samples and standards have different viscosity. However, the systematic error arising from this effect is $<0.2\%$ for integration, and thus is not significant. For the peak height the combined error arising from decomposition and viscosity is around 2% for samples having a viscosity of about 1.4 centipoise. This is mainly due to the difference in viscosity between the samples and the standards. The only way to avoid this error when peak heights are evaluated is to add viscosity-increasing ingredients to the standards and run these separately. When the signal is integrated, this is not necessary until there are very large differences in viscosity.

REFERENCES

1 E. Emerson, J. Org. Chem., 8 (1943) 417.
2 E. F. Mohler and L. N. Jacob, Anal. Chem., 29 (1957) 1369.
3 C. A. Johnson and R. A. Savidge, J. Pharm. Pharmacol. 10 (1958) suppl. 171 T.
4 C. F. Hiskey and N. Levin, J. Pharm. Sci., 50 (1961) 393.
5 D. Svobodova and J. Gasparic, Collect. Czech., Chem. Commun., 33 (1968) 42.

ANALYTICA CHIMICA ACTA, VOL. 145 (1983)

AUTHOR INDEX

continued from outside of cover)

inted in The Netherlands.

CONTENTS

(continued on inside page of cover)